A REVIEW OF RESEARCH
ON
AERONAUTICAL FATIGUE IN THE UNITED STATES

2003 – 2005

Compiled by
James L. Rudd
Air Force Research Laboratory
Wright-Patterson Air Force Base, Ohio, USA

FOR PRESENTATION AT THE MEETING
OF THE
INTERNATIONAL COMMITTEE ON AERONAUTICAL FATIGUE

6 – 10 JUNE 2005

HAMBURG, GERMANY

TABLE OF CONTENTS

9.1. INTRODUCTION

Leading government laboratories, universities and aerospace manufacturers were invited to contribute summaries of recent aeronautical fatigue research activities. Their voluntary contributions are compiled here. Inquiries should be addressed to the person whose name accompanies each item. On behalf of the International Committee of Aeronautical Fatigue, the generous contribution of each organization is hereby gratefully acknowledged.

GOVERNMENT
+ **FAA - Los Angeles Office**
+ **FAA - William J. Hughes Technical Center**
+ **NASA – Glenn Research Center**
+ **NASA – Johnson Space Center**
+ **NASA – Langley Research Center**
+ **USAF Academy**
+ **USAF Aeronautical Systems Center - Engineering Directorate**
+ **USAF Research Laboratory - Air Vehicles Directorate**
+ **USAF Research Laboratory – Materials & Manufacturing Directorate**
+ **US Army Research Laboratory**
+ **National Institute of Industrial Safety – Japan**
+ **Ohio Aerospace Institute**

ACADEMIA
+ **Lehigh University**
+ **Michigan State University**
+ **Purdue University**
+ **University of Utah**
+ **University of Washington**
+ **University of Dayton Research Institute**

INDUSTRY
+ **Engineering Software Research & Development, Inc.**
+ **Fatigue Technology, Inc.**
+ **GP Technologies Inc**
+ **JENTEK Sensors, Inc.**
+ **LSP Technologies, Inc.**
+ **R-Tec**
+ **S & K Technologies**
+ **The Boeing Company**
+ **LexTech**
+ **National Institute of Aerospace**
+ **Alcoa Technical Center**
+ **Northrop Grumman Corporation**
+ **Craig Walters Associates**

References, if any, are listed at the end of each article. Figures are compiled at the end of the review.

The assistance of Charlotte Burns, Universal Technology Corporation, in the preparation of this review is gratefully acknowledged.

9.2. OVERVIEWS

9.2.1 UPDATES TO THE USAF'S AIRCRAFT STRUCTURAL INTEGRITY PROGRAM (ASIP)

Lt Col Lawrence M. Butkus, USAF Aeronautical Systems Center – Engineering Directorate

The U.S. Air Force (USAF) is currently engaged in actively strengthening, formalizing, and expanding its Aircraft Structural Integrity Program (ASIP). The ASIP is a disciplined engineering approach based on a preventative maintenance strategy intended to ensure that adequate structural performance, safety, reliability, and supportability levels are achieved throughout the life of the weapon system. The ASIP applies to all USAF fixed wing, rotary wing, manned, and unmanned aircraft, of which there are currently 52 different types. It consists of five main tasks (Figures 9.2-1-9.2-4) that are executed during the life cycle of an aircraft program. Since a majority of USAF aircraft are in the sustainment phase, most ASIP efforts are focused on Task V – Force Management (Figures 9.2-5-9.2-6). For over 45 years, the ASIP has been successful in preventing structural failure and in minimizing the rate of aircraft lost due to structural causes.

In April 2003, the Air Force initiated a review of ASIP that resulted in actions that will lead to several significant changes to the program. These changes will include:

- The creation of a USAF-wide "virtual" ASIP organization to encompass the ASIP Managers for each aircraft type as well as representatives in each of the USAF's Major Commands
- The designation of Dr. Joseph Gallagher, the Senior Leader for Structures in the Aeronautical System Center's Engineering Directorate, as the leader of the virtual ASIP organization
- The conversion of the ASIP Handbook that offers guidance to a military standard, MIL-STD-1530, that, instead, provides direction
- The formalization annual Aircraft Structural Integrity Team (ASIT) reviews of all weapon systems
- Improved coverage of key issues such as:
    - Risk assessments and management
        - developing requirements for performing risk assessments
        - creating guidelines for using risk assessments in decision-making
        - establishing a risk management framework for structural issues
    - Corrosion detection, prevention, and management
        - developing requirements for minimizing the occurrence of corrosion
        - linking corrosion prevention, surveillance, assessment, and mitigation
    - Guidance pertaining to tailoring of the ASIP for
        - unique systems (e.g. unmanned aerial vehicles [UAVs])
        - new structural design concepts (e.g. unitized structure)
        - advanced materials (e.g. composites and hybrid materials)
        - new acquisition strategies (e.g. "spiral development")
- Major revisions to all ASIP-related documentation
- A drive to more directly link the achievement and maintenance of structural integrity to operational safety, suitability, effectiveness, readiness, availability, and life cycle cost

These efforts will not change the overall focus of the ASIP. To the contrary, the changes are intended to strengthen the ASIP. Improvements to the program will make the ASIP more applicable to newer types of weapon systems, acquisition strategies, and sustainment processes. These improvements will also give the ASIP the flexibility necessary to permit it apply to current weapon systems as well as to those developed in the distant future.

The majority of improvements to the ASIP, including revised documentation, are intended to be in place by the end of 2005. Tasks that carry over into 2006 include the development of training programs and web-based tools to assist ASIP Managers.

9.2.2 HOLSIP WORKSHOPS

Prof. David W. Hoeppner, University of Utah

The following members of University of Utah attended the third international workshop on HOLISTIC STRUCTURAL INTEGRITY PROCESSES held in Breckenridge, CO in 2004:

Dr. Kimberli Jones, Mr. Sachin Shinde, Dr. David Hoeppner, and visiting research scholar Mr. Takao Okada (from JAXA).

Dr. Hoeppner and Mr. Shinde also attended the fourth international HOLSIP workshop held in Stowe, VT during March, 2005.

9.2.3 DATA AND METHODOLOGIES FOR STRUCTURAL LIFE EVALUATION OF SMALL AIRPLANES

Michael Shiao, FAA, William J. Hughes Technical Center

Under FAA funding, the Wichita State University National Institute for Aviation Research, in collaboration with small airplane manufacturers, is developing a structural-life evaluation methodology for small airplanes. The purpose of this task is to support the revision of Advisory Circular (AC) 23-13, “Fatigue and Fail-Safe Evaluation of Flight Structure and Pressurized Cabin for Part 23 Airplanes.” AC 23-13 currently references Flight Standards Services (AFS)-120-73-2, “Fatigue Evaluation of Wing and Associated Structure on Small Airplanes,” which will be superseded by the revised AC 23-13. The original AFS-120-73-2, published in 1973, is based on incomplete usage and material data. The data and results from this research will be included in the revised AC 23-13 for the continued evaluation of structural health for the aging small airplane fleet.

An initial review of published loads spectra and usage data has been conducted by Wichita State University. Typical loads exceedance spectra are shown in Figure 9.2-7. The solid lines are the weighted mean, and the symbols are individual airplanes. As indicated, the scatter with respect to the group mean is large. Scatter can be better understood by examining airplane operational usage statistics such as altitude, airspeed, and flight duration. Flight duration data for typical single-engine airplanes are shown in Figure 9.2-8. Loads spectra can be further analyzed in terms of the statistical moments for load factors and operational usage. The resulting spectra can then be completely specified in terms of the statistical moments and the type of distribution.

Analytical loads spectra that are based on statistical moments have three distinct advantages compared to a completely empirical spectra: (1) load levels that are not contained in the original data can be determined; (2) an analytical relationship between the airplane’s acceleration at its center of gravity and load conditions, such as gust load, maneuver load, and landing load, can be developed; and (3) uncertainties in the loads estimates can be evaluated.

The current AFS-120-73-2 fatigue life evaluation methodology uses S-N curves that were based on full-scale test results of surplus military airplanes. The FAA Fatigue Working Group noted that this approach often produces unrealistic estimates for fatigue life. Furthermore, the S-N data are based on one type of wing structure with no means of directly accounting for stress concentrations and load transfer. Two existing methods, Stress Severity Factor and S-N Fatigue Severity Index, were used as a basis for developing a fatigue life methodology that accounts for structural details, full-scale structural complexities, and loading spectrum. The end result will be a method that uses conventional stress concentration factors (that are functions of the structural detail) and empirical factors to determine the effective stress concentration factor for the structural detail. With a known effective stress concentration factor, fatigue life can be determined from conventional S-N data. Further modifications are required to correct for full-scale structural effects and loading spectrum effects. These modifications are also represented in terms of empirical factors.

Experimental work to generate appropriate empirical factors has begun. A typical test arrangement is shown in Figure 9.2-9.

For clarity, half of the antibuckling fixture has been removed. The shown specimen is loaded at a representative 1-g mean stress level with an appropriate alternating stress level. Antibuckling fixtures are required because many of the specimens must be tested at negative R-values to produce failure in the desired range of cycles.

Final project deliverables are (1) an unlimited distribution document and database that contains credible S-N curves and statistical exceedance spectra, (2) technical data to develop guidance material to support rulemaking, and (3) a structural-life evaluation methodology for small airplanes.

9.2.4 METALLIC MATERIALS PROPERTIES DEVELOPMENT AND STANDARDIZATION

John Bakuckas, FAA, William J. Hughes Technical Center

The 3rd Metallic Materials Properties Development and Standardization (MMPDS) Coordination Meeting was held April 14-17, 2003, in Las Vegas, NV. The meeting was well attended with over 50 participants and was held in concert with the first release of the MMPDS-01 Handbook, the replacement document for MIL-HDBK-5. The Handbook is recognized internationally as a reliable source of aircraft materials data for aerospace materials selection and analysis. Consistent and reliable methods are used to collect, analyze, and present statistically based material and fastener-allowable properties. The Handbook is the only publicly available source in the U.S. for material allowables that the FAA generally accepts as being compliant with the FAR for material strength properties and design values for aircraft certification and continued airworthiness. Moreover, it is the only publicly available source worldwide for fastener joint allowables that comply with the FARs.

This year marks the first year of publication of the MMPDS Handbook and the final year of publication of MIL-HDBK-5. For this year only, MMPDS-01 and MIL-HDBK-5J will be technically equivalent. In the spring of 2004, when the 1st Change Notice of MMPDS-01 is published, MIL-HDBK-5 will be designated noncurrent, and MMPDS will become the only government- recognized source in the U.S. of published design-allowable properties for metallic commercial and military aircraft structures and mechanically fastened joints. This maintains the 65-year legacy of MIL-HDBK-5 and its predecessor the Army-Navy-Commerce Handbook 5.

The MMPDS Handbook can be obtained from the National Technical Information Service, NTIS, at http://www.ntis.gov/ for a nominal fee. The MMPDS Handbook is available in two formats: (1) microfiche for \$116.50 plus shipping and (2) paper copy for \$223.50 plus shipping. The MMPDS Handbook can also be downloaded in PDF format free of charge at the FAA William J. Hughes Technical Center library's website http://actlibrary.tc.faa.gov/.

9.2.5 CONTINUING ANALYSIS SURVEILLANCE SYSTEM RESEARCH PROJECT

Michael Vu, FAA, William J. Hughes Technical Center

Since 1964, all air carriers have been required by regulation to conduct continuous evaluations of their maintenance programs. Specifically, 14 CFR Parts 121.373 and 135.431 require air carriers to establish a Continuing Analysis and Surveillance System (CASS) to evaluate, analyze, and correct deficiencies in the performance and effectiveness of their inspection and maintenance programs. These regulations do not distinguish between maintenance functions the air carrier accomplishes and those that it contracts out. Nevertheless, the responsibility for CASS remains with the air carrier.

CASS is an air carrier quality assurance system and must consist of the following functions: surveillance, controls, analysis, corrective action, and follow-up. Together, these functions form a closed-loop system that allows the air carrier to monitor the quality of its maintenance. In a structured and methodical manner, CASS provides air carriers with the necessary information to make decisions and reach their maintenance program objectives. Furthermore, if CASS is used properly, it becomes an inherent part of the air carrier's way of doing business and helps promote a safety culture within the company.

While the regulation governing CASS is short and offers little guidelines, its sparse language nonetheless requires a complex system. Each CASS must set high goals, and the FAA is empowered by the regulations to require changes to an air carrier's maintenance program if it shows signs of weakness.

To help industry maintenance personnel and FAA inspectors understand and comply with CASS requirements, the FAA Flight Standards Aircraft Maintenance Division asked the Risk Analysis Branch to conduct research on CASS requirements in December 2001.

The Risk Analysis Branch completed the research in October 2002. Three models were developed that illustrate how the structure of CASS can be established based on the air carrier's size and complexity. CASS model 1 is for large 14 CFR Part 121 air carriers with more than 100 turbine-powered aircraft operating worldwide, model 2 is for 14 CFR Part 121 or 135 air carriers with 5 to 20 turbine-powered aircraft operating in a domestic regional network, and model 3 is for air carriers with fewer than five turbine-powered aircraft of ten or more seats operating on demand under 14 CFR Part 135. Each model represents a complete system that should meet, or exceed, the regulatory requirements. Existing air carriers can also use the models as a comparison to their existing CASS and determine its effectiveness. A new entrant carrier can use one of these models to establish its CASS.

The research results are based on the information gathered through research and on-site interviews with industry, FAA, and trade association representatives. Interviews with eighteen 14 CFR Part 121 air carriers, five 14 CFR Part 135 air carriers, four aviation industry associations, and a representative of the Joint Aviation Authorities of Europe were conducted over a 6-month period. Interviews of personnel at the FAA Flight Standards District Office, Certificate Management Office, and Headquarters were also conducted to gain input from the regulatory perspective.

Based on the research materials, AFS-300 developed the advisory circular "Developing and Implementing a Continuing Analysis and Surveillance System," AC 120-79, which was approved April 21, 2003. Following the AC's guidance is one method of complying with the requirements of 14 CFR Parts 121.373 and 135.431.

9.2.6 FAA CERTIFICATION ISSUE PAPER STUDY

Cristina Tan, FAA, William J. Hughes Technical Center

During the design certification of new aircraft, the Aircraft Certification Service uses a system of issue papers (IPs) to document the decision-making process on new, novel, and unique certification issues. This process has been used since the early 1980s. Hardcopies of the IPs have been used for the last 15 years, and the majority of IPs have been addressed through regulations. The 1500 IPs generated over the last 6 years have been stored electronically by project, but no attempt has been made to recover the historical and managerial information they contain. These IPs contain information concerning

- potential revisions to 14 CFR Part 25 (Transport Category Airplane),
- areas where existing policy and guidance are inadequate, and
- technical subjects, which are resource-intensive.

The FAA Certification Issue Paper Study was a research effort to review certification issue papers that were generated in the past 6 years and to develop methods of sorting and evaluating this data would allow the Transport Airplane Directorate to process the information in a more efficient way.
The FAA Issue Paper Database Application (Figure 9.2-10) is a user interface to the IP database. The application was designed in a Microsoft Access environment. This interface has three groups of operations: forms, reports, and queries. The description of each group is explained below.

Forms: Through forms, users can enter new IP data into the system. Users are required to pick from a preset classification, keywords, type of IP, aircraft, and enter other information such as the subject, project, regulation, and the executive summary. There is a provision to hyperlink to the actual IP so users can open the IP document.

Reports: The application can generate reports on the IP database for classifications such as Airframe, Cabin Safety, Flight Test, Propulsion, and Systems. The reports present information on keywords, manufacturer, type of aircraft, and the issue description related to the selected classification.

Queries: The application allows users to query the IP database based on keyword, IP type, classification, applicant, aircraft model, IP status, and regulation. All the results of the query have hyperlinks to the IP document. There is a provision in the application to view the entire database.

Of the over 2000 FAA IPs screened and reviewed, 1167 unique IP records were categorized and entered into the newly created FAA IP database. These records (and all records that may be added in the future) are available for review and development of trend analysis as needed by the certification engineers in the Transport Airplane Directorate. The FAA Issue Paper Database Application provides a simple means of organizing and analyzing certification issues to assist the Transport Airplane Directorate in managing those issues.

9.2.7 METALLIC MATERIAL PROPERTIES DEVELOPMENT AND STANDARDIZATION

John Bakuckas, FAA, William J. Hughes Technical Center

The Metallic Material Properties Development and Standardization (MMPDS) is an effort led by the Federal Aviation Administration (FAA) to continue the Handbook process titled "Metallic Materials and Elements for Aerospace Vehicle Structures" (MIL-HDBK-5). The Handbook is recognized worldwide as the most reliable source for verified design-allowable properties needed for metallic materials, fasteners, and joints used in the design and maintenance of aircraft, missiles, and space vehicles. Consistent and reliable methods are used to collect, analyze, and present statistically based aircraft and aerospace material and fastener-allowable properties.

The objective of the MMPDS is to maintain and improve the standardized process for establishing statistically based design allowables that comply with the regulations, which is consistent with the MIL-HDBK-5 heritage. The United States Air Force (USAF) issued a cancellation notice for MIL-HDBK-5J, effective May 5, 2004. In the notice, a pointer is made to the MMPDS-01 as the replacement document. The MMPDS is now the only government-recognized source in the U.S. of published design-allowable properties for metallic commercial and military aircraft structures and mechanically fastened joints. This maintains the 65-year legacy of MIL-HDBK-5 and its predecessor the Army-Navy Commerce Handbook 5.

A plan was established to manage the MMPDS. The goal is to ensure that the continuity and integrity of the MMPDS document and process is consistent with the MIL-HDBK-5 heritage. To accomplish this goal, a more equitable and sustainable sponsorship is needed for the long-term health of the MMPDS. With current and foreseeable budgetary constraints, the best way to leverage shrinking government resources is to share the funding between multiple agencies. Towards that goal, the FAA is actively pursuing three avenues of funding: drawing increased support from government agencies, drawing increased support from industry, and selling the Handbook and derivative products and using profits for further Handbook development.

Efforts to obtain joint government sponsorship of the MMPDS have been quite successful. During fiscal year 2004 (FY04), a Memorandum of Understanding to support the MMPDS was established with the Joint Council on Aging Aircraft (JCAA). The JCAA has representatives from each of the Department of Defense services, from NASA, and from the FAA. Through the JCAA, in particular, the USAF, the Navy, the Defense Logistics Agency, and NASA, the MMPDS is now a jointly sponsored activity.

Industry has been and continues to be a strategic partner in the development and maintenance of the Handbook. In recent years, suppliers and manufacturers have been the primary source for information entered in the Handbook and have stepped up their efforts through the development of the Industry Steering Group (ISG). Through the auspices of the ISG, web-based products and tools have been developed that support MMPDS industry activities.

Looking ahead, the FAA's goal is to conduct some market surveys and develop strategies to begin the commercialization effort. The next release of the Handbook, MMPDS-02, is planned to be ready for licensing at the 7th MMPDS Coordination Meeting in April 2005.

9.2.8 ASSESSMENT OF HELICOPTER STRUCTURAL USAGE MONITORING SYSTEM REQUIREMENTS

Dy Le, FAA, William J. Hughes Technical Center

One task within the FAA National Aging Aircraft Program is to conduct research to obtain technical guidance and information, including data for use in the health and usage monitoring systems (HUMS) certification procedures contained in Advisory Circular (AC) 29-2C, Section MG-15. This AC addresses airworthiness approval of HUMS and provides guidance for obtaining airworthiness approval for installation and credit validation.

During the first quarter of FY04, one of the research efforts funded by the FAA and completed by the Naval Air Warfare Center, Aircraft Division was to perform a data-driven assessment of various aspects of the helicopter structural usage monitoring process. The objective was to determine the data-sampling rate and the required set of data parameters that needed to be collected for part life extensions, maintenance credits, or trend monitoring. The results of the work, applicable to commercial utility helicopters and tiltrotor aircraft, will be used to provide data to support the certification procedures described in the HUMS AC.

The assessment addressed several structural monitoring system design issues, including the number of aircraft parameters to be monitored and the data rates at which those parameters should be monitored. This assessment used data collected previously by the Navy over several years. The Navy collected extensive data that tracked the development of damage in rotorcraft components. From these data they created damage tables for key rotorcraft components that were used in the current task. They also determined the minimum set of parameters that needed to be monitored to track fatigue damage on key components.
To determine the generic set of parameters that are necessary to determine what phase of flight (e.g., level flight, bank) the rotorcraft is in, an assessment was done to identify the parameters that needed to be monitored to determine the flight phase. An assessment of the effect of varying the number of parameters was performed using flight data for an SH-60R aircraft. In general, if a reduced parameter set is proposed for a monitoring system, certain aspects of the component damage calculations will likely be missed.

The parameters necessary for structural monitoring were separated into three groups: a core set of requirement parameters, a required set of aircraft configuration-specific parameters, and a set of useful but not absolutely necessary parameters. The minimum set of parameters that must be modeled to recognize the ground-air-ground cycles is the six parameters of gross weight, altitude, outside air temperature, air speed, rotor speed, and weight on wheels. Figure 9.2-11 shows that, for the minimum set of six, 75% of the fatigue damage was tracked for over 20% of the life-limited components. If eight more parameters (vertical velocity, roll angle, pitch rate, vertical acceleration, collective stick position, lateral cyclic stick position, longitudinal cyclic stick position, and pedal position) were added for a total of 14 parameters, then 75% of the damage can be tracked for 83% of the components of interest.

While SH-60R-specific data values established for the reduced parameter set are not necessarily applicable to other aircraft models, the maneuvers that are typically damaging are fairly consistent across platforms. As such, the key parameters for this reduced data set study will likely be applicable to other platforms. When a reduced data set is proposed, the specific impact to accurate component damage calculations must be assessed through review of the aircraft-specific damage rate tables. Given the damage tables for a specific aircraft model, a similar analysis can be performed and a minimum data set for that model could be established.

The rate at which the data must be collected is also very important and is driven by how quickly the input parameters change. Parameters must be monitored and recorded at the appropriate rate to ensure that peak information is captured properly and to ensure that the usage monitoring results are accurate. In this task, minimum data rates for regime recognition input parameters were established for two military aircraft, the UH-60 (utility helicopter) and V-22 (tiltrotor aircraft).

Figure 9.2-12 shows the effect of monitoring vertical acceleration, Nz, at 2 Hz and at 8 Hz. At 8 Hz, the peak Nz value is about 1.5 g's. However, when the same signal is monitored and recorded at 2 Hz, the peak information is totally missed. Therefore, if data are collected at 2 Hz or lower, the data peak (representative of a pullup maneuver) would not be captured and recognized as the maneuver flown, and the damage associated with the peak would not be correctly accounted for.

All available flight data for the UH-60 (utility helicopter) and V-22 (tiltrotor aircraft) were used to establish minimum-acceptable data rates. Maneuvers that were deemed military only were removed from the data set, and the required data sets were reassessed to establish the data rate required to capture peak information for a commercial spectrum. For commercial utility helicopters and tiltrotor aircraft, the required data rates were found to be highly dependent on the specific input parameter with data recording rates ranging from 1 to 6 Hz.

The results of this task are documented in the FAA technical report "Assessment of Helicopter Structural Usage Monitoring System Requirements," McCool, K. and Barndt, G., DOT/FAA/AR-04/3, April 2004.

9.2.9 MATERIAL SUBSTITUTION FOR LEGACY AIRCRAFT

R. Perez, Boeing, St. Louis

A summary of work related to material substitution for legacy aircraft is illustrated in Figures 9.2-13, 9.2-14 and 9.2-15.

9.2.10 AGING OF THE CESSNA 402, 402A, 402B AND 402C AND RAYTHEON T34A AND B

Robert Eastin, FAA, Los Angeles Office

The structural certification bases for the subject airplane models had no fatigue requirements. Consistent with this, these airplanes have been operating in the United States without the benefit of any mandated fatigue management strategy (e.g. life limits or damage tolerance based inspection programs). There have been Airworthiness Directives (AD) issued over the years to deal with specific fatigue incidents on a case by case basis but on the whole these models have been relatively free from fatigue problems.

Events over the past several years have brought attention to these airplanes in particular and to the general issue of the aging of the general aviation fleet in the United States. There are clear challenges when it comes to effectively managing fatigue in a fleet of aircraft where fatigue has not been considered a serious threat. There has been significant resistance from owners and operators of the subject models to any mandatory fleet wide regulatory actions. Several public meetings have been held to provide information on the rationale behind FAA actions taken, and others proposed, to minimize the probability of catastrophic failures. In spite of strong resistance from some owners and operators, the FAA took certain regulatory actions to mitigate the risk of additional incidents. However it appears that additional and possibly more restrictive actions may be necessary. For the airplane models involved this is an evolving process and is expected to result in significant changes to how the FAA deals with the aging general aviation fleet. Some of the more relevant facts associated with the Raytheon and Cessna models involved are summarized below.

9.2.10.1 Raytheon T34A and B (See Figures 9.2-16, 9.2-17 and 9.2-18)
The T34A and B are military trainer versions of the Beech Bonanza airplane. The United States Air Force (USAF) procured 348 As with the first delivery in 1953 and the Navy procured 423 Bs with first delivery in 1954. Civil certification was required by the military procurement contracts. The basic wing structure of both models is the same and was designed statically for +6G and –3G limit maneuver load factors. The T34A and T34B were certificated to Part 3 of the Civil Air Regulations (November 1, 1949 version) as acrobatic and utility category respectively. These airplanes started coming into the civil registry during the 1960's as the USAF and Navy released airplanes to the Civil Air Patrol. At present there are approximately 260 active registered airplanes.

These airplanes enjoyed a relatively fatigue free history until April 19, 1999 when T34A, N140SW, suffered a wing separation during mock aerial combat over Rydall, Georgia. Subsequent to this there have been two additional wing separations. One on November 19, 2003 and one on December 7, 2004. Each event resulted in two fatalities and after investigation the NSTB has attributed each wing separation to fatigue.

The primary fatigue location for the 1999 and 2003 failures was at the front spar lower cap at wing station (WS) 34. The appearance of the fractured section was very similar for both failures and was characterized by cracking at multiple sites. For the 1999 failure the wing also had a fracture site at the rear spar lower wing attachment fitting and fatigue cracks were found in the rear spar lower cap at WS 66. For the 2003 failure there was also fracture at WS 66 in the rear spar but no cracking of the lower attachment fitting. The records show that for the airplane involved in the 2004 failure the front wing spars had been replaced in 1996. On this airplane the only fracture was in the center wing front spar lower cap just inboard of the lower wing attach fitting. Fatigue cracks were present at multiple sites. Fatigue cracks were also found in the rear spar lower cap at WS 66 and in the horizontal tail attach fitting. There were no signs of manufacturing or service anomalies reported.

Each failure resulted in certain regulatory actions intended to preclude a repeat failure. The first failure was eventually addressed with AD 2001-13-18 (August 16, 2001) which required Raytheon developed inspections of front spar WS 34, WS 66 and rear spar WS 66 and the lower attach fitting every 80 hours. However the expense and difficulty associated with these inspections motivated the development and approval of four different AMOCs (Alternative Method of Compliance). They all addressed front spar WS 34 with some sort of modification and the rear spar lower attach fitting with inspection but did not include any action for WS 66. The second failure occurred on an airplane that had passed the threshold for inspection given in AD 2001-13-18 , but had not been inspected. This failure underscored the criticality of front spar WS 34 and brought rear spar WS 66 into the spot light. AD 2001-13-18 was revised to rescind the AMOCs until they were revised to include inspections at WS 66. The third failure revealed yet another fatigue critical area that had not been previously addressed. This resulted in AD 2004-25-51 (December 10, 2004) which grounded all civilian registered T34As and Bs.

The T34A and B fleet remains grounded at the time of this writing. A public meeting (Reference FAA website: http://www.faa.gov/certification/aircraft/aceT34PublicMeeting.htm) was held to discuss the situation. Getting these aircraft back into the air will not be easy. There are many issues to resolve such as quantifying the effect of usage in mock aerial combat since all three accident airplanes had been employed for a significant amount of time in this environment. There is also the lack of a fatigue knowledge base (e.g. full scale/component fatigue test results, fatigue and/or damage tolerance assessments, usage profiles). The FAA is considering mandatory modification and life limits amongst other things. The way forward is not clear at this point.

9.2.10.2 Cessna 402, 402A, 402B and 402C (See Figures 9.2-19, 9.2-20 and 9.2-21)
The subject Cessna models are twin engine piston airplanes capable of seating up to nine passengers and have been utilized in a wide variety of applications including scheduled passenger service, cargo delivery, and scenic tours (e.g. Grand Canyon). The 402, 402A and 402B are structurally identical with tip tanks and a dry wing and were designed in the late 1960's. The 402C was designed in the late 1970's and has a higher gross weight, a redesigned wet wing without tip tanks and a redesigned vertical stabilizer. These airplanes were certificated to Part 3 of the Civil Air Regulations (May 15, 1956 version).

These airplanes have enjoyed a relatively fatigue free history. However service experience includes front spar lower cap fatigue cracking on four 402s and two 402As. Cracking was from cap to skin attachment holes and was concentrated in a local area just inboard of the engine. Full scale fatigue testing of a 402 performed after original certification also identified this area as susceptible to fatigue. Additionally there was a fatal wing separation experienced by a 402C attributed to fatigue cracking in the front spar lower cap in this same general area. The in-service findings prompted regulatory actions in 1979 (applicable to the 402, 402A and 402Bs) and 2000 (applicable to 402Cs) that mandated inspections to detect cracking of the front spar lower cap. At the time this was considered sufficient to ensure safety.

In the late 1990's Cessna performed a damage tolerance evaluation (DTE) of these airplanes and based on the results established inspections and other procedures need to insure safety relative to fatigue. These were documented in a Supplemental Inspection Document (SID). Cessna concluded that inspection of the front spar lower cap was not sufficient and that this area needed to be modified at a prescribed "not to exceed" time in service. An external reinforcing strap was subsequently designed by Cessna and they requested that the FAA issue an AD that would mandate strap installation. In response a proposed AD was published for public comment. Resulting comments from owners and operators were generally negative and two public meeting were held in 2004 (Reference FAA website: http://www.faa.gov/certification/aircraft/aceCessna400WingsparPublicMeeting.htm)
to have open discussions on the proposal.

In February of 2005 a pilot of a 402C being used in commuter service sensed a structural problem with the wing and requested maintenance to investigate prior to further flight. This revealed that the spar cap was completely failed and that there was major cracking in the surrounding structure. This prompted another commuter operator to perform inspections and similar but less extensive cracking was found in another 402C.

The 402C findings resulted in the FAA issuing ADs that mandated immediate inspections of all 402C aircraft at relatively short intervals. Additionally, at the time of this writing, the FAA is considering moving forward with issuing ADs that require the installation of reinforcing straps on 402, 402A, 402B and 402C airplanes. This action should alleviate the immediate concern with the front spar lower cap. But, what about other Cessna Twins that share a similar design (e.g. 401, 414)? What about other areas? Should the Cessna developed SID be mandated by AD? These are all hard questions that must be addressed. It is expected that additional actions will not be well received by a community where fatigue management at the overall airplane level is a relatively new concept. Like the T34A and B the way forward is not clear.

9.3. LOADS

9.3.1 CHARACTERIZATION OF TG-10B TAIL LANDING GEAR LOADS

Gregory A. Shoales and James M. Greer, Jr., United States Air Force Academy

This program was funded in its entirety by the Aeronautical Systems Center's Aging Aircraft Support Squadron at Wright-Patterson AFB, Ohio (ASC/AAA).

The United States Air Force Academy (USAFA) operates a fleet of sailplanes to include the TG-10B—commercially known as the L-23 Super Blanik. The L-23 aircraft were acquired by USAFA beginning in 2000 as replacements for the aging Schweizer 2-33 fleet. Since entering service the USAFA TG-10Bs have experienced numerous failures of the tail landing gear and associated support structure during normal cadet flight training operations (Figure 9.3-1). Little explanation for this damage was available from either the acquisition program data or the manufacturer.

The goal of this data collection effort was to help improve the TG-10B program office's (ASC/YTG) understanding of the loads environment that may have contributed to the failures of the TG-10B tail landing gear support structure. It was hoped that such information might be used to prevent such failures in the future. The data collected during this program could also be used to support the redesign of the tail landing gear structure. The program objectives defined to satisfy the program goal were the acquisition of strain, acceleration and operational parameter data. One of the operational parameters of specific interest by ASC/YTG was operations from the USAF Sailplane Landing Area (SPLA) as compared to other surfaces.

To accomplish these objectives, CAStLE personnel installed a self-contained flight data acquisition system (FDAS) in one (1) USAFA TG-10B sailplane. This aircraft was then flown in normal cadet flight operations. The FDAS collected strain and acceleration data using strain gages and accelerometers. The system included a digital data acquisition system (DDAS) which recorded these data. The program continued for the number of the flight hours necessary to sufficiently understand the normal operations tail wheel support loads environment. No special maneuvers were required. The only flight crew interaction was the activation and deactivation of the FDAS as part of the crew checklist via a clearly labeled cockpit switch. Crew members completing data acquisition sorties also completed a brief questionnaire to include additional operations information that helped correlate the recorded data to the operational parameters. Throughout the program CAStLE personnel periodically obtained the data from the DDAS for analysis.

The data show a significant increase in loads severity between all operations conducted on the USAFA SPLA when compared to any other surface evaluated. This includes both landings and ground repositioning operations. While an attempt has been made by the USAFA TG-10B operators to mitigate damage from the SPLA through pilot training, this report's analysis showed that the random nature of the SPLA surface can overwhelm the impact of pilot performance. While this program did not quantify the remaining life of the USAFA TG-10B fleet, it did significantly improve the understanding of how certain operation factors such as SPLA operations affect the structural loads. The program's final report was published as USAFA TR-2005-6, Feb 2005.

9.3.2 OPERATIONAL LOADS MONITORING

Thomas DeFiore, FAA, William J. Hughes Technical Center

Title 14 Code of Federal Regulations (CFR) Part 23 Airworthiness Standards are replete with loads criteria much of which were generated prior to deregulation and, in some cases, prior to the design of both wide-body and fly-by-wire civil aircraft. With the existence of new technology, newer operating rules and practices, and the anticipation of double the air traffic within 10 years, there is a need to develop and implement a system to continuously validate and update the operational flight and ground loads airworthiness certification standards based on actual measured usage.

The Federal Aviation Administration (FAA) has an ongoing Operational Loads Monitoring Program, which includes both flight and landing loads data collection on civil transport aircraft, as shown in Figure 9.3-2.

The output from the Operational Loads Monitoring research provides the technical basis for airframe certification requirements. The research independently assesses the original equipment manufacturers (OEM) design assumptions and aircraft usage analysis. This is a fundamental element of the FAA's regulatory and certification process and is an essential input to confirming the continued safety and airworthiness of the civil transport fleet. The research provides the opportunity to identify operational problems in a proactive manner.

Data from digital flight data recorders (Figure 9.3-3) are acquired, processed, and analyzed and are published in formal FAA reports. Thirty formal loads-related FAA technical reports have been published along with a significant number of technical papers.

The FAA Operational Loads Monitoring team provided specialized operational loads data and analysis for the Aviation Rulemaking Advisory Committee (ARAC) to develop recommendations for the certification criteria for the A380 airplane, 14 CFR Part 25.495, Turning.

The research resulted in the publication of "Side Load Factor Statistics From Commercial Aircraft Ground Operations," DOT/FAA/AR-02/129, Tipps, D., et al., January 2003. Presented in the report are analyses and statistical summaries of landing and ground operations data to provide the FAA with a technical basis for assessing the suitability of the 0.5-g lateral acceleration criteria specified in 14 CFR Part 25.495 for turning, Figure 9.3-4. The data represent 1037 flights, 1039 flights, and 1361 flights of B737-400, B767-200ER, and B747-400 aircraft, respectively. Included is statistical information on vertical and lateral accelerations, yaw angles, ground speeds, and gross weights experienced during touchdown and ground operations. Ground-turning lateral acceleration data were used in the development of a normalization procedure to allow prediction of lateral load factors due to ground turning on other aircraft. While the data contained in the report might indicate that the 14 CFR Part 25.495 may be conservative at the 0.5-g level, when one considers that 14 CFR Part 25.495 takes into consideration asymmetric gear loading for both dry and highly slippery conditions, the retention of the traditional 0.5-g value may well be appropriate. The results of this study clearly indicate, however, that the lateral loads experienced by the larger and heavier transport jets during ground turns are substantially less than those of the smaller jet transports.

Statistical data are presented on the aircraft's usage, flight and ground loads data, and systems operations in the technical report "Statistical Loads Data for Bombardier CRJ-100 Aircraft in Commercial Operations," DOT/FAA/AR-03/44, Rustenberg, J., June 2003. The data presented in the report provide information about the accelerations, speeds, altitudes, flight duration and distance, gross weights, speed brake and spoiler cycles, thrust reverser usage, and gust velocities encountered by the CRJ-100 airplane (Figure 9.3-5) in actual operational usage. The statistical data provided the FAA, aircraft manufacturers, and the operating airline with the information that is needed to assess how the CRJ-100 is actually being used in operational service versus its original design or intended usage. The FAA plans to (1) evaluate existing structural certification criteria, (2) improve requirements for the design, evaluation, and substantiation of existing aircraft, and (3) establish design criteria for future generations of new aircraft using the data. Aircraft manufacturers use the data to assess the aircraft's structural integrity by comparing the actual in-service usage of the CRJ-100 versus its originally intended design usage. While current program research efforts are tailored primarily to support the FAA regulatory community, the data can also provide the aircraft operators with some valuable insight into how their aircraft and aircraft systems are being used during normal flight and ground operations.

The FAA William J. Hughes Technical Center hosted a Gust Specialists Seminar in May 2003 to review and document the Statistical Discrete Gust (SDG) Method, which is used as an alternative procedure for estimating severe gust and turbulence loads. The seminar was the last in a series of seminars going back to 1986 when an international team of specialists, convened by the FAA, met approximately annually to re-evaluate the gust criteria for future generations of commercial transport aircraft. The goals of this international ad hoc committee have been to reduce the number of design criteria to be met and to recommend a design method with the ability to handle advanced technologies such as active controls and gust load alleviation.

The SDG method provides a specification, which accounts for the non-Gaussian statistical structure of the more intense turbulence fluctuations, and the manner in which these interact with the dynamic response of a flexible aircraft. SDG can be interpreted as a generalization of the existing tuned Isolated Discrete Gust (IDG) model to take account of tuning to gust patterns of different shapes. SDG is also expressed in a statistical format that parallels that of the Power-Spectral-Density method, being applicable in both Mission Analysis and Design Envelope forms.

The SDG method has been identified as the only existing method that can handle discrete gust events and relatively continuous turbulence and, moreover, can be used to evaluate highly nonlinear systems. The SDG has not been recommended by the Gust Specialists Committee for consideration as a revised airworthiness requirement, perhaps, at least in part, as a result of perceived computational complexity. However, the SDG remains the only existing method with the potential to meet the goals of the international ad hoc committee.

Additional information can be found at http://aar400.tc.faa.gov/Programs/Aging Aircraft/airbornedata/index.htm.

9.3.3 DOWNLINKING ICING DATA FROM COMMERCIAL AIRCRAFT

James Riley, FAA, William J. Hughes Technical Center

An ice detector warns a pilot when his or her aircraft encounters icing conditions. Some icing encounters are very hazardous and all have a potential effect on aircraft flight safety. If information concerning an icing encounter on one aircraft could be provided in near real time to weather forecasters and other aircraft, the pilots of other aircraft might be able to avoid potentially hazardous icing conditions. Also, archived data from icing encounters will be used in the evaluation and modification of current icing forecast models, which will contribute to the development of better models. The archived information can also be analyzed to develop a better understanding of how often aircraft encounter icing and where the encounters most frequently occur.

The FAA has joined with Goodrich Aerospace to investigate how to capture ice detector information from commercial aircraft. The approach that has been chosen is to downlink icing data (ice and no ice signals) from ice detectors mounted on commercial aircraft to ground stations. Electronic uplinking would be a very efficient way of providing the data to other aircraft. It was decided that it would be best to start with a downlinking demonstration project using commercial aircraft that required minimal modification to its hardware and software, thus minimizing engineering and certification costs. A survey of aircraft in the commercial fleet was completed to determine which aircraft would be most appropriate for the project according to these criteria. The survey found that there are several types of aircraft that could downlink ice detector information with relatively minor hardware and software changes, but these changes would require some hardware engineering and certification work.

However, the B777 was found to only require a software modification, without additional certification, to downlink the ice detector information. The software modifications were coded, and several airlines were contacted to see if they would participate in this project.

Delta Air Lines was the first to participate in the demonstration project and is currently downlinking icing data from the ice detectors on its entire fleet of B777 aircraft. Downlinking icing data started during the 2002-2003 winter icing season and will continue for 1 year. The resulting data is being provided to the National Center for Atmospheric Research in Boulder, Colorado, for use in the evaluation and enhancement of icing forecasting models. The potential safety value of providing such information in near real time to other aircraft will also be assessed. Results thus far look promising. A second airline has expressed interest in joining the project for the next winter season. Once the technical and economic feasibility of downlinking icing data from commercial aircraft has been established by this project, it is hoped that the airlines will participate in downlinking icing data on a routine basis. Participation by regional carriers, which spend quite a bit of time in icing conditions, would be particularly valuable. Broad participation by commercial carriers would lead to the improvement of icing forecasts and to the expansion and improvement of icing information available to pilots

9.3.4 EFFECTS OF MIXED-PHASE ICING CONDITIONS ON AIRCRAFT SURFACES AND AIRCRAFT THERMAL ICE PROTECTION SYSTEMS

James Riley, FAA, William J. Hughes Technical Center

Most aircraft icing in the atmosphere is due to supercooled liquid droplets (droplets at temperatures below 32°F) impinging and freezing on aircraft surfaces. However, many clouds are mixed-phase clouds, containing both supercooled droplets and ice particles. The safety of flight into mixed-phase clouds has been a long-standing question, with limited scientific information available on which to base sound engineering decisions. Most information on in-flight icing is for purely liquid clouds, and certification requirements are written for those conditions. The National Transportation Safety Board has recommended to the FAA that aircraft icing certification requirements be expanded to include mixed-phase icing conditions if necessary, and the FAA has investigated questions bearing on the magnitude of the safety threat that may be posed by mixed-phase conditions.

The FAA determined that testing in an icing tunnel was needed, and a test was conducted in the Cox & Company Icing Wind Tunnel in July 2002 using a wing section equipped with a thermal ice protection system. Analysis of the test results was completed and a report, "Assessment of Effects of Mixed-Phase Icing Conditions on Thermal Ice Protection Systems," DOT/FAA/AR-03/48, Al-Khalil, K., was published in May 2003. This was a collaborative effort involving the FAA, Wichita State University, Cox & Company, and NASA Glenn Research Center.

The test results indicated that in mixed-phase icing conditions, ice accretion resulted mainly from the supercooled water droplets present in the mixed-phase cloud. For glaze ice, which occurs at temperatures close to 32°F, the ice particles in the mixed-phase clouds actually reduced the overall size of the ice accretion, as shown in Figure 9.3-6.

It is believed that this may have been mainly due to shedding or splashing of water from a surface water film due to ice particles bounced in the film and, to a lesser extent, due to erosion of accreted ice by the incoming particles.

The performance of the thermal ice protection system, when used in an evaporative mode (which evaporates all incoming water or ice), did not seem to be adversely affected by the presence of ice particles in the cloud. However, testing the system in a running-wet mode (which prevents freezing in the protected region, with water running back to a less critical area) showed that the power requirements at the leading edge were much higher when ice particles were present in the simulated cloud, as shown in Figure 9.3-7. The bars indicate a cloud consisting entirely of water from the spray bars, but all other conditions are either mixed-phase or consist of ice particles only. Heater No. 4 is at the leading edge of the wing section.

This investigation used state-of-the-art simulation methods and visualization techniques that yielded unique data. Although the ice particles that can presently be simulated represent only a small percentage of the many types found in the atmosphere, the investigators believe that the trends observed in the tunnel will also occur during natural icing encounters.

9.3.5 MODERNIZING GRAPHS ON AIRCRAFT ICING DESIGN CRITERIA

Richard Jeck, FAA, William J. Hughes Technical Center

Title 14 Code of Federal Regulations contains scattered graphs and tables of supplementary data or information, usually in the appendices to the various parts of the CFR. Some of this material would be useful beyond the original vision of the suppliers if the material were in a computer-compatible form so that graphs could be customized or data tables imported directly into computer programs. An example of the benefits of computerizing a particular supplementary graph is illustrated as follows.

Appendix C of 14 CFR Part 25 contains six graphs of design variables that are frequently used by designers of in-flight ice protection systems, by data analysts for icing test flights, icing wind tunnel tests, and by computer modelers of ice shapes on aircraft surfaces. One of the most used figures from 14 CFR Part 25, Appendix C is reproduced in Figure 9.3-8. This, and the five other companion figures, have been published in the CFR since the early 1960s.

Unfortunately, the published versions of some of the figures are of a poor quality, as shown in Figure 9.3-8. The graphical grid spacing is awkward in that it is not evenly matched to the numerical scales marked along the axes. Also, these fixed (printed on paper) versions of the graphs are not convertible to other useful versions (R. K. Jeck, "Converting Appendix C to Other Variables," paper no. 2003-01-2153 in *Proceedings of the FAA In-Flight Icing/Ground De-icing International Conference & Exhibition* (Chicago, IL, June 16-20, 2003)).

These problems can be easily overcome by tabulating the coordinates of the curves in Figure 9.3-8 in a computerized spreadsheet. Then, using the charting capabilities of the spreadsheet software, clean, properly scaled reproductions of the original graphs can be produced at will, as shown in Figure 9.3-9.
The advantages of spreadsheet-based graphs in this example are that they

- have a cleaner, sharper appearance than the printed versions in the CFR.

- have a more convenient grid spacing on the vertical and horizontal axes than the printed versions in the CFR.
- are easier to size and insert electronically into word processors or other computerized documents.
- can be adjusted or customized to suit the needs of various applications.
- can be converted to other useful variables or scales.
- can replace the original graphs with cleaner, better versions in the printed CFR.

In summary, common computer technology can be used to modernize supplementary material that is currently available only in hard copy form in the CFR. When the CFR is made available on compact disc or other computer-compatible media, working files such as spreadsheet versions of graphs can be included and supplied directly to the user to enhance the usability of graphical data.

9.3.6 EXPERIMENTAL STUDY OF SUPERCOOLED LARGE DROPLET IMPINGEMENT ON AIRCRAFT SURFACES

James Riley, FAA, William J. Hughes Technical Center

A major concern in the design and certification of ice protection systems for aircraft is the extent of supercooled water droplet impingement on aircraft surfaces, since this results in the formation of ice. The impingement characteristics of aircraft surfaces can be used to determine the size and location of ice protection systems. Droplet trajectory and impingement computer programs are often used as a cost-effective means for the design of ice protection systems. Current programs have been extensively tested for the icing conditions currently included in the FAA regulations. However, they have not been validated for supercooled large droplet (SLD) icing conditions, which are expected to be added to the FAA regulations soon. Consequently, the FAA determined that tunnel testing was needed to obtain experimental data that could be used for development and validation of droplet trajectory and impingement computer programs. A collaborative effort was undertaken involving Wichita State University (WSU), NASA Glenn Research Center (GRC), and the FAA. Testing was conducted by WSU under an FAA grant in the NASA GRC Icing Research Tunnel. A very extensive data set was obtained, which was then processed and analyzed by WSU. A final report was published: "Experimental Study of Supercooled Large Droplet Impingement Effects," DOT/FAA/AR-03/59, Papadakis, M., et al., September 2003.

The testing used a dye tracer technique that had been used in the past for measuring local impingement efficiency on aircraft aerodynamic surfaces. In this technique, water containing a small amount of water-soluble dye is injected in the form of droplets into the air stream ahead of the body by means of spray nozzles. The surface of the body is covered with blotter material upon which the dyed water impinges and is absorbed. At the point of impact and droplet absorption, a permanent dye deposit (dye trace) is obtained. The impingement limits are obtained directly from the rearmost dye trace on the absorbent material.

It was necessary to update this technique in various ways so it would be appropriate for testing in SLD conditions. The 12-nozzle spray system was expanded to 16 nozzles to provide the required cloud uniformity for the SLD cases. Extensive updates were made to the hardware and software of the laser and charge-coupled device (CCD) reflectometers used for the reduction of the raw impingement data. New calibration curves were developed for the laser and CCD data reduction systems.

Impingement data were obtained for four two-dimensional airfoils and an airfoil with two different simulated ice shapes. Cloud conditions simulated included median volume diameters (MVDs) of 11, 21, 79, 137, and 168 microns. (The MVD is a convenient representative droplet size for the cloud.) The first two conditions are covered by the current regulations, but the last three are SLD conditions.

Droplet trajectory and impingement computations were also performed with the computer program LEWICE. As shown in Figure 9.3-10, a comparison of the experimental data to the computer results indicated that this program tended to overpredict droplet impingement in SLD conditions, especially in the tails of the impingement distribution. This suggests that modifications to LEWICE and probably other such programs will be necessary if they are to be sufficiently accurate to use for design and certification purposes.

9.3.7 AERODYNAMIC EFFECTS OF ICE FORMED IN SLD CONDITIONS

James Riley, FAA, William J. Hughes Technical Center

Aircraft certified for flight in icing conditions must be shown to be able to fly safely within the FAA's icing envelopes that were developed for supercooled clouds and are defined in terms of liquid water content, representative drop size, and temperature. Freezing drizzle and rain are not included in the envelopes, although aircraft may operate in these conditions near the ground. Some clouds contain freezing drizzle- or rain-size drops, referred to as supercooled large droplets (SLD). In recent years, several accidents (claiming more than 90 lives) and incidents have occurred in SLD conditions. At the request of the FAA, the Ice Protection Harmonization Working Group, consisting of representatives of airworthiness authorities, manufacturers, pilot groups, and research organizations in North America and Europe, is considering expanding certification requirements to encompass SLD conditions. In addition to the meteorological characterization of the conditions themselves, information is required on the nature of ice accretions that form in SLD conditions and on the aerodynamic effect on aircraft. This information would also provide an indication of what parts of the ice accretion must be predicted accurately by computational models currently under development. The FAA determined that there was a need for research to develop more information of this kind, and a collaborative effort was undertaken involving the FAA, the University of Illinois, and NASA GRC.

Ice accretion tests were conducted in the NASA GRC Icing Research Tunnel (IRT) using the 78-inch chord model shown in Figure 9.3-11, which is representative of a commuter turbopropeller wing. The objective of the test was to generate SLD ice accretions representative of in-flight accretions. Accretions were documented with photographs, tracings, and ice thickness measurements. Moldings made of three accretions have since been used to generate castings. An analysis of the documentation showed that the accretions had combinations of two or more key features: nodules, horns, and leading-edge glaze. Examination of the limited flight test data in SLD conditions showed similar features.

Aerodynamic performance tests were performed at the University of Illinois using simulated SLD ice accretion features. Testing was performed using an 18-inch chord model having the same airfoil section as the icing model. The key ice accretion features were geometrically scaled in size and simulated with a variety of simple materials. A simulated SLD accretion is shown in Figure 9.3-12.

In the first test phase, key features were tested in isolation. The test results for the nodule simulations indicated that a larger number of smaller nodules resulted in a more severe aerodynamic penalty than a smaller number of larger nodules. Also, nodules located closer to the leading edge also had a larger detrimental effect. Tests with the leading-edge glaze ice simulations showed that larger (i.e., thicker) and rougher ice caused larger aerodynamic degradation than smaller and smoother formations. The horn ice simulations had the largest impact on airfoil performance. Typical effects were observed where larger horns located farther aft caused the most severe penalties.

In the second test phase, combinations of these features were tested to simulate the measured accretions. For SLD accretion with horns, the results showed that the horn dominated the aerodynamics. However, the addition of the leading-edge glaze ice upstream of the horns reduced the effect of the horn, as shown in Figure 9.3-13. That is, the aerodynamic performance was improved with the addition of the leading-edge glaze ice over the horn-only case. The effect was more pronounced as the ratio of glaze ice thickness to horn height increased. The upper and lower surface nodules had very little impact on the aerodynamic performance since they were located downstream of the horns. This means that numerical predictions of SLD accretions with horns should accurately predict the size and location of the horns for proper representation of the aerodynamics.

9.3.8 AIRPORT PAVEMENT DESIGN WORKSHOPS

David Brill, FAA, William J. Hughes Technical Center

A series of technical workshops on FAA airport pavement design software was held by the Airport Technology R&D Branch in FY04. These full-day workshops were held at various locations in the United States and internationally. The purpose of the workshops was twofold:

1. To familiarize users with new developments in the FAA airport pavement design software, including LEDFAA 1.3, COMFAA, and FEDFAA 1.2 Beta—an evaluation version of the FAA's new FAARFIELD software that is planned for 2006.

2. To increase awareness of the FEDFAA 1.2 Beta program among potential users and to encourage participants and members of their organizations to download and evaluate the program. Beta testing is an essential part of the software development process.

During 2004, five workshops were held, with two workshops in the United States, and three internationally. The first U.S. workshop was held in Denver, Colorado, on June 22. The second workshop was held July 29 in Arlington (Crystal City), VA. The Arlington workshop was held in conjunction with the American Society of Civil Engineers International Air Transport Conference. The combined attendance at these two workshops was approximately 75. The workshop attendees represented a variety of organizations, including government, academia, and the private sector. They included consulting engineers, airport operators, civil engineering faculty, and state transportation officials as well as FAA regional and airport district office personnel. The international workshops were held in cooperation with the Japan Ministry of Transport in Tokyo, Japan, on May 26, with the South Korea Transport Ministry on June 1, and with the General Administration of Civil Aviation of China in Beijing, China, on September 27-29.

The FEDFAA 1.2 Beta program was demonstrated at the workshops. The principal difference between FAARFIELD and the current LEDFAA 1.3 standard is the incorporation of three-dimensional (3D) finite element (FE) analysis models in FAARFIELD. The use of 3D FE models will provide more accurate critical design stresses for rigid (concrete) pavement designs. The 3D FE method is used in the new software for both new rigid pavements and rigid pavement overlays. The FEDFAA 1.2 Beta program can be downloaded for evaluation at: http://www.airporttech.tc.faa.gov/naptf/download/index1.asp.

9.3.9 LEDFAA 1.3 SOFTWARE PROGRAM RELEASE

Gordon Hayhoe, FAA, William J. Hughes Technical Center

A new updated version of the FAA's LEDFAA airport pavement design software program was released on April 30, 2004. LEDFAA 1.3 incorporates many new features including:

- updated aircraft libraries containing the A380, A340-500/600, B-717, B-737-900, B-777-300ER, and other newer models;
- GA aircraft category, including many of the common GA, corporate, and regional jets;
- full metric unit capability;
- a change to full 32-bit programming for faster speed and better compatibility with current operating systems.

LEDFAA 1.3 incorporates numerous programming changes that, while not obvious to the user, represent significant technical advances. The failure models (mathematical models within the program that determine the pavement design thickness) have been updated to reflect the results of the flexible (asphalt) pavement full-scale traffic tests conducted at the NAPTF. Structural models have been revised to capture the interaction between all landing gears in a multiple-gear assembly (e.g., A380 or B-747), resulting in a more accurate strain analysis. LEDFAA 1.3 also uses LEAF, a layered elastic analysis program developed by the FAA, in lieu of the older JULEA program. LEAF has been designed to significantly increase the efficiency of layered elastic calculations, and it is fully documented and supportable.

LEDFAA 1.3 was incorporated into Advisory Circular (AC) 150/5320-6D, "Airport Pavement Design and Evaluation," under Change 3 (April 30, 2004). As a result of this regulatory change, LEDFAA 1.3 is now the required FAA pavement thickness design procedure whenever a triple dual-tandem aircraft (e.g., A380 or B-777) is in the aircraft traffic design mix. It is a valid alternate design procedure for all other traffic mixes covered by the AC. Previously (under cancelled AC 150/5320-16), LEDFAA was only allowed to be used for FAA standard designs when the airport was intended to serve the B-777 aircraft.

LEDFAA 1.3 can be downloaded at: http://www.airporttech.tc.faa.gov/pavement/26ledfaa.asp

9.3.10 FAA OPERATIONAL LOADS MONITORING PROGRAM

Thomas DeFiore and John Howford, FAA, William J. Hughes Technical Center

The Code of Federal Regulations, Aeronautics and Space, Airworthiness Standards (i.e., FARs) are replete with loads criteria much of which were generated prior to deregulation and in some cases prior to the design of wide body, regional jet and fly-by-wire civil aircraft. As an aid to keep FAR's current, the United States Federal Aviation Administration (FAA) has established a research program to acquire and maintain an extensive database of in-service operational usage data. These new data provide the FAA with the capability to continuously validate and update the flight and landing load airworthiness certification standards for transport airplanes based on actual measured usage.

Using these data, the FAA reviews fatigue and damage tolerance certification criteria and can prevent future surprises with special studies. Aircraft manufacturers use the data to: (1) update the fatigue and damage tolerance loads on the current fleet, and (2) provide accurate fatigue and damage tolerance loads for both repair of current airframes and design of new airframes. The airlines can benefit as well by using this data for improved maintenance scheduling and trade studies of operational procedures. The data can also provide insight into future service problems. Finally, the general public benefits from the additional level of safety attained from the knowledge of commercial airplane measured operational service usage.

The principal products of the FAA's operational loads monitoring research are published formal reports. The reports are separated into the following four categories: (1) large transport usage, (2) commuter and general aviation usage, (3) ground and landing loads usage and (4) loads analysis methods. Loads reports published in 2003 and 2004 are presented with corresponding web address on the following page. Reports published prior to 2003 can be obtained from the following web address http://aar400.tc.faa.gov/Programs/AgingAircraft/airbornedata/index.htm (See Figures 9.3-14 and 9.3-15)

9.3.11 ACTIVE AEROELASTIC WING PARAMETER IDENTIFIED FLIGHTS COMPLETE

Peter M. Flick, USAF AFRL/VASA

Active aeroelastic wing (AAW) technology can benefit future aircraft designs including unmanned air vehicles, advanced transports, and advanced fighter concepts such as future strike. Design studies have shown that the technology can decrease aircraft weight 5% - 20%, depending on the mission. (See Figure 9.3-15A)

When applied to fighters, the AAW design approach enhances maneuverability by increasing wing control power and improves roll rate at higher dynamic pressures. AAW wings provide large amounts of roll power using conventional control surfaces while controlling air loads and reducing overall aircraft drag. In high altitude, long endurance aircraft, AAW technology can be used to alleviate gust loads and to manage wing warping to increase aerodynamic efficiency.

The Air Vehicles Directorate, in cooperation with the National Aeronautics and Space Administration Dryden Flight Research Centers, and Boeing Phantom Works, successfully completed the first phase of flight research for the AAW. The test platforms was an F/A-18A modified with a split leading-edge flap drive system, a modified flight control computer, and a flexible wing with thinner skins that allowed the outer wing panels to twist up to 5°.

More than 1,600 sensors on the F/A-18A measured parameters such as control surface positions, wing deformation, structural strain frequency response, and accelerations. Engineers will use this parameter identification data to develop new AAW flight control laws and to design guidance for future AAW applications.

AAW is a multidisciplinary, synergistic technology that integrates air vehicle aerodynamics, active controls, and structures together to maximize air vehicle performance.

The concept turns wing aeroelastic flexibility into a net benefit through the use of multiple leading and trailing edge control surfaces activated by a digital flight control system. AAW techniques use air stream energy to achieve this desirable wing twist with very little control surface motion. The wing then creates the needed control forces with outstanding effectiveness. When AAW technology is applied correctly, the wing will twist less (although in an opposite direction) than a conventional wing twists during maneuvering. AAW technology will enable future designers to consider higher aspect ratio and thinner wings with less structural weight than current wing designs.

9.3.12 CHARACTERIZING AEROACOUSTIC LOADS

Douglas Henderson, USAF AFRL/VASM

The Air Vehicles Directorate developed an accessible and extensive database of dynamic acoustic loads that affect aircraft structure and subsystems. This database will allow engineers to produce aircraft with longer structural life, lower maintenance costs, and increased readiness. (See Figure 9.3-15B)

As part of the Small Business Innovation Research program, the directorate worked with UNISTRY Associates, Inc. to develop a new engineering technique that predicts the loads placed on an aircraft during flight by fluctuations in high-frequency sound pressure. The technique takes data from a variety of sources and compiles it onto one curve. This data makes it easier for engineers to compare and use the information to make better design-performance predictions.

The directorate used this new technique to generate a database that demonstrates how sound pressure varies with changes in frequency for various structural configurations, airflow conditions, and data-processing methods. Data on weapons bays and noise generated on pulse-detonated engines make the database particularly valuable. Currently, the database is available to scientists on a CD-ROM; however, the directorate has developed a commercialization plan to place the database on the Internet.

During flight, an aircraft is subjected to strong pressure fluctuations caused by airflow and acoustic resonance. The resulting acoustic loads have high sound pressure levels at high frequencies that can damage weapons, crack nearby surfaces and components, and radiate intense noise. With the directorate-developed database, engineers can assess the effects of this phenomenon and use the knowledge to design aircraft with increased structural life, lower maintenance costs, and increased readiness.

9.4. FATIGUE AND FRACTURE

9.4.1 MATERIAL SUBSTITUTION FOR AGING AIRCRAFT

Andrew Hinkle, S&K Technologies

A significant number of the aircraft in the current military fleet have been in service for over 35 years, and many of these aircraft will continue to be used for another 25 years, because they are operationally effective. The duration of service for these aircraft is well beyond the initial design envelope, and subsequently the accrual of fatigue and corrosion damage has dramatically increased the cost of fleet management. The material substitution paradigm of replacing a damaged component fabricated from a legacy alloy with a component fabricated from a modern alloy is an important element of managing the performance and durability of the USAF aging aircraft.

A number of newer commercially available high strength 7xxx alloys were identified to replace incumbent 7xxx-T6 alloys. Generally, these alloys were combined with a mild overaging (T7x tempers) to reduce stress corrosion cracking. In past years the effort was to characterize the mechanical and corrosion properties of candidate alloys for materials substitution. Now the program has shifted to characterize the potential for fatigue improvements in these alloys and the corrosion-fatigue interaction of the mild-overaged T7 tempers.

Various aging aircraft fleets were examined for components that are currently being replaced on a regular basis particularly components subject to fatigue and corrosion. Study of these components identified a number of 7075-T6 forging that were candidates for material substitution using alloy 7085-T76. This potential replacement alloy has similar static strength, good corrosion resistance and open-hole cyclic fatigue data projects fatigue life improvements of approximately 3 times for the components. A second phase of the program is now underway to demonstrate the fatigue improvements under realistic spectrum load and ultimately on a component. If the results of these further tests prove a long fatigue life, fabricating these components from the replacement alloy will have significant cost avoidance for the USAF.

Another material substitution program compared the corrosion-fatigue life of the legacy alloys with the replacement alloys. Constant amplitude axial fatigue tests were performed in a water vapor saturated N_2 environment, according to ASTM standard E-466. Fatigue specimens were pre-corroded on one of the two L-T surfaces. The magnitude of the fatigue life reduction varies with alloy temper and corrosion type, and the variation is more evident for the lower stress level of σ_{max} = 150 MPa. (Figure 9.4-1) Compared to the decade-drop in fatigue life of corroded specimens relative to the pristine baseline, the differences in pre-corrosion effects between the T6 and T7 tempers are small. In each corrosion state, the T7 temper of 7055 exhibits a slightly longer fatigue life range than 7075-T6511, especially at the low stress. From the materials substitution perspective, the modern alloy in a stress corrosion cracking resistant temper, 7055-T74511, demonstrate similar corrosion-fatigue interaction resistance.

ACKNOWLEDGEMENT

This work was sponsored by the Aeronautical Systems Center, Agile Combat Support Systems Wing, Aging Aircraft Systems Squadron, WPAFB, OH, under Air Force Contract F09650-03-D-0001 administered by S&K Technologies for Major Timberlyn Harrington, Chief, Air Vehicles Branch, ASC/AAAV.

REFERENCES

1) Hinkle, A. J., M. Garratt and L. Yocum, "Improving Airworthiness through Material Substitution", *Proceedings of Aging Aircraft 2005*, Palm Springs, CA, January 2005.
2) Li, D., J. Burns, R. Bush, M. Garratt, A. Hinkle, T. Mills, C. Marks, J. Moran, J. Scully and R. Gangloff, "Characterization of Corrosion-Fatigue Interaction for Aluminum Alloy Substitution", *Proceedings of Aging Aircraft 2005*, Palm Springs, CA, January 2005.

9.4.2 STRUCTURAL DAMAGE MANAGEMENT TOOL (SDMT)

Kevin Boyd and David Newman, S&K Technologies and Alex Litvinov, LexTech

The Structural Damage Management Tool (SDMT) is a software application designed to assist ASIP engineers in determining the effect of environmental degradation on structural life. SDMT integrates an environmental damage prediction model with the US Air Force fatigue crack growth code, AFGROW (ref 1).

The damage prediction model works by estimating a corrosion rate (i.e., thickness loss per year) based on material type, product form and basing location. The estimated corrosion rate is applied to a structural integrity model over the duration of the aircraft's deployment and an "environmentally affected" service life can be estimated. SDMT users are able to run a fracture analysis both with, and without the effect of environmental damage; allowing for a direct assessment of the effects of corrosion and basing strategy on the maintenance intervals of USAF aircraft (Figure 9.4-3).

In FY04, the SDMT graphical user interface (GUI) was significantly enhanced to increase usability. Figure 9.4-2 shows the new SDMT GUI which is responsible for all user input and output (previous versions relied on MS Excel for graphing). The GUI has also been modularized to allow users to have more control over the level of analysis. For example, users without access to NDI images can construct an AFGROW style structural integrity model and still use of SDMT's corrosion prediction and deployment plan functionality.

The Weibull analysis portion of SDMT was updated in FY04 to increase performance and accuracy. The updated Weibull implementation was verified against the commercial Weibull analysis package Weibull++ from Reliasoft (ref 2). Plans for SDMT in FY05 include an enhanced materials database, additional structural integrity solutions and a risk assessment capability.

REFERENCES

1) AFRL/VASM, AFGROW : http://www.siresearch.info

2) Reliasoft : http://www.reliasoft.com

9.4.3 RESONANT FREQUENCIES OF VIBRATING PANELS WITH CRACKS

Mohan M. Ratwani, R-Tec and David Banaszak, USAF AFRL

In-service experience and test results have shown that cracks often initiate in structures subjected to vibratory loads. The resonant frequencies of panels gradually decrease as the cracks initiate and propagate. It is important to know the resonant frequencies (especially the fundamental frequencies) of panels during crack initiation and propagation in order to make life predictions of panels. Fatigue tests under vibratory loads under shaker excitation, using specimen configuration shown in Figure 9.4-4a, are generally carried out at resonant frequencies to obtain fatigue data. Cracks initiate and propagate at locations shown in Figure 9.4-4b, and the resonant frequencies of panels decrease as cracks propagate.

The test data have shown (References 1) that cracks do not initiate at the holes but away from the holes close to the washer as shown in Figure 9.4-4b. The vibratory motion of the plate and initiation of cracks indicates that the plate vibrates with fixity along y-axis (Figure 9.4-4b) like a cantilever beam. For analysis, the vibratory motion of the plate may be considered as bending of a cantilever beam. Mathematical techniques to determine resonant frequencies of panels with cracks are developed in Reference 2. The results of analytical predictions were compared with the test database, generated by the Wright-Patterson Air Force Base (Reference 1), on aluminum specimens subjected to shaker excitation at resonant frequencies. Predicted and observed resonant frequencies at various crack lengths in 85x180 mm panels with 3.2mm thickness and in 170x360 panels with 3.2- mm thickness are shown in Figures 9.4-5, and 9.4-6, respectively. A good correlation between predicted and test resonant frequencies is seen.

REFERENCES

1) Banaszak D and Dale G. A, "Two-Level Factorial Experiment for Crack Length Measurements of 2024-T3 Aluminum Plates Using Temperature Sensitive Paint and Electrodynamics Shakers", Section on Physical and Engineering Sciences Proceeding, American Statistical Association, August 1999.

2) Ratwani M. M, "Development of Validated Crack Measurement System for Vibrating Structures", Report Number AFRL-VA-TR-2002-3005, ADA 399661, January 2002.

9.4.4 FATIGUE CRACK GROWTH RATE EFFECTS ON SINGLE- AND MULTI-LAYERED COLD-EXPANDED AIRCRAFT ALUMINUM

Molly R. Brown and Scott a Fawaz, U.S. Air Force Academy

Through analysis and experimental procedures, it has been determined that cold-working is helpful in extending fatigue life of holes. From the expansion process, these holes are subjected to compressive residual stresses followed by a ring of residual tensile stresses and finally material that is unaffected by the process. Since a ring of compressive residual stresses exists, on a micro-structural level, this material has a more densely packed region. Due to cold-working, fatigue crack nucleation is more difficult since a weak region around the hole is less likely to exist. See Figure 9.4-7. The fatigue resistance has been increased by three times through findings from Fatigue Technology Inc. (FTI), the company that performed cold-expansion for this test.

Background
Structural maintenance personnel first acknowledged this as a problem, and approached CAStLE for assistance. On the aircraft in question, cold-working was done through multiple layers of material. Typically in analysis, it is assumed the process is done one layer at a time, however, that is not the case on the wing skin of the subject aircraft. The outer layer of material is 2024-T3, the second layer is 7075-T6, and the last layer is quenched and tempered 4340 steel. The thickness of the aluminum plates were 0.25 inches while the steel was 0.125 inches thick. The steel is present to reinforce the hole.

As these cold-worked holes begin to age, the question of crack growth rate arises. Once the crack nucleates, how its fatigue crack growth is effected by the change in micro-structure is unknown. Since this process is widely used in weapon systems all through the Air Force, the answer to this problem would be exceptionally useful.

In order to find the crack growth rate, monitoring intermittently was essential. While ideal, using electric potential drop was difficult to use with plates 0.25 inches and over. While doing optical readings at about every 8,000 cycles, a lot of essential crack growth data could be lost. In order to obtain crack growth rates post-mortem, a marker load spectrum was used so that darker bands of crack growth (denoting a higher stress level) could be measured using a scanning electron microscope (SEM) to get more complete crack growth data.

Process
Fatigue crack growth tests were performed on a servo-hydraulic fatigue test frame. The load spectrum used can be seen in Figure 9.4-8. After testing, fractography will be done to create crack growth rate information.

Results
The number of cycles to failure and the maximum stress levels can be seen in Table 9.4-1.
This project shall be completed by the summer of 2005.

9.4.5 MODELING THE FATIGUE PROCESS
Prof. David W. Hoeppner, University of Utah

Extensive work is underway at the University of Utah on modeling the fatigue process from nucleation to instability. A new in situ fatigue machine to attach to a scanning electron microscope has been developed and is in operation. This is the eighth major design iteration of the in situ machines. The effect of microstructure and corrosion exposure on short crack propagation and transition from nucleation to short crack propagation is under study in the effort. This is also related to extensive mechanics based modeling that is underway in the University of Utah programs related to crack nucleation and short crack growth.

9.4.6 EXTRACTION PROCEDURES TO COMPUTE THE T-STRESS FOR 2D AND 3D CRACK PROBLEMS
Ricardo L. Actis, Engineering Software Research & Development, Inc.

The direction of crack growth and the stability of the crack path are influenced by the second term in the asymptotic expansion of the elasticity solution in the neighborhood of a crack tip, called the T-stress. Cracks have been observed to turn sharply in the presence of T-stress. Reliable estimation of the T-stress is therefore important for fracture analysis of complex structures.

The combination of the p-version of the finite element method with a superconvergent extraction procedure based on a path independent integral provides for an accurate and reliable computation of the T-stress for cracks in two-

and three-dimensions. The procedure has been implemented in the finite element analysis program StressCheck[1]. A brief description of the implementation and an example are presented in the following.
The implementation of the T-stress extraction utilizes a path-independent integral based on the Betti-Rayleigh reciprocal theorem. In two-dimensions the T-stress can be computed from the following contour integral:

$$T = E\oint_{\Gamma}\left(\sigma_{ij}^{*}u_i^{FE} - \sigma_{ij}^{FE}u_i^{*}\right)n_j dS$$

where E is the effective modulus of elasticity which depends on whether the analysis is plane-stress or plane-strain, σ_{ij}^{*} are the extraction stress functions in the local Cartesian coordinate system centered on the crack tip, u_j^{*} are the extraction displacement functions in the same coordinate system, $\sigma_{ij}^{FE}, u_j^{FE}$ are the stresses and displacements on Γ obtained from the finite element solution, and n_j are the components of the outward normal to the differential arc length dS. For additional details, see Ref 1. In three-dimensions, the T-stress is computed using the same path-independent integral over a circular path around the crack front at an arbitrary point P. A cutting plane normal to the tangent to the crack edge at is determined and the global components of the stresses and displacements along a circular path contained in the cutting plane are computed from the finite element solution. These stresses and displacements are projected onto the cutting plane and integrated with the extraction function to compute the T-stress. The effective modulus is adjusted based on the ratio of the in-plane normal stresses and the transverse stress.

In Planar and 3D Elasticity, the extraction of the T-stress is provided once a sequence of finite element solutions of increasing polynomial order is available. The user simply enters the radius of the circle for the integration path and selects the node located at the crack tip in 2D or the edge of the crack front in 3D and the program provides the values of K1, K2 and T-stress as shown for the double cantilever beam (DCB) problem in Figure 9.4-9.

The DCB specimen has large positive T-stress that may cause crack path instability under pure mode I loading. A DCB configuration with a/w=0.5 and h/w=0.2 is considered. The 44-element mesh and boundary conditions are shown in Figure 9.4-9a. Two layers of refinement in geometric progression towards the crack tip were used in this case. The following properties were considered for the analysis: E=29x10^6, ν=0.295, plane-strain. The load was applied as a sinusoidal traction distribution along half of each hole with a resultant value P=100. The following values were used for the dimensions: a=1.0, w=2.0, h=0.4, thickness=0.5.

The 3D-prooblem was solved with symmetry constraint imposed on element faces with normal in the direction of the positive or negative z-axis in order to simulate plane-strain conditions. The problem was solved by p-extension and the values of K1, K2 and the T-stress as a function of the number of degrees of freedom (DOF) are shown in Figure 9.4-9b. For p=8 (13388 DOF), K1=3475.6 and T=5784, from where B=2.950 ($B = K_1\sqrt{\pi a}/T$), which is very close to the value B=2.951 reported in Ref [1]. Figure 9.4-9c shows the T-stress at seven equally spaced points along the crack front. Rapid convergence of K_1 and T to their estimated limit values is clearly visible in the table of Figure 9.4-9b.

REFERENCE

1) Chuin-Shan Chen, Roland Krause, Richard G. Pettit, Leslie Banks-Sills, and Anthony R. Ingraffea, *Numerical Assessment of T-stress Computation using a p-version Finite Element Method*, International Journal of Fracture, 107: 177-199, 2001.

9.4.7 FATIGUE EFFECT OF POLISHING 2024-T3 CLAD SHEET

Mark Ofsthun, Boeing, Wichita

2024-T3 clad sheet has been used on exterior skins for several decades. The high fatigue quality makes 2024 a good choice for fatigue designed aluminum pressurized structure. The cladding is a pure aluminum coating applied during the rolling process is used as a corrosion barrier. Polished clad also makes for a good decorative appearance. However, the majority of the airlines prefer a painted surface for their own particular aircraft appearance. The polishing process is a costly and time-consuming operation. The question is whether or not the surfaces benefit

---

[1] StressCheck® is a registered mark of Engineering Software Research & Development, Inc. (www.esrd.com)

structurally from the polishing. If the polishing adds compression residual stresses, there may be some fatigue benefit for polishing clad aluminum.

In order to answer this question, a fatigue test program was conducted using .040 2024-T3 clad sheet. A sheet that was sent to the mill for polishing was cut into two pieces, half the piece was polished the other set aside. Fatigue coupons were cut from each piece and fatigue tested to determine if there was any difference in polished 2024-T3 clad sheet relative to an unpolished 2024-T3 clad sheet.

In this study, two types of specimens were tested, the first was a un-notched axial fatigue coupon. The other specimen was a flexure specimen, which is a bending specimen. Figure 9.4-10 provides a sketch of the test specimen. The fatigue test results, Figure 9.4-11, indicated that there was no difference in fatigue performance of un-polished and polished 2024-T3 clad sheet. On the axial fatigue specimens, a slight (3%) increase in the average fatigue life of the polished was observed. In flexure fatigue a slight (3%) decrease in the average fatigue life of the polished was observed. These slight differences can be attributed to normal test scatter. On airplanes that are to be painted, not polishing the aluminum sheet can reduce costs and not degrade the fatigue quality.

9.4.8 LASER DEPOSITED TITANIUM

Mark Ofsthun, Boeing, Wichita

Building complex parts from titanium often require large and expensive blocks of material. Typically, these parts are extracted from forgings. Machining these parts is difficult and the forging process inherently has residual stresses and during the machining of these parts, the parts often relax causing distortion and if severe enough, rejection of the parts themselves. A unique manufacturing method developed by the Aeromet Company is taking a titanium powder, and depositing it on a base plate of titanium using a CO_2 laser beam. A schematic of the laser deposited process is shown in Figure 9.4-12. The parts are Hot Isostatic Pressed (HIP'd) to remove potential voids. The result is a part that is near net shape and residual stress free. Thus reducing machining time and cost as well as significantly reducing warpage potential. Figure 9.4-13 shows a sample laser deposited part.

As part of the investigation of the potential use of laser deposited titanium, a small fatigue study was conducted. The fatigue test specimen was axial loaded two ended lugs. The lugs were tested in the direction of the nozzle (X) and in the direction of the build-up (Z). After depositing and HIP'ing the parts were solution treated and aged. The reason for the additional solution treating and aging was to improve the static properties. Extensive static testing indicated that the mill annealed laser deposited properties were slightly lower than wrought products. The fatigue study was a minimum effort. Additionally, all test coupons were shot peened. Results shown in Figure 9.4-14 indicated that the solution treated and aged laser deposited material was quite competitive with mill annealed plate. Surprisingly, the X direction was the weaker fatigue properties. The two lots tested in the Z direction both performed better than mill annealed plate. The X direction were significantly lower than the Z direction which is exactly the opposite of the static properties.

With minimum warpage, reduce machining time and the good fatigue properties, laser deposited titanium may be a key process in making cost competitive complex titanium parts. Other potential benefits include the repair of large titanium parts.

9.4.9 EFFECTS ON FATIGUE PROPERTIES OF PAINT STRIPPING OF ALUMINUM SHEET WITH NANOCOMPOSITE MEDIA

Mark Ofsthun, Boeing, Wichita

Removal of paint from commercial airplanes is not a simple matter. Chemical strippers have environmental concerns. Rough media can damage surfaces thus degrading fatigue properties. Plastic Media Blasting for example has been found to cause some degree of fatigue damage when used 3-5 times. Wheat starch, however has been proven not to degrade the fatigue properties at all. However, wheat starch is not terribly effective at removing paint from aluminum surfaces.

United Technology has recently developed a media composed of Nanocomposite. This material is composed of several materials that has numerous advantages that makes it a good media for paint stripping. Some of these advantages include: not susceptible to water or humidity, less dust, fast stripping rate and causes less damage to the aluminum substrate than most media. Figure 9.4-15 is a photograph of nanocomposite media.

In order to prove its acceptability to commercial aircraft, an extensive test program was undertaken. Included in the review were: surface roughness, clad penetration, residual stresses, paint adhesion and most importantly, fatigue. The nanocomposite paint stripping media passed all the tests performed. The fatigue results included the fist media developed referred to as Magic 1™. During the development of the nanocomposite media, United developed two additional versions called Magic 2™ and Magic 3™. Magic 2™ was developed for improved rate stripping and Magic 3™ was developed for removing cured fay seal.

The fatigue testing composed of un-notched basic fatigue coupons. The coupons were painted and stripped four times and compared to specimens that were painted with no subsequent stripping. Figure 9.4-16 provides the fatigue test results of Magic 1™. Figure 9.4-17 provides the fatigue test results of Magic 2™ and Magic 3™. From these figures it can be easily determined that nanocomposite paint stripping does not adversely affect the fatigue performance of clad aluminum sheet.

9.4.10 EFFECTS ON FATIGUE PROPERTIES OF LASER DRILL PERFORATED TITANIUM SHEET

Mark Ofsthun, Boeing, Wichita

Acoustic tests have indicated that drilling small holes with lasers can help reduce noise in titanium sheet. However, laser cutting leaves a heat affected zone which is known to drastically reduce fatigue quality. In the evaluation of laser drilling, a small fatigue evaluation was conducted in order to assess the potential impact on fatigue properties of titanium sheet (Ti 6Al-4V) with laser perforated sheet.

The laser perforation was done by Aerospace Systems & Technologies Ltd. Panels were perforated with hole diameter of .004 inch diameter in .032 gage titanium (5% POA – Percent of Area) and .002 inch diameter in .050 gage titanium (.3% POA). A sketch of the perforated panels is provided in Figure 9.4-18. The results were tested against drilled and deburred open holes. The laser perforated specimens were tested with and without chemical etching to determine if etching could improve the fatigue performance. A sketch of the test coupons are provided in Figure 9.4-19.

Test results are shown in Figure 9.4-20 where it can be seen than for the .3 POA, the laser perforated performed better than an open hole coupon. Whereas 5POA was worse than an open hole. As the tests were limited, it was not establish if the effect was due solely to the POA or if the thickness lead to increased heat affected zone in the thicker titanium. Additional studies will be required to establish exact causes, be it is likely the POA is the largest driver to the fatigue quality. The results indicate that the approximately 5000 laser drilled holes were roughly equivalent to a single drilled and deburred open hole (.25 inch diameter). When the POA was .3%, the performance was about 10% better in fatigue strength (KSI) than the baseline open hole. At 5% POA, there was a 13% reduction in fatigue strength (KSI) than the baseline open hole. Chemical etching had little effect on the fatigue strength of laser drilled holes in titanium.

9.4.11 FATIGUE EVALUATION OF CNC STYLIST FORMING

Mark Ofsthun, Boeing, Wichita

Making complex shaped parts can be done a number of ways. Machining the parts out of thick block or plates is one method. This method involves intensive machining and excessive waste of materials. Forming the parts out of sheet metal can be quite cost effective. Stretching or bending the sheet metal can accomplish the forming process. However, stretch forming can lead to structural concerns as micro cracking can occur. As a result, stretch forming is typically done in the O condition or W condition and is limited to a maximum thinning of 5%. DJ Engineering in Augusta Kansas has developed a new, patented, method of forming complex parts referred to as CNC Stylist Forming. This process is a based upon using a special forming tool with a solid backing plate and slowly by pressure, form the part. Figure 9.4-21 shows a sample tool and formed part using the patented forming process.

This CNC Stylist Forming process is capable of stretch forming materials (in the O or W Condition) up to 30% level of thinning with little risk of micro cracking. Naturally, there is a concern for the effect on the material properties for such a significant amount of strain. In order to determine the effect of the CNC Stylist forming on 2024 bare sheet (.16 gage) and 7075 bare sheet (.20 gage), three pans like that shown in Figure 9.4-21 of each material were formed. For each material, the pans were formed to 5%, 15% and 30% thinning. The pans were designed to form to a uniform thickness along the slope such that no machining of the surfaces would be required to establish the basic static and fatigue properties of the materials when CNC Stylist formed. Included in the evaluation was unformed material from the same lot for comparison. After forming, the pans were aged to 2024-T42 and 7075-T73 respectively. The specimens utilized in the evaluation were static tension coupons and fatigue notched axial coupons (Kt = 1.5).

Results of the static tests are shown in Figure 9.4-22. From this plot it can be seen that the NC Stylist Forming had some effect on the static properties on both alloys. The ultimate strength was the least affected and the modulus was the most effective and yield was in between in terms of affected properties. It should be pointed out that the amount of degradation for the level of forming was surprisingly minimal.

Figure 9.4-23 contains a similar plot for the axial fatigue testing. The 2024-T42 was barely affected by the CNC Stylist forming. The 12 percent reduction in fatigue life was surprisingly little for the amount of forming. The fatigue results paralleled the drop in static elongation properties. The effect on the 7075 material was much more drastic however. 7075 sheet fatigue life dropped in half from the 5% CNC Stylist Forming. Additional forming resulted in additional decreases in fatigue performance. The slope of the 7075 curve between 5 and 30% in Figure 9.4-23 was similar to the static Fty curve in Figure 9.4-22.

The patented CNC Stylist Forming process is an innovative way of forming complex shaped parts. Understanding its capabilities and mechanical properties affords many potential applications to improves manufacturing capabilities while maintaining high levels of structural integrity.

9.4.12 AFRL Technology Aids Aircraft Manufacturing Industry

Jim A. Harter, USAF AFRL/VASM

The Cessna Aircraft Company used AFRL-developed software to certify the damage tolerance of the new Cessna Citation Jet 3 (CJ3) aircraft. Cessna used Air Force Growth (AFGROW) crack life prediction software to verify the CJ3 met all requirements to earn Federal Aviation Administration certification. The CJ3 is the first aircraft to receive Cessna's certification using AFGROW, and the company plans to use this software program for all of its future projects.

AFRL developed AFGROW to evaluate the reliability and risk of current Air Force platforms. AFGROW effectively predicts structural crack growth over time. It helps engineers determine service life for existing aircraft structures and creates preventative maintenance schedules. Additionally, engineers can use AFGROW during the initial design process to help build structures that are more resistant to structural cracking.

9.4.13 AFGROW

Jim A. Harter, USAF AFRL/VASM

AFGROW is one of the fastest and most efficient structural crack life prediction tools and is available free of charge online. Many major aerospace companies, such as Cessna and Boeing, use AFGROW, but scientists can apply AFGROW to any structure that experiences fatigue cracking.

From the Wright Brothers era through the late 1960s, engineers used "safe life" design, a philosophy that assumed quality control would detect all manufacturing flaws before an aircraft could enter service. Adhering to this perspective, engineers estimated the number of operating hours it would take for structural cracks to form and then based aircraft service life expectancy on these estimates.

This approach changed in 1969 as a result of a prominent aircraft accident at Nellis Air Force Base, Nevada. On December 22 of that year, an F-111A Aardvark with just over 100 flight hours crashed when its left wing separated during a pull-up maneuver. This incident was of particular concern to accident investigators because they determined quality control personnel had failed to detect the crack prior to aircraft delivery. In addition, they ascertained it had taken a relatively short time for the crack to cause wing separation.

In response to this accident, the Air Force abandoned the safe life approach for a damage tolerance design philosophy, which assumes the presence of cracks too small for postmanufacture quality assurance inspectors to detect. Consequently, engineers now base aircraft inspection schedules on how long they estimate it will take preexistent cracks to cause component failure and possible aircraft loss.

At first, engineers assumed a loglinear relationship existed between crack growth rate and the crack driving parameter (i.e., stress intensity factor). However, the crack growth rate/stress intensity relationship is not necessarily log-linear. For example, depending on the structural material in use, there may be a point in a crack's life when it undergoes a sudden burst of growth that leads to rapid fracture. The only accurate way to predict when such variations will occur is to calculate and plot crack growth at each point in an aircraft's operational cycle, a process that requires millions of calculations, some of which took earlier, less powerful computers months to complete.

Today, better computational resources and Air Force Research Laboratory (AFRL) research have exponentially advanced the science of crack growth prediction. The laboratory has led the way for over a decade with its Air Force Growth (AFGROW) crack life prediction software. Essentially, AFGROW lets users assume a structure starts out with a crack length of their choice and reveals how the surrounding structure and stresses will affect the crack's growth. It calculates crack growth point by point in the aircraft's structural life, frequently doing so in a matter of seconds. AFGROW is one of the fastest and most efficient crack life prediction tools available today. Although AFGROW is a tool employed largely for aerospace applications, engineers can apply it to any type of structure that experiences fatigue cracking.

AFGROW is a user-friendly computer program that interfaces with Microsoft® Windows®, allowing users to cut and paste information between the Windows clipboard and applications such as Microsoft Excel. This capability enables users to compare experimental data points—charted in Excel, for example—to AFGROW's predictions. This effective integration with existing Windows-based programs saves time and money by eliminating the need for AFGROW developers to create new companion programs.

Leveraging this concept, AFRL engineers developed a new plug-in geometry interface that allows AFGROW to interface with StressCheck®, an industry-wide structural analysis program capable of calculating stress intensity (K) factors in a Windows environment. Before this achievement, AFGROW users had to make assumptions about how a structure's three-dimensional quality would affect the intensity of the structural stresses that lead to crack formation. The new interface, however, makes it possible for Stress-Check to feed AFGROW this information throughout the crack life prediction process, eliminating assumptions and further improving AFGROW's accuracy.

Scientists successfully demonstrated the new interface's effectiveness by calculating crack formation over time from the internal edge of any userdefined notch (i.e., rounded indentation on the outside edge of a surface). Currently, scientists are further expanding this demonstrated capability to determine stress crack formation for more complex structures. Eventually, they hope to enable AFGROW to make accurate predictions for hole shapes more complex than the simple cylinder-shaped holes it can now model. For example, they would like to evaluate cracks near countersunk holes.

Found in all types of aircraft, holes of this shape facilitate the countersinking of screws into an aircraft's skin to keep the surface smooth. Because these holes have angular sides, cracks can form at any angle and at various depths in the aircraft skin. Associated crack prediction calculations are very difficult because there are an infinite number of possibilities related to the crack's placement and direction of growth. However, the enhanced AFGROW capability could manage this complexity by using the external K-solving code to return stress intensity values for the given cracking configuration.

AFGROW developers also hope to use the new geometry interface to enable the program to analyze crack growth from several holes simultaneously. Presently, AFGROW users can study one or two cracks at one hole only; AFGROW takes into account how the crack(s) at a given hole are influenced by other holes in the geometry or template, but it cannot currently show how multiple cracks growing at the same time can affect one another.

The AFGROW program and supporting information are available to interested parties online and free of charge through the structural integrity research Web site, www.siresearch.info. Once users complete this site's free registration process, they will have access to forums that address problems and approaches for solving them.

Through these participative, virtual discussion areas, users can ask questions, provide input regarding potential future updates and enhancements to AFGROW, and enter comments pertaining to other AFRL-developed analysis tools. Site members can also register to receive e-mail notification of AFGROW updates, including upcoming training dates for the several classes AFGROW developers conduct each year. Additionally, site members can link to an AFGROW-specific site containing downloads for the AFGROW user manual and related documentation, as well as past and present versions of AFGROW program code. Other available downloads include a manual designed to help users use AFGROW with other Windows programs and a bug search that lists known program bugs, describes corrective actions, and provides the opportunity to report bugs not currently identified.

Current AFGROW Capabilities of Version 4.009e.12 (LEFM Based) are:

Stress Intensity Solutions:

Twenty-Two Classic Models	Tension, Bending and Bearing Cases
User-Defined Models	Advanced Models (Two through cracks, Through cracks with hold effects, Unsymmetric corner cracks at holes)
Weight Function Solutions	Offset Holes and Cracks
Composites Bonded Repair Capability	Oblique Cracks
User-Defined Solutions	

Loading Spectra:

FALSTAFF	Twist
User-Defined	Exceedance Plotting

Retardation Models:

No Retardation	Closure Model	FASTRAN Model
Modified Willenborg Model	Wheeler Model	Hsu Model

Crack Growth Rate Models:

Walker Equation	NASGRO Equation and Material Database
Harter T-Method	Table Look-Up
Forman Equation	Interactive Growth Rate Plotting and Data Overlay Capability
Environmental Growth Rate Capability	

Input/Output:

Graphical User Interface (GUI)	Crack Growth Animation	Beta Table Output (COM)
Real Time Crack Growth Plotting Capability	Component Object Model (COM) Capability	XML I/O
Text Based Input and Output	Ability to Restart at a Given Point in a Spectrum (COM)	

Other Tools:

Crack Initiation	Cycle Counting
View Plots in Excel	

Recent activities related to AFGROW are described in Figures 9.4-24 through 9.4-27.

9.4.14 FRETTING FATIGUE

Prof. David W. Hoeppner, University of Utah

Significant amount of work in the area of fretting fatigue has been performed at the University of Utah from 2003-2004.

The purpose of this study was to understand the fretting fatigue mechanism by characterization of the fretting damage transition to cracking in 7075-T6 aluminum alloy. Determination of the influence of fretting on fatigue life and identification of the damage threshold for 7075-T6 aluminum alloy were also performed. An additional goal of this study was to identify causes and mechanisms related to fretting fatigue by fractographic inspection of surfaces using scanning electron (SEM) and confocal microscopy. A fretting map was created for 7075-T6 aluminum alloy fatigue specimens fretted on 7075-T6 aluminum alloy pads by varying displacement amplitude and normal force.

Results indicated that a fretting fatigue damage threshold exists in this material that varies with respect to applied axial and normal stresses and the thickness of the material. The exposure to fretting while under cyclic loading substantially reduces life of the specimens compared to fatigue.

The fretting damage transition to cracking was tracked through interrupted tests. SEM and confocal images of the specimens revealed that fretting plays a role in crack nucleation. Another observation was that pit depth was not the most critical factor in the crack nucleation due to the fretting. Many other factors play important roles in crack formation from fretting damage zones. The presence of subsurface constituent particles beneath the fretting damage also assisted to crack formation and ultimately to fracture. Fretting degradation depends on the axial stress, normal stress, microstructure and thickness of the material. A larger grain size is more susceptible to increased fretting degradation and a smaller grain size has more resistance to fretting.

Sachin Shinde completed his Ph.D. research in spring-2005. Dr. Hoeppner and Mr. Shinde attended the Fourth International Symposium on Fretting Fatigue held at Lyon, France in May, 2004.

9.4.15 LOAD HISTORY EFFECTS RESULTING FROM COMPRESSION PRECRACKING

Mark A. James, National Institute of Aerospace; Scott C. Forth, NASA Langley Research Center and John A. Newman, U.S. Army Research Laboratory

Compression precracking (CPC) has seen renewed interest lately as a possible alternative procedure for generating fatigue crack growth threshold data with minimal load history effects [1,2]. Using the CPC method, specimens are precracked with both maximum and minimum loads compressive (negative). Compressive yielding occurs at the crack-starter notch, resulting in a local tensile residual stress field through which the fatigue crack must propagate. Although the tensile residual stress field contributes to the driving force for precracking, it also introduces the possibility of history effects that may affect subsequent fatigue crack growth during testing that follows precracking. The tensile residual stress field elevates the local driving force at the crack tip, promoting higher crack growth rates than would be expected from the applied loading. These higher growth rates result from two effects: an elevated maximum stress-intensity factor and delayed closure development. Three-dimensional finite element analyses (FEA) and experimental testing were used to characterize the load history effects induced by compression precracking [3]. The analysis results indicate that for low tensile loading levels near the threshold region, the residual stresses cause the calculated crack tip driving force to differ from the applied driving force by 25% or more. In addition, significant crack growth of about two or three times the estimated plastic zone size is needed to grow away from the residual stress field and reduce the calculated crack tip driving force to within 5% of the applied driving force. Figure 9.4-28 is a plot of selected results for an aluminum alloy. The results were generated under constant ΔK loading after compression precracking. The initial crack growth rate corresponds to an R=0.7 loading condition (fully open crack due to the tensile residual stress field) for the given applied ΔK. Also included are plastic zone size estimates from 3D FEA and a standard equation. Experimental results also show that growth of about two to three times the estimated plastic zone size is necessary to establish steady growth rates under constant ΔK loading for these testing conditions.

REFERENCES

2) Tabernig, B. and Pippan, R., "Determination of the Length Dependence of the Threshold for Fatigue Crack Propagation," Engineering Fracture Mechanics, 69, 2002, pp. 899-907.
3) Forth, S.C., Newman, J.C., Jr., and Forman, R.G., "On Generating Fatigue Crack Growth Thresholds," International Journal of Fatigue, Vol. 25, 2003.
4) James, M. A., Forth, S. C., and Newman, J. A., "Load History Effects Resulting from Compression Precracking," *Fatigue and Fracture Mechanics: 34th Volume, ASTM 1461*, S. R. Daniewicz, J. C. Newman, Jr., and K.-H. Schwalbe, Eds., ASTM International, West Conshohocken, PA, 2004.

9.4.16 RESIDUAL STRESS EFFECTS ON NEAR-THRESHOLD FATIGUE CRACK GROWTH IN FRICTION STIR WELDS IN AEROSPACE ALLOYS

Reji John and Kumar V. Jata, US Air Force Research Laboratory, Materials & Manufacturing Directorate, AFRL/MLLM

Friction stir welding (FSW) is being explored as a potential tool for manufacturing aluminum and titanium aerospace structures. Several joint configurations, butt, lap and fillet joints have been made in the production of such exploratory structures. The knowledge of fatigue and fatigue crack growth behavior in the weld zone is required to provide an understanding and tools to assess the damage tolerance issues in friction stir welded joints and structures. The US Air Force conducted a study [1-3] on near-threshold fatigue crack growth in friction stir welded aluminum alloy 7050-T7451 and a titanium alloy Ti-6Al-4V. Tests were conducted on weld coupons using three geometries: compact tension, C(T), eccentrically loaded single edge, ESE(T), and center-crack tension, M(T). Different stress ratios (R) were employed to understand the effects of residual stresses in the heat affected zone (HAZ) of the alloy. Residual stresses were measured on samples machined from the friction stir welded plates prior to testing. The results showed that residual stresses play a key role in the crack growth parallel to the weld-path in the HAZ. Although friction stir welding introduced "low" residual stresses in the friction stir welded plate, this study showed that fatigue crack growth along the weld can still be significantly affected by residual stresses. This residual stress effect was demonstrated using specimen configurations corresponding to bending and tensile loading. At low R (=0.05), the C(T) specimen showed significantly higher fatigue threshold and low crack growth rate compared to the M(T) specimen. At R=0.8, the differences in crack growth rate between the C(T) and M(T) geometry were considerably reduced. Analysis of ΔK - K_{max} behavior near threshold for various Al alloys and Ti-6Al-4V showed evidence of the dominant influences of residual stresses. Parametric analyses were conducted using uniform residual stress distributions along the crack plane. This study demonstrated that the fatigue threshold was significantly altered even in the presence of "low" residual stresses, sometimes leading to threshold values lower than that of the parent material. Additional analyses of the residual stress effects in the weld region are in progress.

REFERENCES

1) Jata, K.V., Sankaran, K.K., and Ruschau J.J., Metallurgical and Materials Transactions, Vol.31 A, September 2000, pp. 2181-2192.
2) John, R. and Jata, K.V., "Residual Stress Effects on Near-Threshold Fatigue Crack Growth in Friction Stir Welds," Proceedings of Symposium on Friction Stir Joining and Processing, The Minerals, Metals, and Materials Society, TMS, pp. 57-69, November 2001.
3) John, R., Jata, K.V., and Sadananda, K., "Residual Stress Effects on Near-Threshold Fatigue Crack Growth in Friction Stir Welds in Aerospace Alloys,' International Journal of Fatigue, Vol. 25, pp. 939-948, 2003.

9.4.17 SPARKING OF TITANIUM DURING SANDING AND DEBURRING

Irfan Rosidi and Antonio C. Rufin, Boeing, Seattle

High production volumes, the need to use shop resources efficiently, and ergonomics have led to a greater use of tools and techniques designed for high material removal rates. In the case of sanding and deburring of titanium, the use of these rather aggressive processes can increase the risk of sparking and surface damage resulting in a potential loss of fatigue quality. It is recognized, that it is very difficult to sand or deburr titanium without ever producing a single spark, and it is not clear what rework options are available once sparks are produced. It is therefore desirable to establish the possible circumstances under which a moderate level of sparking might be permissible from a durability standpoint, along with developing a better understanding of the factors affecting the fatigue quality of sanded edges in titanium.

An early Boeing study demonstrated that sparking during edge finishing operations on titanium can create a significant loss in fatigue properties of the material, and confirmed the presence of a metallurgically altered layer in surfaces that had been exposed to severe sparking. Subsequent observations showed that a small amount of material removal by a more benign process such as chemical etching could eliminate the sparked layer from the material surface, and thus allow recovery of some of the loss in fatigue performance.

The initial objective the more comprehensive follow-on test program, which is described here, was to evaluate the fatigue performance of sparked titanium that had undergone either 0.0002-inch (typical, per surface) material removal by light etching or a larger amount of material removal by chem-milling. For comparison, baseline groups of titanium coupons without any exposure to sparking, with and without chem-milling, were used. Flat notched specimens (with a stress concentration [K_t] based on net stress of 1.5) were manufactured and fatigue tested. Additional specimens were added later to investigate the effect of polishing, transverse scratches/marks, multi-step operations with different operators, types of sanders and sanding speed, direct sandblasting, and etch levels.

One of the significant results from this program was the absence of the type of thermal surface damage that was observed in the first study, which had dealt with more extreme (and perhaps somewhat unrealistic) sanding conditions. However, the tests also did reveal a great deal of fatigue sensitivity to the lay (direction of dominant sanding marks) of the part. Transverse sanding marks a fraction of one thousandth of an inch deep on a corner on edges where sparking occurred during sanding resulted in significantly degraded fatigue lives.

A single normal chemical etch of a sparked, transversely sanded edge did not help, but the more significant amount of material removal by chem-milling restored the fatigue life of the part to the baseline, as-chem-milled (no sanding) condition. Direct sandblasting of the sanded surface also seemed to restore the fatigue performance to the baseline condition. The same effect was observed with mechanical polish plus a light chemical etch of the sanded surface, provided the following requirements were met: (1) sanding was limited to the edge of the part, (2) sanding and polishing were performed in a manner that left no visible transverse sanding marks, and (3) no adherent fines (molten titanium particles shed during the sanding process) were created during either sanding or polishing.

Most of the work just described targeted titanium sheet products. A parallel study focused on titanium plate (> 0.188 inch thick) and the effects of shot peening, abrasive cleaning (sand blasting), and light sanding on sparked material with adherent fines. The latter can be difficult to remove completely and tend to aggravate the condition of the surface by creating thermally affected zones (and, if severe enough, cracks) beneath them. Flat notched and open hole fatigue test specimens were used in this effort. The adherent fines were investigated in the notched coupons only. Test results (Figure 9.4-29) indicate that shot peening and/or abrasive cleaning (sand blasting) after sanding relieve the detrimental effect of sparking and adherent fines. Light sanding alone as a final finishing process did not have much influence in removing the effect of sparking and (especially) molten fines. Examination of the specimens after testing indicated that all fractures on the sparked and lightly sanded specimens initiated at adherent fines, in spite of having attempted to remove the fines by light sanding. In fact, some of the fractures originated away from the center notch, indicating that the defects caused by the fines were more severe than the nominal specimen stress concentration of 1.5. There were no apparent adverse effects on the open hole specimens from sparks generated by the rotary deburring process evaluated in this program.

9.4.18 DESIGN FOR LONGITUDINAL SINGLE-SHEAR LAP JOINT FATIGUE IMPROVEMENT

Karen D. MacKenzie, Boeing, Seattle

Longitudinal single-shear lap joints are used to join aircraft fuselage skins in a straightforward and inexpensive manner. However, these lap joints maybe problematic in terms of fatigue performance. Historically, to increase fatigue life, the skin thickness is increased locally at the joint and fastener diameter is chosen to further reduce bearing stresses. The joint thickness step is typically accomplished by either bonding a doubler in this area or milling the skins down to their final thickness with a thicker pad at the joint. However service experience has shown the local skin padding and prudent fastener diameter selection by themselves are not adequate to prevent early fatigue failures.

Boeing has developed a lap joint with reduced tension, bearing and bending stresses. It addition, the outer skin is the more critical of the two for ease of crack detection.

This design was tested for pressure fatigue performance in a full scale single-aisle, 5 abreast fuselage section and successfully completed 378,000 cycles (5 lifetimes) without a crack. The new joint will be subjected to the complete range of fuselage fatigue loads in a full-scale twin-aisle fuselage section in 2003 and 2004.

9.4.19 EXPERIMENTAL FRACTURE MECHANICS

E.A. Patterson, Michigan State University

Work on modelling crack closure in polycarbonate using photoelasticity was concluded in 2003 [1] although further research to link this experiment-based model to analytical models is being discussed in collaboration with Professor Neil James at the University of Plymouth, UK. The work demonstrated that crack tip closure phenomena could be modelled quantitatively and that contact at the flanks did not correlate with effective stress intensity factors when this occurred. A review of optical techniques for measuring crack tip stress fields [2] was conducted which included an assessment of the factors influencing the choice of a technique for a particular investigation, such as ease of use and capital costs. This work identified thermoelastic stress analysis as having significant under-developed potential and recent work has focussed on its use for monitoring fatigue cracks [3]. New methodologies based on genetic algorithms have been developed to allow the location of the crack tip and amplitude of the stress intensity factor, ΔK to be evaluated during the growth of a fatigue crack using a sensitive infra-red camera [4]. The new methodology is non-destructive and non-invasive in that no surface preparation is necessary although a spray-coating with a water-based matt black paint is desirable but not essential. Continuous monitoring of the crack location and stress intensity factor is viable in real engineering components without *a prior* knowledge of the applied loading or history. It has been demonstrated that the thermoelastic measurements provide a direct evaluation of the effective stress intensity factor and opening loads in the presence of crack closure phenomena. (See Figure 9.4-30)

REFERENCES

1) James, M.N., Pacey, M.N., Wei, L-.W., Patterson, E.A., 2003, ‘Characterisation of plasticity-induced closure-crack flank contact force versus plastic enclave’, Engineering Fracture Mechanics, 70(17):2473-2487.
2) Patterson, E.A., Olden, E.J., 2004, ‘Optical analysis of crack tip stress fields: a comparative study’, Fat & Fract. Engng. Mater. & Structures, 27(7):623-636.
3) Diaz, F.A., Patterson, E.A., Tomlinson, R.A., Yates, J.R., 2004, ‘Measuring stress intensity factors during fatigue crack growth using thermoelasticity’, Fat & Fract. Engng. Mater. & Structures 27(7):571-584.
4) Diaz, F.A., Yates, J.R., Patterson, E.A., 2004, ‘Some improvements in the analysis of fatigue cracks using thermoelasticity’, Int. J. Fatigue, 26(4):365-376.

9.5. PROBABILISTIC METHODS

9.5.1 PROBABILITY OF FRACTURE (PROF) SOFTWARE UPDATE

Peggy C. Miedlar, Alan P. Berens and Peter W. Hovey, University of Dayton Research Institute

Increasing attention is being given to the use of non-deterministic methods in the planning of maintenance actions based on of the many stochastic factors that influence structural integrity in an aging fleet. An example of a risk analysis tool that is amenable to aging aircraft applications is the computer program PRobability Of Failure (PROF).

PROF is a structural risk analysis program designed around the data available from the USAF Aircraft Structural Integrity Program (ASIP). PROF models the growing population of fatigue cracks at a stress riser as a function of flight hours. The crack size distribution is modified at specified maintenance times depending on the inspection capability and repair quality. Single flight probability of failure, is calculated as a function of flight hours by combining the distributions of crack size, fracture toughness and maximum stress in a flight. The single flight failure probability (hazard rate) is then converted to the distribution of flight hours to failure. Risk analysis through PROF is modular in that it calculates risks on a per detail basis. More complex scenarios are assessed by combining the results of multiple runs.

The PROF program is currently being modified to provide information that is specifically directed at the process for making decisions regarding the timing of structural maintenance. In particular, algorithms are being added that will combine the risks from the major control points of a single airframe and will combine risks associated with selected multi-element damage scenarios. This information can be used to assess the status of individual airframes as a function of flight hours. To account for the distribution of flight hours of the individual airframes in a fleet, the individual airframe data will be aggregated to predict the expected fleet reliability as a function of flight hours and calendar time. For example, the safety associated with various maintenance intervals can be compared in terms of the expected number fleet failures as function of calendar time; see Figure 9.5-1. Further, given the costs of inspecting and repairing cracks, the intervals can also be compared in terms of the expected costs of maintenance and failures.

PROF can perform the analysis requirements included in Mil-Std-882D, 10 February 2000, entitled "Standard Practice for System Safety". This is an approach that has proven useful in the management of safety risks, with a key component the assessment of mishap risks. The assessment is based on both the severity of the consequences and the likelihood of occurrence of a mishap. There are four suggested levels of severity and five suggested levels of likelihood of occurrence. The quantitative mishap probability values are based on individual aircraft and the qualitative levels are based on the entire fleet. The assignment of the quantitative values to the probability values depend on fleet size. The mishap risk assessment values are used to rank hazards in terms of their associated mishap risks and are used to define categories of risks and the level of management for the acceptance of risks. When addressing risk analysis decisions, military leaders want to know the risk assessment value being anticipated.

ACKNOWLEDGEMENT
This work is sponsored by the Aeronautical Systems Center, Agile Combat Support Systems Wing, Aging Aircraft Systems Squadron, WPAFB, OH under Air Force Contract F09650-03-D-0001 administered by S & K Technologies for Major Timberlyn Harrington, Chief, Air Vehicles Branch, ASC/AAAV.

REFERENCE

1) Berens, A.P., Hovey, P.W., and Skinn, D.A., 1991. *Risk Analysis for Aging Aircraft Fleets, Volume I - Analysis*, WL-TR-91-3066, Wright Laboratory, Wright-Patterson Air Force Base, OH, October 1991.
2) Hovey, P.W., Berens, A.P., and Loomis, J.S., 1998. *Update of the PROF Computer Program for Aging Aircraft Risk Analysis, Volume 1 – Modifications and User's Guide*, AFRL-VA-WP-TR-1999-3030, Air Force Research Laboratory, Wright-Patterson Air Force Base, OH, November 1998.
3) Miedlar, P.C., Berens, A.P., Hovey, P.W., and Thomsen, M.L., 2004. "Aging Aircraft Maintenance Planning," *Proceedings of the 2004 USAF Aircraft Structural Integrity Program Conference,* Memphis, TN, December 2004.

9.5.2 INTEGRATED PROBABILISTIC RISK ASSESSMENT TOOLS

Kevin Boyd, Andrew Hinkle and David Newman, S&K Technologies; Michael Shiao, FAA Tech Center; Lt Col Scott Fawaz, U.S. Air Force Academy; and Alex Litvinov, LexTech

Probabilistic-based risk assessments are becoming a fundamental part of an aging aircraft's ASIP Program. As structural integrity problems arise on certain aircraft, tools are needed to assess the impact to the rest of the fleet. In many circumstances, fleet management decisions must be made quickly that can be very costly and/or effect aircraft availability. Therefore, analytical software tools and data must be available to assist ASIP Managers, Chief Engineers and their System Program Directors (SPDs) in making these critical evaluations. The Integrated Probabilistic Risk Assessment Tools (IPRAT) program provides tools that enable probabilistic risk assessments and promote probabilistic damage tolerance analysis, maintenance-based planning (Figure 9.5-2). By employing probabilistic methods, multiple design conservatisms can possibly be reduced, allowing life-limited structures to operate well beyond their original design lives, reducing downtime, operating costs and increasing fleet readiness.

After finalization of requirements needed to support the USAF Air Logistics Centers (ALC's), the first effort developed an updated, standalone version of the University of Dayton Research Institute's Probability of Fracture (PROF) risk assessment software. This updated program includes algorithms to calculate risks associated with multiple control points on an airframe and combine multiple individual airframes to calculate fleet reliability. Another task that is included in this effort will link the PROF code to the deterministic fatigue crack growth code, AFGROW. The second effort is a cooperative agreement between the FAA Hughes Technical Center, ASC/AAA, USAFA and SKT. This program involves the integration of advanced Monte Carlo and other probabilistic risk assessment methods with the AFGROW program. The Monte Carlo approach provides complete flexibility in choice of distributions used to represent inspection data while linking with other probabilistic methods enable quicker and fewer calculations.

The linking of these two risk assessment approaches with the deterministic fatigue crack growth software, AFGROW, will provide an ASIP engineer with a robust tool for evaluating aging aircraft risk, inspection scheduling and long-term maintenance costs. With the help of integrated toolsets, SKT believes that ASIP engineers will be able to more efficiently manage risk and maintenance costs in aging aircraft structure.

ACKNOWLEDGEMENT
This work was sponsored by the Aeronautical Systems Center, Agile Combat Support Systems Wing, Aging Aircraft Systems Squadron, WPAFB, OH, under Air Force Contract F09650-03-D-0001 administered by S&K Technologies for Major Timberlyn Harrington, Chief, Air Vehicles Branch, ASC/AAAV.

REFERENCES

1) Miedlar, P.C., Berens, A.P., Hovey, P.W., and Thomsen, M.L., 2004. "Aging Aircraft Maintenance Planning," *Proceedings of the 2004 USAF Aircraft Structural Integrity Program Conference,* Memphis, TN, December 2004.

2) Shiao, M. C., K. Boyd and S. Fawaz, "A Risk Assessment Methodology and Tool for Probabilistic Damage Tolerance-Based Maintenance Planning", *Proceedings of Aging Aircraft 2005,* Palm Springs, CA, January 2005.

9.5.3 CRACK GROWTH BASED PROBABILITY MODELING OF S-N RESPONSE, AND INFLUENCES OF ENVIRONMENT AND MICROSTRUCTURE

D. Gary Harlow and Robert P. Wei, Lehigh University

Fracture mechanics based probability modeling has been applied to the analysis of conventional S-N data on a high strength bearing steel (SUJ2 steel) into the very high cycle (VHC) domain; i.e., up to 10^{10} cycles, with over 300 data points at 8 stress levels. It focused upon the probabilistic analysis of and the likely underlying causes for the observed distributions in fatigue lives in the 10^4 to 10^{10} cycle regime; these distributions could not be adequately represented by traditional statistical analyses. The results show that the fatigue lives and the associated distributions (i.e., the S-N response) resulted naturally from fracture mechanics based crack growth analyses, with cracking originating from a microstructural, or mechanical, heterogeneity (e.g., an inclusion, Figure 9.5-3). The overall S-N response is shown to be consistent with the probabilistic distributions for the size and location of crack nuclei, and possible influences of near-surface residual stresses and test environment. These findings show a clear connection between crack growth and S-N response, and show a path for mechanistic understanding of S-N behavior of engineering materials.

Figure 9.5-4 shows the cumulative distribution functions (cdfs) computed from the crack growth model and the corresponding experimental data. None of the cdfs can be represented very well by a Weibull cdf, especially for $\Delta\sigma$ below 1,700 MPa. Based on statistics alone, a more complex (and mechanistically questionable) cdf would be needed to represent the data, as well as the significant increases in statistical scatter as $\Delta\sigma$ decreases. In terms of the fracture mechanics based model, on the other hand, the cdfs at $\Delta\sigma$ above 1,700 MPa reflect principally a single mode of crack-growth failure that is determined by the distribution in the size if inclusions near the specimen surface. The cdfs at the lower stresses reflect failure that had originated at both surface and subsurface inclusions, and the modeling effort reflect considerations of stress intensity factor differences, surface residual stresses and the influences of test environment. These factors need to be examined systematically for a range of materials and test conditions.

Figure 9.5-5 captures one plausible interpretation for the behavior of the S-N data on SUJ2 steel; namely, principally in terms of environmental influences, as crack growth in this high strength steel is expected to be significantly enhanced by atmospheric moisture. The influence of surface residual stresses is assumed to be mitigated by "shakedown" during initial fatigue loading. The experimental data are shown by the gray symbols, and the expected S-N curves in the deleterious and inert environments are superimposed as solid and dashed dark lines. The difference between the two lines reflects the expected increase in fatigue crack growth rates and the reduction in endurance limit by the deleterious environment. For this steel above about 1,300 MPa nearly all of the fatigue failure would be expected to be associated with cracks that nucleated at the surface and environmentally enhanced crack growth, which is consistent with observations. At and below about 1,300 MPa (i.e., as the stress corrosion threshold is approached), nucleation and growth from surface inclusions becomes less dominant, and indeed, failures from both surface and internal nucleation are observed. The distribution for the probability for crack growth from surface and subsurface nucleation sites may be represented schematically by the inset to reflect this environmental influence, and the S-N behavior can be well represented by a probabilistic version of the "rule of mixture" for the two nucleation modes for crack growth.

This investigation provides an additional framework for understanding S-N behavior and serves a bridge for linking the traditional fatigue and fracture mechanics communities. It is hoped that the effort will lead to additional research to better understand the key variables that affect metal fatigue, and quantification of the influences of key random variables on the distribution in fatigue lives.

REFERENCES

1) Harlow, D. Gary, Wei, Robert P., Sakai, Tatsuo and Oguma, Noriyasu, "Crack Growth Based Modeling of S-N Response," 3rd International Conference on Very High Cycle Fatigue (VHCF-3), Kyoto and Shiga, Japan, September 16-19, 2004 (Plenary Lecture) 542-552.

2) Sakai, T., Takeda, M., Tanaka, N., Kanemitsu, M., Oguma, N. and Shiozawa, K., "Characteristics S-N Property of High Carbon Chromium Bearing Steel in Ultra-Wide Life Region Under Rotating Bending," *Material Science Research International Special Technical Publication* - 1 (May 2001) 41-46.

9.6. DAMAGE TOLERANCE

9.6.1 DAMAGE TOLERANCE-BASED SKIN REPAIR SOFTWARE

Michael Shiao, FAA, William J. Hughes Technical Center

The effect of structural repairs on aircraft structural integrity is one of the critical issues that need to be addressed for the assurance of aircraft continuing airworthiness and operational safety. In addition, the Aging Airplane Safety Interim Final Rule requires the use of damage tolerance-based inspection programs on airplanes with multiple engines and ten or more passengers used in scheduled operations (operation within the state of Alaska is exempt) was published on December 6, 2002. To assist the small airplane industry in complying with this aging rule, an integrated design assessment tool, Repair Assessment Procedure and Integrated Designs for Commuters (RAPIDC), has been developed. RAPIDC is an automated static strength and damage tolerance analysis tool for skin repairs and antenna installations. It is a PC Windows-based software with user-friendly, point-and-click graphical user interface (GUI) features. It has an advisory system to provide repair guidelines as needed. An extensive material and fracture parameter database was also created for easy data access. RAPIDC Version 2.0 was released January 31, 2003, via the Internet at the following website:

http://aar400.tc.faa.gov/ Programs/AgingAircraft/Commuter/RAPID.

The latest version includes a built-in finite element module (FEM), an automatic FEM mesh generator, a load spectrum generator, and static and damage tolerance analysis modules for fuselage skin repairs and antenna installations. The built-in FEM is used to determine fastener load transfer of mechanically fastened multiple layers. An automatic mesh generator eases users' effort for model preparation. Typical fuselage skin repairs are shown in Figures 9.6-1(a) through 9.6-1(d).

The built-in doubler configurations for antenna installations are shown in Figures 9.6-2(a) through 9.6-2(e). Only the circular cutout is allowed.

A new capability for irregular fastener pattern was also implemented into the RAPIDC design process. This capability allows users to place fasteners as they were found in an operational environment, as illustrated in Figures 9.6-3 (a) and 9.6-3(b), rather than the straight line previously required by the program. This feature is especially critical for the designs of the elliptical, sausage, and teardrop doublers.

A detailed repair assessment report is automatically generated. The report includes all the design parameters and configurations, analysis methodologies, and results from damage tolerance analysis.

Typical results such as fatigue crack growth history, residual strength, and critical crack length are plotted in Figures 9.6-4(a) and 9.6-4(b).

9.6.2 DARWIN® -- A NEW METHODOLOGY FOR SURFACE DAMAGE TOLERANCE ASSESSMENT

Joseph Wilson, FAA, William J. Hughes Technical Center

A new probabilistic methodology has been developed for predicting the risk of fracture associated with aircraft jet engine rotors and disks subjected to surface damage. The methodology, defined by the Rotor Integrity Subcommittee of the Aerospace Industries Association, was recently implemented in Design Assessment of Reliability With Inspection (DARWIN®), a probabilistic fracture mechanics software code developed by Southwest Research Institute under FAA research and development (R&D) Grants.

DARWIN is being developed in collaboration with major engine manufacturers (General Electric, Honeywell, Pratt & Whitney, and Rolls-Royce). The 2000 R&D 100 award-winning program computes the probability of fracture as a function of the number of flight cycles, considering random defect occurrence and location, random inspection schedules, and several other random variables. A user-friendly GUI is included to handle the otherwise difficult task of setting up the problem for analysis and viewing the results.

Aircraft turbine rotors may be subjected to rare, critical events (e.g., uncontained engine failures) due to the presence of metallurgical (e.g., hard alpha) and manufacturing (e.g., surface damage) defects that can occur during the manufacturing process. A probabilistic methodology is particularly well suited to the efficient design of components subjected to rare, critical (i.e., life-limiting) events, because it allows the designer to adjust nominal component parameters to meet quantitative reliability requirements.

Previous releases of DARWIN have focused on the risk assessment of titanium aircraft engine rotor disks with potential inherent (hard alpha) defects. Inherent defects can occur anywhere within a disk, so a volumetric zone-based risk integration methodology is used to account for this uncertainty.

In contrast, surface damage is present only on the exterior surfaces of a component and is often located at features (e.g., boltholes) or along other machined surfaces. Additional crack geometries were introduced in the DARWIN 4.x releases to model surface features. A feature-based methodology is used to estimate risk in which the disk risk is approximately equal to the sum of the risks associated with the individual features. For a typical disk, the number of features associated with surface damage assessment is relatively small compared to the number of zones associated with inherent defect-based assessment.

The initial framework for surface damage-based risk assessment is shown in Figure 9.6-5 mission profile definition are the stress, temperature, and stress gradient values at discrete time steps.

A number of enhancements were added in the recent 4.2 code release, including PC and Linux versions, the capability to execute the analysis code directly from the GUI, and improved deterministic crack growth assessment and visualization. A capability for modeling surface damage based on three-dimensional finite element geometry is currently under development for the 5.0 release (Figure 9.6-6).

9.6.3 CHARACTERIZATION OF FATIGUE BAHAVIOR OR AIRCRAFT FUSELAGE STRUCTURES

John Bakuckas, FAA, William J. Hughes Technical Center

A major focus of the structural integrity research supporting the FAA National Aging Aircraft Research Program has been the assessment of fatigue mechanisms in aircraft structure through computational and experimental analysis. Emphasis has been placed on determining the causes, growth mechanisms, and consequences of widespread fatigue damage (WFD). Knowledge of multiple-site damage (MSD) nucleation time, pattern, and distribution, as well as its subsequent growth and effects on residual strength, is a prerequisite for planning an acceptable program to preclude the occurrence of WFD.

As part of the FAA's core capability, a unique, state-of-the-art Full-Scale Aircraft Structural Test Evaluation and Research facility has been established at the FAA William J. Hughes Technical Center for testing large curved panels representative of aircraft fuselage structure. This facility provides experimental data to support and validate analytical methods under development, including WFD prediction, repair analysis and design, and new aircraft design methodologies. The fixture, shown in Figure 9.6-7, is designed to simulate the actual loads an aircraft fuselage structure is subjected to while in flight, including differential pressure, longitudinal load, hoop load in the skin and frames, and shear load.

Several programs have been undertaken to investigate the fatigue and residual strength characteristics of fuselage structure. A variety of fuselage panels were tested and analyzed, including undamaged panels and panels manufactured with crack-like slits to simulate initial damage scenarios. In addition, a panel with polyisocyanurate foam was tested to assess its effect on fatigue behavior. For each panel tested, strain surveys were first conducted to ensure proper load transfer from the load application points to the panels. Fatigue damage was quantified in terms of crack initiation, crack distribution (location and size), and subsequent growth. Residual strength tests were conducted to determine the effects of damage states on load-carrying capacity.

Test results during the strain survey revealed a high local-bending deformation along the critical outer rivet row in the lap joint area, the same area where MSD cracks initiated. As shown in Figure 9.6-8, there is more local bending for a curved panel CVPB compared to the flat panel test results. The flat panels tested had identical joint construction to the curved panel CVPB. For both panels, the maximum strain occurred at the inner skin surface.

The majority of fatigue life was spent in initiating and forming cracks. Cracks initiated from the inner-faying surface at rivet holes in the outermost fastener row in the lap joints and progressed through the thickness, as illustrated in Figure 9.6-9. Once first linkup occurred, crack growth rate increased substantially.

Although multiple cracking did not have an effect on the overall global strain response, it significantly reduced the fatigue life and residual strength, as shown in Figure 9.6-10.

In addition, the application of polyisocyanurate foam to fuselage panels was effective, enhancing crack growth performance. More details can be found in Bakuckas, J.G., Bigelow C.A., and Tan, P., "Characterization of Fatigue Behavior of Aircraft Fuselage Structures," *Proceedings From the International Committee on Aeronautical Fatigue* (ICAF 2003), Lucerne Switzerland, May 2003.

9.7. CORROSION/FATIGUE

9.7.1 AN INVESTIGATION INTO THE STRUCTURAL INTEGRITY OF A RETIRED USAF C-130E CENTER WING BOX TO SUPPORT USAF ASC/AAA AVHM PROGRAM

Kevin Boyd and Michael Stuerman, S&K Technologies and Lt Col Scott Fawaz and Gregory Shoales, U.S. Air Force Academy

S&K Technologies, in cooperation with the United States Air Force Academy (USAFA) is performing a structural integrity evaluation and documentation of a Center Wing Box (CWB) structure from a decommissioned C-130E aircraft. This evaluation consists of three main phases scheduled during FY04 & FY05.

Phase I involves the evaluation of newly developed, in-situ ultrasonic Non-Destructive Inspections (NDI) of select CWB Fatigue Critical Locations (FCL's). Specifically, the inspections examine wing skins, stringers, beam caps, and inner to outer wing rainbow fittings for the presence of corrosion and cracking. Phase I NDI indications are depicted in the notional 3-Dimensional representation of the CWB, shown in Figure 9.7-1. The inspected locations were selected and prioritized based upon their safety limits as established by Damage Tolerance Analysis (DTA) and immediate fleet concerns. The spatial locations of the selected FCL's are illustrated in Figure 9.7-2.

Phase II includes the intact removal of the CWB and further component parceling to facilitate traditional secondary NDI evaluations. Phase II findings will be used to demonstrate the validity of the Phase I NDI results. Traditional secondary NDI consists of visual, fluorescent liquid penetrant, or eddy current methods as deemed appropriate.

Phase III will focus on macro and micro fractographic analysis of limited CWB components in order to fully characterize damage mode(s). These CWB components will be selected based upon the combination of Phase I and Phase II NDI findings, FCL design data, and by review of fleet wide historical failure analysis reports. Microscopy permits the differentiation of damage modes involving Stress Corrosion Cracking (SCC), fatigue, and / or corrosion fatigue by identifying features such as initiation sites, fatigue striations, crack branching, and/or inter- versus trans-granular cracking. Presently, Phase I is complete and Phase II & III are progressing.

S&K Technologies Inc. and the USAF Academy will use the comprehensive failure mode evaluation results along with newly measured flight loads data to perform detailed structural integrity analyses of the CWB. The structural analyses will, in part, employ AFGROW along with S&K Technologies' Structural Damage Management Tool (SDMT). Results and data from this program will serve to provide information to the C-130 SPO (WR-ALC/LB) to assist the ASIP manager with fleet management decisions.

ACKNOWLEDGEMENT

This work was sponsored by the Aeronautical Systems Center, Agile Combat Support Systems Wing, Aging Aircraft Systems Squadron, WPAFB, OH, under Air Force Contract F09650-03-D-0001 administered by S&K Technologies for Major Timberlyn Harrington, Chief, Air Vehicles Branch, ASC/AAAV.

REFERENCES

1) Cordell, T. and Maj. Harrington, T., "Air Vehicle Health Management," Technical Presentation Given During the Aging Aircraft Strategy Session at the 2005 Aging Aircraft Conference.

9.7.2 FATIGUE CRACK EVOLUTION IN PRE-CORRODED 2024-T3 ALUMINUM

K. van der Walde and B.M. Hillberry, Purdue University and J.R. Brockenbrough, Alcoa Technical Center

Localized corrosion has widely been observed to have deleterious effects on structures subjected to fatigue loading [1,2]. Research work on corrosion-nucleated fatigue crack growth in aluminum has been performed at Purdue University and the Alcoa Technical Center under the sponsorship of Alcoa. The thrust of this work has been to understand corrosion pit morphology and to further understand, and model, ensuing crack growth brought about by fatigue loading. A fracture mechanics framework is brought to bear on this problem [3].

Multiple crack initiation was addressed by fractographic analysis of numerous pre-corroded 2024-T3 aluminum fatigue specimens. It was observed that over half of the specimens analyzed failed as a result of multiple crack initiation. Quantitative fractography revealed that stress level and corrosion exposure duration are positively correlated with *n*, the number of failure-causing crack-nucleating pits per specimen. An algorithm was developed to numerically simulate the growth process of multiple cracks. In applying this model to the test data it was found that the inclusion of multiple crack effects is of particular importance at high stress level. It was also found that, of the many crack-nucleating flaw combinations that could have resulted from the pitting observed on fracture surfaces, the actual combination generally yielded one of the lowest possible lives. This observation fostered an extreme-value approach to life prediction using as the input random plane cross-sectional images of pitting corrosion. Figure 9.7-3 shows a comparison of the experimentally observed fatigue lives and those obtained using this life prediction approach.

Further insight into pit-nucleated crack growth has been gained from scanning electron microscopy of interrupted crack growth test specimens. Following corrosion exposure, these specimens were fatigue tested for prescribed numbers of cycles (determined as percentages of the known average expected lives) and then monotonically overloaded, thus exposing cracks in intermediate stages of growth. Analysis of these cracks has proven invaluable in understanding shape evolution and initiation location. Figure 9.7-4 shows a crack emanating from a pit in 2024-T3 aluminum which was cycled for 20% of its total expected life.

The Alcoa/Purdue corrosion fatigue work conducted has attempted to address several of the key issues in corrosion-nucleated fatigue crack growth. While the damage evolution of fatigue cracks in corroded structures is quite complex, it is shown that simplified modeling strategies can be implemented to assess residual life.

REFERENCES

1) Sankaran, K.K., Perez, R., and Jata, K.V., 2001, "Effects of pitting corrosion on the fatigue behavior of aluminum alloy 7075-T6: modeling and experimental studies," *Materials Science and Engineering*, A297, pp. 223-229.

2) Bray, G.H., Bucci, R.J., Colvin, E.L, and Kulak, M., 1997 "Effects of prior corrosion on the S/N fatigue performance of aluminum sheet alloys 2024-T3 and 2524-T3," *Effects of the Environment on the Initiation of Crack Growth*, *ASTM STP 1298*, Van Der Sluys, W.A., Piascik, R.S., and Zawierucha, R., Eds, ASTM.

3) van der Walde K. A Model For Fatigue Crack Growth In Pre-Corroded Aluminum, Ph.D. Dissertation, To be published May 2005, Purdue University.

9.7.3 STRESS CORROSION CRACKING IN 7079-T6 SHEET MATERIAL

Molly Brown and Scott Fawaz, U.S. Air Force Academy

The Center for Aircraft Structural Life Extension (CAStLE) at the United States Air Force Academy has been assigned to study stress corrosion cracking (SCC) in AA 7079-T6 as part of the Aeronautical Systems Center, Aging Aircraft Division's (ASC/AAA) Air Vehicles Health Management program. CAStLE was introduced to this problem to help alleviate a short inspection interval burden. Currently, models are being generated by data from thick sheet SCC testing, which are assumed to be very conservative.

Background

For this effort, specimens were taken from actual skin material, where this problem in the fleet resides. The sheet was then machined by electrical-discharge machining (EDM) into ESE(T) specimens and pre-cracked in accordance with ASTM E647. The schematic for an ESE(T) specimen is illustrated in Figure 9.7-5.

The SCC testing will be done in an aqueous environment while using a constant-displacement method of loading. The specimen shall be instrumented using a back face strain gage in order to calculate crack opening. Data on the strain gage will be taken at regular intervals. Load readings will also be done concurrently. This will generate data for load and crack opening displacement, which can later be reduced to crack growth rate vs. stress intensity data.

Progress

The load frame has been designed, but validation has not been done. See Figure 9.7-6. The environmental chamber has been designed as a clear pipe of PVC with one fixed end and one opening end for access to instrumentation. Inlet valves were integrated so that moist air may be constantly forced through the system. In line with the specimen, a load cell will be fixed to the bottom plate of test frame. Load will be applied by tightening a threaded rod, providing constant displacement throughout the test. The specimen will be loaded in the test frame so that clevises are fixed to the load cell and the threaded rod. The need for good alignment has been addressed, and will be ensured for each data reading.

Use of the constant displacement method was verified by experts in the field who suggested this method over constant load testing. Furthermore, constant displacement testing, which is more commonly used for this type of test, would give much smoother, slower-increasing stress intensity data than a constant load test. This is particularly desirable for taking data manually, as will be done here.

During January 2005, the validation of crack growth readings was most important. Measurements were done by a traveling optical microscope and by clip-on displacement gage to verify the back face strain gage readings. Data from this portion of testing is not yet available.

Progress
Thus far, validation has been under way to determine whether the compliance equations in ASTM match the experimental data. This information is not yet available. The entire program should be finished by the summer of 2005.

9.7.4 COMPRESSION BUCKLING TESTS OF Z-STIFFENED PANELS WITH SIMULATED GRINDOUTS

James M. Greer, Jr., Daniel W. Hill and Scott A. Fawaz, U.S. Air Force Academy and Ron Logan, Northrop Grumman Corporation Integrated Systems

The objective of this investigation was to determine the effect of corrosion grindouts on the compressive strength of B-707 upper wing skin panels. Three representative geometries were considered. One configuration represented the minimum strength wing panel (40 ksi, Configuration #1, or C1), and one represented the maximum strength wing panel (64 ksi, Configuration #3, or C3). A third configuration was also tested. These panels, denoted Configuration #2 (C2), were mistakenly manufactured with thicker stiffeners, but were tested nonetheless to provide additional data for this study. Two pristine panels in each configuration were tested, and damage was introduced into each of the other panels in the form of uniform spanwise grindouts. These grindouts ranged from 35% to 63% of the panel skin thickness, and were meant to simulate severe in-service corrosion grindouts.

Twenty-seven panels were manufactured in the three aforementioned configurations. All panels consisted of a skin sheet with five evenly spaced Z-stiffeners. Panel configurations are shown in Figure 9.7-7. The skin was of 7075-T6 aluminum sheet material. The stiffeners were formed (bent) from 7075-0-BARE coil stock, then solution heat treated and aged per the SAE AMS2770G specification to the T62 temper before attaching them to the skin. The bend radii for the stiffeners was 4.3 mm (0.17 in). The material properties for the aluminum used to fabricate the panels are listed in Table 9.7-1.

Grindouts were made to the panels along the full length of the panel on the skin opposite the middle stiffener. The grindout geometry is shown in Figure 9.7-8. Grindouts varied in depth from 34.8% to 62.6% of the skin thickness, denoted as t_c in Figure 9.7-8.

All panels were tested under displacement-controlled conditions to panel failure. Loading was applied along the stringer axis. The results are shown in Table 9.7-2 and Figure 9.7-9. Where three tests were conducted on similar configurations, the outlying result was discarded. However, results were so consistent, this only occurred twice. Results were very repeatable.

By modifying the panel buckling calculation methods of Johnson, Euler, and Gerard, the behavior of panels with grindouts was modeled. A modified Johnson-Euler method (see, e.g., Reference [1]) worked best for modeling damaged C1 and C2 (long) panels, and a modified Gerard method [2] worked best for modeling the C3 (short) panels. This follows from the large amount of plastic deformation in the stringers of C3 panels vs. C1 and C2 panels (see Table 9.7-2). The modification to these methods consisted of decreasing the skin thickness of the entire affected (center) bay by the maximum grindout depth. Plots of these methods vs. the experimental results are shown if Figures 9.7-10, 9.7-11 and 9.7-12.

The test results indicate that uniform grindouts along the stiffener length, provided the middle stiffener (only) is affected, and the fastener is reattached snugly with new rivets, caused only minor degradation in panel buckling strength. Moreover, by modifying the analysis methods of Johnson, Euler, and Gerard, curves can be generated that depict strength degradation as a function of grindout depth for these panels. The shorter (C3) panels experienced significantly more plasticity prior to collapse than did the longer (C1 and C2 panels). It is for this reason that the Gerard method was more appropriate, and better at modeling, the C3 panels. These curves give the structural engineer a new tool for assessing the degradation in strength to B-707 upper wing skin panels due to grindouts.

REFERENCES

1) M. C.-Y. Niu, *Airframe Structural Design*. Hong Kong: Conmilit Press LTD, 1998.

2) G. Gerard, "Handbook of Structural Stability: Part V - Compressive Strength of Flat Stiffened Panels," Technical Note 3785, National Advisory Committee for Aeronautics, Washington, Aug. 1957.

9.7.5 FAILURE MODE DETERMINATION OF UPPER WING SKIN WITH VARIABLE CORROSION

Molly R. Brown and Scott A. Fawaz, U.S. Air Force Academy

The Center for Aircraft Structural Life Extension (CAStLE) at the United States Air Force Academy investigated the fatigue performance of artificially exfoliated transport aircraft upper wing skin as part of the Aeronautical Systems Center, Aging Aircraft Division's (ASC/AAA) Air Vehicles Health Management program. Specimens were prepared by milling 7075-T651 aluminum to reflect a thickness loss at a depth: width ratio of 5:1 while maintaining a profile of a smooth contour as would be seen by natural corrosion processes. An artificial corrosion process performed by using EXCO per ASTM G34 simulated sufficient corrosion for representation on the upper wing skin. In order to obtain a representation of varying amounts of corrosion, multiple depths of corrosion were modeled. These changes in thickness varied between five and seventy percent in a 0.25 inch plate. Fatigue was introduced by applying a compression-dominated load spectrum from the aircraft at wing station (WS) 320. These specimens were run to two design lifetimes or failure.

Background

Corrosion was artificially simulated to create a similar scenario as would be on the upper wing skin. The majority of each specimen's surface area was masked with beeswax so that submersion in the corrosive liquid would only reach the machined contour of the specimen. Corrosion was formed using the common EXCO process per ASTM G34, which is popular for inducing severe types of exfoliation corrosion [ASM Handbook, Evaluation of Exfoliation Corrosion p 243 vol 13 1992].

This design was not used at the start of the program, but it evolved around February 2004. The other design had the potential to yield at the edges of the impression since they were too close to the edges of the specimen. Many geometries of hourglasses were experimented with until the simple geometry was implemented (see Figure 9.7-13).

The impression that simulates corrosion had a requirement that it met the amount of thickness loss that was required and that it kept the same angle of descent into the impression. From those two guidelines, the span of the pit and the radius of the partial sphere to be machined into it were determined. A diagram of the machining concept is in Figure 9.7-14.

After testing had completed for five specimens, it was noted by the customer that since exfoliation corrosion was found to be fatigue insensitive (see CAStLE-Failure Mode Determination of Upper Wing Skin), fasteners should be introduced to the specimen to create more of a stress concentration. This would obviously create a specimen that was more likely to fail due to fatigue, as well.

To ensure a proper replicate of the wing skin for testing, a steel pin was chosen where the fastener may have a tolerance of -0.005/-0.015 and the hole may have a tolerance of +0.005/-0.035 inches. Essentially, this ensured a "snug" fit between the steel pin (precision dowel pins were used here) and the specimen.

Progress
The test program's progress is reported in Table 9.7-3. Also noted is a scatter in number of cycles to failure as seen in the below equation. Scatter is considered sufficiently low when the standard deviation of the log of the number of cycles to failure is less than or equal to 0.15.

$$\sigma_{\log(N_f)} \leq 0.15$$

Conclusion
Testing will continue until a complete set of data has been taken. This will include three specimens of each corrosion condition between 15% and 75% thickness losses in 5% increments. The program should conclude in June of 2005. At that time, the results will be published.

9.7.6 FATIGUE PERFORMANCE OF EXFOLIATED TRANSPORT UPPER WING SKIN MATERIAL

Molly Brown and Scott Fawaz, U.S. Air Force Academy

Aluminum hourglass specimens were artificially corroded on three material orientations: LT, ST, and LS and subjected to a compression-dominated transport upper wing skin (UWS) load spectrum. Half of the 18 specimens were of the orientation shown in Figure 9.7-15 and loaded in the L direction; the other half had the L and T directions swapped and were loaded in the T direction. Twelve specimens had damage consisting of a grindout on the LT surface (see Figure 9.7-15), the surface of which was then artificially corroded using a technique developed by the Corrosion Kinetics Laboratory at the Ohio State University [1] (other specimen surfaces were masked with lacquer). Six of these 12 specimens were further damaged by corroding a small area on the LS or ST surface (no grindout). Six other specimens had corrosion only on the small LS or ST area. The specimen population is summarized in Table 9.7-4.

The load spectrum consisted of 468,172 cycles per pass. Twenty passes of the spectrum (over nine million cycles) constituted two aircraft lifetimes. This is a compression-dominated spectrum, with 58% of the loads in the spectrum being compressive (min load –193 MPa or –28 ksi, max load +115.8 MPa or +16.8 ksi, median value –114.5 MPa or –16.6 ksi, mean value –26.9 MPa or –3.90 ksi).

The first set of two-lifetime fatigue tests was completed with no specimen failures. Testing took place in 100% humidity at (nominally) 75°F. Specimens were analyzed using an optical microscope to determine the area and volume of the corroded region, and a scanning electron microscope was used to determine the crack nucleation site.

Since there were no failures after 20 spectrum passes, all specimens were tested again using a modified load spectrum in which the spectrum tensile stresses were increased by 20%. Eight of eighteen specimens survived the second, more severe, spectrum without failure. Three specimens were damaged in test anomalies. The results of these tests are summarized in Tables 9.7-5 and 9.7-6. Specimen dimensions are indicated in Figure 9.7-16. Holes were drilled in a few of the specimens for the purpose of *in-situ* SEM examination. Most specimens did not have these holes, and in all cases the holes were covered by the wedge grip surfaces during testing.

It is noteworthy that none of the specimens failed during the first fatigue test (20 passes, two lifetimes). This indicates that under severe environmental conditions, as simulated by the 100% relative humidity with the corrosive compound in the intergranular fissures, laboratory induced intergranular and exfoliation corrosion damage in UWS is fatigue insensitive for the configuration tested. Since the stresses are lower outboard of WS 320, this conclusion likely holds for wing stations outboard of WS 320.

REFERENCES

1) Frankel, Gerald S. and Rokhlin, Stanislav I. "Intergranular and Exfoliation Corrosion Rate Studies" The Ohio State University, 23 February 2003.

9.7.7 FATIGUE PERFORMANCE OF TRANSPORT AIRCRAFT UPPER WING SKIN MATERIAL

Molly R. Brown and Scott A. Fawaz, U.S. Air Force Academy

The Center for Aircraft Structural Life Extension (CAStLE) at the United States Air Force Academy investigated the fatigue performance in terms of total life of artificially exfoliated transport aircraft upper wing skin as part of the Aeronautical Systems Center, Agile Combat Support Squadron's (ASC/AAA) Air Vehicles Health Management program. The specimens were hourglass in shape to ensure a uniform stress distribution through the width of the gage section. They were corroded on three material orientations, LT, ST, and LS and subjected to the compression-dominated load spectrum of the at upper wing station (UWS) 320. The specimens were loaded in both the LT and TL direction. Fatigue testing was done on spanwise (LT) and chordwise (TL) oriented specimens. An electrochemical corrosion process was performed by the Fontana Corrosion Center at the Ohio State University on the 7178-T6 aluminum to create intergranular corrosion (IC) followed by exfoliation corrosion (EC). The first set of fatigue tests, simulating two aircraft design lifetimes, was completed with no failures in the 18 specimens. All specimens were then tested again using a modified load spectrum which increased the spectrum tensile peak stresses by 20%. Eight of eighteen specimens survived the second, more severe, spectrum without failure. After completion of the fatigue tests, the specimens were analyzed using optical and electron microscopy to determine the area and volume of the corroded region in addition to the size and location of the crack nucleation site.

Background

Exfoliation corrosion typically occurs on the UWS due to protective coating breakdown between the cadmium plated steel fasteners and the aluminum alloy 7178-T6. Once the protective cadmium coating is ineffective, a galvanic cell is created between the steel fasteners and the wing skin material.

In order to consider extending the service life and possibly deferring maintenance, the fatigue criticality of the exfoliated specimens must be determined. In other words, will mode I fatigue cracks nucleate in the corroded upper wing skin?

Process

The hourglass specimens were machined from actual UWS aircraft material—AA 7178. Since exfoliation corrosion is found in a variety of conditions, loading directions for the test were chosen to be both longitudinal and transverse. For a diagram showing where the material originated, see Figure 9.7-17 and Figure 9.7-18.

The specimens were tested using a load spectrum to simulate the loads experienced on the upper wing skin. The stress model is a wing bending moment calculation. Also, the wing geometry and panel properties are considered in wing stresses. Due to panel thickness and other geometries, wing stresses start to peak around WS 320 and increase inboard. The maximum stress in the spectrum was 16.8 ksi and the minimum stress was -28 ksi. The specimens ran to failure or to the equivalent of two lifetimes. Specimens that did not fail during the first test were then exposed to another, more severe, spectrum that was altered by using a multiplication factor of 1.2 on the tension peaks. To be consistent with MIL-STD-1530B, the fatigue tests were run to two lifetimes, 40,000 hours. Testing to two full lifetimes was conservative since a portion of the fatigue life had been used in service.

Results

Of the eighteen specimens tested, fifteen useful data points were obtained. No data was collected for three specimens that were damaged by testing anomalies. In Table 9.7-7**,** the results are listed by orientation and corrosion location, along with the result of two sets of fatigue tests.

It is important to note that none of the specimens failed during the first fatigue spectrum. This means that under severe environmental conditions, the corroded upper wing skin is insensitive to fatigue in its first two lifetimes, 40,000 flight hours, at WS 320. Since the stresses are lower outboard of WS 320, the conclusion can be drawn that exfoliation damage from WS 320 and outboard is fatigue insensitive. Only two of the fracture surfaces were found to have nucleated at a corrosion site. Of those specimens where nucleation did not occur at corrosion, the nucleation sites varied.

When the program was in review with the customer, a more severe stress state (involving a hole) would be beneficial to the model created in the end. From that, the project "CAStLE-Failure Mode Determination of Upper Wing Skin, Variable Corrosion" was initiated.

9.7.8 IN-SERVICE UPPER WING SKIN FATIGUE TESTS

James M. Greer, Jr., Cornelis B. Guijt, Stephan Verhoeven and Scott A. Fawaz, U.S. Air Force Academy

The focus of this project was the effect of exfoliation corrosion on fatigue life, where the cyclic loading is represented by a spectrum for a transport upper wing skin station. The load spectrum consisted of 468,172 cycles per pass. Twenty passes of the spectrum (over nine million cycles) constituted two aircraft lifetimes. This is a compression-dominated spectrum, with 58% of the loads in the spectrum being compressive (min load –193 MPa or –28 ksi, max load +115.8 MPa or +16.8 ksi, median value –114.5 MPa or –16.6 ksi, mean value –26.9 MPa or –3.90 ksi). Related work in this area was done by Bellinger, Komorowski, Liao, Carmody, and Peeler, subjecting in-service specimens to constant-amplitude, compression-dominated loading [1].

The in-service specimens were not removed from the aircraft with testing in mind (poor specimen geometry), so prototype specimens of the same configuration as the in-service specimens were fabricated, instrumented and tested to verify the loading scheme (Figure 9.7-19.). Spectrum testing of the prototype article was successfully completed to two aircraft lifetimes (20 passes of the spectrum). The in-service part was then tested. Spectrum testing of the aircraft part was done in the same manner as the prototype testing: Tabs were adhesively bonded to the specimen, and containers (bags) were placed on the surface of the specimen to ensure that the fastener holes were subjected to the salt-water environment. A deficient adhesive bondline on one tab led to premature failure of the specimen after approximate 3.5 spectrum passes (about 50 hours of testing), but the specimen was repaired and testing continued. After 13 spectrum passes (182 hours of testing) the specimen was inspected and two cracks were observed growing from a fastener hole (see Figure 9.7-20). The specimen was sectioned for examination.

Fractographic analysis indicated a likely nucleation site (an inclusion with high silicon content) on one side of the fastener hole near the countersink knuckle (Figure 9.7-21). On the other side of the hole, again at the countersink knuckle, the crack appeared to start at a corrosion pit. At neither side of the hole in Specimen #1 did any feature associated with intergranular attack or exfoliation appear to have a role in crack nucleation. It is not known if these cracks nucleated during laboratory testing or in service.

A second in-service part was tested, again in a corrosive environment, and it too failed at 1.3 additional lifetimes (13 spectrum passes). The specimen failed in the grips and was not repairable. The test section was sectioned as indicated in Figure 9.7-22, and the sections were subjected to 3-point bending in an attempt to open any existing cracks at the hole edges. No cracks were observed at holes 1 or 2, but hole 3 exhibited a crack on its left edge (see Figure 9.7-22 for L/R orientation). This crack nucleated at a corrosion pit at the bottom of the fastener hole (Figure 9.7-23). On the other side of the hole, some interesting features had formed that appear to be the early stages of crack nucleation, and may have been caused by irregularities in the surface due to exfoliation (Figure 9.7-24). These features are the only ones to date that indicate exfoliation possibly having a role in crack nucleation in this compression-dominated spectrum test.

In summary, all cracks found initiated from something other than exfoliation corrosion, although there were indications of some crack nucleating features adjacent to one side of one hole at 1.3 additional lifetimes.

REFERENCES

1) N. Bellinger, J. Komorowski, M. Liao, D. Carmody, F. T., and D. Peeler, "Preliminary Study into the Effect of Exfoliation Corrosion on Aircraft Structural Integrity," in *Proceedings of the 6th Joint FAA/DoD/NASA Aging Aircraft Conference*, (San Francisco, CA), September 2002.

9.7.9 CORROSION FATIGUE

Prof. David W. Hoeppner, University of Utah

Substantial work in the area of corrosion fatigue has been performed at the University of Utah from 2003-2004. Much of this work was based on previous research, including that performed for the Corrosion Fatigue Structural

Demonstration program administered by Lockheed Martin for the Air Force Research Lab, which was completed in early 2003.

The importance of corrosion fatigue research is well known and continues to be an important area of study. The main focus of the latest corrosion fatigue research at the University of Utah was to gain an increased understanding of how microstructure influences pit growth, pit-to-crack transition, and critical crack propagation to fracture. Two thicknesses of 7075-T6 aluminum alloy were etched and then subjected to concomitant corrosion fatigue in a 3.5% NaCl environment. Testing was interrupted at various intervals to obtain information on pit generation, growth, and potential cracking. 7075-T6 aluminum alloy was selected for experimentation based on its applicability to the aging aircraft community, as this alloy has been used for wing and fuselage structures on both military and commercial aircraft in the past.

Results indicated that microstructure has a significant influence on pit-to-crack transition and fatigue crack propagation. Fatigue cracks in a concomitant corrosion fatigue environment propagated only when the crack growth rate was greater than the pit growth rate. Short cracks (<100 μm) in a corrosion fatigue environment were strongly influenced by grain boundaries and crystallographic grain orientation. Constituent particles competed with corrosion pits as critical crack nucleation sites, an example of which is shown in Figure 9.7-25. Post-fracture analysis confirmed the presence of non-critical cracks within the corroded region, related to pitting and constituent particles.

REFERENCE

1) Jones, K., 2004, "Effect of Microstructure on Pit-to-Crack Transition in 7075-T6 Aluminum Alloy," Ph.D. dissertation, University of Utah.

9.7.10 RELIABILITY ALGORITHMS FOR CORROSION-FATIGUE DAMAGE EVALUATION IN AIRCRAFT STRUCTURES

Dr. Dan M. Ghiocel and Dr. Letian Wang, Ghiocel Predictive Technologies Inc.

The overall scope of this DOD research effort is *to develop a prototype engineering computational tool for predicting aircraft component reliability and life-cycle cost under corrosion-fatigue damage.* The intent is to reduce the cost of maintaining aging aircraft while ensuring reliability. The cost reduction benefits can be derived from reduced unscheduled high cost maintenance on aircraft and planning for lower cost aircraft logistics center inspection and maintenance. By developing physics-based stochastic models for idealizing the operating environment, pressure loading, structural behavior and material corrosion-fatigue progressive damage*, the component reliability analysis and the maintenance cost analysis are approached from an advanced engineering understanding and modeling* [1]. The research project emphasis is on the crevice corrosion effects on aircraft joint fatigue life. Selected case studies included joints of the B-707, C-141 and K-135 aircrafts.

Using the prototype tool, called ProCORFA [2], the aircraft designer or maintenance engineer can quickly perform *what-if* analyses to see how different design modifications affect a component's risk of failure, the predicted life and/or the induced maintenance costs. The main efforts of this research project focused on computational modeling aspects including: (i) stochastic modeling of progressive corrosion-fatigue damage, (ii) stochastic component stress analysis, (iii) reliability calculations including maintenance uncertainties and Bayesian updating based on new field data, and (iv) stochastic modeling and optimization of overall cost given the component reliability constraints. The stochastic corrosion damage models employed are described elsewhere [1]. A multiscale stochastic analysis approach (Figure 9.7-26) was employed to compute local stress distributions around the rivets [2]. To perform efficiently the nonlinear stochastic finite analysis advanced response surface approximation models were employed. The stochastic stress analyses included random variations in material properties, manufacturing tolerances, riveting, hole expansion, residual stresses, plus the stochastic corrosion variation in the vicinity of the rivets (Figure 9.7-27).

REFERENCES

1) Ghiocel, D.M. and Tuegel, E.J. "Reliability Assessment of Aircraft Structure Joints Under Corrosion-Fatigue Damage", Chapter 28 in the "Engineering Design Reliability Handbook", CRC Press, December, 2004, at http://www.crcpress.com/shopping_cart/products/product_detail.asp?sku=1180&parent_id=&pc=
2) ProCORFA software at http://www.ghiocel-tech.com within the Engineering Tools page.

9.7.11 UNDERSTANDING OF ENVIRONMENTAL CRACKING IN AGING AIRCRAFT STRUCTURE

Robert S. Piascik, Stephen W. Smith, John A. Newman and Scott A. Willard, Langley Research Center

The understanding of local loads is one of many issues that are critical when assessing the airworthiness of aging aircraft structural components, especially when the aircraft structure exhibits environmental damage. It is not unusual for aircraft to continue operation 20 to 40 years after reaching the economic design life. These are the years that aircraft become more susceptible to local corrosion in regions that are difficult to inspect but critical to continued aircraft airworthiness. As time dependent corrosion damage processes become more prevalent, additional "first-order-effects" that influence structural integrity must be considered. The aim of this study is to highlight a few cases that illustrate how environmental assisted damage will require additional understanding as aircraft structures age.

Case #1 Environmental Assisted Cracking of an Aluminum Aircraft Forging

Forty-year-old transport aircraft were found to have cracked horizontal stabilizer tie box forgings. The large forging, approximately two meter by one meter in size, is located in the tail of the aircraft and is the attachment point for the horizontal stabilizer. Non-destructive examination of the fleet revealed that many of the large aluminum alloy (7075-T6) forgings contained numerous cracks capable of leading to component failure and potential loss of aircraft. Figure 9.8-28 shows the crack surface of a 24 cm (9.5 inch) crack that initiated in the mid-thickness region of a fastener hole. The distinct variations in color along the length of the crack surface are accumulated corrosion products that reveal the crack front configuration along the length of the crack. These results show that severe crack tunneling occurred; after crack initiation, the tunneled crack propagated nearly 7.5 cm (3 inch) along the forging interior before the crack penetrated the surface of the forging. Both energy dispersive spectroscopy (EDS) and Auger analysis were performed to identify chemical contaminants associated with the crack surface corrosion products. No definitive contaminants were detected and no variation in chemical composition was linked to the dramatic variation in the surface corrosion along the length of the crack. These results suggest that crack environment (chemical composition) had not changed appreciably during crack growth and also suggests that the dramatic variation in crack surface discoloration is the result of a variation in corrosion product thickness rather than corrosion product chemistry. A failure analysis was conducted revealing the following: (1) cracks propagated along an intergranular (IG) crack path, (2) crack regions exhibited evidence of corrosive environment and (3) no fatigue striations were observed on the crack surfaces. Based on these findings and the belief that sustained loading was dominant in regions of cracking, stress corrosion cracking (SCC) was identified as the root cause of cracking and the horizontal stabilizers were replaced with a more SCC resistant 7000 series alloy.

The results of additional studies have suggested environmental fatigue may also be a likely cause of cracking in the horizontal stabilizer in addition to SCC. A review of tie box local loads suggests that a small cyclic load is likely applied along with sustained loads (residual stress and fit-up stress) that produce a high mean stress ($R = K_{min}/K_{max}$) fatigue (ripple) loading. Laboratory fatigue crack growth (FCG) tests were conducted at high R to simulate possible tie box local ripple loads (high sustained loads with superimposed small cyclic loads). The laboratory air (relative humidity ranging from 30 to 60%) and high relative humidity (RH >95%) FCG test results are shown in Figure 9.8-29. The FCG tests were conducted using material extracted from a tie box forging that exhibited cracking and test specimens were fabricated to ensure that fatigue crack paths were in the identical crack direction to that observed in service. Four FCG test results are shown in Figure 9.8-29; three constant Kmax tests were conducted to simulate high R ripple loads and a low mean stress constant R =0.05 test. For the constant Kmax = 13.2 MPa√m test (square symbols), the applied stress ratio ranged from 0.7 to 0.9 and for the Kmax = 6.6 MPa√m test (circle symbols), the applied stress ratio varied between R = 0.1 and R = 0.9. The constant Kmax = 11.0 MPa√m test (diamond symbols) were conducted at a stress ratio ranging from 0.1 to 0.9. The high R data from the constant Kmax tests converge at low ΔK suggesting an extremely low FCG threshold of approximately 0.7 MPa√m. The R=0.05 test results (triangle symbols) reveal a low mean stress FCG threshold of approximately 3.0 MPa√m. It is important to note that the high humidity crack growth data (diamond symbols) exhibit similar behavior compared to the laboratory air FCG rates. It is not until the FCG growth threshold is approached that high humidity FCG rates become ΔK independent, for ΔK < 0.7 MPa√m. Knowing the load frequency (5 Hz), a da/dt = 2.5x10-6 mm/sec was calculated for the ΔK independent crack growth behavior. The calculated da/dt result from Figure 9.8-29 is identical to the SCC crack growth rates determine by SCC testing of the identical material in 95%RH environment at a sustained load equivalent to a Kmax = 11.0 MPa√m.

Figures 9.8-30a and 9.8-30b are micrographs showing metallographic cross sections of a crack from a tie box forging and a laboratory air specimen crack that propagated by high R ripple loads, respectively. Each micrograph shows the crack-tip region and the surrounding microstructure. Extensive metallographic examinations have shown that the laboratory air cracks produced under high mean stress exhibit an IG crack path similar to the cracks found in the tie box forging. In addition, these examinations have shown that IG crack surfaces produced at high mean stress ripple loads do not exhibit striations; an observation consistent with the crack surfaces produced in-service. These results are not unexpected; striations are normally not detected on aluminum fatigue crack surfaces produced at extremely small (near threshold) cyclic amplitudes.

For this case, local sustained loads and high mean stresses are a likely result of forging residual stress and component fit-up stress. The sustained loads, in combination with extremely small ripple loads, can produce rapid environmental enhanced IG cracking. SCC in combination with intergranular environmental assisted fatigue (EAF) is probable. The data shown in Figure 9.8-29 illustrates that an understanding of local loads is paramount when predicting damage tolerance of aging aircraft components susceptible to time dependent corrosion; here, small operation loads (ripple loads) continue to produce rapid crack growth rates compared to low mean stress. To emphasis these findings, the following example is given. Assuming both SCC and EAF, total environmental crack growth (EAC) is defined as $(a)_{EAC} = (a)_{SCC} + (a)_{EAF}$. From Figure 9.8-29, the following "highly conservative" estimate of $(a)_{EAC}$ is made to highlight the extremely rapid growth rates that could occur. Assuming a $K_{SCC} = 11.0$ MPa√m and a $da/dt_{SCC} = 2.5x10\text{-}6$ mm/sec, the crack will grow 7.8 cm/year by SCC. Obviously this would not occur and the true environmental spectrum (time of crack-tip wetting) would have to be factored to establish a reasonable $(a)_{SCC}$. Assuming a small ripple load of $\Delta K = 1.5$ MPa√m crack growth rates would increase by a factor of 10. Again, without knowing local loading frequency and usage factors, a simple "highly conservative" yearly EAC crack growth $(a)_{EAC} = 78$ cm/yr (assuming a load frequency of 5 Hz). Although these calculations are overly conservative, it illustrates how rapidly cracks can grow in the tie box forging and when factored over 20 to 40 years, it strongly suggests that understanding first order effects (local loads, time of wetness, cyclic behavior, etc.) is critical when time dependent aging processes are involved.

Case #2 Propagation of Damage by Compressive Loads

Intergranular corrosion or exfoliation corrosion is a well-known environmentally induced damage mode that can occur in aluminum aircraft structural alloys. Structural analysis usually considers exfoliation a thinning process that reduces the load carrying capability of the structural component. For these analyses, tensile loads are usually considered damaging unless the corrosion is so extensive that structural buckling becomes an issue when compressive loads are dominant. It is obvious that these structural membrane load considerations are extremely important, but it is also critical to understand local-load-corrosion-damage interactions. Here, local loads that are normally thought to be benign can interact with time dependent corrosion damage ultimately producing a local stress state that rapidly degrades the integrity of the aging structure. For example, upper wing skins are typically considered to operate at fatigue loads that are dominated by compressive loads with small tensile loads. These compressive dominant operational loads are typically thought to be benign unless relatively substantial corrosion damage occurs. Recent, studies have shown that compressive dominant loads can interact with small levels of corrosion resulting in reduced fatigue strength.

Laboratory studies have shown that compressive loads can exacerbate local corrosion damage. Laminar (IG) cracks were found to propagate from IG corrosion damage under a compressive fatigue load environment. Center-hole test coupons that simulate the local stress state in an upper wing skin fastener hole were tested using a typical compression dominated upper wing skin load spectrum. Small regions of IG corrosion were introduced along the hole inside diameter at the 11 to 1 o'clock or 5 to 7 o'clock orientations; here, the intergranular corrosion formed penetrations along the pancake shaped grain boundaries of the upper wing skin. The IG penetrations are typically parallel to the direction of the applied compressive fatigue load illustrated in Figure 9.7-31. After compressive load fatigue testing, detailed examinations revealed that laminar cracks initiated at the preexisting IG damage and propagated to the 3 and 9 o'clock orientations. It is important to note that the laminar cracking (LC) propagated in a direction parallel to the applied load and is a likely result of a micro-buckling damage mode produced during compressive loading. Once compressive load produced LC reached the tension load dominated portion of the hole, fatigue crack nucleation occurred followed by FCG as illustrated in Figure 9.7-31. The micrographs in Figure 9.7-32 show the 6 to 9 o'clock portion (similar to Figure 9.7-31) of a coupon cyclically loaded in compression and tension (–16.5 MPa√m and + 5.5 MPa√m). Similar to the illustration in Figure 9.7-31, the micrographs show that compression dominated LC propagated from the small region of IG corrosion to the tension hole orientation where a fatigue crack nucleated and propagated under the tension portion of the load spectrum. These results show that structural integrity can be influenced by a small amount of corrosion damage located in seemingly benign locations and orientations, and the progression of damage can be greatly influenced by what are considered non-damage-propagating loads.

9.8. TESTING

9.8.1 RESONANT FREQUENCIES OF VIBRATING PANELS WITH CRACKS AND BONDED COMPOSITE PATCHES

Mohan M. Ratwani, R-Tec and David Banaszak, USAF AFRL

Current emphasis is on repairing cracked metallic aircraft structures with composite patches. This repair concept has worked well for cracks initiating and propagating under fatigue loading. Currently, this repair concept is being applied to cracks initiating and propagating under vibratory loads. The resonant frequencies of panels gradually decrease as the cracks initiate and propagate. When a cracked structure is repaired the resonant frequency increases due to added stiffness provided by the repair patch. It is important to know the resonant frequencies of panels after repair to make life predictions of panels.

Efficient mathematical techniques and a software program are developed (Reference 1) for predicting resonant frequencies of cracked panels with bonded repairs. The results of analytical predictions were compared with the test database (References 2) generated by the Wright-Patterson Air Force Base on aluminum specimens repaired with composite patches (Figure 9.8-1) and subjected to shaker excitation at resonant frequencies. Predicted and observed resonant frequencies at various crack lengths in 170x36 panels with 1-mm thickness and in 170x360 panels with 3.2-mm thickness are shown in Figures 9.8-2, and 9.8-3, respectively. A good correlation between predicted and test resonant frequencies is seen.

REFERENCES

1) Ratwani M. M, "Development of Validated Crack Measurement System for Vibrating Structures", Report Number AFRL-VA-TR-2002-3005,ADA 399661, January 2002.
2) Banaszak D, Dale G. A and Baust D. J, "Effectiveness of Damped Fiberglass Patches on Vibrating 2024-T3 Plates", Proceedings of SAMPE 2001 Conference, Long Beach California, May 2001.

9.8.2 DESTRUCTIVE EVALUATION OF AGING SMALL AIRPLANES

Michael Shiao, FAA, William J. Hughes Technical Center

By 2010, the average age of the fleet of small airplanes (~180,000 aircraft) will approach 40 years. However, little is known about the consequences of the aging process of small airplanes. Comprehensive teardown inspections provide critical information to determine the condition of high-time operational aircraft. Data developed from teardown inspections can be used to provide guidance for maintaining structural and systems integrity. Limited teardown inspections of large civil aircraft have been performed, which resulted in a limited and proprietary knowledge base. There is no such knowledge base for small airplanes. Therefore, FAA research of teardown investigation on small airplanes would provide an excellent opportunity to gain knowledge and insight required to support rulemaking, advisory circular preparation, and findings of compliance for small aircraft.

In September 2002, the FAA initiated a research project to evaluate two high-time commuter airplanes, both Cessna 402 models. The 402 was chosen because of its design commonality with several other commuter-class airplanes. The first aircraft, a 402A model built in 1969 with 19,700 flight hours, was primarily used for flying tourists through the Grand Canyon. The second aircraft, a 402C model built in 1979 with 25,500 flight hours, was owned by Cape Air/Nantucket Airlines who flew commuter routes to islands in Massachusetts, Florida, the Virgin Islands, and Puerto Rico. The state of the structure and mechanical and electrical systems are being evaluated using destructive and nondestructive techniques. Specific observations made of the two aircraft selected for teardown investigation are being documented and generalized as applicable to the small airplane fleet in operation today.

The research is being conducted primarily at the National Institute for Aviation Research Aging Aircraft Research Laboratory at Wichita State University. The teardown evaluation involves two phases on each aircraft: an inspection phase and a teardown phase. In the inspection phase, over 100 visual inspections are performed on the airframe and aircraft systems along with detailed visual inspection of the aircraft wiring. Then, supplemental inspections are conducted on critical structural areas using NDI techniques such as visual, dye penetrant, magnetic particle, and eddy current. In addition, aircraft maintenance records, service bulletins, and airworthiness directives are being reviewed, including service difficulty and accident/incident reports for the Cessna 402 aircraft. The teardown phase includes disassembly of the aircraft (Figure 9.8-4), inspection of aircraft systems' components, investigation of advanced NDI methods (such as magneto optic imaging shown in Figure 9.8-5), laboratory testing of aircraft wiring, detail disassembly of aircraft sections, and microscopic examination of critical structural areas in the airframe (Figure 9.8-6).

Several industry participants are assisting with many aspects of the project. Cessna is providing technical and engineering support along with certified technicians to perform the supplemental inspections. Cessna's piston service center is providing service bulletins and service requirements applicable to the 402 aircraft. The FAA provided the 402A model, while Cape
Air/Nantucket Airlines provided the 402C and technicians to support the inspection and disassembly of the aircraft. The FAA Airworthiness Assurance NDI Validation Center is participating in the program by monitoring the supplemental inspections and investigating advanced NDI methods that may be applicable to this type of commuter aircraft. The FAA Small Airplane Directorate and the Wichita Aircraft Certification Office are assisting in the review of service difficulty and accident/incident reports along with certification requirements for these aircraft.

The inspection phase for the Model 402A was completed in March 2003, and the teardown phase was completed in September 2003.

9.8.3 CHARACTERIZATION OF TEST BED AIRCRAFT

Robert McGuire, FAA, William J. Hughes Technical Center

In response to the initiation of the new Aging Mechanical Systems Program, the FAA purchased a B747-136 (Figure 9.8-7) to serve as a program test bed for investigating aging mechanical systems. The aircraft was decommissioned in a manner to ensure the continued functionality of its mechanical and electrical systems. The test bed is available to support any future testing of mechanical systems.

In December 2002, the FAA technical note "Mechanical Systems Characterization of Boeing 747 Aging Systems Test Bed Aircraft," DOT/FAA/AR-TN02/119, was published. The report indicates that most systems, required for ground testing, were found to operate and function, or were serviced to operate and function, in accordance with the basic system functionality requirements specified in the Boeing 747-100 Maintenance Manual. These systems include the following: pneumatic system, hydraulic system, trailing-edge flap systems, leading-edge devices, aileron system, spoiler system, elevators, horizontal stabilizer, hydraulic shutoff valves, air conditioning, fuel system, landing gear system, lighting, doors and escape hatches, cargo handling, potable water, and lavatories.

Several systems were found to be nonoperational and would require a substantial financial expenditure in replacement components to make them operational. It was decided to leave these systems alone at this time; they include cabin pressurization, autopilot, navigation, communication and radio equipment, entertainment systems, interphone and public address system, oxygen system, ice and rain system, and fire systems.

9.8.4 ATR42 IMPACT TEST

Allan Abramowitz, FAA, William J. Hughes Technical Center

On July 30, 2003, the FAA conducted a vertical impact test of a high-wing regional commuter airplane. The test was conducted at the FAA William J. Hughes Technical Center. The objective of the test was to evaluate the impact response of the fuselage, floor tracks, seats, and anthropomorphic test dummies on a large high-wing regional commuter airplane when subjected to a severe, but survivable, impact. An ATR42, a 42 passenger twin-engine turboprop, high-wing airplane (Figure 9.8-8) was dropped from a height of 14 feet above the ground and impacted the surface with a final velocity of 30 feet per second. This is consistent with the vertical velocity change found in the Seat Dynamic Performance Standard 14 CFR Part 25.562(b)(1). The airplane was configured to simulate a typical flight condition, including seats, simulated occupants, simulated fuel, and cargo. The data collected in this test will supplement existing data and help provide the basis for future dynamic seat certification standards for commuter category airplanes. This is the last in a planned series of commuter airplane tests conducted by the FAA.

The airplane had a wingspan of 81 feet, weighed approximately 35,000 pounds, contained approximately 9000 pounds of simulated fuel (water), and 2100 pounds of luggage. The plane was configured with two simulated engines. Seven instrumented anthropomorphic test dummies and sixteen mannequins represented the crew and passengers. The airplane contained three different types of seats: the standard ATR current-generation seats, a 16-g-rated experimental seat, and an experimental energy-absorbing seat.

The airplane sustained substantial structural damage, especially at the fuselage/wing mating area of the cabin (Figure 9.8-9).

The test was well attended by Technical Center employees, the general public, the aviation community, and by local, state, and federal officials. There was extensive media coverage at the local, national, and international level in the newspapers and on television.

9.8.5 DESTRUCTIVE EVALUATION AND EXTENDED FATIGUE TESTING OF RETIRED AIRCRAFT STRUCTURES

John Bakuckas, FAA, William J. Hughes Technical Center

Airframe teardown inspections and extended fatigue testing are an effective means for structural evaluations and assessments for continued airworthiness of high-time operational aircraft, particularly those approaching their design service goal (DSG). Essential information and data for evaluating airframe structures that are susceptible to widespread fatigue damage (WFD) are obtained from teardown inspections. Teardown destructive inspections and extended fatigue testing can provide key information for developing programs to preclude WFD. While the expertise and knowledge base to conduct teardown inspections are well established by the large commercial airframe original equipment manufacturers (OEM) and military sectors, comprehensive guidelines and data that are documented and available to broader aviation community are lacking.

The FAA and Delta Air Lines have teamed to develop the protocol for airframe teardown inspections and extended fatigue testing. This 3-year project started September 2002. For this initiative, 11 fuselage lap joint panels susceptible to WFD, each approximately 8 by 12 ft, from a retired Boeing 727 passenger aircraft that is near its DSG are being evaluated as shown in Figure 9.8-10. In seven panels, the state of multiple-site damage (MSD) will be characterized using nondestructive inspection (NDI) and destructive fractographic examination. For the remaining four panels, the state of MSD will be advanced through extended fatigue and then assessed through NDI and destructive fractographic evaluation.

Prior to removing the panels from the aircraft at the storage site, conventional NDI evaluations were conducted per standard industry practices. A large number of crack indications were found along the lap joint in stringer 4R. Postremoval inspections conducted in a laboratory environment with controlled conditions confirmed these findings.

A teardown protocol was established to characterize the state of damage; to measure crack sizes, shapes, and distributions; to study crack initiation sources and sites; and to determine crack growth characteristics. A procedure was established to disassemble joints and reveal fracture surfaces using a section of the lap joint with both visual and NDI crack indications at several fasteners, as shown in Figure 9.8-11. One-inch-square pieces were cut from the joint with the fasteners in the center of each piece. The pieces were mounted in a stereomicroscope to determine the location of the cracks around the fastener and to examine the region around the base of the fastener. Two cuts were then made through the fastener hole interface away from the cracks to remove the fastener. The samples were then soaked in a solution to soften the sealant and pry open the layers. A slot was then machined in the plane of the crack leaving a 0.05″ ligament in front of the crack tip. The samples were cooled using liquid nitrogen, and the ligament was broken, using a pair of pliers, to expose the fracture surface of the crack.

Extended fatigue testing of four panels will be performed using the Full-Scale Aircraft Structural Test Evaluation and Research (FASTER) fixture located and operated at the FAA William J. Hughes Technical Center. The FASTER fixture was modified to add the unique capability to apply a variable-loading profile to a fuselage panel.

The objectives of the extended testing are to (1) propagate the state of damage beyond one DSG; (2) characterize and document the state of damage through real-time NDI, high-magnification visual measurements, and posttest destructive inspections; and (3) correlate analysis methods to determine crack detection, first linkup, and residual strength. Each panel will be subjected to load spectra, simulating the actual in-service flight load conditions. Testing of the first panel containing the lap joint along stringer 4L was initiated in FY04. There were no NDI crack indications on this panel prior to testing. As of September 2004, 20,000 pressurization cycles had been applied with no crack indications.

This project supports the upcoming Notice of Proposed Rulemaking for WFD and provides the data needed to calibrate and substantiate WFD assessments from real structures with natural fatigue crack initiation and accumulation representative of commercial transport use over an extended period of time (20-30 years). A critical product from this project will be guidance material that can be used in developing and assessing programs for continued airworthiness.

9.8.6 IMPROVED TEST METHODS AND ANALYTIC MODELS FOR REPRESENTING FATIGUE CRACK GROWTH BEHAVIOR IN THE NEAR THRESHOLD REGIME

R.G. Forman and J.M. Beek, NASA Johnson Space Center; S.C. Forth, NASA Langley Research Center and V. Shivakumar, Barrios Technology

Present accomplishments are briefly described on a development program supported by NASA and the FAA for improving and validating test methods and analytic models for representing fatigue crack growth rate behavior in the near threshold regime. This development effort is important to the application of damage tolerance analysis for high cycle fatigue-loaded components, particularly in meeting planned FAA rules for aircraft propellers and rotorcraft dynamic components.

The current progress in this program is the completion of initial experimental efforts to compare threshold regime data obtained from C(T) specimens with similar data from M(T) specimens. All threshold testing was conducted using the ASTM recommended constant R load-shedding procedure. The specimen materials were obtained from single plates, approximately 6 mm thick, of Ti-6Al-4V MA titanium and 2024-T851 aluminum. The results of these tests for both materials indicated that C(T) specimen data showed the typical "fanning-out" behavior in the threshold regime, but the M(T) specimen data did not show the fanning-out behavior. This is surprising because an M(T) specimen has significantly less constraint (i.e., from a negative T-stress) compared to a C(T) specimen which has a positive T-stress, and thus, less predicted crack closure resulting from load shedding.

Since full range crack growth rate data (from threshold to crack instability) were obtained for load ratio, R, values of 0.1, 0.4, 0.7 and 0.8, satisfactory NASGRO equation curve fits were constructed for each material. The threshold data for the C(T) specimens were also fitted to the NASGRO threshold equation that predicts the variation in threshold, ΔK_{th}, with R, plus the value of the fanning-out constant, C_{th} (See Figure 9.8-12). By comparing the curve fits derived from the C(T) specimens with the data from the M(T) specimens and letting the parameter $C_{th} = 0$, the resulting curves accurately matched the M(T) data for both materials (See Figures 9.8-13 and 9.8-14 for the Ti-6Al-4V results). This indicates that more conservative and possibly more valid threshold values for ΔK_{th} (i.e., no fanning-out behavior) can be satisfactorily derived from existing curve fits (using the NASGRO equation with $C_{th} > 0$) to C(T) specimen data by modifying C_{th}. This assumption has further been verified from analysis of earlier test results from M(T) and C(T) specimens of 7075-T7351 forged aluminum.

To further investigate threshold test procedures and the cause of threshold variations, additional testing will be performed on other commonly used structural alloys, including 7050-T7451 aluminum plate and D6AC forged steel. These efforts will also include a study of the importance of specimen size and flaw type (e.g., surface and corner type flaws) on threshold values and the effect of notch sharpness in minimizing the amount of load shedding in threshold testing (e.g., using a crack-like linear EDM notch extension made with 0.025 mm diameter wire). Also being studied are alternate specimen geometries which will simulate the characteristics of the M(T) specimen but allow much faster cyclic loading and use of less specimen material, similar to that possible for C(T) specimens.

9.8.7 F/A-18 FULL-SCALE TESTING

T. Callihan, Boeing , St. Louis

Status of F/A-18 full scale testing is summarized in Figure 9.8-15.

9.8.8 F-15 FTA6 TEST ARTICLES

M. Golike, Boeing, St. Louis

The efforts described in the F-15 FTA6 test articles, teardown/inspection and teardown analysis process are described in Figures 9.8-16, 9.8-17 and 9.8-18.

9.8.9 THE AIR VEHICLES COMBINED ENVIRONMENT EXPERIMENTAL VALIDATION FACILITY IS UPGRADED

Kenneth B. Leger, USAF AFRL/VASV

The Air Vehicles Directorate Combined Environment Experimental Validation Facility is the largest thermal-acoustic validation facility in the world. The facility provides state-of-the-art validation capabilities to all government agencies and to industry and academia through cooperative research and development agreements. (See Figure 9.8-18A)

The directorate recently oversaw the completion of a $19 million military construction project to upgrade a pre-existing World War II static test building located at Wright-Patterson Air Force Base. The result, the Combined Environment Experimental Validation Facility, is the world's premier aerospace vehicle structure research and development facility. It has various acoustic chambers capable of subjecting specimens (up to 4.5 ft by 9 ft in size) to temperatures up to 2,500°F and sound pressure levels up to 173 dB. Its random fatigue validation capabilities include exerting 20,000 lbs random force dynamic vibration and/or 25,000 lbs controlled variable force dynamic vibration on specimens.

Researchers are using these capabilities to simulate the different environments encountered by air and space vehicles. Using simulation data, they can develop accurate prediction methods for structural response and acoustic fatigue life of advanced structures used on air and space vehicles. In addition, they are researching vibration technologies that may enable lower-cost and higher-performance flight vehicles. Some examples of this research include hypersonic flight vehicle structures, thermal protection system advancements for current space platforms and future space operation vehicles, field repair of fatigue cracking, and buffet suppression.

The building housing the Combined Environment Experimental Validation Facility was built in 1944 as a static test facility for the B-36 Peacemaker, an intercontinental bomber aircraft. The b-36 had a 230 ft wing span and was 162 ft long. The building was large enough to allow the B-36 to be raised vertically with its nose pointing straight up.

The facility's mission is to further aerospace structure technologies through research and development. Through modeling techniques, analytical prediction, and exposing structures to the stresses of noise, vibration, and heat, researchers study the conditions experienced by air and space vehicles during flight. Scientists use the results of this research to solve various aircraft dynamics problems and ultimately increase aircraft readiness levels.

9.9. COMPOSITES

9.9.1 NONDESTRUCTIVE INSPECTION OF COMPOSITE REPAIRS

Cu Nguyen, FAA, William J. Hughes Technical Center

In the aviation industry, structures repaired in the composite shop are generally cured in autoclaves, but repairs made on the aircraft may be done under more varied conditions and efforts must be made to ensure that the repaired composite components are mechanically sound.

Funded through the FAA Airworthiness Assurance Center of Excellence, Iowa State University undertook the development and implementation of two complementary NDI methods for composite repairs: Computer-Aided Tap Tester (CATT) and Air-Coupled Ultrasonic Testing (AC-UT).

The tap test needs only one-sided access but has a limited probing depth. The CATT, being a semiautomated and quantitative technique, can be used to map out the interior conditions of a repaired part (see Figure 9.9-1).

The AC-UT, shown in Figure 9.9-2, is most effective in the transmission mode that inspects the entire thickness of the structure. The AC-UT technique, with its obvious advantage over water-coupled ultrasound, has the potential to be a practical NDI tool for airplane inspection. A primary objective of the current work is to correlate the interior conditions of a repair with the features in the image from the CATT and AC-UT techniques.

In this work, the CATT and the AC-UT system were applied to a number of composite repairs, both good and defective, on test panels and real components. The results were described and compared. One test panel containing a defective repair was destructively sectioned. The findings were compared to both the AC-UT and the CATT images.

After scanning with the CATT and the AC-UT system, the repair panel slated for destructive sectioning was cut with a diamond saw, polished, and examined under an optical microscope. Figure 9.9-3 shows the saw cut surface and the cross section of the repair.

The CATT and the AC-UT images were enlarged to true size and physically matched to the sectioned surface. These direct comparisons are shown in Figure 9.9-4 for the CATT image and in Figure 9.9-5 for the AC-UT image. In Figures 9.9-4 and 9.9-5, the delamination matched very well with both images. Overall, the features in both the CATT and the AC-UT images corresponded quite well with the internal conditions of the repair.

Both the CATT and AC-UT systems were recently field tested at the United Airlines facility and at American Trans Air, both in Indianapolis, IN. The CATT system was used to image two hail-damaged components at United Airlines, a B737 trailing edge and an upper panel of an Airbus A320 horizontal stabilizer. The AC-UT system was used to inspect the B737 trailing edge by mounting the air-coupled transducers on a yoke that was hand held. Results from these field tests correlated well with the sectioned repair and indicated that the imaging capabilities of both the CATT and AC-UT make these methods far more intuitive, accurate, and user-friendly than currently used methods such as coin tap and mechanical impedance analysis.

9.9.2 QUALITY ASSURANCE METHODS FOR FIBER-REINFORCED COMPOSITES

Curtis Davies, FAA, William J. Hughes Technical Center

General aviation has primarily dominated the recent growth of new composite aircraft and composite material applications in primary structures. Figure 9.9-6 shows three types of composite structure aircraft that are currently being certified. With this growth of general aviation composite applications, certification issues have emerged with respect to the exact philosophy of quality control and assurance methods required to guarantee a safe and consistent material supply.

Unlike metallic materials used in structural part manufacturing processes, the material properties of composite materials are dependent on the fabrication process. Therefore, it is essential that material procurement and processing specifications used to produce composite structures contain sufficient information to ensure that critical parameters in the material manufacture and structural fabrication process are controlled and they maintain adherence to the expected part requirements. Due to the wide variety of composite structures now emerging for certification (particularly for general aviation aircraft), control of the materials is rapidly becoming a vital issue with respect to the overall assurance of safety.

In composites, a key link in the overall part and application success is the material and process specifications used for the design. Currently, most general aviation manufacturers generate material and process specifications that are unique to them, and each manufacturer places those unique requirements upon the material vendor. These multiple material and process specifications then cause the vendor to tailor the same material supplied to different companies in order to meet the companies' individual specification. This leads to an unstable material supply that requires additional control at the airframe manufacturer to guarantee adherence to the specification and design application. Metallic materials do not suffer the same complication in manufacture and delivery because of availability of common industry specifications.

The performed research identified all criteria for both material procurement specifications and material fabrication specifications based on known quality assurance methodology. It also identified areas requiring quality assurance development. In the areas needing additional technology or research for manufacturing and fabrication process controls, this project proposed new investigations to develop a methodology to meet the goal of consistent and reliable control of composite products.

For material procurement control criteria, the following items were considered: basic fiber, matrix, and cured component characteristics; chemical, mechanical, and physical properties; safety and health information; transportation; storage; handling; and testing, including type, number, and frequency of tests. For processing control criteria, the following were considered: process information, including fabrication methods and environmental conditions; inspection criteria at each operation; storage and handling throughout the process; process controls (cure cycle parameters, out time); materials; test specimen construction and processing; personnel qualifications; and tool proofing and control.

The developed guidelines for material procurement and processing specification requirements included the best industry practice in testing, data analysis, inspection, material and process control as enumerated in the surveyed specifications, investigators experience, and industry review.

The following FAA technical reports were produced giving guidelines in material procurement and processing specification requirements for unidirectional prepreg tape material systems.

- "Guidelines for the Development of Process Specifications, Instructions and Controls for the Fabrication of Fiber-Reinforced Polymer Composites," DOT/FAA/AR-02/110, Bogucki, G., et al., March 2003.

- "Guidelines and Recommended Criteria for the Development of a Material Specification for Carbon Fiber/Epoxy Unidirectional Prepregs," DOT/FAA/AR-02/109, McCarvill, W., et al., March 2003.

The Material Specification Guidelines report (DOT/FAA/AR-02/109) recommends guidance and criteria for the development of material specifications for carbon fiber-epoxy unidirectional prepreg tape materials used on aircraft structures. A team of industry experts in material specifications, part processing, qualification programs, and design allowables prepared these recommendations. The purpose of this report was to establish recommendations to guide the development of new and revised composite prepreg material specifications. A generalized approach to the development of a shared composite material database was proposed. The approach in this document will remove the restrictions placed on the methods developed by the Advanced General Aviation Transport Experiments to allow a broader market to use the shared database.

The Processing Specification Guidelines report (DOT/FAA/AR-02/110) provides (1) a set of guidelines for the development of process information for the fabrication of continuous fiber-reinforced polymer composite laminate test panels used in the generation of mechanical properties and (2) an approach for the validation of composite fabrication processes used during the certification of composite aircraft structure. A team of industry experts in generating material specifications, processing of composite materials, qualification program management, and design allowables development prepared these guidelines. The guidelines use state-of-the-art processes and sound engineering practices currently used within the aerospace industry.

The success of the initial project led to a second phase to produce similar documents for a fabric carbon fiber system and a liquid resin molding (LRM) system (e.g., resin transfer molding, vacuum-assisted resin transfer molding, and resin film infusion). Phase II will add guideline information for fabric reinforcement and guidance and recommendations for advanced LRM systems. LRM processes are unique in that the raw materials are, many times, from multiple sources. No single producer is able to certify that the combined constituents conform to expected standards. In addition, the combining of the materials in the part fabrication creates more unknowns in the repeatability of the engineering properties and adds complexity in the validation and FAA certification process.

This work provides the first level baseline for the establishment of material procurement and processing control, which will meet FAA requirements. The ultimate goal is to provide a catalyst to the initiation of industry standardization that the metallic materials community has enjoyed for years. These documents form the basis for a new FAA Advisory Circular that will be released in FY04. With the initiation of Phase II, a larger range of applications will develop standardized control methodology.

9.9.3 QUANTITATIVE ASSESSMENT OF CONVENTIONAL AND ADVANCED NDI TECHNIQUES FOR DETECTING FLAWS IN COMPOSITES HONEYCOMB AIRCRAFT STRUCTURES

Dave Galella, FAA, William J. Hughes Technical Center

The aircraft industry continues to increase its use of composite materials. The extreme tolerance to damage and the high strength-to-weight ratios of composites have motivated designers to expand the role of fiberglass and carbon graphite in aircraft structures, most notably in the area of principal structural elements. This has placed greater emphasis on developing improved NDI methods that are more reliable and sensitive than conventional NDI. The FAA Airworthiness Assurance NDI Validation Center (AANC) at Sandia National Laboratories has been pursuing this goal by studying a number of composite structure inspection methods.

Through participation in the Commercial Aircraft Composite Repair Committee Inspection Task Group, AANC has been investigating the need for improved inspections of composite structures. Most composite honeycomb structure inspections are performed visually and supplemented by tap test methods. Tap testing uses an audible change in acoustic response to locate flaws. Other more sophisticated NDI methods, such as ultrasonics or thermography, have been applied to an increasing number of applications to detect voids, disbonds, and delaminations in adhesively bonded composite aircraft parts. Low-frequency bond testing and mechanical impedance analysis tests are often used to inspect thicker laminates.

A probability of detection (POD) experiment was recently completed that compared the ability of conventional and advanced NDI techniques to detect various flaws within typical aircraft honeycomb panels. Figure 9.9-7 shows a common honeycomb sandwich construction. A series of composite honeycomb specimens with statistically relevant flaw profiles were inspected with tap test equipment and more sophisticated techniques introduced to automate and improve composite NDI. The honeycomb specimens were fabricated with either fiberglass or carbon laminate skins with a three-, six-, and nine-ply thickness. Each specimen had a 1-inch Nomex® core. Engineered flaws representing skin-to-core disbonds, ply delaminations, crushed core, and impact damage of varying sizes were contained throughout the specimen set. The specimens were inspected at numerous airline maintenance shops and third-party repair facilities by actual inspectors using a variety of inspection methods. Methods used as part of this study included manual tap hammers, automated tappers, low- and high-frequency bond testers, mechanical impedance analysis, pulse-echo ultrasonics, thermography, shearography, laser Doppler velocimetry, C-scan ultrasonics, laser ultrasonics, air-coupled ultrasonics, acoustography, and phased array imaging devices. In all, eight conventional and ten advanced NDI techniques were studied. Figure 9.9-8 shows an airline inspector using a bond-testing device on one of the test panels.

From the collected data, performance curves were produced to establish both a baseline of current inspection techniques and to demonstrate the improved performance through the use of more advanced NDI techniques and procedures. The study presents the results from a wide array of NDI methods and identifies the limitations and optimum applications for specific inspection methods. Figure 9.9-9 shows the results for several conventional NDI devices used to inspect the six-ply carbon test panels. The curves show the relationship of the POD for each technique used in the test. Curves above and to the right represent the better performing inspection methods.

9.9.4 A COMPARISON OF CEN AND ASTM TEST METHODS FOR COMPOSITE MATERIALS

Peter Shyprykevich, FAA, William J. Hughes Technical Center

A detailed comparison was performed to assess the equivalence of the Committee for European Standardization (CEN) and ASTM International test methods. Both methods are identified as test methods to be used to determine composite material properties in the SAE International Aerospace Material Specifications (AMS) 2980 and 3970. The comparison was done to understand the differences between the two methods and to facilitate data acceptance and standardization. The comparison included both the parameters associated with the two comparable test methods and the additions and changes listed in the AMS specifications. For tests where only one method is specified in the AMS specifications, a second comparable ASTM or Suppliers of Advanced Composite Materials Association (SACMA) test method was used for the comparison. A total of 16 different mechanical and chemical test methods were compared.

For each type of test, the comparison focused on the geometric features of the specimen and test fixture, parameters associated with the test procedure, data reduction, and reporting. For every parameter listed in the comparison tables, an assessment of the equivalence was made using a 0-4 rating scale. An FAA report, “A Comparison of CEN and ASTM Test Methods for Composite Materials,” DOT/FAA/AR-04/24, Adams, D., June 2004, summarizes the comparisons of the test methods and emphasizes the most significant differences between the test methods.

Based on the comparative assessments, it was determined that for 4 of the 16 types of tests, follow-on testing was needed to obtain additional test data to completely assess the test method equivalency. Their selection was not a reflection of their degree of equivalency relative to the other types of tests. The four types of tests subjected to follow-on testing were (1) lamina compression testing to assess the effects of gage length, (2) laminate compression testing to assess the effects of the loading method, (3) in-plane shear testing to investigate the effects of specimen thickness, and (4) constituent content determinations to investigate the effects of specimen size and weighing accuracy and method availability.

The comparison tests were performed on laminates made from Toray T700G/2510 carbon/epoxy unidirectional prepreg tape and from Fibercote T300/E-765 3K plane weave carbon/epoxy prepreg fabric. The mechanical tests were at room temperature and at an elevated temperature of 180°F with infused moisture.

For example, Figure 9.9-10 shows a comparison of the unidirectional compression test data at room temperature. The figure shows that there is a reduction in compressive strength with an increase in gage length, particularly for tape laminates.

Both test methods use the modified ASTM D 695 fixture; however, ASTM requires a 3/16″ gage length, while SACMA requires a 1/2″ gage length. The ASTM test fixture is shown in Figure 9.9-11, and the SACMA fixture is shown in Figure 9.9-12. As expected, the longer gage length CEN specimens produce lower compression strengths, especially for the unidirectional tape laminates.

The study has provided a blueprint to compare different test methods for the harmonization of different test standards. In this particular case, the study will allow acceptance of material data into MIL-HDBK-17 for worldwide use.

9.9.5 BONDED STRUCTURES SAFETY AND CERTIFICATION RESEARCH

Curtis Davies, FAA, William J. Hughes Technical Center

Bonding is used in numerous manufacturing and repair applications on civil aircraft structures. This includes small airplanes, transport aircraft, and rotorcraft. An example of a bonded structure that was used in a recently certified airframe design is shown in Figure 9.9-13. The technical issues for bonding are complex and require cross-functional teams for successful applications.

The structural integrity of bonded joints can be weakened by a number of factors, including manufacturing defects that occur during airframe production, operational defects, and damage that occurs during operation. Over the last 30 years, major aircraft companies have developed strategies to ensure that these issues are controlled during production of bonded aircraft structure.

In addition to the mechanical aspects of the joint, two other areas require further study: (1) the inspection techniques to detect imperfections or defects and (2) the quality assurance of bonded joints before certification and during service. One goal in this area is to determine what types of defects can and cannot be identified through NDI.

Over the last several years, the FAA William J. Hughes Technical Center has investigated a number of areas associated with bonded structures. These investigations have centered on (1) how bondlines found on general aviation (GA) aircraft differ from traditional structural bonds, (2) surface preparation of composite materials, and (3) the analysis of adhesively bonded composite joints. Details of these investigations are available in reports at the FAA William J. Hughes Technical Center library website http://actlibrary.tc.faa.gov.

Even though more and more airframe designs are using composite joints, an approved, recommended procedure for characterizing and procuring adhesive does not exist in the industry. Currently, most airframe companies propose and iterate on a procedure with an FAA Aircraft Certification Office to develop a test plan for qualifying allowables to use for bonded joints. Material and processing specifications for the adhesive are also developed during this process. These test plans and specifications are unique for each application. One purpose of this program is to develop standardized characterization and procurement methodologies for developing adhesives to be used in aircraft structural bonding applications.

Historically MIL-HDBK-17, which the FAA sponsors, has proposed an overall philosophy for the development of adhesive characterization for bonding. The Handbook covers available test methods as well as some design considerations for bonded joints. It does not describe a methodology for generating design-allowable properties for a selected adhesive system or a procurement procedure for the adhesive.

In 2004, the FAA organized an effort to benchmark bonded structures as part of its ongoing composite safety and certification initiatives. The primary objective was to document the technical details that need to be addressed for bonded structures, focusing on safety issues and certification considerations. Examples of proven engineering practices used to address selected technical details will also be documented as part of this effort. The process of benchmarking existing technology will provide direction for future research and development (R&D) in the field. A strong alliance with the industry, other government groups, and academia for safety and certification issues is expected to result from the benchmarking process.

The first step in this effort was to create a comprehensive survey to address questions and concerns associated with bonded structures from discussions with experts and practitioners from around the world. Airframe manufacturers, material suppliers, and other groups in the aircraft and adhesive bonding industry completed the survey. This gave an understanding of the state of bonded structure applications and technology.

The collected output of the survey was reviewed at an FAA-sponsored workshop held in June 2004. With the same industry representatives, the trends in the survey data were reviewed, and the group agreed on further actions related to bonded structures. The results of the survey and the workshop will become part of an FAA technical report on best practices in bonded structures that will be published in the future.

The approach of working with government, academia, and industry experts will yield documents that provide a practical engineering guide, with educational value for an expanding work force. Over time, the FAA will continue to seek input from industry and other government agencies in drafting consistent policy and guidance for bonded structures for successful industry applications.

9.9.6 TESTING AND EVALUATION OF EXPANDED TECHNOLOGY PRODUCTS IN COMPOSITE MATERIALS

Jude Restis, Fatigue Technology Inc.

Composite structures can be assembled faster and more easily with the use of expanded technology products. Expanded technology products include interference fit bushings, interference fit rivetless nutplates, expanded fit grommets and one-sided expanded nuts.

One example where the use of this technology saved manufacturing time is the assembly of composite to metallic joints. In one application, because of the thermal mis-match between the metallic and composite materials, the metallic structure was fatigue critical. To provide the desired fatigue life in the metallic component it would have to be cold worked. In order to perform typical cold working, the components would have to be de-stacked to only expand the metallic component. FTI developed a method of using expanded fit bushings in both components, with closely controlled expansion levels in each component. Using this technology, allowed the structure to be assembled without disassembly for cold working. By controlling the level of expansion in each component, the desired fatigue benefit can be achieved in the metallic component without damage to the composite component.

The use of expanded technology products in composites also provides structural benefits such as open hole compression capability, protection from wear and tear damage, and increased lightning strike resistance.

In order to use expanded technology products in composites, FTI has undertaken extensive tests to evaluate the material behavior with expansion, and to quantify the benefits. This test program includes; damage, retention, static and fatigue with no load transfer, static and fatigue with load transfer, lightning strike, corrosion and conductivity.

9.9.7 AIR VEHICLES DIRECTORATE SOFTWARE AIDS IN A-10 MAINTENANCE ISSUE

1st Lt Luis E. Martinez and Jim A. Harter, USAF AFRL/VASM

The Air Vehicles Directorate developed software that the Ogden Air Logistics Center (OO-ALC) used to design the first A-10 boron patch. This software, as part of the Composite Repair of Aircraft Structures (CRAS) program, provides a design and analysis tool for bonded repairs that decreases maintenance and support costs while increasing aircraft availability.

The directorate coordinated with Boeing to develop CRAS software. CRAS provides validated and demonstrated technology improvements for bonded repair design and analysis of bonded repairs to a damaged metallic structure.

This technology was transitioned to OO-ALC, who used it to design a patch for an A-10 wing segment. Technology challenges addressed by CRAS and applied to patch performance include nonelliptical patch configurations, out-of-plane bending, residual thermal stress, skin thickness effects, elastic-plastic bond-line analysis, proximity influence of adjacent patches, and tapering effects.

In the past, cracks in aging aircraft structures were repaired with mechanically fastened repairs to restore static strength and restrict damage growth. These repairs were easily installed, but they had significant drawbacks including weight addition, parent material removal, and stress riser introduction. Currently, adhesively bonded composite repairs are a desirable alternative.

Bonded repairs are lightweight, thin, corrosion resistant, and conform to the original structure. They eliminate stress risers because “bonding” a composite patch to the structure eliminates the need to drill holes for fasteners. In addition, the composite patch does not interfere with nondestructive inspection of the underlying damaged structure.

CRAS is a Microsoft Windows® application. It creates and analyzes designs for bonded composite repairs to metallic structures with cracks and corrosion grindout areas. It also uses a finite element model generator to analyze repairs for holes, holes with grindouts, dents, and cutouts. The Windows Graphical User Interface displays the CRAS results, which can be printed.

In the first practical application of the CRAS software, OO-ALC scientists designed a patch used to repair a corrosion grindout on the A-10’s upper wing surface. The CRAS software is also being used to fix a crack in the A-

10 wing station 90. Use of these patches will decrease fleetwide A-10 depot time, resulting in decreased maintenance costs and increased aircraft availability for the warfighter.

9.9.8 COMPOSITE REPAIR OF AIRCRAFT STRUCTURES

1st Lt Luis E. Martinez and Jim A. Harter, USAF AFRL/VASM

The Composite Repair of Aircraft Structures (CRAS) program provides a design and analysis tool for bonded repairs that decreases maintenance and support costs while increasing aircraft availability. The CRAS software facilitates designs of bonded composite patches for relatively flat repair configurations. Those designs may be used as the starting point for critical or complex repairs that will generally undergo final design by finite element procedures. The Windows-based software uses an iterative design process in which the patch design is continuously modified until it meets all specified design criteria. CRAS was used to design patches for corrosion grind-outs on an A-10 upper wing skin at Ogden ALC. (See Figure 9.9-14)

9.9.9 ENTERPRISING COMPOSITES DESIGN AND STRUCTURAL ANALYSIS TOOL DEPLOYED TO ROTORCRAFT INDUSTRIAL PARTNER

USAF Air Force Research Laboratory (AFRL)

AFRL researchers and the University of Dayton Research Institute developed a unique composite material design and structural analysis tool to provide design solutions, reduce design cost, and improve flight operations safety for military, industrial and commercial helicopters and other rotorcraft. The new, laboratory-developed design and analysis tool provides rapid solutions early in the design process to assess component damage tolerance and has the potential to trim component risk reduction costs and schedules by as much as 50%. The new technology also enables mission enhancement improvements in certification and supportability.

The team's new tool provides a quicker and less expensive means to characterize and predict the behavior of flawed or damaged structures used to build the associated aircraft. Researchers coordinated with the United Technologies Research Center to develop the technology and transferred it to the Sikorsky Aircraft Corporation. Scientists are adapting the new tool for rotorcraft applications for the Department of Defense.

9.9.10 BONDED REPAIR OF THICK/COMPLEX STRUCTURES

1st Lt Luis E. Martinez and Jim A. Harter, USAF AFRL/VASM

The Bonded Repair of Thick/Complex Structures program will expand the use of bonded repairs into thick and complex structures. This program has developed a repair for the F-16 341 bulkhead attach flange radii. A demonstration of structural health monitoring (SHM) has been completed to show the feasibility of SHM on this complex part. The program is also validating the CRAS software on actual fuselage pieces in several different repair configurations. Two bonded repair situations that are not clearly understood will be explored in this program: stress corrosion cracking (SCC) and compression dominated structure. The factors that affect SCC and structures in compression will be quantified, and the data will be used to update the current bonded repair guidelines. (See Figure 9.9-15)

9.9.11 DURABLE LOW-COST FUSELAGE MONOCOQUE STRUCTURE

Karen D. MacKenzie, Boeing, Seattle

The challenge of aluminum fuselage design is developing a low cost, lightweight monocoque structure with good static and fatigue performance. These goals are often in conflict, that is, a benefit to one is a detriment to the other. However, Boeing has developed a monocoque design that incorporates several cost and weight reduction features while meeting all FAA/JAA structural requirements.

This structure includes several innovative features. It includes a new method of transferring stringer load to the frame without separate clips. It takes advantage of high speed machining advancements and includes monolithic frames that attach to the skin without separate shear ties. It also includes monolithic machined floor beams and an innovative seat-track attachment that resulted in further weight reduction. The design simplifies the assembly process, requires fewer fasteners and requires less tooling.

A full-scale single-aisle fuselage section (as shown in Figure 9.9-16) was designed and subjected to 5 lifetimes (378,000) pressure fatigue cycles. A complete post-test inspection found no crack initiation.

Boeing then designed and built a full-scale twin-aisle fuselage section (as shown in Figure 9.9-16) that will be subjected to a full set of fatigue loads (body bending and shear, floor loading and pressure). The fatigue, fail-safe and static testing of this structure will be completed in 2003 and 2004.

9.9.12 EVALUATION OF AGING COMPOSITE HORIZONTAL STABILIZERS

Matthew Miller, Boeing, Seattle

Major carbon-fiber-reinforced polymer (CFRP) structural applications entered service in the late 1970s / early 1980s and are beginning to be retired. Boeing has acquired two ship sets of the NASA ACEE 737 CFRP Horizontal Stabilizers as shown in Figure 9.9-17. These stabilizers have been in continuous airline service for the past 18 years. Their age along with a varied operational climate make these components ideal for the investigation of the effects of long-term environmental exposure and in-flight loading on complex composite primary structure. These components are being used to validate design, analysis, certification, inspection, and repair philosophies that are widely used throughout the fleet.

Following simulated inspection using standard procedures provided to the airlines, one or more of the stabilizers will be the subject of a thorough teardown examination. This will include detailed inspection for signs of structural distress such as delaminations in the composite structure, an assessment of the quality of repairs, and an examination of the interface between the aluminum and graphite-epoxy components for signs of corrosion. In addition, physical and mechanical properties in the CFRP including degradation in the resin, breakdown in the adhesion to the fibers and chemical composition changes will be evaluated. The effectiveness of design features such as lightning strike protection will be assessed. The stabilizers will are also being used to investigate new and emerging NDE procedures. Additional static or fatigue testing may be undertaken for comparison with comparable data generated during the original certification program.

A preliminary evaluation shows that the stabilizers are in generally satisfactory condition. However, retirement from service was prompted in at least one case by stringer delamination adjacent to the inboard region of the upper surface adjacent to the fuselage. It is believed this resulted from unanticipated “step” loads induced while work was being performed on adjacent components.

9.10. REPAIR AND LIFE EXTENSION

9.10.1 BONDED REPAIR OF CORROSION GRIND-OUTS

Stephan Verhoeven, Cornelis Guijt and Scott Fawaz, U.S. Air Force Academy

The US Air Force is operating a large fleet of aging aircraft. Some examples of problems that aging aircraft can encounter, among others, are fatigue and corrosion. This research focuses on bonded repair of exfoliation corrosion in the upper wing skin of a military transport aircraft. In the past, bonded repairs have shown to be a very effective repair method, in situations where riveted repairs did not work, and/or replacement of the part was cost prohibitive or impossible due to the lack of replacement parts.

Upper wing skins on this transport, made out of 7000 series aluminum, have shown extensive exfoliation damage, mainly around the fastener holes. Exfoliation corrosion is a form of intergranular corrosion associated with high strength aluminum alloys. Heavily worked alloys with a microstructure of elongated grains are especially susceptible to exfoliation. Corrosion products will build up along the grain boundaries and eventually result in layers of the material peeling or flaking off.

The current approach to deal with this damage is to remove the exfoliated material by grinding it out, and not replacing the removed material. Depending on the location on the wing, local grind-outs are allowed up to 25% of the skin thickness. If the exfoliation extends beyond this limit, this approach is no longer allowed since too much material is lost. Replacement of the wing plank might be necessary, making this damage very costly.

The purpose of this project was to develop a bonded repair method that restores structural integrity to corrosion grind-outs that are deeper than the current allowable grind-out depth of 25% of the skin thickness, so that severe corrosion cases can be handled without the possible need for replacement. To significantly expand the current T.O. limits, grind-outs with a depth of 66% of the skin thickness were considered.

One of the most important requirements was that the repairs needed to be flush with the contour of the wing skin. Three different types of repairs were considered: 1. Aluminum repair 2. Boron-epoxy repair 3. Hybrid repair, a combination of aluminum and boron-epoxy. Specimens were tested in fatigue in order to come to the most efficient and durable repair concept.

It was found that:

- The application of a flush repair seems a viable repair option for corrosion damage that is exceeding the current T.O. limits, in a compression dominated structure.
- Fatigue tests, both constant amplitude and spectrum loading, showed that from a durability standpoint the best options are either a hybrid repair or an aluminum repair.
- Hybrid repairs are preferred based on:
  - slowest crack growth
  - damage tolerant patch
  - no compression problems under realistic flight loading conditions
- Aluminum patches can be a good alternative if residual thermal stresses and thermal stresses under operating conditions become a problem.
- Aluminum repairs showed no patch cracking problems.
- Boron-epoxy should be avoided due to delamination problems under compressive fatigue loading.
- Keeping the grind-outs as small as possible does put pressure on design guidelines for bonded repairs. Depending on location/loading/operating temperature, patches could need re-sizing.
- Cracks do grow in compression-compression fatigue cycle due to thermal residual stresses (boron and hybrid)

9.10.2 FATIGUE OF SHOT PEENED 7075-T7351 SENB SPECIMEN - A 3-D ANALYSIS

Takashi Honda, National Institute of Industrial Safety, Japan and Mamidala Ramulu and Albert S. Kobayashi, University of Washington

This exploratory study addresses the effect of shot peening on fatigue crack growth in the presence of a crack tip or a corner singularity in 7075-T7351 aluminum specimens. Nine as-received and twenty four shot peened (Alman scale: 0.004A, 0.008A, 0.012A and 0.016A) single-edged notch bend (SENB) and eighteen three point bend (TPB) specimens, all of which were machined from a 8.1 mm thick 7075-T7351 aluminum plate, were fatigued with the crack in the L-T direction. The entire surface of the specimens were shot peened to reduce if not eliminate crack closure [1]. The cast steel shots generated a rougher surface than the surface of the 7050 aluminum alloy which was peened with glass beads [2]. Cyclic load was applied at 2 to 15 Hz with load ratios, R = 0.1 or 0.8. The crack tunneling profiles were recorded in thirty three SENB specimens, which were either fatigued to failure or fatigued to a predetermined number of cycles and fractured. The eighteen as-received and shot peened (0.004A and 0.016A) TPB specimens (without pre-notching) were fatigued to failure at various stress levels and an *S-N* diagram was constructed. The striations in the SEM micrographs were used to calculate the crack growth rate, *da/dN*. The residual stress distribution in as-received and shot-peened (0.004A to 0.016A) specimens were measured by using an X-ray diffraction stress analyzer. The stress intensity factor, K, along the curved and tunneled crack front in the SENB specimen was obtained through the J integral computed from a 3-D finite element analysis. The 3-D K along the curved and tunneled crack front in a loaded SENB specimen with residual stress was obtained by the superposition of the 3-D K of a loaded SENB specimen without residual stress and the 3-D K of an unloaded SENB specimen with residual stress.

No significant difference was noted between the crack front profiles at failure of the as-received and shot-peened (0.004A and 0.016A) SENB specimens at R = 0.8 and at R = 0.1. The observed two order of magnitude increase in the fatigue life of R = 0.8 over that of R = 0.1 was due to the 78 percent decrease in $\Delta\sigma$ for the latter.

The residual stress distributions in as-received and shot-peened (0.004A to 0.016A) specimens are shown in Figure 9.10-1. The maximum subsurface compressive residual stress increased and moved inwards with increasing shot peening intensity, consistent with published results. Figure 9.10-2 shows the 3-D stress intensity factor, K, of the loaded SENB specimen at successive crack growth. The maximum local *K with residual stress* is equal to the nominal fracture toughness of 7075-T7. Figures 9.10-3 and 9.10-4 show the *da'/dN* versus ΔK relations at the center and the left side of SENB specimens, as received and shot peened at intensities of 0.004A to 0.016A, respectively. *da'* in these figures represents the forward motion of the crack front growth. As expected, the residual stress generated by shot peening did not affect the crack growth rate at the center of the crack front as shown in Figure 9.10-4. Shot peening, however, affected the crack growth rate at the edge of the crack front. The crack growth rate at the initial phase of crack growth, i.e. at the machined notch tip, in the shot-peened specimens is significantly higher than that of the as-received specimen. The crack growth rate of all shot-peened SENB specimens, except that shot peened at 0.008A, converged together at the higher ΔK, i.e. after substantial crack propagation. The crack propagation rate of the as-received specimen was lowest for all driving forces.

Previous study of shot peened, 7075-T7351 TPB specimens [3], suggested that the higher crack growth rates at the left side of the shot peened SENB specimens was due to the surface damage inflicted by the shots. The SEM photographs of the fracture and side surfaces of an SENB specimen shot peened at 0.016A showed large embedded defects caused by the subsurface folding at the machined notch tip and resulted in a higher crack growth rate at the initial phase of fatigue crack propagation. The smaller embedded defects in the subsurface folded texture along the specimen surface accelerated crack growth rate in the subsequent phase of crack growth. Thus the beneficial effect of the residual compressive stress is offset by the subsurface damage, both of which are induced by shot peening of 7075-T7351 aluminum SENB specimen.

REFERENCES

1) X. Y. Zhu and W. J. D. Shaw (1995). Correlation of Fatigue Crack Growth Behaviour with Crack Closure in Peened Specimen. *Fatigue & Fract. of Eng'g Mat'ls & Struct.* **18**, 811-820.
2) P. K. Sharp and G. Clark (2001). The Effect of Peening on the Fatigue Life of 7050 Aluminum Alloy. DSTO-RR-0208, Department of Defense, Australia.
3) T. Honda, M. Ramulu and A. S. Kobayashi. Effect of Shot Peening on Fatigue Crack Growth in 7075-T7351. To be published in ASTM Journal of Testing and Materials

9.10.3 BONDED REPAIR OF COMPOSITE SANDWICH STRUCTURES

Peter Shyprykevich, FAA, William J. Hughes Technical Center

With the increasing use of fiber-reinforced composite sandwich structures in aircraft components, it has become necessary to develop repair methods that will restore the component's original design strength without compromising its structural integrity. One of the main concerns is whether large repairs are always necessary to restore strength or whether smaller, less-intrusive repairs can be implemented instead. Cure temperature can also become an issue if the repair patch requires curing at 350°F. Residual thermal stresses due to the bonding of the patch to the parent structure may induce further damage to the component. With these concerns in mind, the main objective of this study was to evaluate the effectiveness of scarf repairs applied to sandwich structures, given several bonding repair variables.

The first task investigated the performance of different airline depots in repairing picture frame shear elements using two different repair methods: the Society of Automotive Engineers (SAE) Commercial Aircraft Composite Repair Committee (CACRC) developed a wet lay-up procedure and an OEM prepreg procedure. Each method had different cure temperatures and used different materials. Furthermore, the wet lay-up method required an extra ply, while the OEM method did not. Another difference between the two methods involved the scarf overlap: the wet lay-up method used the conventional 0.5-inch scarf overlap, while the OEM method used a steeper 0.25-inch scarf overlap. All the repaired coupons achieved at least 92% of the average pristine strength regardless of the repair method, as illustrated in Figure 9.10-5, except those coupons from one airline depot that seemed to have been poorly bonded.

The second task performed in this investigation examined the effect of different repair variables on repair performance. The variables considered included three different scarf overlaps, two different core cell sizes (1/8 and 3/8 inch), and impact damage inflicted on the repair. Test results on large four-point bending beams with 1/8- and 3/8-inch cells are shown in figures 9.10-6 and 9.10-7. There was no change in strength or failure strain as a function of increasing scarf overlap for the 1/8-inch cells (figure 9.10-6); however, when barely visible impact damage was inflicted on the overlap area of these coupons, a decrease in failure strain of up to 20% was found for the small overlap length coupons, figure 9.10-7. The behavior of the 3/8-inch cells was quite different as the failure strain decreased for the 0.5-inch overlap length for the undamaged large four-point bending beams, Figure 9.10-6.

The damaged 3/8-inch cell coupons exhibited the same trend with respect to scarf ratio, i.e., overlap length (Figure 9.10-7). Furthermore, damage inflicted in the scarf area caused a decrease in the strength and strain capacities on the order of 10% and 23%, respectively, relative to the undamaged coupons. From the test results, it is apparent that the optimum overlap length is 0.25 inch irrespective of core cell size. It was also found that the 1/8-inch core beams had higher failure strains than the 3/8-inch core coupons for both undamaged and damaged states.

The research performed validates the use of the CACRC repair procedures that are documented in numerous SAE publications and establishes the optimum scarf length for repair of facesheets of composite sandwich structures.

9.10.4 CRACK GROWTH OF ROTORCRAFT MATERIALS

Dy Le, FAA, William J. Hughes Technical Center

One milestone of the FAA National Aging Aircraft Program Plan is to review and update 14 CFR Part 29 regulations and AC material regarding aging issues. The goal is to include damage tolerance (DT) requirements in 14 CFR Part 29.

In 2000, the FAA started the rulemaking process and initiated several joint rotorcraft research and development efforts to support the implementation of the DT requirements and the development or revision of applicable ACs. The FAA plans to implement the DT rule in the future.

One of the research efforts funded by the FAA and conducted by the University of California, Irvine was to examine and quantify the impacts of current life enhancement methods on fatigue life in rotorcraft by focusing on the development and validation of a generalized crack growth analysis model appropriate for all possible rotorcraft components and operating conditions.

To improve the fatigue life of metallic components, especially in the rotorcraft industry, shot peening is widely used. Shot peening is a cold-working process primarily used to extend the fatigue life of metallic structural components. Small spherical particles, typically made of metal with a high hardness, are made to impact the surface of the structural component at a velocity of 40-70 m/s. The shot-peening process consists of multiple repeated impacts of a structural component by these hard spheres causing local plastic deformation, as shown in Figure 9.10-8. The elastic subsurface layers should theoretically recover to their original shape during unloading. However, continuity conditions between the elastic and plastic zones do not allow for this to occur. Consequently, a compressive residual stress field is developed in the near-surface layer of the structural component. Since fatigue cracks generally propagate from the surface of structural components, the resulting surface compressive residual stress field is highly effective in improving the early fatigue behavior of metals. The compressive residual stress field can significantly decrease the crack growth rate of short surface cracks. As a result, the extension of fatigue life of shot-peened structural components can be determined.

Despite the complexity of the shot-peening process, there have been attempts to determine the residual stress field using approximate approaches and closed-form solutions. However, application of the Hertzian contact theory and an approximate elastic-plastic analysis for the surface layer can better estimate the distribution of the compressive residual stress field due to shot peening, as shown in Figure 9.10-9. Residual stress distributions with better precision can be obtained with the use of numerical methods and computer simulation of the whole shot-peening process. Typically, the shot-peening simulation is divided into two steps. The first step is a dynamic analysis of the shot workpiece contact, which is aimed at the determination of boundary conditions for the second elastic-plastic step. The second step is a quasi-static elastic-plastic analysis, which produces the distribution of residual stresses.

Early models used to predict residual stresses describe the shot-peening process as a quasi-static case. As a result, the velocity of the shot is not taken into account, and empirical parameters are used. The newly enhanced model developed under this current research takes the primary shot-peening factors into consideration, including characteristics of the material, diameter, and velocity of the shot.

The flow chart in Figure 9.10-10 depicts the enhanced model for the calculation and prediction of the residual stresses due to shot peening. In this enhanced model, no empirical relations or parameters are used.

The approach used in this research to model fatigue crack growth in shot-peened structural components, as shown in Figure 9.10-11, consists of (1) using the finite element alternating method for computing fracture mechanics parameters for the crack and (2) using the approximation approach based on the plastic strip model for predicting crack growth rates.

The crack is modeled by the Symmetric Galerkin Boundary Element Method as if it were in an infinite medium. The finite element method is independently used for the stress analysis of the uncracked structural component subjected to the applied loading. Proper superposition of two solutions was applied through the use of an iterative-alternating procedure. The effect of the residual compressive stress field on crack propagation was performed via an analysis of shot-peened 7075-T7351 aluminum plates (1.8-mm-thick, double-edged specimens). Figure 9.10-12 shows the fatigue crack growth (da/dN) data versus the stress-intensity factor range (ΔK) of 7075-T7351 specimens. AGILE 3D and NASGRO models were used to simulate the tests and demonstrate the effect of the shot peening on fatigue crack growth.

The plot in Figure 9.10-13 depicts the effects of shot peening on fatigue crack growth. Full validation of the developed model for the calculation and prediction of the residual stresses due to shot peening and other life enhancement techniques is needed for use in advisory materials. Design optimization techniques, through which the fatigue lives of rotorcraft components can also be optimized, will also become available for use in advisory materials.

9.10.5 EVALUATION OF CRACK GROWTH IN THE PRESENCE OF RESIDUAL STRESSES FROM THE COLD EXPANSION PROCESS

Jude Restis, Fatigue Technology Inc.

The split-sleeve cold expansion process of Fatigue Technology Inc. (FTI) has been used for over 35 years by the aircraft industry to improve the fatigue life of structures by inducing compressive residual stresses around holes.

Current methods of predicting the fatigue life and crack growth from cold expanded holes demonstrated a lack correlation between the predicted and actual crack growth and have also been shown to be very sensitive to possible errors. Since a good correlation of the predicted and real crack growth is essential to an accurate and efficient damage tolerance program, the applicability and effectiveness of the current method is questionable.

A preliminary three-dimensional Finite Element Analysis (FEA) investigation into the crack mechanics indicated that the crack front shape of a cold expanded hole was distinctly different than crack growth from a non-cold expanded hole. A series of fatigue tests of 7075-T651 open hole dogbone specimens were run to investigate the crack front shape. The results showed that the crack front shape was significantly different from a cold expanded hole than a non-cold expanded hole and varied with thickness.

The distinct P shaped crack front shape was investigated further by growing a crack from a cold expanded hole in a 3-D Finite Element Analysis Model. At this stage in the development of the model, Crack Tip Opening Angle (CTOA) was used as an indicator of relative speed of crack growth in various directions rather than associating it with an absolute crack growth rate. The model showed a similar crack front shape via the simple CTOA criterion as the experiments due to the complex thru thickness residual stress distribution. This thru thickness distribution was the cause for the P shaped crack and the faster crack growth observed on the entry side than the exit side surface of the cold expanded specimens.

Because the crack front shape of a cold expanded hole is different than a non cold expanded hole, any prediction method is better served by accurately modeling the real crack growth rather than correlating the life with a model of a physical different crack shape with a slower crack growth rate.

Research focus will continue on accurately predicting the growth pattern before moving to predicting rate of crack propagation. Once the crack growth pattern is properly modeled, work will begin on crack growth and fatigue life prediction methodology.

9.10.6 STRUCTURAL WEIGHT SAVINGS UTILIZING RESIDUAL COMPRESSIVE STRESS AND DERIVATIVE PROCESSES

Jude Restis, Fatigue Technology Inc.

The science of inducing residual compressive stress around fastener (and other) holes has shown a great tolerance for applied tensile stress. Fatigue life improvement from the incorporation of these beneficial residual stresses has been well documented over the past three decades. A new emphasis utilizing the benefits of Cold Expansion residual stresses to reduce structural weight has been investigated and will be discussed.

Testing and advanced analysis tools have shown the structural weight savings using Cold Expansion. Several test programs have been initiated comparing the structural weight at a fixed fatigue life between non-cold worked holes and cold worked holes. Structural weight was removed in test samples that were processed with the cold expansion process until the test life was the same as the non-cold worked case. Conservative test results showed a 30% structural weight reduction with cold expansion. Similar testing and analysis was run on other advanced processes such as a rivetless nutplate system (ForceTec), and a high interference fit bushing installation system (ForceMate). Both of these systems also showed significant weight savings over more traditional systems.

9.10.7 EFFECT OF COLD EXPANSION ON THE FATIGUE LIFE OF HOLES WITH STRESS RATIO = -2.0

Jude Restis, Fatigue Technology Inc.

FTI completed testing to investigate the feasibility of using cold expansion, or the installation of expanded ForceTec Rivetless nut plates or ForceMate bushings for the retrofit of lower longerons of a fighter aircraft subjected to a compression dominated fatigue spectrum. The test coupons were open hole and made from Ti-6Al-4V (STA). The test fatigue loads were constant amplitude cycles with a stress ratio $R = -2.0$ and maximum gross stress of 30ksi. Three configurations were tested comparing them to a baseline of a non-cold expanded hole. The objective was to demonstrate that cold expansion or the ForceTec nut plates or bushings provided at least a 2:1 Life Improvement factor (LIF). Crack growth was also measured to determine crack initiation.

Fatigue crack growth analyses were made with regression of fatigue life back from failure or back from the fatigue crack lengths measured. At least two of the ForceTec specimens went to run out of 108,000 and 138,000 cycles without failure. LIF's were determined two ways; assume the crack initiation life is 50% of the test life to failure and, subtracting the analytical crack growth life from the test life to failure. For cold expanded holes the LIF > 2.88 with a minimum of 2.12 for a single specimen. For the ForceTec (bushed) holes the LIF> 13,23 for an average of three specimens. The minimum LIF was 4.06 for a single specimen. Based on these results it was recommended to repair the lower longerons using ForceTec Nut plates or ForceMate bushings as appropriate.

9.10.8 ANALYSIS AND FATIGUE TESTING OF A NEW FASTENING SYSTEM FOR THE F-16

Jude Restis, Fatigue Technology Inc.

TukLoc is a replacement fastening system for the problematic NAS 1734 "Elliptical Press Nut" which has shown a propensity to leak, migrate in the hole, and develop premature fatigue cracks in the F-16 Wing. The most significant improvement over the legacy product is the interference fit generated as a result of cold expanding the TukLoc into the parent material.

Low load transfer, constant amplitude fatigue testing of 0.25" TukLoc nuts, Hi-Lok fasteners (0.003" interference) and NAS 1734 nuts in 2024 and 7075 aluminum were conducted to determine the fatigue life benefit. The approximate amount of load transfer was 8% for the stress levels tested. TukLoc nuts provided life improvement in line with the solid shank interference fit Hi-Lok fasteners at the highest stress level of 22.5 ksi. At the intermediate stress level of 18.5 ksi, the fatigue life of TukLoc nuts was greater than the Hi-Lok nuts. Comparison of the TukLoc nut with the NAS 1734 nut showed a significant fatigue life improvement for TukLoc nuts at all stress levels.

A finite element analysis (FEA) was conducted to better qualify the fatigue life improvement of the TukLoc nut. The FEA results indicated that the lowest stress amplitude at all three loads occurred in the Hi-Lok fastener followed by the Tukloc nut and finally NAS 1734. The lowest mean stress occurred in the TukLoc nut followed by the HiLok fastener and finally NAS 1734. The life improvement of the HiLok nut was directly attributable to the high interference fit that was large enough to induce plastic deformation. The installation of a HiLok with this level of interference would be expected to severely score and mark the hole, though that was not included in the FEA modeling. The life improvement of the TukLoc nut was related to the combination of an interference fit and residual compressive stresses. The residual compressive stresses resulted in the lowest mean stress at all stress levels and the interference fit reduced the stress amplitude below that of the NAS 1734 nut.

Both the FEA and experimental testing results indicated that the fatigue life improvement of TukLoc nuts over NAS 1734 was significant. The results indicated that the combination of the residual compressive stress and the interference fit resulted in similar or higher fatigue lives than the tested HiLok fastener and significantly higher fatigue lives than NAS 1734 nuts.

9.10.9 TIME SAVINGS, STRUCTURAL WEIGHT SAVINGS AND INCREASED FATIGUE QUALITY USING ADVANCED BULKHEAD FITTINGS

Jude Restis, Fatigue Technology Inc.

Typical structural bulkhead penetrations for electrical, hydraulic, fuel or other systems can be complex involving many parts, may include adding structural weight for web padups and may decrease structural fatigue quality with satellite penetrations for fasteners.

Testing and analysis has been performed on a new bulkhead fitting system developed by Fatigue Technology Inc. This new bulkhead fitting system, FleXmate, takes advantage of the known benefits of cold expansion and the benefits of high interference fit expanded bushings with the ability to adapt to many fitting configurations. It also offers the advantages of reduced part count, elimination of satellite fastener holes and can reduce weight by reducing web padups for fittings penetrations.

9.10.10 EFFECT ON THE FATIGUE PROPERTY OF SHOT PEENED TITANIUM AND STEEL WHEN SUBJECTED TO ELEVATED TEMPERATURES

Mark Ofsthun, Boeing, Wichita

Shot peening is a process in which small spherically shaped media are projected to the surface of the metallic structure. The media leaves residual compressive stresses at the surface. This results in the failure origin being driven to sub surface where stress concentrations are lower. This is similar to cold working except the beneficial residual stresses are significantly lower and shallower for shot peening than cold working. Figure 9.10-14 depicts the shot peen process and the typical residual stress pattern. Typical shot peen fatigue benefits are shown in Figure 9.10-15.

In order to improve fatigue quality by shot peening, coverage and intensity are critical elements to successful fatigue quality improvement. Additionally, because the compression stresses of shot peening are shallow, elevated temperatures must also be considered when depending on shot peening as a fatigue quality enhancement. When the material is exposed to elevated temperatures, the beneficial residual stresses may be relieved and significantly reduced, thus reducing some of the fatigue quality enhancement of shot peening. Figure 9.10-16 shows how the fatigue quality of titanium (6Al-4V mill annealed), and a 180 ksi Nickel Alloy (NA 718, 180-200 ksi) can be affected by exposure to elevated temperatures. Figure 9.10-16 shows little impact on fatigue performance of the high temperature exposure for un-peened specimens. But a significant loss in fatigue performance for the shot peened specimens exposed to the high temperatures. Nonetheless, it needs to be pointed out that an overall improvement in fatigue quality was still observed for these two alloys despite the elevated temperature exposure.

9.10.11 E-BEAM WELD REPAIRS

Mark Ofsthun, Boeing, Wichita

Large monolithic structure are designed to reduce costs by reducing part count and assembly time. However, these parts require larger stock size and require significant machining. Scrapping such parts because of machining errors, particularly late in the fabrication sequence, would be a significant expense. Therefore, it is necessary for large monolithic parts to have a repair plan to correct machining errors.

Electron Beam is a process, which fuses metals using kinetic/heat energy from electrons that are emitted from an electron beam gun. These electrons are accelerated at approximately 2/3 the speed of light, which generates the energy to fuse materials such as titanium. Figure 9.10-17 shows a schematic of the e-beam weld process.

If large titanium parts were to have machining errors, e-beam plug weld could be a potential repair, provided the material properties were not significantly affected. The major concern would be the heat affected zones reducing the fatigue quality of the base material. In order to determine the effect of e-beam plugs on base material properties, fatigue tests were conducted on titanium (Ti 6Al-4V mill annealed) forgings. The specimen configurations are shown in Figure 9.10-18. The fatigue tests consisted of a low Kt specimen with round plugs, oval plugs, and baseline (no plugs). The plugs were made of the same material as the specimens themselves (mill annealed Ti 6Al-4V). The plugs were welded in a vacuum using the e-beam process shown in Figure 9.10-17. After welding, the fatigue specimens were inspected for defects using x-ray and ultra sound and were then machined from the weld blanks to the final test configuration with the plugs located .25 inches from the notch. The specimens surfaces were machined down .05 inches per side to remove weld splatter. The notch was a stress concentration of 1.5. The intention was to determine if for the short distance from the notch would influence the fatigue properties. The results of the fatigue tests are shown in Figure 9.10-19.

Figure 9.10-19 indicates that there was some effect on fatigue performance for the circular plug weld. A fatigue life degradation of 15% was observed for the circular shape plug. The oval shape plug indicated no degradation. Some of the fatigue nucleation sites appear to be in the heat affected zone. His would indicate that the e-beam repair plug could be a design repair with reasonably minimum impact on the fatigue quality. These results should not be applied to edge repairs. Nor should they be applied to repairs where surface clean-up is not possible. The general condition of the surfaces where the welding takes place is very poor. It is anticipated that much more severe fatigue degradation would result if the surfaces were not cleaned up.

9.10.12 C-130 DURABILITY PATCH DEMONSTRATION A SUCCESS

David L. Banaszak, USAF AFRL/VASV

The Air Vehicles Directorate successfully demonstrated a life-extending structural damping patch for the C-130 (Hercules) aircraft. The patch has the potential to prevent, or significantly delay, the development of high-cycle fatigue cracking, decreasing repair costs and increasing operational readiness. The demonstration's success opens the door to increase the use of damping treatments to mitigate high-cycle fatigue cracking currently occurring in many aircraft.

The directorate worked with the North Carolina Air National Guard (NCANG) to demonstrate a life-extending structural damping patch n an operational C-130. The patch, created and installed by Damping Technologies, Inc., was made from layers of aluminum and a viscoelastic material. For the demonstration, the patch was attached to a panel behind one of the C-130's engines. Engineers selected the C-130 aircraft panel because of its frequent cracking rate. Previously, the panel required repairs in about half of NCANG's C-130 fleet.

Prior to the demonstration, the directorate collected vibration and temperature data on the designated panel during five flights, using an AFRL-developed data acquisition system called the Damage Dosimeter. After the patch was applied, the directorate collected vibration and temperature data for seven additional flights. When engineers compared data from these two sets of flights, they found the patch decreased strain on the panel. This outcome indicated that the patch could increase the panel's life by 4.6 times. The directorate plans to keep the patch on the C-130 for the remainder of its life for continual evaluation.

Fatigue cracking, caused by vibration, is common on most aging aircraft. Energy from sources, such as airflow, acoustic loads, or engine vibration, can cause vibration in the panel. A damping patch dissipates this vibrational energy, decreasing the panel's peak deflections during each flight.

Typically, panels with fatigue cracking are repaired using a reinforcing panel fastened with rivets. The reinforcement helps the panel survive the load, but the rivets introduce stress risers and transmit the vibration to the surrounding structure, causing fatigue cracking to spread. This phenomenon, called "crack chasing," requires these surrounding areas to be reinforced, which can create additional problems. The damping patch prevents crack chasing by dissipating vibrational energy without transmitting it to the surrounding structure.

9.11. NON-DESTRUCTION INSPECTION

9.11.1 LASER BOND INSPECTION (LBI) OF COMPOSITE AIRCRAFT STRUCTURES

Craig T. Walters, Craig Walters Associates and Jeff L. Dulaney, LSP Technologies, Inc.

To reduce weight and improve fuel efficiency, composites are being used in aircraft construction at an accelerating rate. The presence of material defect regions in these composite aircraft structures could lead to disastrous failure of the structure under flight loads. These defective regions may be in the composite laminate itself or in adhesive bonds in the structure, and may arise as a result of damage in the service life of the aircraft, or in the original manufacturing process through production error. Many classes of these defective regions are undetectable by conventional NDI techniques such as ultrasonic probing because the nature of the material defect does not change the ultrasound transmission and reflection characteristics. An example of service damage that might be difficult to detect would be laminate weakening due to excessive heating. Examples of hard-to-sense adhesive bond manufacturing defects include a “kissing bond” (good mechanical contact with no strength) or a weak adhesive due to improper mixing or curing.

A new inspection technology invented at Boeing and under development at LSP Technologies, Inc. (LSPT) and Craig Walters Associates (CWA), offers a practical solution to locating composite damage/defect regions in laminate and laminate-adhesive bonds in aircraft structures. This inspection technique, known as Laser Bond Inspection (LBI), is a proof-testing method that applies a well-controlled dynamic stress to the composite structure, and senses the failure of weak laminate or weak adhesive bonds in response to the stress. The dynamic stress is generated by a pulsed laser beam interaction with the composite structure as discussed below. The controlled stressing of the composite material has no effect on the material or bond if it is not damaged, defective, or substandard.

The LBI process has been developed using a laser device originally built for laser shock processing (LSP) of metals for improved fatigue life. However, the requirements for a laser to implement the LBI process are different from those for LSP. On-going work efforts are focused on developing an advanced laser device architecture configured specifically for the LBI application that will reduce both the size and cost of the presently used research design. This advancement is essential for rapid insertion of the LBI process into aircraft manufacturing plant operations and aircraft maintenance depots.

Aircraft manufacturing and aircraft maintenance will greatly benefit by the detection of defects in composite materials used in structural components. Anticipated benefits include the detection of weak areas in composite laminate or adhesive bonds that conventional testing cannot locate. In addition, aircraft structures that have been in service, and may have been damaged will be able to be inspected by using the laser bond inspection process. (See Figure 9.11-1)

REFERENCES

1) R Bossi, K Housen, and W Shepherd, "Application of Stress Waves to Bond Inspection," Paper presented at SAMPE 2004. Long Beach, CA, May, 2004.

9.11.2 DEVELOPMENT OF SONIC INFRARED IMAGING (THERMOSONICS) FOR AIRCRAFT STRUCTURES

Dave Galella, FAA, William J. Hughes Technical Center

A new nondestructive inspection (NDI) technique is being developed that combines sound energy and infrared (IR) imaging to detect frictional heating produced by cracks, delaminations, and disbonds that could be in aircraft structures. This technique, known as sonic IR imaging, or thermosonics, was first applied in 1999 by researchers at Wayne State University (WSU) who found that short pulses of ultrasound (50 to 500 ms) at frequencies of 20 to 40 kHz could cause defects, such as cracks, in solid objects to heat up and become detectable to an IR camera. This patented technology offers both broad area inspection capability and high sensitivity to surface breaking and near-surface cracks.

As shown in Figure 9.11-2(a), the IR image shows no visible cracks at a bolthole prior to ensonification. After ensonification of the same hole, the IR image, Figure 9.11-2(b), clearly shows radial cracks at the 6 and 9 o'clock positions and a circumferential crack between these points.

Since 1999, research on the use of thermosonics for aircraft inspection has been funded at WSU by the FAA through its Airworthiness Assurance Center of Excellence as part of the National Aging Aircraft Research Program.

To date, several prototype systems have been developed. One system, located at the FAA Airworthiness Assurance NDI Validation Center (AANC) facility in Albuquerque, New Mexico, is shown in Figure 9.11-3 inspecting a turbine disk. Other experimental prototypes at WSU are shown in Figures 9.11-4 and 9.11-5. Both of these figures show ultrasonic sources that have been modified so that they can be held stable against an inspection surface during ensonification. The ultrasonic head, shown in Figure 9.11-5, consists of a precisely tuned block of aluminum with three ultrasonic horns attached. These three horns vibrate simultaneously when the sound pulse is activated and provide three coherent sound sources rather than one source, as provided by the configuration shown in Figure 9.11-4.

Testing of these hand-held prototypes is ongoing, both in laboratories and in the field. Figure 9.11-6 shows the one-horn version being tested on the B737 test bed at the AANC.

Considerable progress is being made in the studies of this new NDI technique, although it should be recognized that this technology is still in its infancy and many fundamental issues still remain to be investigated and understood.

One such phenomenon recently discovered is called acoustic chaos. This phenomenon occurs in the test part when fractional multiples of the input excitation frequency are present during ensonification. The relationship between this chaotic waveform and the sonic IR signal strength is not yet understood, although there are strong indications that the IR signal is much larger when acoustic chaos is present than when it is not. It is not yet clear how different frequency components of a sonic vibration contribute to the heating of the crack, how various sonic vibration modes contribute to relative displacements of crack surfaces, nor what are the overall optimal parameters for using the method in practice. Further study is ongoing to determine the origin of acoustic chaos and its effect on sonic IR heating.

9.11.3 AUTOMATED SIGNAL ANALYSIS SYSTEM FOR AIRCRAFT WHEEL INSPECTION

Cu Nguyen, FAA, William J. Hughes Technical Center

Aircraft wheels are subject to excessive stresses during landing and takeoff cycles. As such, it is a requirement to periodically inspect aircraft wheels to ensure their structural integrity. Eddy-current inspection is a widely used technique for inspecting aircraft wheels, since it is faster and easier to implement than other NDI techniques. The analysis of these eddy-current signals, however, generally depends on decisions of the human operator.

Funded as part of the FAA's Airworthiness Assurance Center of Excellence (AACE), Iowa State University, in collaboration with Northwest Airlines and ANDEC in Toronto, Canada, developed and implemented an automated signal analysis (ASA) system for aircraft eddy-current wheel inspections. The system is currently in beta-site testing at Delta Air Lines.

ASA systems are very useful for NDI, largely due to their ability for rapid analysis of large amounts of data with enhanced accuracy and consistency. It minimizes human errors and probability of false calls while increasing the inspection speed and accuracy.

A schematic of the ASA wheel inspection system is shown in Figure 9.11-7. The wheel is manually mounted on a rotating table. Information about the type of wheel is fed into the software to determine the scan plan. The eddy-current probe is held against the wheel and moved downward as the wheel is rotated, which ensures that 100 percent of the wheel is scanned. During each revolution, 2500 samples of data for each channel are collected. The data collected are then displayed on a time-based digital strip chart, an impedance plane, or a C-scan (plan view) image. The digital strip chart is superior to a paper strip chart since an operator can scan through and zoom in on signals and save the data for future use. The impedance plane is a tool used to obtain a visual representation of the shape and path of a defect in the wheel.

The ASA system developed here can image the C-scans as horizontal and vertical channels as well as functions of magnitude. These imaging tools enable the operator to analyze defects in the wheel graphically by scrolling over signals, such as holes, cracks, and notches, and viewing the raw signal in a window on the same screen, as shown in Figure 9.11-8.

The ASA system runs on any personal computer (PC) equipped with an input/output card and can control the functions of data acquisition and storage. The main window, shown in Figure 9.11-9, has three main buttons: Scan, Plot, and Image. To effectively analyze the signals while minimizing false alarms, the software uses a statistical method to calculate the appropriate threshold of data for different areas of the wheel, since different parts of the wheel have varying noise patterns. The program detects different areas of the wheel with a device known as an analog to digital converter card. This card assists the program's algorithm to determine a threshold value by the amount of data collected per rotation. The algorithm then determines the appropriate threshold level based on a predefined parameter for that portion of the wheel and the local amount of variation during a given time interval.

During normal eddy-current inspections, most false alarms are caused by spikes of noise, which cause unusually large amplitudes in the signal. Using ASA, these false alarms are avoided because the spike signals only show up during one revolution of the wheel. Real defects in a wheel would show up during more than one consecutive revolution because they exist in three dimensions and it takes several revolutions to mark the locality. With the spatial correlation capability, the program can easily detect these occurrences.

The developed system uses software called Wheel Inspection and Signal Analysis to control a marker system to mark the locations of cracks in the wheel. The marker board receives inputs from the computer software via the parallel port and the encoder that is used to generate pulses for rotating the turntable. When the software detects a crack in the wheel, the marker pen is actuated to mark the circumferential position of the wheel during the following rotation. This enables the operator to physically locate the crack on the wheel for further detailed hand inspection.

The ASA system has been designed to help make the wheel inspection procedure faster and more efficient. The user can easily correlate a feature on the wheel to the electronic strip chart and also follow the formation of the complex impedance trajectory of this feature. C-scan images allow visualization of feature size and location on the wheel, in contrast to paper strip charts, which require experience to recognize the number of flaws, flaw size, and location. Automatic retrieval of old data of the wheel, displays of difference images between the current and previous data, and image registration techniques all enhance the process of monitoring flaw initiation and growth. Using automatic signal classification to obtain online decisions about signal type and marking flaw locations on the wheel expedites the wheel inspection process and increases its reliability. The C-scan display helps visualize the wheel inspection data in an image form and also predicts the flaw size. Similar systems like this can be developed for other aircraft applications such as engine disk, impeller bores, and fuselage skin panels.

9.11.4 DRY-COUPLED PROBES FOR ULTRASONIC INSPECTIONS OF AIRCRAFT STRUCTURES

David Galella, FAA, William J. Hughes Technical Center

An important part of any ultrasonic procedure is the couplant that transfers the sound energy between the ultrasonic probe and the inspected structure. Oil- or water-based gels are commonly used for manual inspections, while water immersion or bubbler systems maintain a constant level of coupling for automated units. There are numerous inspection procedures where liquid couplants are a detriment. A majority of the common problems with couplants is related to the time-consuming application and removal of the couplant. In addition, some advanced aircraft structures prohibit the application of couplants, part immersion, or contact techniques to prevent contamination or degradation of the materials or coatings.

To avoid the problems associated with the liquid-coupling medium, dry-coupled probes are being developed at Northwestern University for ultrasonic inspections with longitudinal and transverse ultrasonic waves at frequencies up to 10 MHz. This project is supported by the FAA as part of its National Aging Aircraft Research Program.

The probes use a flexible polymer coupling substrate that easily deforms around irregularities when in contact with the inspection surface. One conceptual design of the dry-coupled probes is a rolling probe that consists of a nonrotating stator with an ultrasonic transducer and a rotating rotor with the polymer substrate. This rolling probe design looks very promising for high-speed, ultrasonic scanning of large airframe components.

Dry-coupled probes have advantages for inspecting aircraft components with limited access and various spatial orientations. These inspection conditions may result in an inconsistent application of couplant. In the case of conventional contact probes, even the partial loss of couplant from the probe face causes substantial variations in the signal amplitude. This is most likely to occur when the probe is manually scanned over the inspection area. On the other hand, manual scanning with the dry-coupled rolling probes demonstrated very stable coupling, minimal fluctuations, and high repeatability of the ultrasonic signals, regardless of the spatial orientations of the aircraft components.

The probes consist of commercially available normal incidence or angle beam ultrasonic transducers. These transducers can be easily replaced or adjusted when different inspection frequencies, bandwidths, or incident angles are required. Minimal time is required to reconfigure the probe from one application to another. Some probe designs contain either several different ultrasonic transducers at different incident angles or a variable-angle unit for rapid adjustments of incident angles.

Figure 9.11-10 shows that the dry-coupled rolling probes are designed to work with conventional, portable ultrasonic flaw detectors. Advanced scanning and data acquisition systems may also be used when high-quality ultrasonic imaging is preferred. The results of the ultrasonic inspection can be presented as A-, B-, or C-scan images. For image acquisition, the probes use an internal miniature encoding module.

A DC-10 Service Bulletin calls for the ultrasonic inspection of the horizontal stabilizer constant and outer section skin panels for evidence of cracking. All interior and exterior surfaces of the upper and lower outboard skin panels as well as interior and exterior surfaces of the upper and lower center section skin panels have to be inspected. Figure 9.11-11 shows the probe that was used for B-scan ultrasonic imaging of the DC-10 horizontal stabilizer.

The current inspection procedure is based on the transducer scanning with A-scan data acquisition to measure the depths and lengths of the detected cracks. The crack lengths are measured using manual marks on the skin panel for initial and final transducer positions. This data acquisition and measurement procedure is quite time-consuming, cumbersome, and is not very reliable.

An alternative ultrasonic procedure is under development that will inspect the DC-10 horizontal stabilizer using dry-coupled rolling probes. These probes have proven to be very effective for linear scanning and B-scan imaging. All necessary information on the depth and length of the crack can be acquired and displayed in B-scan format using any portable ultrasonic flaw detector. Figure 9.11-12 shows a B-scan image of several fastener holes with fatigue cracks emanating from the holes.

Even though the dry-coupled rolling probes are a fairly new ultrasonic inspection tool, recent field tests demonstrated that the probes are highly effective for a number of applications on advanced aircraft materials and structures.

9.11.5 AIRWORTHINESS EVALUATION OF AGING SMALL AIRPLANES

Michael Shiao, FAA, William J. Hughes Technical Center

By 2010, the average age of the fleet of small airplanes (~180,000 aircraft) will approach 40 years. However, little is known about the consequences of the aging process of small airplanes. Comprehensive teardown inspections provide critical information to determine the condition of high-time operational aircraft. Data developed from teardown inspections can be used to provide guidance for maintaining structural and systems integrity. Limited teardown inspections of large civil aircraft have been performed, and these have led to a limited and proprietary knowledge base. There is no such knowledge base for small airplanes. Therefore, FAA research of teardown investigation on small airplanes would provide an excellent opportunity to gain knowledge and insight required to support rulemaking, advisory circular preparation, and findings of compliance for small aircraft.

In September 2002, the FAA initiated a research project to evaluate two high-time commuter airplanes, both Cessna 402 models. The 402 model was chosen because of its design commonality with several other commuter-class airplanes. The first aircraft, a 402A model built in 1969 with 19,700 flight hours, was primarily used for flying tourists through the Grand Canyon.

The second aircraft, shown in Figure 9.11-13, a 402C model built in 1979 with 25,500 flight hours, was last owned and operated by Cape Air/Nantucket Airlines who flew commuter routes to islands in Massachusetts, Florida, the Virgin Islands, and Puerto Rico.

This research project was conducted at Wichita State University and was supported by several industry partners. Cessna provided technical and engineering support along with certified technicians to perform the supplemental inspections. Cessna's piston service center provided service bulletins and service requirements applicable to the 402 aircraft. Cape Air/Nantucket Airlines donated the second aircraft, a 402C model, and provided technicians to support the inspection and disassembly of the aircraft. The FAA AANC participated in the program by monitoring the supplemental inspections and investigating advanced NDI methods that may be applicable to this type of commuter aircraft. In addition, the FAA Small Airplane Directorate and the Wichita Aircraft Certification Office assisted in the review of service difficulty and accident/incident reports along with certification requirements for these aircraft.

The teardown evaluation involved two phases on each aircraft: an inspection phase and a teardown examination phase. In the inspection phase, over 100 visual inspections were performed on the airframe and aircraft systems along with detailed visual inspections of the aircraft wiring. Supplemental inspections were then conducted on critical structural areas using NDI techniques such as dye penetrant, magnetic particle, and eddy current. In addition, aircraft maintenance records, service bulletins, and airworthiness directives were reviewed, including service difficulty and accident/incident reports for the Cessna 402 aircraft. The teardown phase includes disassembly of the aircraft, inspection of aircraft systems components, investigation of advanced NDI methods such as magneto optic imaging (shown in Figure 9.11-14), laboratory testing of aircraft wiring, detail disassembly of aircraft sections, and microscopic examination of critical structural areas in the airframe, as shown in Figure 9.11-15.

The research was completed in September 2004. In general, damage locations and damage sources through visual inspection, nondestructive investigation, and destructive investigation in structures as well as electrical and mechanical systems were identified. Typically, corrosion and fatigue damage at various structural components were found. Wiring damage due to chafing, rubbing, exposed shield, and several other improper maintenance practices were observed. The FAA Small Airplane Directorate will use the information to develop guidance to help maintain the safe, continued airworthiness of small airplanes.

9.11.6 VISUAL INSPECTION RESULTS OF SELECTED B-737 AND B-747 DUAL-LOAD PATH FLIGHT CONTROL COMPONENTS

Robert McGuire, FAA, William J. Hughes Technical Center

A task within the FAA Aging Aircraft Research Program has assessed the condition of aging flight control linkages and determined if there were previously unidentified conditions that could lead to unsafe conditions if there was a failure in the component. Of particular interest were safety-critical, single component dual-load path elements. Dual-load path elements are defined by the Aging Transport Systems Rulemaking Advisory Committee as "An assembly having primary and secondary load paths where both paths are in an integral part of a single component (element)." Generally, these are hardware components that are integral or collocated, intended to last the life of the aircraft, difficult to visually inspect, and receive inputs from multiple independent sources for redundancy and reliability.

The two problems associated with dual-load path elements are (1) an undetected degradation (e.g., corrosion) or failure will mean that the designed-in redundancy may be compromised so that a subsequent failure could create an unsafe condition and (2) common-mode failures leading to deterioration of both load paths due to collocation could cause an unsafe condition. Additional maintenance practices, including the application of advanced NDI techniques, can be proposed to further enhance the operational safety.

Researchers at the FAA ANNC studied the single element, dual-load path linkages from primary flight control systems on B-737 and B-747 commercial aircraft that had been retired in the previous 6 months. The work was done in cooperation with the manufacturer.

Twenty-one dual-load path components were identified for this study. Each specimen received three phases of in-depth visual inspections (aided by a fiberscope when appropriate) that examined the component as installed on the aircraft, after removal and cleaning, and after being completely disassembled. The inspections searched for any visual signs of erosion, corrosion, excessive wear, fretting, cracks, impact damage, or other mechanical degradation. Some components were also inspected against OEM specifications.

While the component-level findings would not necessarily affect the continued safe flight and landing of their respective aircraft, the inspection results did yield some findings that may be of interest to the industry. Two B-737 Mach trim actuators, tested by the OEM, performed sluggishly and were deemed nonairworthy. The B-747 specimens of interest included three aileron actuator links (inboard aileron) with excessive bearing wear, one tube assembly (inboard elevator) that had numerous fatigue cracks ranging from 15-20 mm long on the outer load path, and one rod assembly (inboard elevator) had a 25-mm fatigue crack on the outer load path. Since the inner and outer load paths of both the tube and rod assemblies mentioned above are permanently bonded together, a visual inspection cannot be done on all areas of these components.

As a result, a recommendation was made that visual inspections should be supplemented with an eddy-current inspection and a reference standard be developed to investigate and validate the results from visually inaccessible areas. As it is unknown whether these findings are the result of a trend or an anomaly, additional aged dual-load path inspection specimens will be acquired. The first testing phase identified subjects for further study. Because of the small size of the sample set and the source of the samples (retired, nonairworthy aircraft), it was inappropriate to draw any definitive conclusion concerning the condition of parts in current service.

9.11.7 AIRCRAFT STRUCTURAL HEALTH MONITORING USING PERMANENTLY MOUNTED SENSORS

J. Timothy Lovett, Jentek Sensors, Inc.

On-board eddy current sensor networks can provide aircraft structural health monitoring by detecting and monitoring fatigue damage at numerous locations. To be practical, these sensors and arrays must be low cost, thin, conformable, durable and reliable over years of service.

JENTEK Sensors Inc. is actively developing this capability utilizing Meandering Winding Magnetometer (MWM®) Arrays. MWM-Arrays are made from thin metal windings between layers of durable, conformable polymer materials, with a total thickness of about 100 μm, or 0.004 in. These sensor arrays do not require local electronics (within 8 meters) at each sensor. As a result, low cost networks can be devised to monitor numerous on-board locations. Furthermore, these eddy current sensors can be attached at locations of interest with a thin layer of adhesive or they can be embedded in joints. They can be covered with an approved sealant or protective coating, or completely encapsulated, if desired.

Figure 9.11-16 provides photographs and schematics of linear and circular MWM-Array sensor constructs. The technique used to fabricate MWM-Arrays permits sensor drive windings and sense elements to be arranged to optimize sensitivity to fatigue cracking at particular locations. The circular MWM-Array, for example, is fabricated with concentric sensing elements. When mounted to encircle a fastener hole, it provides crack propagation information as the crack propagates outward from the fastener hole and passes beneath the concentrically arranged sense elements.

Figure 9.11-17 provides data from an MWM-Rosette (circular array) mounted on an aluminum fatigue specimen. The crack is picked up first by channel 1, the innermost sensing element, as indicated by the decrease in measured conductivity. As the crack grows, the signal from Channel 1 gradually increases until it approaches saturation as the crack tip moves beyond the region of Channel 1 sensitivity. At about the same time, the crack tip is moving into the region of Channel 2 sensitivity, as indicated by the decrease in conductivity. By knowing the spatial positioning of the channels and their range (at the frequencies in use) it is possible to track the crack tip (and therefore, crack length) to within a few thousandths of an inch.

Similarly, linear arrays can be fabricated to monitor crack propagation between fastener holes. Figure 9.11-18 illustrates a four-hole joint specimen (work completed under a NAVAIR SBIR Phase II), representative of an aircraft structural joint, with embedded linear MWM-Arrays. Following installation of the MWM-Arrays and bolting the specimen, it was cycled in a load frame to induce fatigue cracking at the fastener holes. The MWM-

Arrays successfully detected and monitored crack progression throughout the test and remained functional even after the specimen had failed.

Figure 9.11-19(a) illustrates a ten-hole specimen used in a multi-site damage study funded by Air Force/Lockheed Martin, after completion of similar tests with 4-hole specimens for NAVAIR. The ten-hole specimen was constructed similar to the four-hole specimen, with embedded linear MWM-Arrays mounted between the holes in the lower and upper rows. The equipment set-up with the specimen in the load frame and the 37-channel probes are shown in Figure 9.11-19(b). The crack tip progression data are shown in Figure 9.11-20. The colored lines indicate progression of crack tips from one hole towards another as a function of number of cycles. As in the four-hole specimen tests, the MWM-Arrays successfully monitored crack growth throughout the test with the sensors embedded at the interface between the metal plates.

This fatigue monitoring capability has also been successfully demonstrated in one full scale fatigue test (P-3 Orion at Lockheed Martin) and several component tests, with additional full-scale tests pending. Transition to the fleet is expected in the near-term.

9.11.8 PRODUCTION OF NDI RELIABILITY STANDARDS WITH FATIGUE CRACKS WITHOUT STARTER NOTCHES USING MOUNTED SENSORS

J. Timothy Lovett, Jentek Sensors, Inc.

Standards for qualification and calibration of NDI techniques have traditionally relied upon specimens with simulated flaws. These simulated flaws have been produced by machining, electro-discharge machining (EDM), laser cutting or other methods. Simulated flaws produced by these means differ considerably from the actual flaws that need to be detected by NDI means, and sensor response to simulated flaws also differs from the response to actual flaws.

Starter notches are often used to produce specimens with fatigue cracks. The starter notch is then machined away leaving a surface breaking fatigue crack. There are, however, important differences in crack morphology between these and genuine fatigue cracks. In addition, the process of machining away the notch may change the near-surface properties of the remaining material. Uncertainty in crack initiation time is another factor that can make it very difficult to control crack size in the specimen. To produce a small crack, one has to rely on estimated number of cycles to crack initiation based on experience. The actual number of cycles to initiation will vary significantly from specimen to specimen.

JENTEK Sensors Inc. has developed and demonstrated capability to monitor initiation and growth of fatigue cracks in specimens of interest using mounted inductive sensors. The sensors provide early crack detection and sizing capability without removing the specimen from the load frame. This provides an opportunity to produce NDI reliability standards with fatigue cracks without starter notches, which require no subsequent machining, thus avoiding any other surface modification. This can be accomplished in simple geometries, at edges, in complex geometries, and even for layered constructs.

The Meandering Winding Magnetometer sensor arrays (MWM-Arrays) are configured with a single drive winding and an array of sensing elements. Sensing elements can be arranged to optimize sensitivity to cracks in particular locations and orientations. The sensor is flexible, extremely thin (100 μm) and lightweight and can be mounted on the specimen with common adhesives.

This has been recently demonstrated in several materials and specimen designs. In one example, two seven-channel MWM-Arrays were mounted inside a hole in an aluminum dog-bone specimen, as shown in Figure 9.11-21 (a.). The sensing elements were positioned along the sides of the holes where fatigue cracks were likely to form. Conductivity and lift-off data from the arrays are shown in Figure 9.11-22. The array mounted on the left side of the hole indicated no change in either conductivity or lift-off but the array on the right side clearly indicated the progressive growth of fatigue cracks. As the cracks increased in depth with increasing load-cycles, the affected channels registered a continuing decrease in conductivity, as shown in Figure 9.11-23. Figure 9.11-21 (b.) shows a similar fatigue test specimen with two holes, each of which contains a sensor array with sensing elements at the three-o'clock and nine-o'clock positions for detecting and monitoring cracks. Figures 9.11-24 and 9.11-25 show a similar approach for generating cracks at the apexes of a slot in a flat IN-718 plate.

In another example, a linear MWM-Array was mounted in the cavity at the center of a shot-peened 4340 steel specimen, as shown in Figure 9.11-26. The data from the seven-channel sensor are shown in Figure 9.11-27. Monitoring the permeability, as measured by the MWM-Array, permits termination of fatigue tests when cracks as small as 75 μm. have developed. After one of the tests, the specimen was scanned with another MWM-Array to produce the permeability image shown in Figure 9.11-28. This image reveals two adjacent fatigue damage zones with cracks at the two locations in one of the zones identified by the permanently mounted MWM-Array during the fatigue test.

9.12. ENGINES

9.12.1 THE DEPARTMENT OF DEFENSE MANTECH LASER PEENING INITIATIVE

Jeff L. Dulaney, David F. Lahrman and Richard D. Tenaglia, LSP Technologies, Inc.; David W. See, USAF AFRL/MLMP; and Walter N. Roy, Army Research Laboratory

Laser peening (also known as laser shock peening) is an innovative surface enhancement technology used to increase the resistance of aircraft gas turbine engine compressor and fan blades to foreign object damage (FOD) and to improve high cycle fatigue (HCF) life. Laser peening has been implemented into production operations for treatment of turbine engine blades for the B1-B Lancer (F101 engine), the F-16 Falcon (F110 engine), and the F/A-22 Raptor (F119 engine). Figure 9.12-1 shows a schematic of laser peening of an Integrally Bladed Rotor (IBR) for the F/A-22 Raptor. Implementation of laser peening has provided considerable savings in maintenance and inspection costs and boosted engine reliability, crew safety, and mission readiness. Laser peening is recently being developed as a method to toughen gears and other propulsion system components for military and commercial helicopters.

Laser peening drives a high-pressure shock wave into a material surface using a high-energy laser pulse. The plastic deformation caused by the shock wave results in compressive residual stresses in the surface of the part. The beneficial compressive residual stresses typically extend as deep as 1.0 to 1.5 mm below the surface or five to ten times deeper than conventional shot peening. Deep compressive residual stresses increase the resistance of components to surface-related failures such as fatigue, fretting fatigue, and stress corrosion cracking.

Relatively high processing costs and low throughput previously limited widespread acceptance of laser peening for applications other than aircraft engines. Under the Department of Defense Manufacturing Technology Laser Peening Initiative, considerable progress has been made to decrease the cost and to increase the throughput of laser peening. The Air Force and Army ManTech programs being conducted at LSP Technologies, Inc. are achieving the project goals of reducing the cost of laser peening by 50 percent to 75 percent and increasing processing throughput by six to nine times compared to earlier methods. Numerous improvements have been made to the laser systems used for laser peening to increase their robustness for production processing of parts and to increase productivity. LSP Technologies, Inc. developed an automated RapidCoater™ system to apply and remove process overlay coatings used during laser peening. As a result of these technical breakthroughs, laser peening for numerous military and industrial applications has become feasible and economical.

REFERENCES

1) David W. Sokol, Allan H. Clauer, and Ravi Ravindranath, "Applications of Laser Peening to Titanium Alloys," Presented at the ASME/JSME 2004 Pressure Vessels and Piping Division Conference, San Diego, CA, July 25-29, 2004.
2) AMPTIAC Quarterly, Richard D. Tenaglia, David F. Lahrman and David W. See, “Preventing Fatigue Failures with Laser Peening,” Volume 7, Number 2, 2003.

9.12.2 ON-AIRCRAFT ENGINE DISK CRACK DETECTION

William Emmerling, FAA, William J. Hughes Technical Center

On-aircraft disk crack detection research seeks to develop technologies (made available by the significant advances in computational and communications technology) that can identify a crack in a turbine engine disk in flight prior to failure. Under the Aircraft Catastrophic Failure Prevention Program, the initial focus of this effort is on fan disks.

The FAA initiated discussions with the Department of Defense and NASA to review the status of engine failure detection technologies, with specific interest in fan disk failures. In a November 2000 meeting at Naval Air Warfare Center (NAWC) Aircraft Division, Patuxent River, MD, with technology developers, it was clear that successes had been achieved in the laboratory, and that various technologies held promise. The overwhelming desire of the technology developers was to obtain data from a full-scale engine test. In April 2001, the FAA Uncontained Engine Failure Technical Community Review Group agreed to provide a full-scale test. The Naval Air Systems Command, FAA, U.S. Air Force, and NASA Glenn Research Center teamed up, in what could be considered a model application of collaboration, to explore and develop promising technologies to detect cracks in on-aircraft turbine engine disks in real time.

Testing was completed at the NAWC Weapons Division China Lake Survivability Laboratory on a NAWC-supplied TF-41 turbine engine, shown in Figure 9.12-2. Four thousand four hundred and seventy-four cycles were completed to propagate an embedded fault in the fan disk shown in Figure 9.12-3. The data generated will provide valuable insight to advance the state of the art in disk crack detection techniques. Previous disk crack detection testing has been conducted in a spin pit, but this is the first time a crack has been propagated in a full-up engine test. The full-up engine environment provides additional challenges in the form of real interactions from the environment and additional engine stages.

The FAA's investment in the demonstration test, along with NAWC China Lake providing the engine, resulted in a cost-effective demonstration of technologies. A significant effort was invested in the development and propagation of the fault prior to testing in the engine. This included analysis (Figure 9.12-4), electron discharge machining, and initiation of the crack under laboratory conditions to maximize the confidence that the crack would propagate during the short full-scale test. Inspection of the disk after spin-pit testing is shown in Figure 9.12-5. Seven technology developers participated in the test. Technologies being explored included acoustic emission, crack wire mesh indicators, vibration, and proximity measurement to detect of the change in the disk as the crack grows. This demonstration has created a cornerstone for government collaboration in aircraft safety research to pursue on-aircraft engine disk crack detection technology development.

9.12.3 UNCONTAINED ENGINE DEBRIS DAMAGE ASSESSMENT MODEL VERSION 2.0.2 RELEASED

Donald Altobelli, FAA, William J. Huges Technical Center

Naval Air Warfare Center Weapons Division (NAWCWD) China Lake and their support contractor, Survice Engineering Company, delivered version 2.0.2 of the Uncontained Engine Debris Damage Assessment Model (UEDDAM) for compliance with proposed revision to AC 20-128, which is currently in development by FAA ARAC.

Figure 9.12-6 shows a typical engine disk failure debris layout. Figure 9.12-7 shows how a typical spray pattern of debris would exit a turbine engine from a compressor disk failure.

In February 2003, a training session took place for the ARAC to familiarize airframe and engine manufacturers with version 2.0.2 of the model and solicited comments.

NAWCWD China Lake and Survice Engineering assembled the user's manual, briefing materials, and generic examples that took the group through the computer program in a very detailed lesson. Modeling tools were used to analyze a simplified airplane to give all participants experience using the analysis features.

The tool uses a Monte Carlo analysis to analyze the hazard to the airplane in accordance with the rotor burst guidance. The analysis can randomly simulate fragment impacts like a real event and repeats the analysis many times to develop the probability of hazard.

Bombardier completed their assessment and provided a favorable written report to ARAC that includes recommendations for improvement.

The UEDDAM vulnerability assessment tools automate the analysis and allow trade-off studies to be performed. This enhances the safety of commercial aircraft by providing the means to critically examine the threat posed by uncontained engine debris and allows steps to be taken to mitigate the threat. Figure 9.12-8 shows a computer model from an analysis.

The uncontainment research effort has produced several reports that are the result of years of effort in support of developing the revisions to AC 20-128, "Design Precautions for Minimizing Hazards to Aircraft from Uncontained Turbine Engine and Auxiliary Power Unit Rotor Failure." A revised compact disc containing all the reports was distributed at the 32nd ARAC meeting in November 2002.

9.12.4 TECHNOLOGY TRANSFER OF HIGH-STRENGTH FABRICS FOR BALLISTIC PROTECTION OF FLIGHT-CRITICAL COMPONENTS FROM UNCONTAINED ENGINE FAILURES

Donald Altobelli, FAA, William J. Hughes Technical Center

Over the years, several civil aircraft accidents with catastrophic consequences have occurred when fragments from in-flight engine failures damaged critical aircraft components. To reduce the probability of such incidents in the future, the FAA sponsored research to develop and apply advanced technologies and methods for mitigating the effects of uncontained engine bursts. These materials would not stop the largest fragments, like the compressor disc segment from the Sioux City accident. However, the loss of all hydraulic systems in that accident was attributed to smaller debris liberated by the failure rather than a direct hit by the large piece. In support of this FAA objective, SRI International completed a research program to evaluate the ballistic effectiveness of fabric structures made from advanced polymers and has developed a computational ability (using the DYNA-3D model developed at Lawrence Livermore National Laboratory) to design fragment barriers. SRI focused on three commercially available high-strength polymer materials—PBO (Zylon), aramid (Kevlar), and polyethylene (Spectra). To allow the end user to design fabric barriers with reasonable computer time, SRI converted the detailed model to a simplified shell model, see Figure 9.12-9.

The purpose of the current AACE program with the University of California-Berkeley (UCB) and Boeing is to transfer the technology from the SRI program to industry and determine the suitability of Zylon (which showed the most promise in the SRI work) as ballistic protection against uncontained aircraft engine fragments.

UCB completed small-scale ballistic testing of Zylon and Kevlar to verify the modeling techniques developed by SRI. Large-scale (actual blade fragment sizes) ballistic tests were completed by SRI that simulated the typical aircraft installations, as shown in Figure 9.12-10. Figure 9.12-11 shows an actual fan blade segment being stopped by the fabric barrier.

Prior to the ballistic tests, modeling was done by SRI and UCB to predict the number of fabric layers necessary to stop the fragment. The predictions were very accurate when compared with the experimental data and resulted in a reduction of tests necessary to characterize the barrier protection.

Boeing conducted independent material development tests on Zylon to verify its strength and environmental impact on the material. All the testing and analysis will be documented in an FAA report.

9.12.5 TECHNOLOGY TRANSFER OF MULTILAYER COMPOSITE FABRIC MODELING FOR GAS TURBINE ENGINES CONTAINMENT SYSTEMS

Donald Altobelli, FAA, William J. Hughes Technical Center

The purpose of this research effort is to use the FAA-funded fabric material model for aircraft barriers developed by SRI International in the design of engine containment barriers. A generic containment model has been developed by Honeywell Engines to assist industry in using this modeling tool for engine fabric containment predictions. In addition, the intention is to help standardize the methods for analysis so FAA Engine Certification engineers can make better judgments on new engine containment designs.

Arizona State University has completed quasi-static testing on Zylon and Kevlar materials on an engine containment ring configuration and built a containment ring model for Honeywell.

NASA-Glenn Research Center (as part of their engine containment program) has conducted several ballistic tests in their gas gun facility in support of this program. These tests were simulated by Honeywell using the material models supplied by SRI. The data from this testing has been the basis for the generic model developed by Honeywell.

Results will be documented in an FAA technical report to be released next year.

In August 2003, SRI and Honeywell presented a training course on the currently developed model to FAA Engine Certification engineers.

9.12.6 LS-DYNA NONLINEAR FINITE ELEMENT MODELING -- AEROSPACE QUALITY CONTROL PROGRAM

Don Altobelli, FAA, William J. Hughes Technical Center

Over the last 10 years, engine and airframe manufacturers have used nonlinear dynamic computational tools (primarily LS-DYNA) to simulate high-speed events such as engine blade rotor failures and bird strikes. Failure mechanisms in the events are studied in the design process. Figure 9.12-12 shows an example of an actual engine blade-off test and a failure model simulation of the test showing similar results.

Prior to the availability of accurate modeling, expensive engines and available rig tests were used for development and certification. Modeling these events has saved significant time and money during development and has greatly enhanced safety by understanding the dynamics of the event. Aviation industry standards need to be established for these modeling techniques. Developing advisory materials will help applicants and Aircraft Certification Office engineers review and approve design changes.

In the mid-1990s, the FAA Aircraft Catastrophic Failure Prevention Program started a research project to develop aircraft material models that could be used in this analysis. Figures 9.12-13 and 9.12-14 are model simulations from the engine containment and engine uncontainment barrier tasks, respectively.

It became apparent that improved quality control and standardization were needed for the FAA certification engineers to be able to evaluate LS-DYNA for certification credit. Further investigation revealed that Livermore Software Technology Corporation (LSTC) (developer of LS-DYNA) has an extensive quality control system for modeling vehicle crashes for the industry. The LSTC's quality control effort has strong support of the automotive industry. The research showed a need for a similar effort with the aircraft industry.
Because the velocities and strain rates of aircraft turbine engine uncontained events happen much faster than car crashes, LS-DYNA requires a separate set of standards to be developed for an aircraft industry quality control program.

In FY03, the FAA teamed with NASA Glenn Research Center (GRC) to bring aircraft and engine manufacturers together to develop analytical methods to model uncontained engine failures. Currently, the team has created several generic aircraft problems that will be used as benchmarks by LSTC in establishing an aircraft industry quality control system. This program will be on-going to establish and maintain quality control for the aircraft industry.

The Aircraft Catastrophic Failure Prevention Research Program is also conducting research and training necessary to support the FAA certification office engineers in understanding and standardizing the LS-DYNA modeling capability for certification. In this fiscal year, two training sessions were conducted to familiarize the FAA engine certification engineers with the LS-DYNA modeling research effort and the limitations of the code. In the future, it is anticipated that additional training will be provided.

This work is part of the NASA Turning Goals into Reality Aircraft Safety Team Award shared by NASA GRC, the FAA, and industry titled "Jet Engine Containment Concepts and Blade-Out Simulation."

9.12.7 AIRCRAFT SHIELDING MATERIAL CHARACTERIZATION

Don Altobelli, FAA, William J. Hughes Technical Center

Small uncontained engine fragments that strike the aircraft can cause a catastrophic failure of aircraft systems, and the prevention or mitigation of debris damage is not currently in FAA regulation requirements. Figure 9.12-15 shows typical debris that can be generated in an uncontained engine failure. Implicit in the approach for multiple smaller fragment mitigation is the capability to shield critical components from debris. The FAA is working with industry to develop materials and a design capability for this fragment impact situation. The velocities and strain rates of these events happen faster than car crashes but slower than military events. As such, the two standards for impact analysis do not apply to aircraft engine failure and require a significant effort to extend to aircraft engine applications.

Modeling a ballistic impact is critical to determining the aircraft vulnerability to debris generated during engine failures. Research is underway by a team led by the University of California-Berkeley (UCB) with members from The Boeing Company and the Lawrence Livermore National Laboratory. Under an Airworthiness Assurance Center of Excellence grant, an improved material model for aluminum and an initial characterization of polycarbonate and generic composite aircraft material was developed. Extensive testing and analysis in this program have produced excellent data enabling better characterization of aluminum 2024-T3 material. Figure 9.12-16 shows a ballistic impact in a piece of aluminum tested at UCB.

Future work in this area will develop additional test data to verify composite and titanium material behavior.

9.12.8 AUTOMATED ENGINE DISK SLOT INSPECTION

J. Timothy Lovett, Jentek Sensors, Inc.

Inspection of slots in jet engine disks is made more difficult by the presence of fretting damage. In response to requests from fleet managers, JENTEK Sensors, Inc., has demonstrated the ability of the Meandering Winding Magnetometer (MWM®) Array to detect small fatigue cracks in the fretting region of engine disk slots. Conformable MWM-Arrays have been incorporated into an automated engine disk slot inspection system. Prototype systems have been delivered to the FAA and U.S. Air Force, and recently a second generation system has been delivered to the U.S. Navy for production use.

Figure 9.12-17 shows a close up view of the MWM-Array probe and the 37 channel sensor that performs the inspection of the disk slot. The flexible sensor array is mounted on a probe containing an inflatable bladder. After the probe with the sensor is inserted into the slot, the bladder is inflated, causing the sensor to conform to the curvature of the inside surface of the slot. The array is then scanned along the slot. JENTEK GridStation® software converts the sensor array output to conductivity and lift-off values and generates an image of the spatial distribution of these values. The lift-off is the proximity of each of the 37 sensing elements to the conductive surface at any point in the scan. Figure 9.12-18 provides conductivity and lift-off images from scans of two different slots. The presence of a crack is indicated in the lower conductivity image by the sharp drop in conductivity, shown as the red area against the otherwise blue background. This slot contains a crack while the other slot has no crack.

The generation of lift-off values is an important advantage of the model-based inversion approach employed by the GridStation software. By accurately measuring, monitoring and imaging lift-off, assurance is provided that the inspection is being performed correctly and that good inspection coverage is achieved. The green fields displayed in the lift-off images provide real-time feedback to the system operator to confirm validity of the measurement.

Under a Navy sponsored program with funding from NAVAIR, a similar system has been developed by JENTEK for inspection of slots in the stage 1-2 compressor spool of an engine. This inspection is performed with the disk in the engine, after removal of the upper compressor case, upper fan duct and blades (see Figure 9.12-19). This system has been successfully demonstrated at the Oceana I-level facility on an operational jet engine.

Both the table-top (Depot) and the top-half (I-Level) inspection configurations offer a substantial increase in inspection throughput and the potential to significantly reduce costs, while providing enhanced capability over conventional inspection methods.

9.12.9 PREDICTING THE INTEGRITY OF CERAMIC PARTS WHEN LOADS AND TEMPERATURES FLUCTUATE OVER TIME

Noel Nemeth, NASA Glenn Research Center

Brittle materials are being used, or considered, for a wide variety of high-performance applications that operate in harsh environments, including static and rotating turbine parts for unmanned aerial vehicles (UAV's), auxiliary power units (APU's), and distributed power generation. Other applications include thermal protection systems, dental prosthetics, fuel cells, oxygen transport membranes, radomes, and Micro-Electro-Mechanical Systems (MEMS). In order for these high-tech ceramics to be successfully used for structural applications that push the envelope of materials capability, the design engineer must consider that brittle materials are characterized and analyzed differently than metallic materials. Unlike ductile metals, brittle materials display a stochastic strength response because of the combination of low fracture toughness and the random nature of the size, orientation, and distribution of inherent microscopic flaws. This plus the fact that strength of a component under load may degrade over time due to slow crack growth (SCG) means that a probabilistic based life prediction methodology must be used when optimizing the trade-offs of failure probability, performance, and useful life. The NASA developed CARES/*Life* code predicts the probability of ceramic components failing from spontaneous catastrophic rupture when these components are subjected to multiaxial loading and SCG conditions. Enhancements to CARES/*Life* now allow for the calculation of component survival probability when loading and temperature vary over time. This capability is referred to as transient reliability analysis and can be used to predict component reliability (probability of survival) for situations such as thermal shock, startup and shutdown conditions in heat engines, and cyclic loading. The methodology has been developed with the following features:

- Transient cyclic fatigue modeling
- Ability to efficiently compute transient reliability for any number of loading cycles
- Transient proof testing analysis capability
- Ability to account for fatigue and Weibull parameters that change over the operating temperature range

This technology is considerably more sophisticated than the common approach of making predictions based on a maximum stressed point at some snapshot in time because *it considers the whole history of loading and the multiaxial stress distribution throughout the entire component to predict probability of survival*. The probability of survival algorithm uses results from transient finite element analysis, where loading profiles are broken into discrete time steps.

Figures 9.12-20 and 9.12-21 show an example of thin silicon nitride disks (20 mm diameter x 0.3 mm) rapidly heated by a laser. The experimental data was taken from the literature. Figure 9.12-20 is a schematic of the laser heating method. Starting at the center of the disk, the laser spirals out towards the edge of the disk over a time interval of approximately 1 second. The heating of the central portion of the disk causes high tangential tensile stresses along the edge of the disk. Figure 9.12-21 shows the transient CARES/Life predictions as a function of stress compared to experimental data. The disk prediction is shown based on analysis of disk # 3 (solid line) and disk #9 (dotted line). The 3-point flexure bar data was used to calibrate (characterize the material stochastic fracture behavior) the CARES/*Life* probabilistic models.

9.12.10 LIFE PREDICTION IN A PROBABILISTIC DESIGN SPACE – FOR BRITTLE MATERIALS WITH TRANSIENT LOADS

Noel Nemeth, NASA Glenn Research Center

Analytical techniques have progressively become more sophisticated and it is now possible to consider the probabilistic nature of the entire space of random input variables on the lifetime reliability of brittle structures. This has been demonstrated with NASA's CARES/Life code combined with the commercially available ANSYS/PDS software. The ANSYS Probabilistic Design System (PDS) is a commercial probabilistic analysis tool, which is an integral part of the ANSYS Finite-Element Analysis program. The ANSYS/PDS allows the effects of probabilistic loads, component geometry, and material properties to be considered in the finite element analysis. The NASA CARES/Life code predicts the time-dependent probability of failure of brittle material structures under generalized thermo-mechanical loading – such as that found in a turbine engine hot-section. We have coupled ANSYS PDS with CARES/Life so that the effects of stochastic variables of component geometry, loading and material properties on the predicted life of the component can be assessed. We are able to do this for:

- Fully *transient* thermo-mechanical loading
- Cyclic loading

Interestingly, in this implementation the material parameters associated with reliability analysis – the Weibull and fatigue parameters – can themselves be made stochastic. This would simulate batch-to-batch variations in the material reliability response or, alternately, the statistical uncertainty of the estimated parameters from the true parameters as derived from experimental rupture data. This enables more realistic assessment of brittle material component integrity. This capability will be useful in the design of ceramic turbine blades and vanes, thermal protection system parts, dental prosthetics, solid oxide fuel cells, and MicroElectroMechanical Systems (MEMS) as well as other applications that employ brittle materials.

A simplified turbine vane model simulating engine startup and shutdown is provided below as an example. Details of this analysis can be found in reference 1. The stator vane was assumed to be composed of a typical silicon nitride. The effect of a probabilistic engine startup/shutdown load profile, and probabilistic Weibull and fatigue parameters on the predicted integrity for a given number of startup/shutdown engine cycles is examined.

For the probabilistic analysis 11 input parameters were identified as random quantities and assigned statistical distribution function to quantify their randomness. The random input variables impacting the Finite-Element analysis include material properties, thermal boundary conditions and the start-up time of the load cycle. The heat transfer coefficient was assumed to be a coupled random value dependent on the variability of the heat transfer mechanism coupled with the randomness of the mass flow. The random input variables affecting only the CARES/Life part of the analysis include the brittle material Weibull and fatigue parameters. The distribution types as well as the distribution parameters, while not based on measured data, nevertheless represented very realistic values.

The transient operation is characterized by 4 phases. There is phase 1 start-up lasting 50 seconds, followed by phase 2 consisting of 850 seconds of hold time. Phase 3 is a 200 seconds long shutdown followed by phase 4, which is 800 seconds of hold time for cooling down. This transient profile is illustrated in Figure 9.12-22 for one loading cycle. The figure shows maximum temperatures and stresses versus time. Figure 9.12-23 shows the stator vane thermal profile at 75 seconds – the moment of maximum transient loading.

Figure 9.12-24 shows the average predicted failure probability (the so-called total probability) versus loading cycles for two probability methods – the Monte Carlo simulation and response-surface Method – as well as a conditional (deterministic) finite element analysis using averaged properties. This “total probability” is just the average of all the individual simulation trials. The differences between the deterministic and probabilistic analysis were due to highly non-linear and skewed probability distributions. These results show that not taking stochastic response into account can lead to un-conservative design. Better correlation between Monte-Carlo simulation and response-surface would be gained as the number of simulations increased. In this case we used 400 simulations for Monte-Carlo.

Figure 9.12-25 shows the results of the sensitivity analysis reported by PDS. It can be seen that most of the input variables significantly impacting the failure probability either influence the temperature results and/or the stresses of the finite-element analysis. All of these input variables have a strongly non-linear influence on the conditional failure probability.

It should be emphasized that an important conclusion of the observed significant difference between the conditional failure probability and the total failure probability is that ignoring the random influences previously outlined may lead to a non-conservative design. The conditional failure probability itself may be acceptably low, but the total failure probability could be, as in this example, two orders of magnitudes higher, which might not be considered as safe enough.

In the end what we have succeeded to accomplish is demonstrating the combining of a probabilistic life prediction methodology for transient loading with a generalized probabilistic finite element analysis program. This is a useful combination that can be applied to other interesting problems such as, for example, the effect of the re-entry envelope on the reliability of certain passive ultra-high-temperature thermal protections systems, or for dental prosthetics, on the effect on reliability of random loading direction and loading magnitude over time. It would also be useful in MEMS lifing where tolerances on dimensions can be a significant fraction of the overall part size.

REFERENCES

1) Reh, S., Palfi, T., and Nemeth, N. N., “Probabilistic Analysis techniques Applied to Lifetime Reliability Estimation of Ceramics”. Paper ID - APS-II-49 Glass. JANNAF 39th CS/27th APS/21st PSHS/3rd MSS Joint Subcommittee Meeting, December 1-5, 2003, Colorado Springs, Colorado.

9.12.11 HIGH TEMPERATURE FATIGUE LIFE ANALYSIS SOFTWARE

Vinod Arya, University of Akron

A computer code FLAPS (Fatigue Life Analysis Programs), for characterizing and predicting fatigue and creep fatigue resistance of metallic materials in the high temperature, low-cycle and high-cycle fatigue life regimes for isothermal and nonisothermal fatigue, has recently been developed by Vinod Arya of University of Akron, Ohio. The code comprises eleven high-temperature life prediction methodologies, and enables the user to assess the life of structural components under different known loading situations. The code is written in a user friendly and interactive manner. An accompanying manual, illustrating the use of programs and containing various examples has also been developed. The programs in the code use the Total Strain version of Strainrange Partitioning (TS SRP), and several other life prediction methods described in the manual. An extensive database has also been developed in a parallel effort. The database is probably the largest source of high temperature, creep-fatigue test data available in the public domain and can be used with other life prediction methods as well. The life prediction computer code FLAPS is a useful tool for application in a wide range of industries including automotive and off-highway vehicles, power generation equipment, manufacturing tool and the aerospace industry.

The software, users manual, and database are all in the public domain and can be obtained by contacting Gary Halford at (216) 433-3265 or Vinod Arya at (216) 433-2816. Request for obtaining an executable copy of the code, manual and other relevant material can be addressed to either of these two persons at NASA-Glenn Research Center, MS 49-7, 21000 Brookpark Road, Brook Park, OH 44135.

9.12.12 DISTRIBUTION OF INCLUSION INITIATED FATIGUE CRACKING IN POWDER METALLURGY UDIMET 720 CHARACTERIZED

Peter J. Bonacuse, Pete Kantzos, Robert Barrie, Jack Telesman and Tim Gabb, NASA Glenn Research Center

In the absence of extrinsic surface damage, the fatigue life of metals is often dictated by the distribution of intrinsic defects. In powder metallurgy (PM) alloys, relatively large defects occur rarely enough that a typical characterization with a limited number of small volume fatigue test specimens will not adequately sample inclusion initiated damage. Counter intuitively, inclusion initiated failure has a greater impact on the distribution in PM alloy fatigue lives as they tend to have fewer defects than their cast and wrought counterparts. Although the relative paucity of defects in PM alloys leads to higher mean fatigue lives, the distribution in observed lives tends to be broader. In order to study this important failure initiation mechanism without expending an inordinate number of specimens, a study was undertaken where known populations of artificial inclusions (seeds) were introduced to production powder. Fatigue specimens were machined from forgings produced from the seeded powder. Considerable effort has been expended in characterizing the crack growth rate from inclusion initiated cracks in seeded PM alloys. A rotating and translating positioning system, with associated software, was devised to map the surface inclusions in LCF test bars and monitor the crack growth from these inclusions. Figure 9.12-26 illustrates the measured extension in fatigue cracks from inclusions on a seeded LCF test bar subjected to cyclic loading at 0.8% strain range and a strain ratio ($\varepsilon_{max}/\varepsilon_{min}$) of zero. Notice that the observed inclusions fall into three categories: some don't propagate at all (arrest), some propagate with a decreasing crack growth rate, and a few propagate at increasing rates that can be modeled by fracture mechanics. Figure 9.12-27 shows the measured inclusion initiated crack growth rates from ten interrupted LCF tests plotted against stress intensities calculated for semi-elliptical cracks with the observed surface lengths. The expected scatter in the crack growth rates for stress intensity ranges near threshold is observed. This data will be used to help determine the distribution in growth rates of cracks emanating from inclusions as well as the proportion of cracks that arrest under various loading conditions.

REFERENCES

1) R&T 2001, NASA/TM-2002-211333, p. 136
2) Bonacuse, Peter J.; Kantzos, Pete; Telesman, Jack; Gabb, Timothy; and Barrie, Robert; *Modeling Ceramic Inclusions in Powder Metallurgy Alloys*, Fatigue 2002, Proceedings of the Eighth International Fatigue Congress, Stockholm, Sweden, June 3-7 2002.
3) Gabb, T. P.; Telesman, J.; Kantzos, P. T.; Bonacuse, P. J.; and Barrie, R. L., Initial Assessment of the Effects of Nonmetallic Inclusions on Fatigue Life of Powder-Metallurgy-Processed Udimet(TM) 720, NASA/TM-2002-211571, September 2002

9.12.13 MODELING THE DISTRIBUTION IN INITIAL CRACK SIZE FOR NON-METALLIC INCLUSIONS

Peter J. Bonacuse, Pete Kantzos, Jack Telesman and Tim Gabb, NASA Glenn Research Center

Non-metallic inclusions can lead to anomalously low fatigue lives in high strength materials. To investigate the effect of inclusions on fatigue life, without testing a large number of specimens, precursor Udimet 720 power metal was seeded with fully characterized samples of ceramic (alumina) inclusions. These "seeded" inclusions were meant to simulate naturally occurring inclusions but at a much higher occurrence rate. Two different compositions and sizes of alumina inclusions were chosen for the seeding study: approximately 50 micron (RAM90) and 150 micron (T64) average diameters. Fracture surfaces of fatigue specimens that were cut from extruded and forged pancakes were examined to determine the size and shape of the inclusions that initiated the fatigue failures. Given measured parameters of the seeds prior to their introduction to the powder, a computer simulation was devised to estimate the size distribution of the fracture initiating inclusions by approximating the inclusions as three dimensional ellipsoids. It was assumed that the largest computed inclusion area perpendicular to the load would be the most likely to initiate and propagate a crack. It was found that the distribution of largest simulated inclusion cross section did not always correlate well with distribution of inclusion fracture surface areas observed. It was also observed that cracks tended to start at the maximum asperities of the inclusion and not necessarily through the maximum cross section (Figure 9.12-28). A solution for the projected area of a randomly oriented ellipsoid was derived to determine if this might provide better correlations. Figures 9.12-29 and 9.12-30 show that the simulated distribution of the largest projected area does provide excellent correlations with fracture surface observations. The orientations of the inclusions were assumed to be random but correlated to the forging strains (Gaussian distribution).

9.12.14 CONFIDENCE INTERVALS FOR CRACK GROWTH PARAMETERS AND LIFE PREDICTIONS OF CERAMIC COMPONENTS

Jonathan Salem, NASA Glenn Research Center

Slow crack growth (SCG) parameters for glasses and ceramics are determined by either strength-based or fracture mechanics based test methods. Strength-based methods employ smooth test specimens, such as flexural beams or tensile specimens, and estimate SCG material parameters from strengths measured over different time intervals. Loading is generally done in a static fashion (i.e., "static fatigue") or in a continuously increasing fashion (i.e., "dynamic fatigue"). The strength-based methods are practical because the tests are simple, inexpensive, and usually accomplished quickly.

Strength-based methods directly sample the preexisting flaw distribution within or on the surface of the test specimens. Thus the cracks develop from at least some of the same sources that are expected to cause failure in a component manufactured in a similar fashion from the same material. Only the strength-based approaches have been standardized and, as a result of the critical nature of flight hardware, data for design of such components is usually generated with these standardized test methodologies.

The disadvantage of strength-based methods is that the SCG results are subject to the inherent scatter in the strength of ceramic materials. Thus the estimation of SCG parameters from strength data can result in poor statistical reproducibility, and an estimate of the parameter variances is necessary to the design process.

Closed form, approximate functions for estimating the variances and degrees-of-freedom associated with the slow crack growth parameters n, D, B, and A^* of the function $v = A^*(K_I / K_{Ic})^n$ as measured using constant stress rate ("dynamic fatigue") strength testing were derived by using propagation of errors [1]. Estimates made with the resulting functions and slow crack growth data for a sapphire window were compared to the results of Monte Carlo simulations. The comparisons indicate that with linearization, good estimates of the variances of parameters n, D, B, and A^* can be made by propagation of errors if the coefficients of variation of the input parameters are not too large.

Parametric variation of the input parameters was used to determine an acceptable range for using closed form approximate equations derived from propagation of errors (Figure 9.12-31). The functions can be used with the NASA codes CARES/Life and NASGRO to generated confidence intervals on deterministic and probabilistic life predictions (Figure 9.12-32).

REFERENCE
1) "Estimation and Simulation of Slow Crack Growth Parameters from Constant Stress Rate Data," J.A. Salem and A. Weaver, To be published in *Fracture Mechanics of Ceramics*, Vol. 12, K. White, R.C. Bradt, D. Munz, M. Sakai, eds., Plenum Press (2005).

9.12.15 CRACK GROWTH PROPERTIES FOR CVD ZnSe USED IN OPTICAL APPLICATIONS
Jonathan Salem, NASA Glenn Research Center

The International Space Station FEANICS (Flow Enclosure Accommodating Novel Investigations in Combustion of Solids) module contains eight, 63 mm diameter zinc selenide (ZnSe) windows that allow observation of various combustion experiments, as shown in Figure 9.12-33. ZnSe is a soft, weak ceramic that exhibits crack growth in the presence of water and a large average grain size. This results in single grains dominating behavior by fracturing at energies lower than expected from macro-crack data. Thus hardware, such as a window fabricated from polycrystalline CVD (chemical vapor deposited) ZnSe, will contain large grains that fail at single crystal fracture energies.

The design of fracture critical components for the International Space Station requires life analysis for conditions ranging from 40 to 90% humidity. In order to design windows sufficient to sustain the mission pressure cycle, the literature on CVD ZnSe was reviewed [1]. Unfortunately, the publications have a tendency to give incomplete information both in terms of the data analysis and in terms of the experimental techniques used, and the original data is not available. Therefore much of the data analyzed in this paper was digitized from plots in original publications. This was necessary not only to get a complete set of crack growth parameters for 100% humidity, but also to determine the scatter in the data.

For 100% humidity, the slow crack growth parameters of the equation

$$v = AK_I^n \tag{1}$$

for macro-crack failure were $n \approx 40$ and $A_{macro} \approx 1000$ m/s (MPa√m)$^{-n}$. Unfortunately, because of the low fracture toughness and large grain size of CVD ZnSe, failure can occur from relatively small cracks at low energies not represented by macro-crack parameters. In order to determine parameters for small-crack failure, two approaches were used: (1) strength-based data was analyzed using small crack fracture energies, and (2) macro-crack curves were shifted to the small crack region by a simplistic formula:

$$A_{Single} = A_{Macro}\left(\frac{K_{IcMacro}}{K_{IcSingle}}\right)^n \tag{2}$$

For 100% humidity, the slow crack growth parameters for small-crack or single crystal failure were estimated to be $n \le 40$ and $A_{single} \ge 10^{20}$ m/s (MPa√m)$^{-n}$ as shown in Figure 9.12-34. Reasonable agreement between the strength-based data and the shifted macro-crack data was exhibited for both 45% relativity humidity air and water. Strength and Weibull modulus for currently available CVD ZnSe was measured by testing of circular plates. The average strength for 100% humidity was 57.8 ± 6.5 MPa. The Weibull modulus and characteristic strength as estimated with the maximum likelihood estimator were 9.6 and 60.6 MPa, respectively, in good agreement with literature on well polished test specimens. Fracture toughness measurements ranged from 0.33 to 0.9 MPa√m, with the lower values representing failure from small flaws within grains and the larger values representing macroscopic cracks in dry environments.

REFERENCE
1) "Estimation of ZnSe Crack Growth Properties for Design of the FEANICS Windows, J.A. Salem, NASA TM 213359 (2005).

9.12.16 EFFECTS OF HIGH TEMPERATURE EXPOSURES ON FATIGUE LIFE OF DISK SUPERALLOYS

T.P. Gabb and J. Telesman, NASA Glenn Research Center and P.T. Kantzos, Ohio Aerospace Institute

Recent research has been focused on examining (ref. 1) the effects of extended exposures and extended cycle periods on the fatigue resistance of two disk superalloys. Powder metallurgy-processed, supersolvus heat treated Udimet® 720 and ME3 (ref. 2) fully machined fatigue specimens were exposed in air at temperatures of 650 to 704°C for extended times. They were then tested using conventional fatigue tests with a total strain range of 0.70% and min/max strain ratio of 0 to determine the effects of prior exposure on fatigue resistance. Subsequent tests having extended dwells at minimum strain in each fatigue cycle were then performed to determine cyclic exposure effects.

The effects of various prior exposures at 650°C to 704°C for 100 to 1029 hours were first evaluated on Udimet 720 fatigue life and failure modes. Resulting Udimet 720 fatigue lives at 650°C, including prior exposed and unexposed lives, could be generally grouped according to failure initiation sites, (Figure 9.12-35). Specimens failing from surface oxide-initiated cracks had about 80% lower lives than those failing from internal cracks at inclusions or grain facets. Cyclic dwell tests at 650°C were then performed with a dwell time based on the longest prior exposure time at 650°C divided by the subsequent log mean cyclic life. These tests reduced mean lives by 90% from unexposed, conventional test lives, and invariably failed from surface oxide-initiated cracks, (Figure 9.12-36). Cyclic dwell lives were lower than the pre-exposed lives, suggesting the damage produced by each fatigue cycle and a dwell exposure can interact.

Further discriminating evaluations were performed using disk alloy ME3, also sometimes referred to as Rene′ 104 and ME16. Cyclic dwell tests were first performed at the same strain conditions as before, giving a log mean cyclic life of 26,362 cycles and test duration of 439 h, (Figure 9.12-37). This test duration time was then used as the prior exposure condition. The contribution of environmental attack was then isolated by comparing prior exposures of 704°C/439 h in air versus vacuum. Prior exposure in air reduced fatigue life about 50% from unexposed levels, and usually induced surface oxide-initiated failures. Prior exposures in vacuum did not significantly reduce subsequent mean fatigue life from unexposed levels, indicating the air environment was strongly contributing to the damage. Long exposures could also be detrimental by reducing beneficial compressive residual stresses produced near the specimen surface during machining. These effects were evaluated by electro-polishing away the surface layer on several specimens before conventional fatigue testing. The fatigue lives of these specimens showed more scatter than unpolished specimens, but fatigue life was not consistently reduced by the electro-polishing. This indicated relaxation of beneficial compressive residual stresses was not strongly driving the life reductions due to exposure. Cyclic dwell testing was again most damaging, reducing mean fatigue life about 90% in comparison to unexposed, conventional fatigue test life. Therefore, the mixing of fatigue and environment damage in each cycle was the most important consideration in determining exposure effects on life.

It can be concluded that exposure effects could significantly influence disk superalloy fatigue lives, by shifting the failure initiation sites from internal defects to environment-affected surface layers. Prior exposures of specimens can be used to help approximate some aspects of the exposure effects that may occur during service in aerospace gas turbine engines, by activating to some degree a fatigue cracking mechanism at surface oxidation. However, more realistic cyclic dwell tests produced the lowest lives, and could give more accurate indications of exposure impacts on service lives.

REFERENCES

1) T. P. Gabb, J. Telesman, P. T. Kantzos, J. W. Smith, "Effects of High Temperature Exposures on Fatigue Life of Disk Superalloys", Superalloys 2004, ed. K. A. Green, H. Harada, T. E. Howson, T. M. Pollock, R. C. Reed, J. J. Schirra, S. Walston, TMS, Warrendale, PA, 2004, pp. 269-274.
2) T. P. Gabb, J. Telesman, P. T. Kantzos, K. O'Connor, "Characterization of the Temperature Capabilities of Advanced Disk Alloy ME3", NASA/TM-2002-211796, Washington, D.C., Aug. 2002.

9.12.17 INCORPORATING RESIDUAL STRESSES IN LIFE PREDICTION OF TURBINE ENGINE COMPONENTS

Reji John, James M. Larsen, Jay Jira and Bryan Sanbongi, US Air Force Research Laboratory, Materials & Manufacturing Directorate, AFRL/MLL

A technology development program known as Engine Rotor Life Extension (ERLE) [1] has been initiated by the United States Air Force. ERLE has the goal of extending the useful lifetime of major, fracture-critical components in currently fielded gas turbine engines, without increasing the risk of component failure. A broad range of related technologies such as life prediction and fracture mechanics, nondestructive evaluation, engine usage and health monitoring, and component repair have been targeted for achievement of this goal. The total life of an engine component can be determined as the sum of crack initiation life and crack propagation life. Crack propagation life typically includes the small and large crack growth regimes. Current life management practice (Engine Structural Integrity Program, ENSIP) by the U.S. Air Force uses a damage-tolerance-based method for managing the life of safety-critical components. This approach is based on systematic inspections of critical life-limiting locations in components. The inspection intervals are determined as 50% of the predicted crack growth life from an assumed initial flaw size. Using nondestructive inspection (NDI) techniques, the components are inspected for location-specific crack sizes. The component design lifetime is based on a crack initiation criterion, but if a crack is detected prior to this mandatory component retirement lifetime, then the component is retired immediately.

The prediction of the crack growth behavior at critical locations in a component is based on the expected thermo-mechanical loading conditions and the assumed crack growth behavior of the material. Shot-peening is used to retard crack growth at critical locations in most of the legacy engines. Shot-peening introduces significant near-surface (within 0.15–0.20 mm) compressive stresses. The benefits of these compressive residual stresses in improving fatigue life, retardation of crack growth and resistance to foreign object damage have been extensively demonstrated. However, current damage-tolerance-based life management practices, i.e. Predictions of crack initiation life and crack propagation life, do not explicitly account for the residual stresses induced by surface enhancement procedures. Incorporation of surface-treatment induced residual stresses in life management is a key technology in the ERLE initiative. Hence, AFRL/MLL has initiated many programs addressing incorporation of residual stresses in crack growth life prediction.

Surface measurements on post-service disks showed that significant residual stresses were retained in these components at the end of current design life [2]. The magnitude of the retained surface stresses was about 30-50% of the initial stresses [2]. This degree of surface residual stress relaxation is consistent with lab studies [3]. Accurate life prediction of crack growth in the presence of residual stresses requires the knowledge of the surface and sub-surface residual stresses along the crack plane. Hence, a benchmark program was initiated by AFRL/MLL to measure detailed depth measurements of residual stresses in post-service disks. Crack growth analyses showed that even retention of only 20-50% of the original residual stress distribution can yield greater than 2X increase in crack growth life, compared to the current baseline predictions that exclude residual stresses [4]. Thus, combining data from the field with detailed laboratory experiments and analysis, a reduced level of residual stress could be established and implemented in life management practice. Monitoring residual stresses at critical locations during service can help reduce the potential increase in risk associated with disk life extension. Life management based on such threshold residual stress level will require NDI-based accurate monitoring of residual stress at critical locations. Recent depth measurements have shown that the most substantial residual stress relaxation occurs close to the surface [4]. Sub-surface residual stress relaxation is not as severe as that observed on the surface [4]. Hence, AFRL/MLL has initiated a program to develop NDI techniques that are capable of measuring sub-surface residual stresses in titanium and superalloys. Such residual stress inspections are in addition to current crack inspections being conducted under the ENSIP program. Therefore, successful implementation of a life prediction methodology using residual stresses requires two critical NDI technology developments. These are: (1) accurate and reliable NDI techniques sensitive to crack extension in the surface and depth directions, and (2) NDI techniques to monitor surface and subsurface changes in residual stresses in components. AFRL/MLL has initiated programs aimed at developing these advanced NDI techniques.

REFERENCES

1) Larsen, J.M., et al., “The Engine Rotor Life Extension (ERLE) Initiative and It’s Opportunities to Increase Life and Reduce Maintenance Costs,” presented at AeroMat 2001, Long Beach, CA, 12 June 2001.

2) Vukelich, S., Berkley, S., Russ, S., and Bradley, E. F., "Residual stress measurement and its application to achieve predicted full life potential of low cycle fatigue (LCF) engine disks," Proceedings of The 9th International Symposium on Transport Phenomena and Dynamics of Rotating Machinery, Honolulu, Hawaii, February 2002.
3) Buchanan, D.J., John, R., and Ashbaugh, N.E., "Thermal Residual Stress Relaxation in Powder Metal IN100 Alloy," Journal of ASTM International, Submitted, May 2004.
4) John, R., Larsen, J.M, Buchanan, D.J., and Ashbaugh, N.E., "Incorporating Residual Stresses in Life Prediction of Turbine Engine Disks," Fatigue 2002, Proceedings of the Eighth International Fatigue Conference, Editor: A.F. Blom, Engineering Materials and Advisory Services Ltd, West Midlands, UK, pp. 1063-1070, June 2002.

9.12.18 FATIGUE VARIABILITY AND MECHANISM-BASED LIFE PREDICTION

J.M. Larsen and A.H. Rosenberger, US Air Force Research Laboratory and S.K. Jha, Universal Technology Corp.

Current approaches to life management of fracture critical turbine engine components tend to treat the uncertainty in lifetimes arbitrarily. Therefore, a significant part of the useful life of a component may remain unutilized. The sustainment and replacement costs and their impact on fleet readiness calls for a reevaluation of the present paradigm. The Materials Damage Prognosis Program initiated by the Defense Advanced Research Projects Agency (DARPA) is aimed at reliably increasing the utilization of the useful capability of a component or system by an integrated approach to life management [1]. One of the key elements of this approach is to develop a physically-based life prediction methodology that is based on a real time awareness of the damage state of the material [1]. Consistent with this goal we have examined the physical basis for variability in fatigue lifetimes of several turbine disk materials as well as materials potentially considered for engine applications [2-7]. We show that the largest contribution to the variability in fatigue lifetimes comes from superposition of variability of at least two separate mechanisms at the same stress levels. We propose a life prediction methodology that is based on the variability in the worst-case failure mechanism.

Depending on the material, the superposition of mechanisms seemed to be related either to the duality in the state of deformation of the material [2,6] or due to dual crack initiation modes [7]. For example, in the $\alpha+\beta$ titanium alloy, Ti-6Al-2Sn-4Zr-6Mo (Ti-6-2-4-6), the variability in life increased with decreasing stress level (σ_{max}) as shown in Figure 9.12-38. However, at lower stress levels, the experimental points had a step-like shape [2] with respect to the Cumulative Distribution Function (CDF). This is shown at the σ_{max} level of 860 MPa in Figure 9.12-39. This indicated that, the increased variability with decreasing σ_{max} resulted from superimposition of variability associated with two failure mechanisms (designated as Type I and Type II in Figure 9.12-39) [2]. Detailed characterization of the crack initiation sites revealed that, the life limiting failures (i.e., Type I) nucleated in a surface primary-α (α_p) particle that had its basal pole along the loading axis and was surrounded by a region of high activity of prism <a> type slip [6]. It was hypothesized [3,6] that the crack initiation or the onset of propagation in the Type I failures occurred during the heterogeneous deformation state of the sample, i.e., in the initial fatigue cycles leading to small lifetimes (on the order of 10^4 cycles). On the other hand, in the Type II, crack initiation occurred after deformation was more homogeneously distributed leading to up to two orders of magnitude longer lifetimes.

In another example, a nearly fully-lamellar γ-TiAl based alloy showed almost flat fatigue life behavior, i.e., lives differed by orders of magnitude within a very narrow range of σ_{max} [7]. This is shown in Figure 9.12-40. The experimental points, again, had a step-like shape with respect to the CDF as shown in Figure 9.12-41 for the σ_{max} level of 475 MPa and the temperature of 600ºC. The flat fatigue-life behavior was shown to be due to the segregation of lives into two mechanisms. This depended on whether failure occurred by immediate propagation of a surface nucleated crack (leading to lives on the order of 10^3 cycles) or alternately, by subsurface crack nucleation (leading to lives on the order of 10^6 cycles) [7].

The common factor between both materials was that their fatigue behaviors were marked by two mechanisms such that the first mechanism (smaller lifetime) was caused by early crack nucleation/onset of propagation. The variability in this mechanism was related to the variability in the small + long crack propagation [6,7] in these materials. A life prediction methodology is proposed that takes into account the dual nature of fatigue variability. In this methodology, life prediction is based on the variability in the worst-case mechanism, i.e., variability in crack growth from the life-limiting microstructural parameter. This is illustrated in Figure 9.12-42 (a) and (b) respectively for Ti-6-2-4-6 [6] and the γ-TiAl based alloy [7]. A significant reduction in the uncertainty in life and, therefore, a greater utilization of the useful life, can be achieved as illustrated in the figure.

REFERENCES

1) L. Christodoulou and J. M. Larsen, "Using Materials Prognosis to Maximize the Utilization Potential of Complex Mechanical Systems," *JOM*, March 2004, p. 15, 2004.
2) S. K. Jha, J. M. Larsen, A. H. Rosenberger, and G. A. Hartman, "Dual Fatigue Failure Modes in Ti-6Al-2Sn-4Zr-6Mo and Consequences on Probabilistic Life Prediction," *Scripta Materialia*, Vol. 48, p. 1637, 2003.
3) S. K. Jha, J. M. Larsen, A. H. Rosenberger, and G. A. Hartman, "Microstructure Based Variability in Fatigue Life of Ti-6Al-2Sn-4Zr-6Mo," *Probabilistic Aspects of Life Prediction*, ASTM STP 1450, W. S. Johnson and B. M. Hillberry, Eds., ASTM International, West Conshohoken, PA, pp. 116-127, 2004.
4) S. K. Jha, M. J. Caton, J. M. Larsen, and A. H. Rosenberger, "Superimposing mechanisms and their effect on the variability in fatigue lives of a nickel-based superalloy," in *Materials Damage Prognosis,* J. M. Larsen, et. al. eds., TMS publications, 2005, in press.
5) M. J. Caton, S. K. Jha, J. M. Larsen, and A. H. Rosenberger, "Divergence of Mechanisms and the Effect on the Fatigue Life Variability of Rene`88 DT," in *Superalloys 2004*, p. 305, 2004.
6) S. K. Jha, J. M. Larsen, A. H. Rosenberger, and C. Annis, "Prediction of the worst-case fatigue failures in an α+β titanium alloy," in *Materials Damage Prognosis,* J. M. Larsen, et. al. eds., TMS publications, 2005, in press.
7) S. K. Jha, J. M. Larsen, and A. H. Rosenberger, "The role of competing mechanisms in the fatigue life variability of a nearly fully-lamellar γ-TiAl based alloy," Acta Materialia, Vol. 53, p. 1293, 2005.

9.12.19 SIMULATION OF THREE-DIMENSIONAL CRACK GROWTH IN AEROSPACE COMPONENTS

Reji John and Lt Sigfried Haering, US Air Force Research Laboratory, Materials & Manufacturing Directorate, AFRL/MLLMN

A technology development program known as Engine Rotor Life Extension (ERLE) [1] has been initiated by the United States Air Force. ERLE has the goal of extending the useful lifetime of major, fracture-critical components in currently fielded gas turbine engines, without increasing the risk of component failure. A broad range of related technologies such as life prediction and fracture mechanics, nondestructive evaluation, engine usage and health monitoring, and component repair have been targeted for achievement of this goal. The total life of an engine component can be determined as the sum of crack initiation life and crack propagation life. Crack propagation life typically includes the small and large crack growth regimes. These cracks typically occur at complex features requiring the use of three-dimensional (3D) crack propagation simulation tools for accurate crack growth life prediction [2]. Hence, AFRL/MLLMN initiated two programs to develop 3D crack propagation tools capable of predicting crack growth in components under realistic engine service conditions.

The objective of the first program was to incorporate advanced capabilities in the fracture mechanics software, ZENCRACK [3]. The new capabilities include cyclic and time-dependent load spectra, residual stress effects on crack growth, generalized Willenborg retardation, user-defined crack fronts (e.g. for transition from semi-elliptic to through cracks) and automatic large 3-D crack growth. ZENCRACK was also interfaced to ANSYS in addition to enhanced interfaces to ABAQUS and MSC.MARC. Advanced numerical crack growth integration algorithms were developed for superposition load systems (e.g. static residual stresses and cyclic loading). New 3-D meshing features to minimize element distortion were developed. Fatigue and time-dependent crack growth data can be specified as a function of stress ratio and temperature using Paris Law segment data, tabular data or in a ZENCRACK user subroutine. AFRL/MLLMN is evaluating this code using feature specimens in which corner cracks emanate from holes. In addition, ZENCRACK was recently used to simulate deformation modes in disks due to cracks at critical locations [4].

The objective of the second program was to develop a finite element based crack propagation analysis software, FRANC3D. The current version of openly available FRANC3D is based on the boundary element method [5, 6]. Application of FRANC3D for analysis of engine components under service loading conditions required integration with finite element codes such as ANSYS and ABAQUS. The first phase of this program is directed towards development of ANSYS based crack propagation analysis. Evaluation of the interim version of this code is in progress at AFRL/MLLMN. Additional capabilities including analysis under engine service conditions effects are being planned.

REFERENCES

1) Larsen, J.M., et al., "The Engine Rotor Life Extension (ERLE) Initiative and It's Opportunities to Increase Life and Reduce Maintenance Costs," presented at AeroMat 2001, Long Beach, CA, 12 June 2001.
2) Russ, S. M., Rosenberger, A. H., Larsen, J. M., Berkley, R. B., Carroll, D., Cowles, B. A., Holmes, R. A., Littles, J. W., Jr., Pettit, R. G., and Schirra, J. J., "Demonstration of Advanced Life-prediction and State-awareness Technologies Necessary for Prognosis of Turbine Engine Disks," Health Monitoring and Smart Nondestructive Evaluation of Structural and Biological Systems III, Proceedings of SPIE, Vol. 5394, 2004, pp. 23-32.
3) Chandwani, R., Cook, G., Timbrell, C., Wiehahn, M., Basu, A., Sharma, A.M., and Chakrabarti, P., "Improved Life Prediction of Turbine Engine Components Using A Finite Element Based Software Called Zencrack," AFRL-ML-WP-TR-2004-4014, SBIR Phase II Final Report, Air Force Research Laboratory, Wright-Patterson AFB, OH, USA, September 2003. Available at http://www.zentech.co.uk/zencrack.htm.
4) Brockman, R.A., Huelsman, M.A., and John, R., "Simulation of Deformation Modes for Damage Detection in Turbine Engine Disks," in Materials Damage Prognosis, J. M. Larsen, L. Christodoulou, J. R. Calcaterra, M. L. Dent, M. M. Derriso, W. J. Hardman, P. Hoffman, J. W. Jones, and S. M. Russ (Editors), The Minerals, Metals, and Materials Society, TMS, 2005.
5) FRacture ANalysis Code (FRANC3D) for simulating arbitrary non-planar 3D crack growth. Available at http://www.cfg.cornell.edu/software/software.htm.
6) Carter, B.J., Wawrzynek, P.A., and Ingraffea, A.R., "Automated 3D Crack Growth Simulation," International Journal of Numerical Methods in Engineering, Vol. 47, pp. 229-253, 2000.

9.13. FIGURES/TABLES

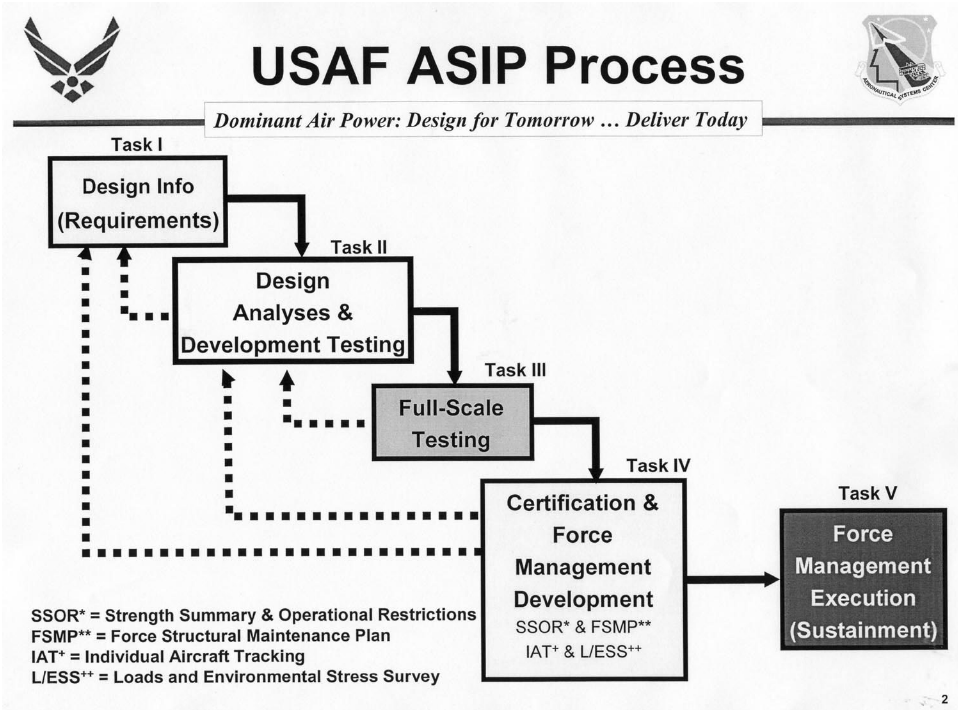

Figure 9.2-1

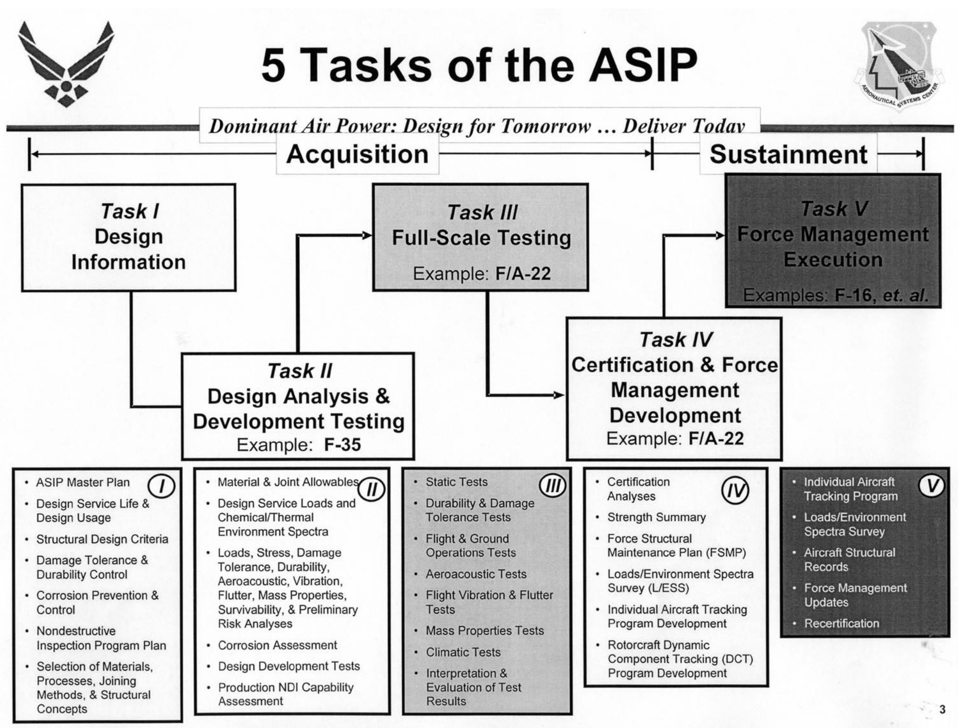

Figure 9.2-2

5 Tasks of the ASIP

Dominant Air Power: Design for Tomorrow … Deliver Today

TASK I	TASK II	TASK III	TASK IV	TASK V
DESIGN INFORMATION	**DESIGN ANALYSIS & DEVELOPMENT TESTING**	**FULL-SCALE TESTING**	**CERTIFICATION & FORCE MANAGEMENT DEVELOPMENT**	**FORCE MANAGEMENT EXECUTION**
ASIP MASTER PLAN	MATERIALS AND JOINT ALLOWABLES	STATIC TESTS	CERTIFICATION ANALYSES	INDIVIDUAL AIRCRAFT TRACKING PROGRAM
DESIGN SERVICE GOAL AND DESIGN USAGE	LOAD & STRESS ANALYSES	DURABILITY TESTS	STRENGTH SUMMARY	LOADS/ ENVIRONMENT SPECTRA SURVEY
STRUCTURAL DESIGN CRITERIA	DESIGN SERVICE LOADS & DESIGN CHEMICAL/THERMAL ENVIRONMENT SPECTRA	DAMAGE TOLERANCE TESTS	FORCE STRUCTURAL MAINTENANCE PLAN	AIRCRAFT STRUCTURAL RECORDS
DAMAGE TOLERANCE & DURABILITY CONTROL PROCESS	DURABILITY & DAMAGE TOLERANCE ANALYSES	FLIGHT & GROUND OPERATIONS TESTS	LOADS/ ENVIRONMENT SPECTRA SURVEY DEVELOPMENT	FORCE MANAGEMENT UPDATES
CORROSION PREVENTION & CONTROL	CORROSION ASSESSMENT	AEROACOUSTIC TESTS	INDIVIDUAL AIRCRAFT TRACKING PROGRAM DEVELOPMENT	RECERTIFICATION
NONDESTRUCTIVE INSPECTION PROGRAM PLAN	AEROACOUSTIC DURABILITY, VIBRATION & FLUTTER, & MASS PROPERTIES ANALYSS	FLIGHT VIBRATION TESTS	ROTORCRAFT DYNAMIC COMPONENT TRACKING PROGRAM DEVELOPMENT	
SELECTION OF MATERIALS, PROCESSES, JOINING METHODS, & STRUCTURAL CONCEPTS	PRELIMINARY RISK ANALYSIS	FLUTTER TESTS		
	SURVIVABILITY ANALYSIS	MASS PROPERTIES TESTS		
	DESIGN DEVELOPMENT TESTS	CLIMATIC TESTS		
	PRODUCTION NDI CAPABILITY ASSESSMENT	INTERPRETATION & EVALUATION OF TEST RESULTS		

4

Figure 9.2-3

Description of ASIP Tasks

Dominant Air Power: Design for Tomorrow … Deliver Today

Task I: **Design Information –** Develop structural design criteria, including strength, rigidity, damage tolerance and durability

Task II: **Data Analyses & Development Testing –** Determine the environment, perform preliminary and final structural analyses based on these environments and size the airframe to meet strength, rigidity, DT and durability criteria

Task III: **Full-Scale Testing –** Obtain sufficient flight and ground testing to validate the structural analyses

Task IV: **Certification & Force Management Development –** Develop the Force Structural Maintenance Plan (FSMP), adapt the process to collect usage and aging data, and estimate the economic service life for the airframe

Task V: **Force Management Execution –** Collect and analyze data for force structure decision-making and modify FSMP to keep the force safe and affordable

5

Figure 9.2-4

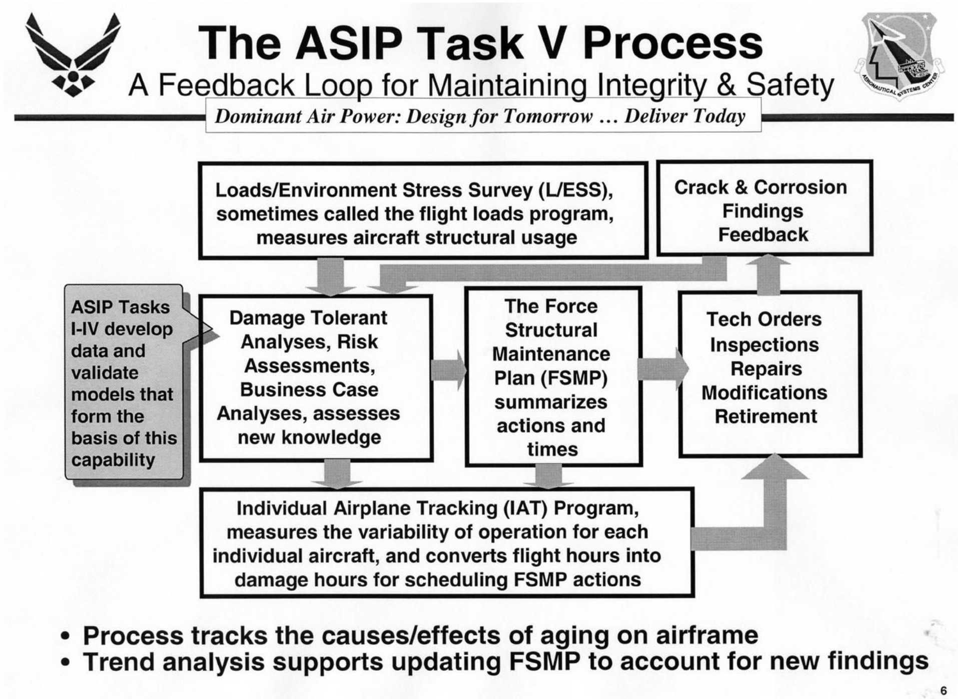

Figure 9.2-5

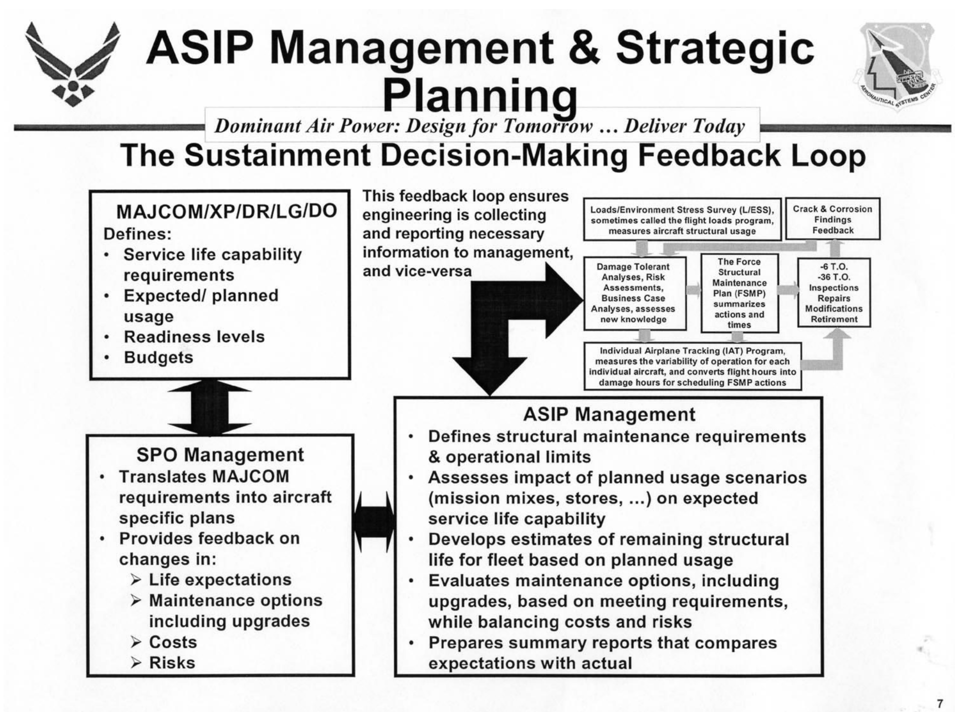

Figure 9.2-6

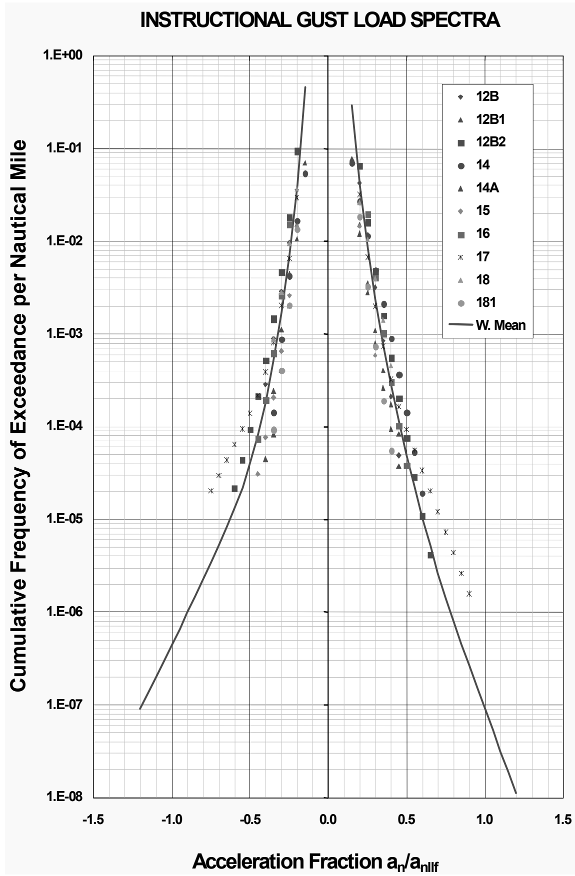

Figure 9.2-7 Instructional Single-Engine Airplane Gust Exceedance Spectra

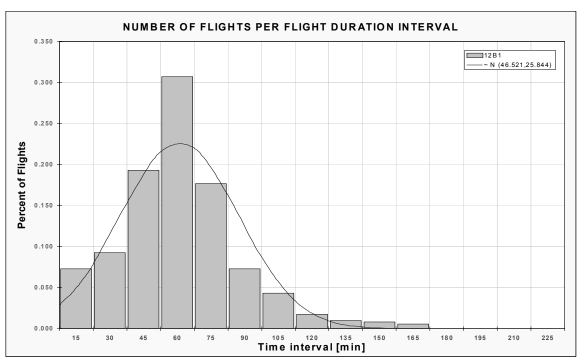

Figure 9.2-8 Single-Engine Flight Duration

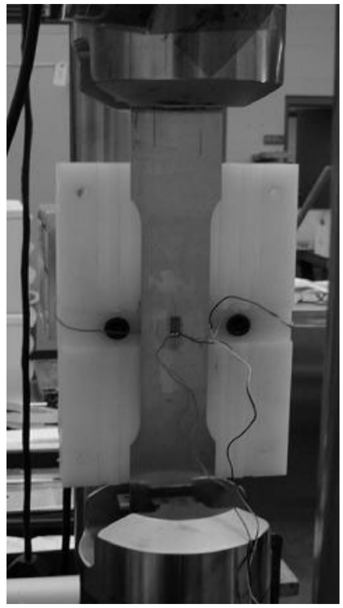

Figure 9.2-9 Test Specimen With Strain Gages and Antibuckling Fixture

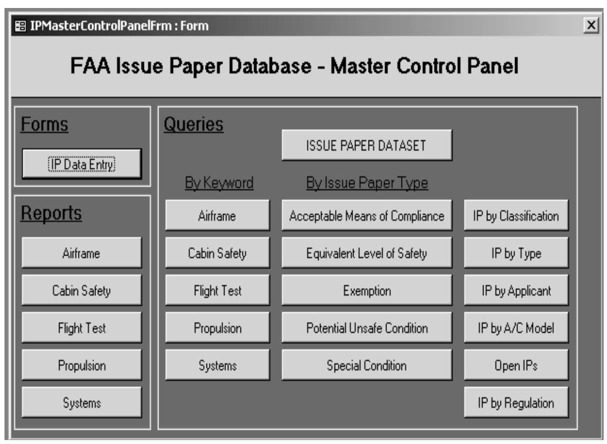

Figure 9.2-10 Master Control Panel Screen Layout

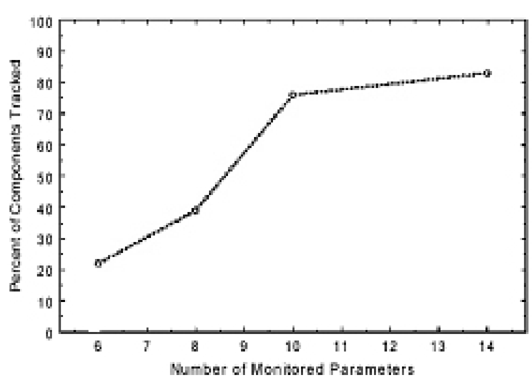

Figure 9.2-11 Number of Monitored Parameters

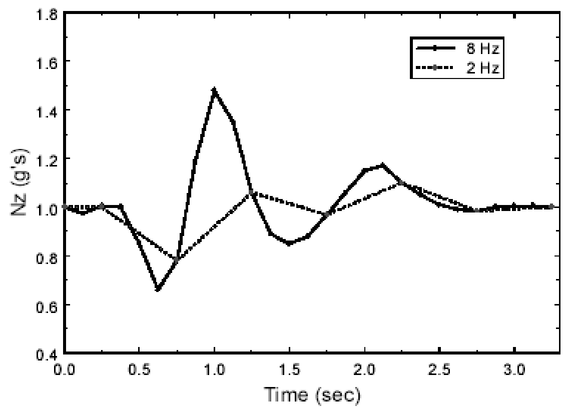

Figure 9.2-12 Effect of Data Rate on Vertical Acceleration

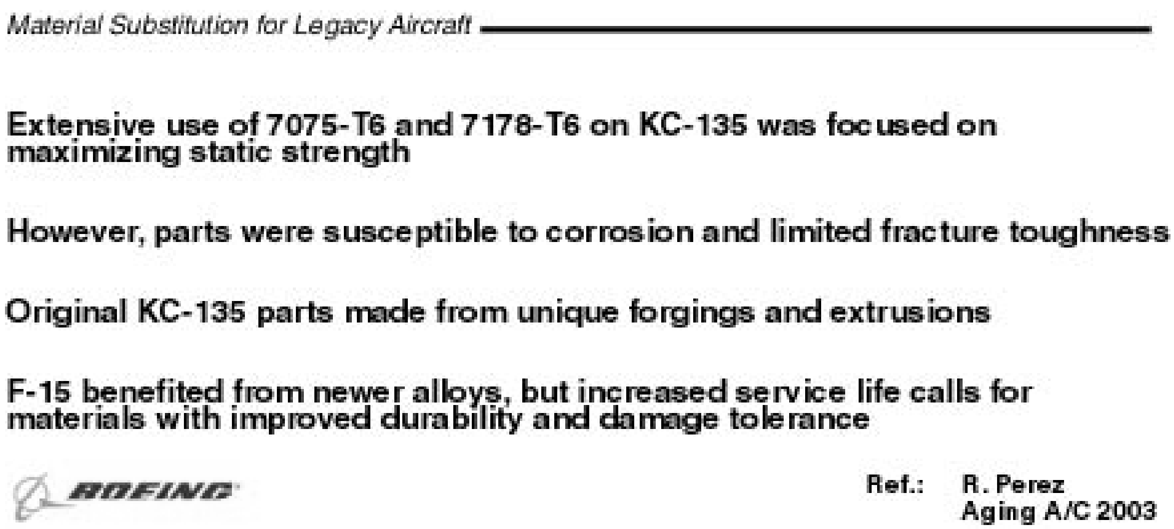

Figure 9.2-13

Preliminary Candidate Materials

Material Substitution for Legacy Aircraft

Plate	Extrusions	Forgings	Sheets
7049-T73X	7049/7149-T73X	7175-T74	2524-T3
7075-T73X, T76X	7075-T73X, T76X	7249-T7452	7055-T762
7475-T6X, T73X, T76X	7050-T73X, T74X T76X	7085-T7452, T7652	
7050-T74X, T76X	7150-T6X, T7X		
7040-T74X	7175-T73X		
7150-T6X, T7X	7055-T74X, T76X, T77X		
7055-T77X			
7085-T7X			
2324-T39			

BOEING

Ref.: R. Perez
Aging A/C 2003

Figure 9.2-14

Conclusions

Material Substitution for Legacy Aircraft

- Newer alloys have better combination of strength, corrosion resistance, durability and damage tolerance
- Many alloys are readily available and offer a return on investment
- Material issues can be overcome to ensure successful substitution in legacy aircraft

BOEING

Ref.: R. Perez
Aging A/C 2003

Figure 9.2-15

T34

- Procured as military trainer; USAF T34A, USN T34B.
- No fatigue requirements in certification basis (CAR3, 11/1/49) .
- Operated in US under civil registry starting in 1960's without any mandated fatigue management strategy.

Figure 9.2-16

T34 Accident and AD Overview

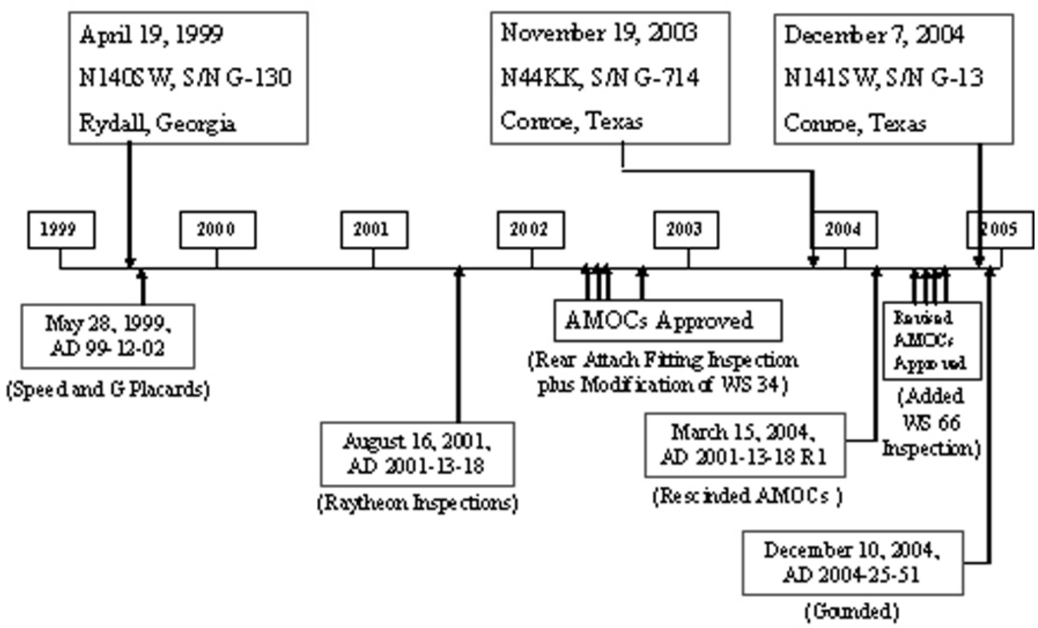

Figure 9.2-17

T34 Fracture Locations

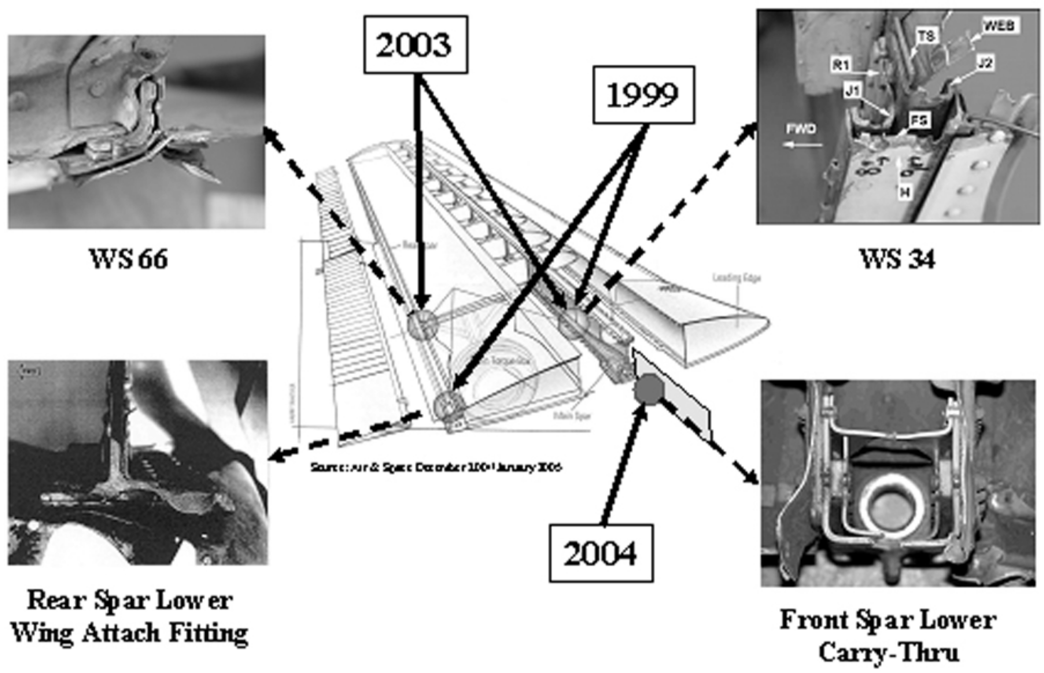

Figure 9.2-18

Cessna 402, 402A, 402B, 402C

• Wide range of usage including scheduled commuter, cargo delivery, scenic tours.

• No fatigue requirements in certification basis (CAR3, 5/15/56) .

• Operated in US starting in 1960's without any mandated fatigue management strategy.

Figure 9.2-19

402, 402A Cracking Locations

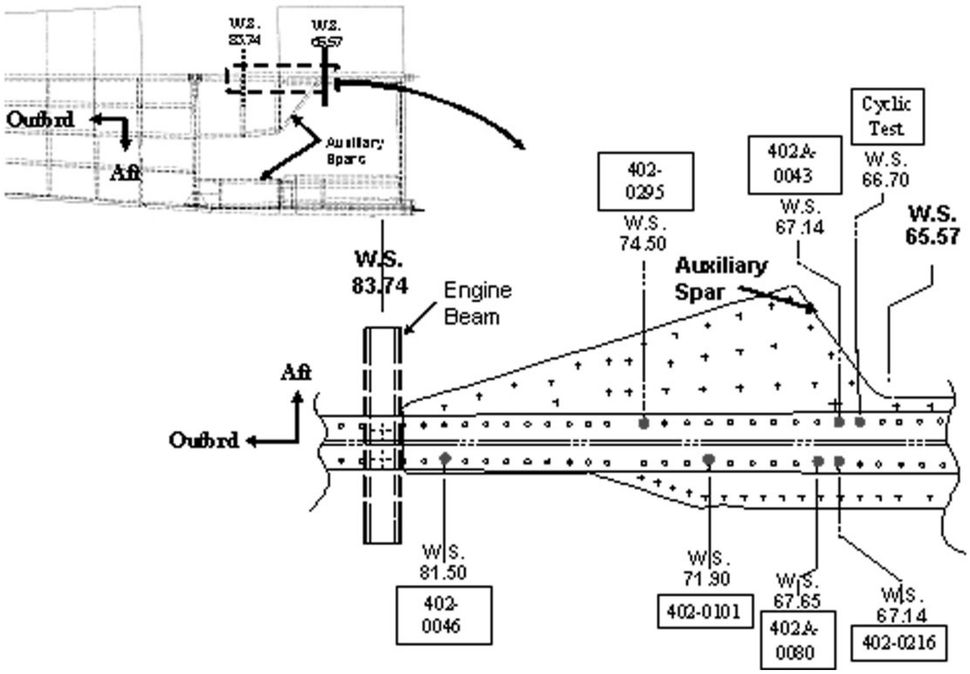

Figure 9.2-20

Model 402, 402A, 402B Wing Strap

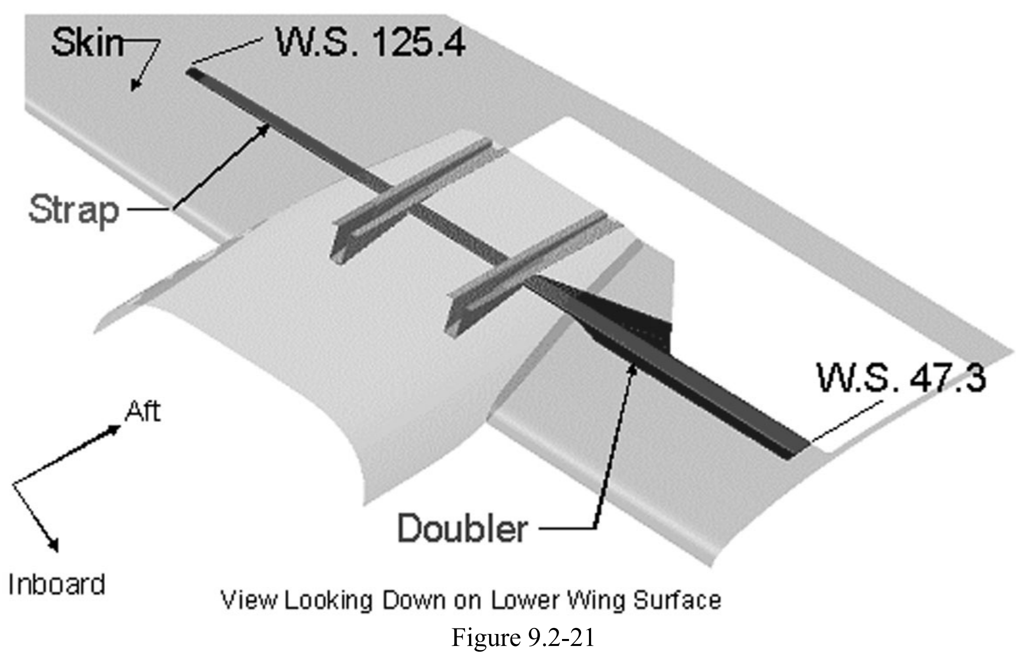

Figure 9.2-21

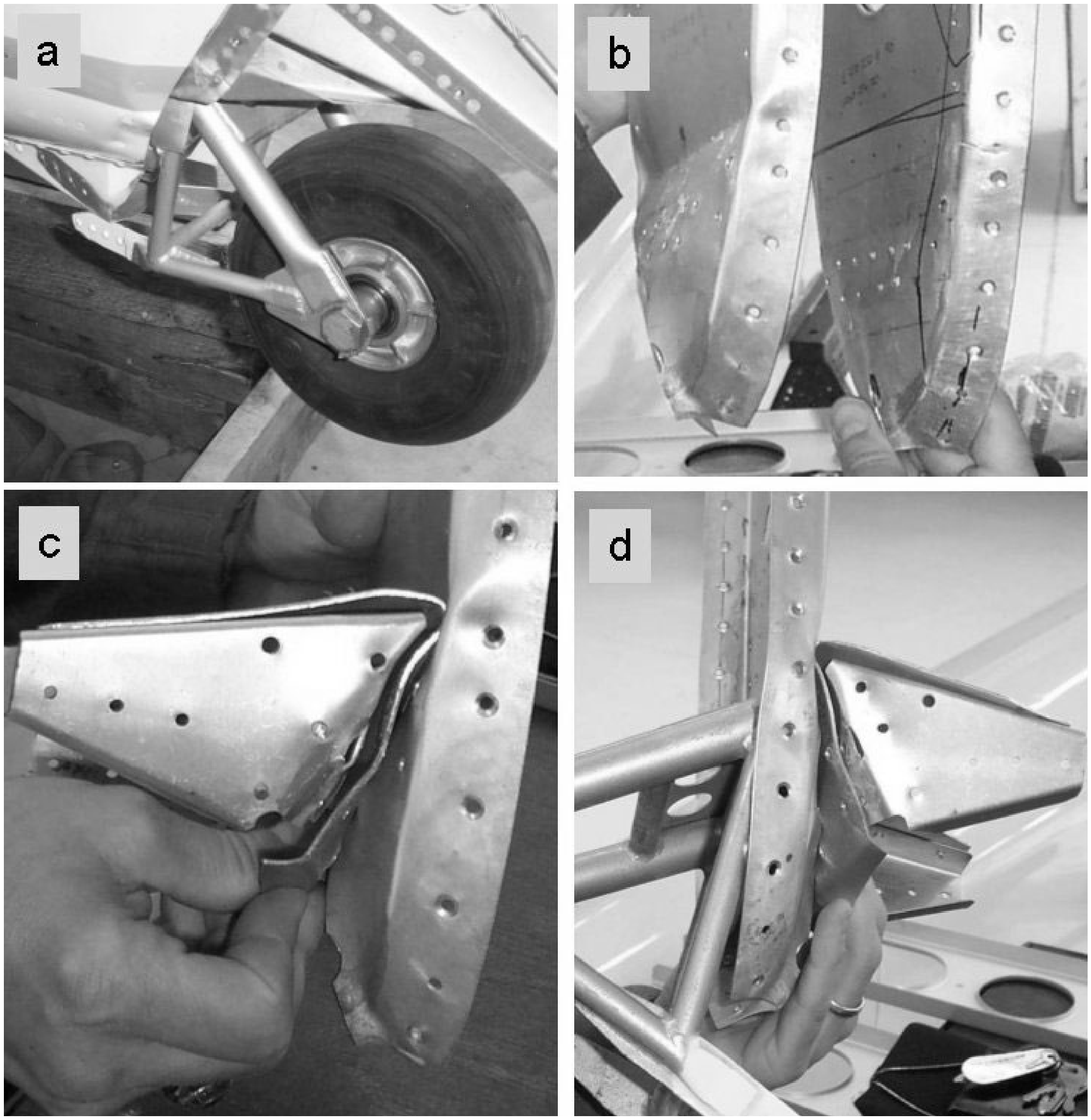

Figure 9.3-1 Photographs of typical damaged structure found after tail gear failure showing a) common ground observation after “hard” landing with failure of shear rivets, b) damage cased to aft spar by rigid tail gear truss upper flange and c,d) subsequent damage to substructure behind upper flange. Also shown in d) is the assembled relative orientation of tail gear structure without surrounding fuselage skin.

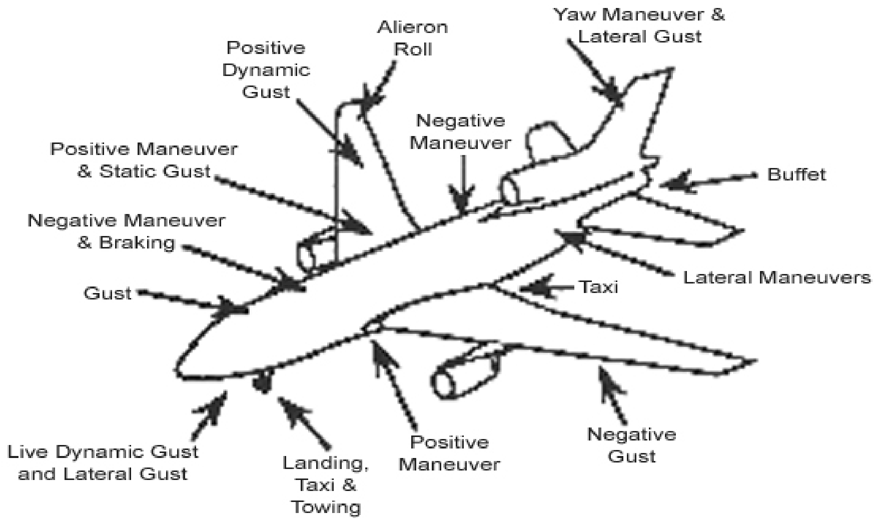

Figure 9.3-2 Typical Aircraft Loads

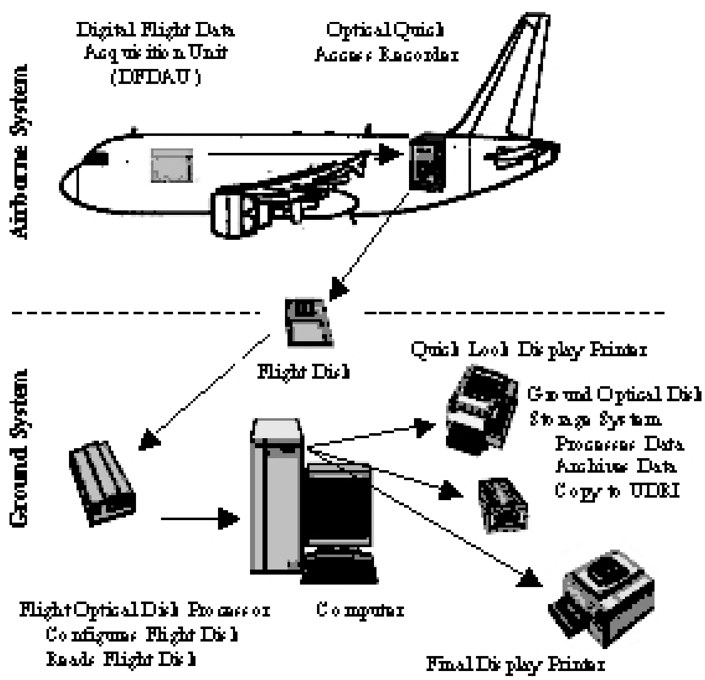

9.3-3 Optical Disc Flight Data Flow

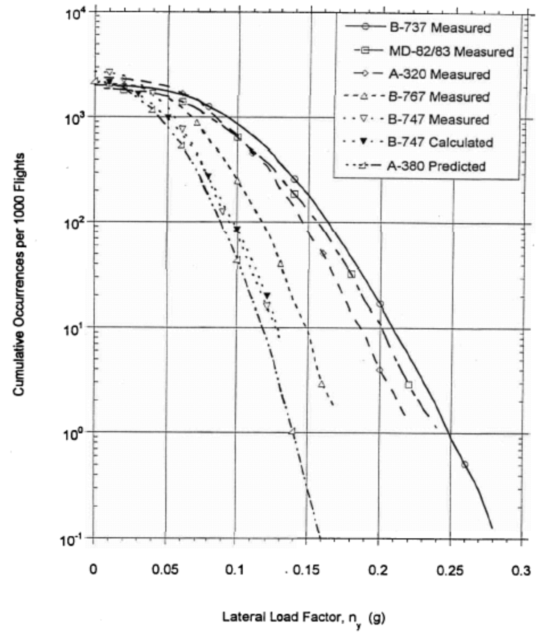

Figure 9.3-4 Comparison of Measured and Calculated Cumulative Frequency of Ground Turning Lateral Load Factor, Taxi-in

Figure 9.3-5 CRJ-100 Airplane

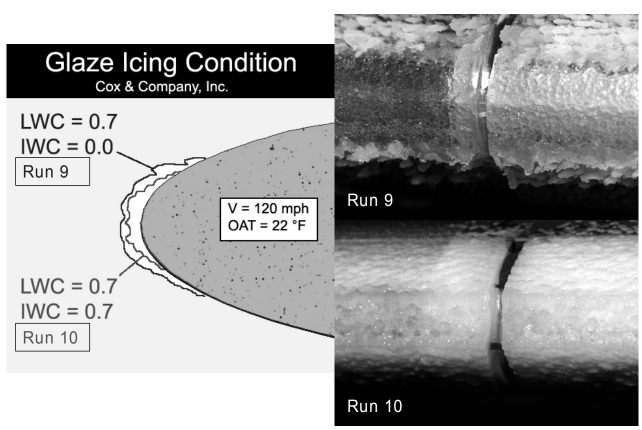

Figure 9.3-6 Comparison of Glaze Ice Accretions in Purely Liquid and Mixed-Phase Conditions

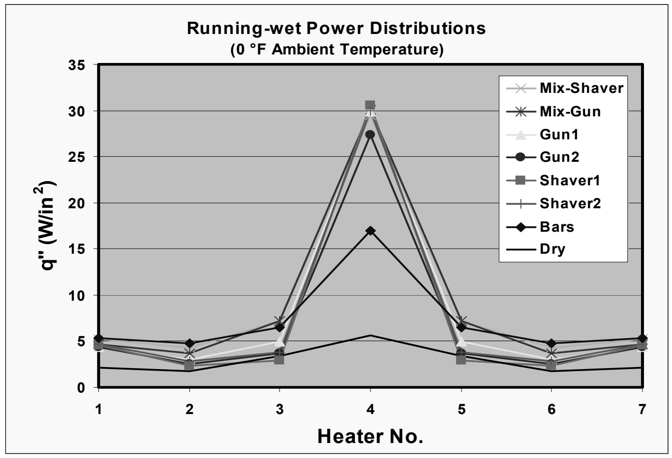

Figure 9.3-7 Power Distributions for a Thermal Ice Protection System in the Running-Wet Mode for Several Icing Conditions

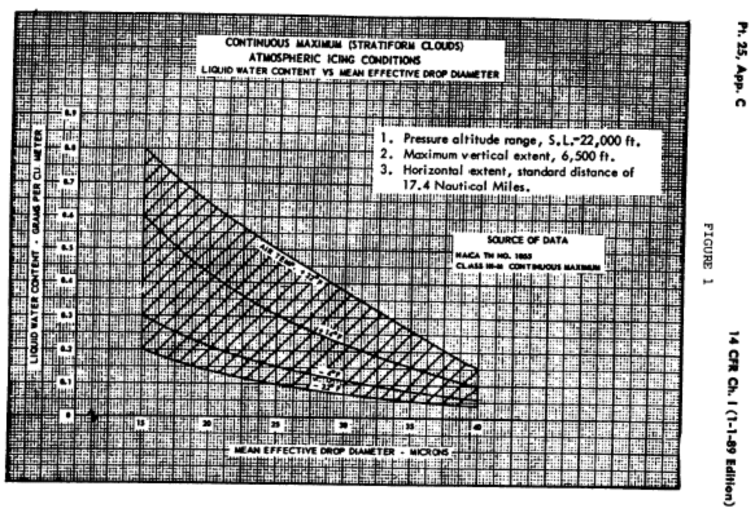

Figure 9.3-8 Continuous Maximum (Stratiform Clouds) Atmospheric Icing Conditions (reproduced from 14 CFR Part 25, Appendix C)

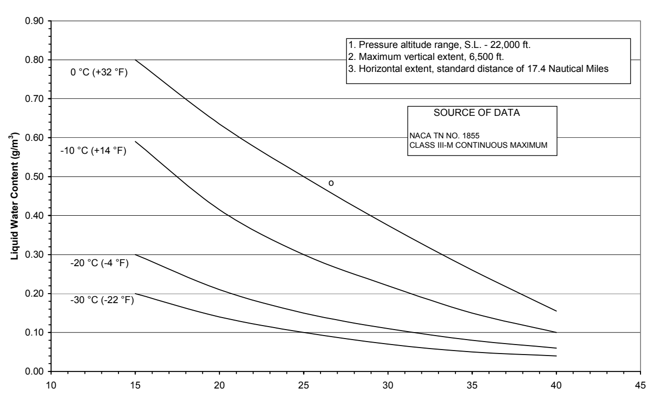

Figure 9.3-9 Continuous Maximum (Stratiform Clouds) Atmospheric Icing Conditions (produced using spreadsheet software)

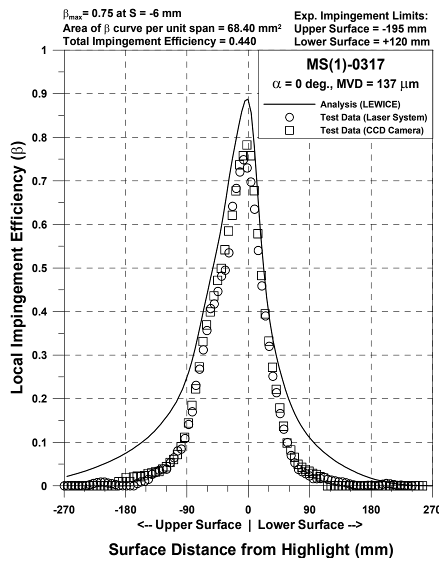

Figure 9.3-10 Experimental and Predicted Impingement Curves for an MS(1)-0317 Airfoil

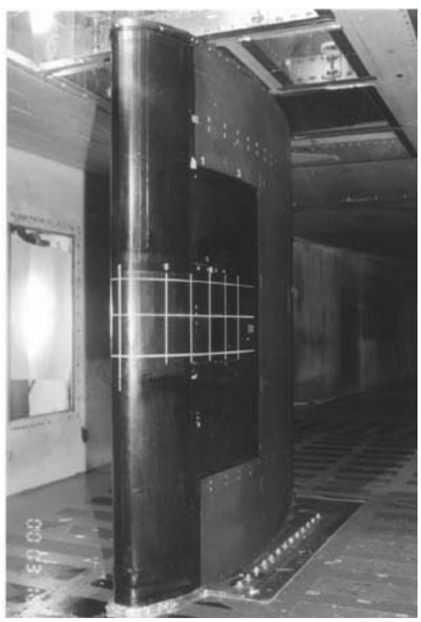

Figure 9.3-11 Commuter Turbopropeller Wing Model Installed in the NASA GRC IRT

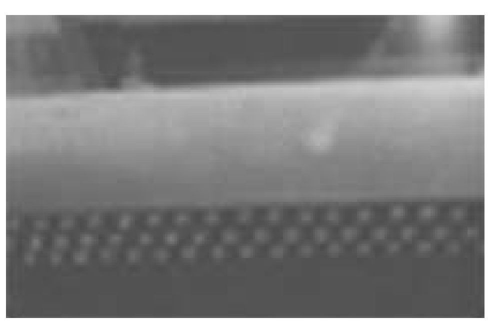

Figure 9.3-12 An SLD Ice Accretion Simulation Used for Aerodynamic Testing

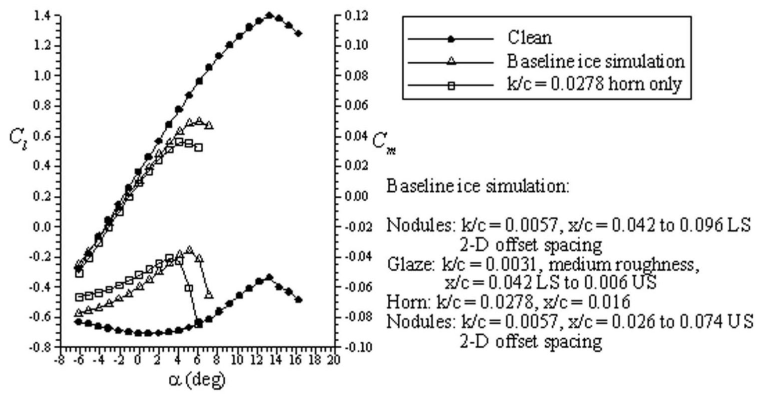

Figure 9.3-13 Comparison of Lift Performance With Baseline SLD Ice Accretion Simulation Versus a Horn Simulation Only

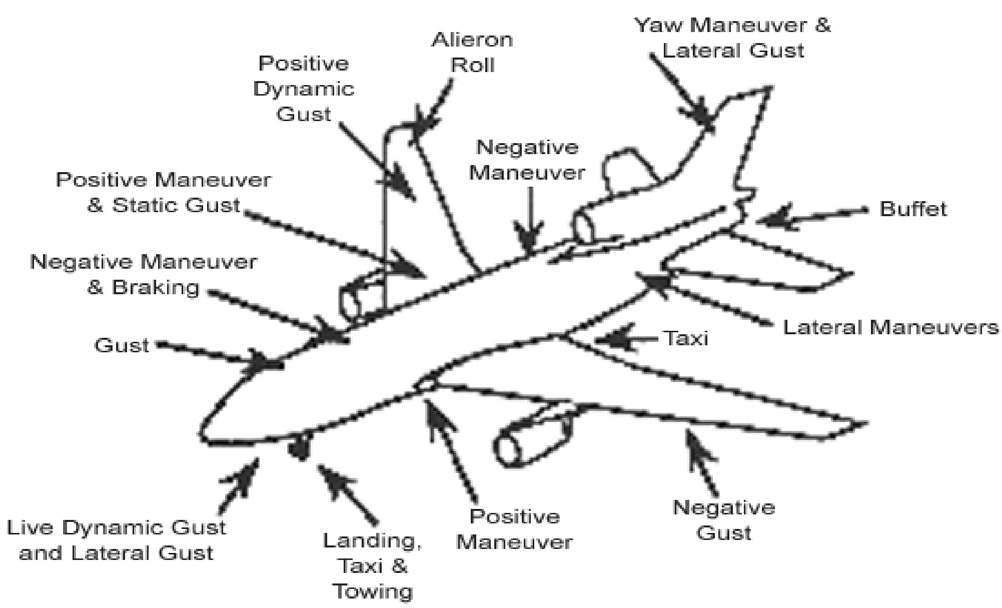

Figure 9.3-14

DOT/FAA/AR-04/47	Cumulative Aircraft Video Landing Parameter Surveys Summary Report - London City Airport, Philadelphia International Airport and Atlantic City International Airport, December 2004
DOT/FAA/AR-04/20	Documentation of the Linear Statistical Discrete Gust Method, June 2004
DOT/FAA/AR-03/62	Using Modern Computing Tools to Fit the Pearson Type III Distribution to Aviation Loads Data, September 2003
DOT/FAA/AR/-03/44	Statistical Loads Data for Bombardier CRJ-100 Aircraft in Commercial Operations, July 2003
DOT/FAA/AR-02/129	Side Load Factor Statistics From Commercial Aircraft Ground Operations, January 2003
DOT/FAA/AR-04/44	Statistical Loads Data for the B-747-400 Aircraft in Commercial Operations, January 2005

Figure 9.3-15 FAA Operational Loading Monitoring Published Reports 2003-2004

Figure 9.3-15A

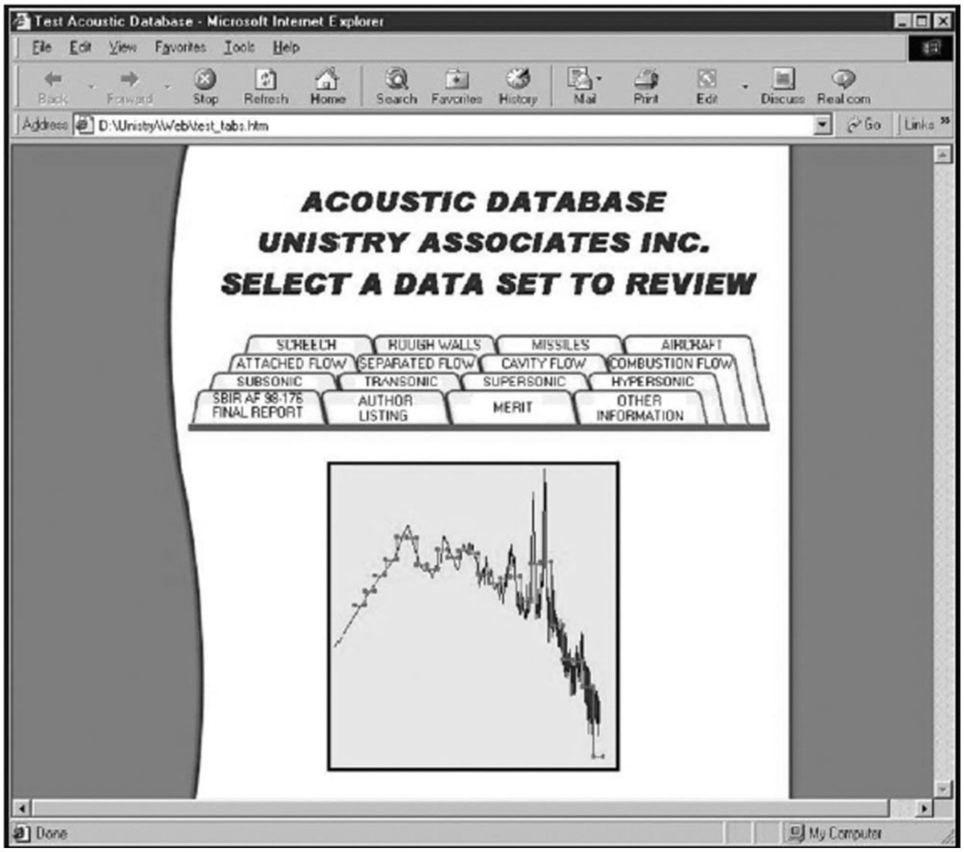

Figure 9.3-15B

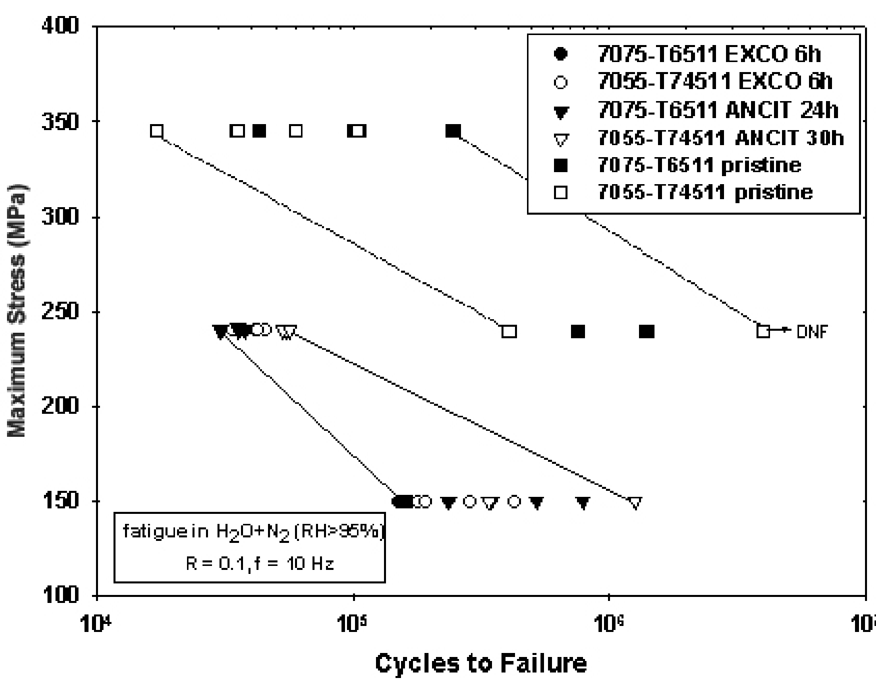

Figure 9.4-1 S-N Data Plots Comparing the Fatigue Resistance of Pristine and Pre-corroded Specimens of the Two 7000 Series Alloys. Dashed Lines Between Data Points Show the Range of Data Currently Available to Group Pristine and Pre-Corroded Specimens, Without Assuming a Trend.

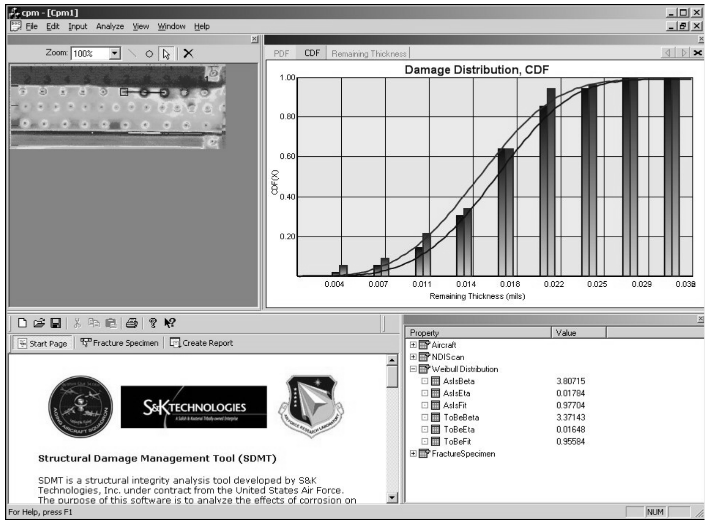

Figure 9.4-2 SDMT Interface

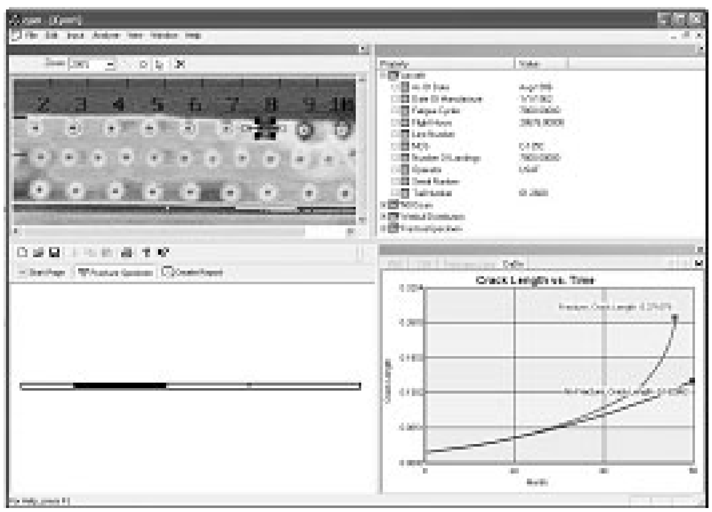

Figure 9.4-3 Crack Growth Analysis

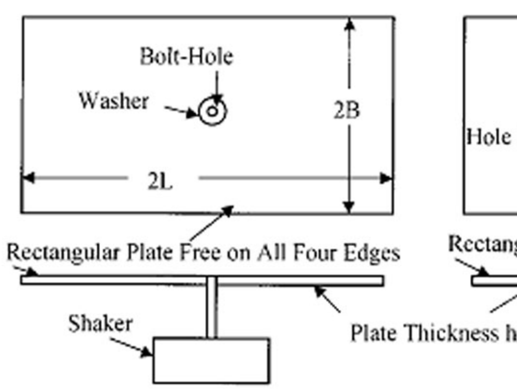

Figure 9.4-4a Test Specimen Geometry

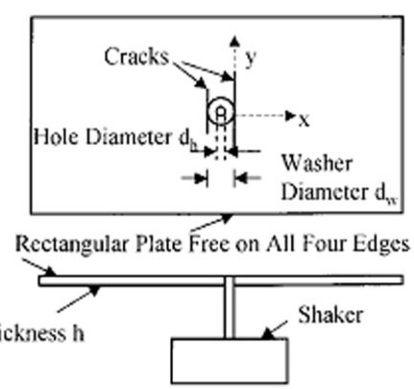

Figure 9.4-4b Crack Initiation Locations

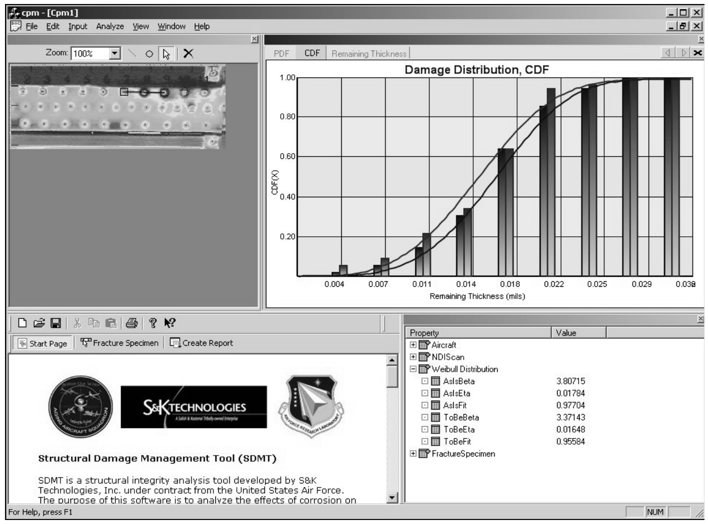

Figure 9.4-2 SDMT Interface

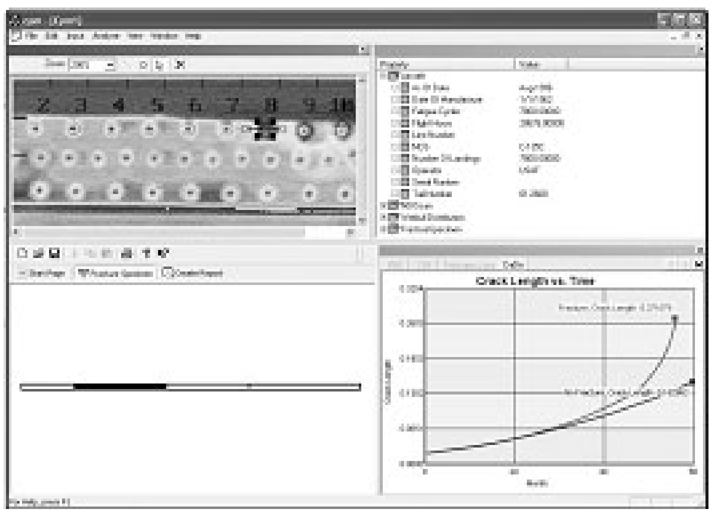

Figure 9.4-3 Crack Growth Analysis

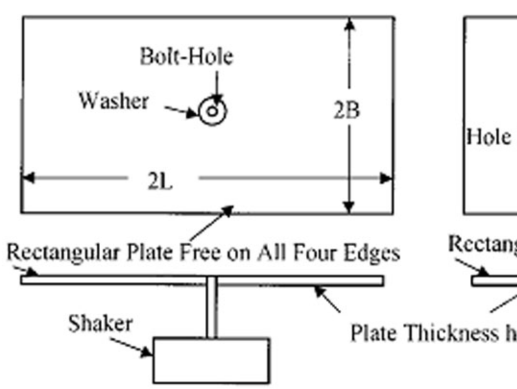

Figure 9.4-4a Test Specimen Geometry

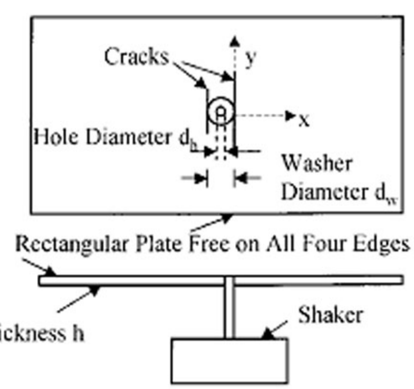

Figure 9.4-4b Crack Initiation Locations

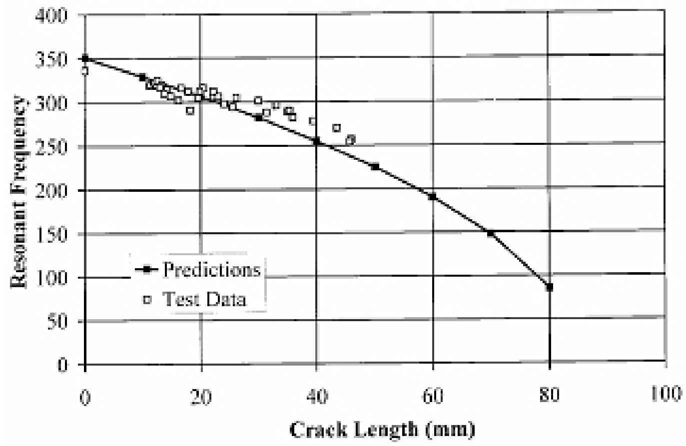

Figure 9.4-5 Predicted and Observed Resonant Frequencies at Various Crack Lengths in 85x180x3.2-mm Specimens

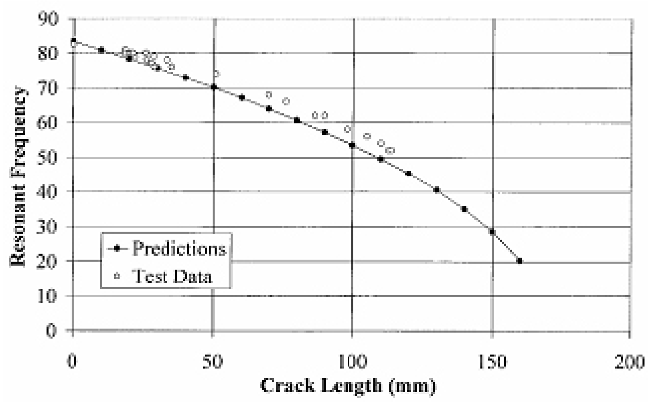

Figure 9.4-6 Predicted and Observed Resonant Frequencies at Various Crack Lengths in 170x360x3.2-mm Specimens

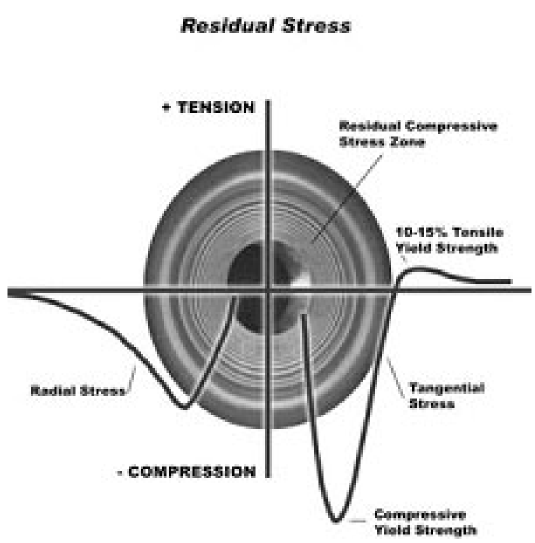

Figure 9.4-7 Schematic showing region of compressive and tensile residual stresses from cold expansion around a hole. Courtesy of FTI

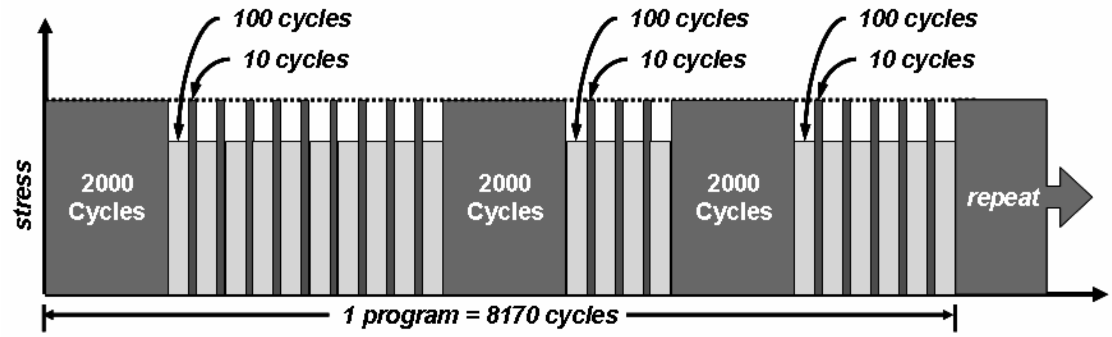

Figure 9.4-8 80% Marker Spectrum Where the Stress for the 100 Cycle Segments are Reduced to 80% of the Max Stress

Table 9.4-1 Testing Progress; Maximum Stress Versus Number of Cycles to Failure

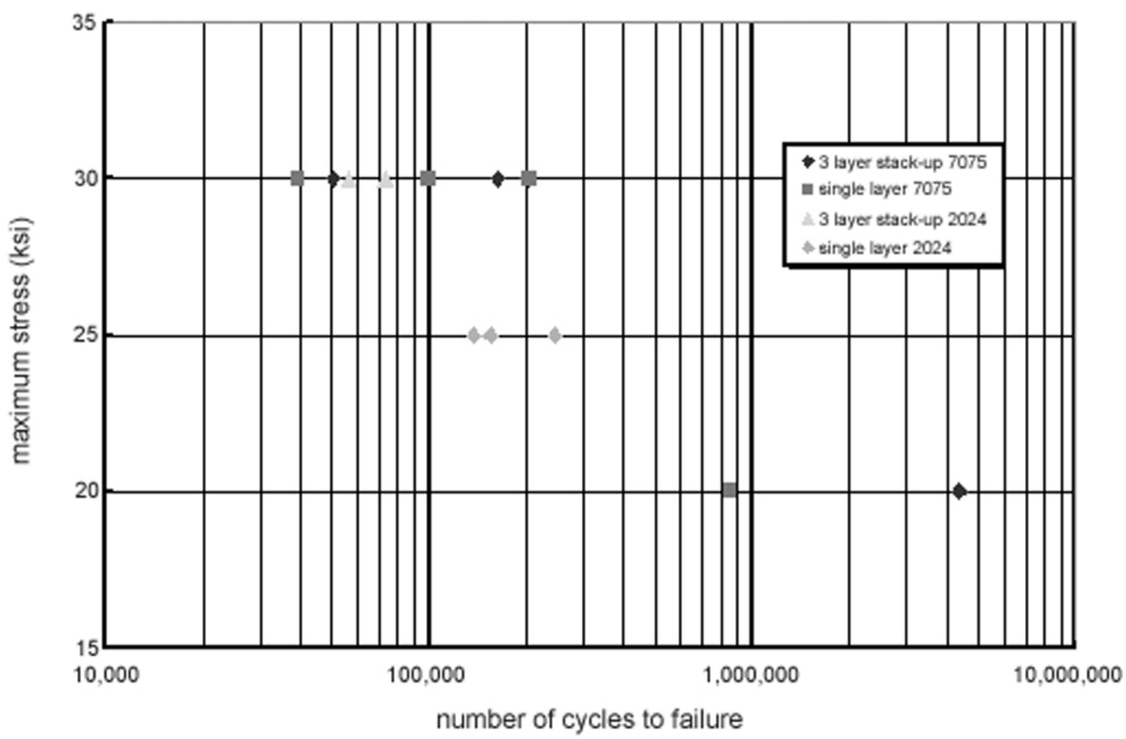

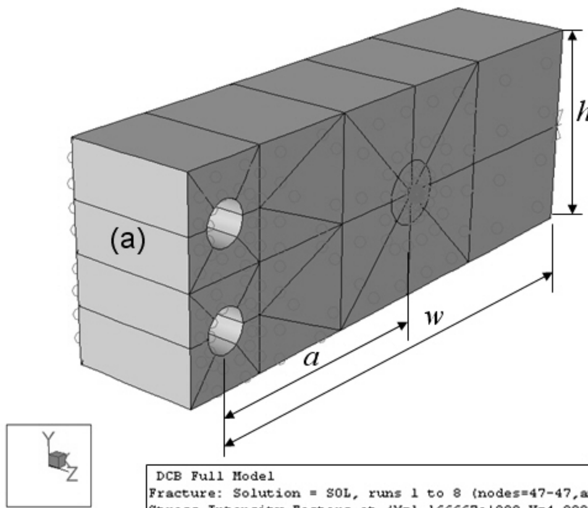

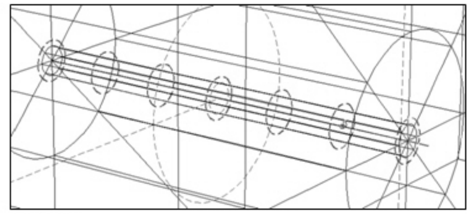

DCB Full Model
Points: Solution = SOL, runs #8 to #8
System=Global

(c)

N	Z	T-Stress Run #8
1	-2.499500E-001	5.783919E+003
2	-1.666333E-001	5.783981E+003
3	-8.331667E-002	5.783974E+003
4	-1.387779E-017	5.783979E+003
5	8.331667E-002	5.783975E+003
6	1.666333E-001	5.783984E+003
7	2.499500E-001	5.783919E+003

DCB Full Model
Fracture: Solution = SOL, runs 1 to 8 (nodes=47-47,angle=360.0),
Stress Intensity Factors at (X=1.166667e+000,Y=4.000000e-001,Z=-4.700134e-004)

(b)

DOF	K1	K2	T-Stress	Limit_K1	Limit_K2	Limit_T-Stress
217	1482.685	(0.000)	3559.947	3471.019	(0.000)	5795.523
782	3041.285	(0.000)	5629.416	3471.019	(0.000)	5795.523
1403	3340.071	(0.000)	5585.947	3471.019	(0.000)	5795.523
2500	3457.547	(0.000)	5767.338	3471.019	(0.000)	5795.523
4115	3480.592	(0.000)	5760.952	3471.019	(0.000)	5795.523
6380	3480.442	(0.000)	5772.722	3471.019	(0.000)	5795.523
9427	3477.495	(0.000)	5779.592	3471.019	(0.000)	5795.523
13388	3475.643	(0.000)	5783.979	3471.019	(0.000)	5795.523

Figure 9.4-9 DCB Specimen. (a) Finite Element Mesh, (b) Fracture Mechanic Parameters K1, K2 and T-stress at Mid-plane, (c) T-stress at Equally Space Points Along the Crack Front.

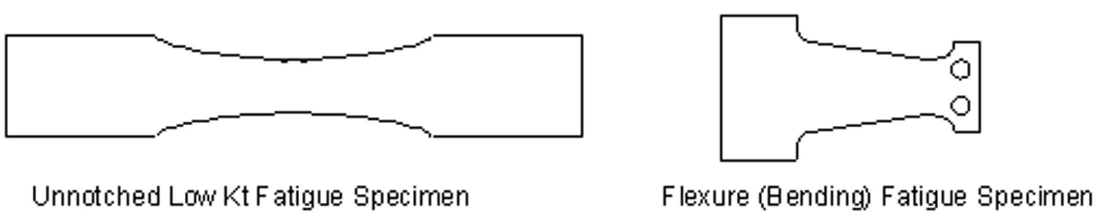

Figure 9.4-10 Fatigue Specimens

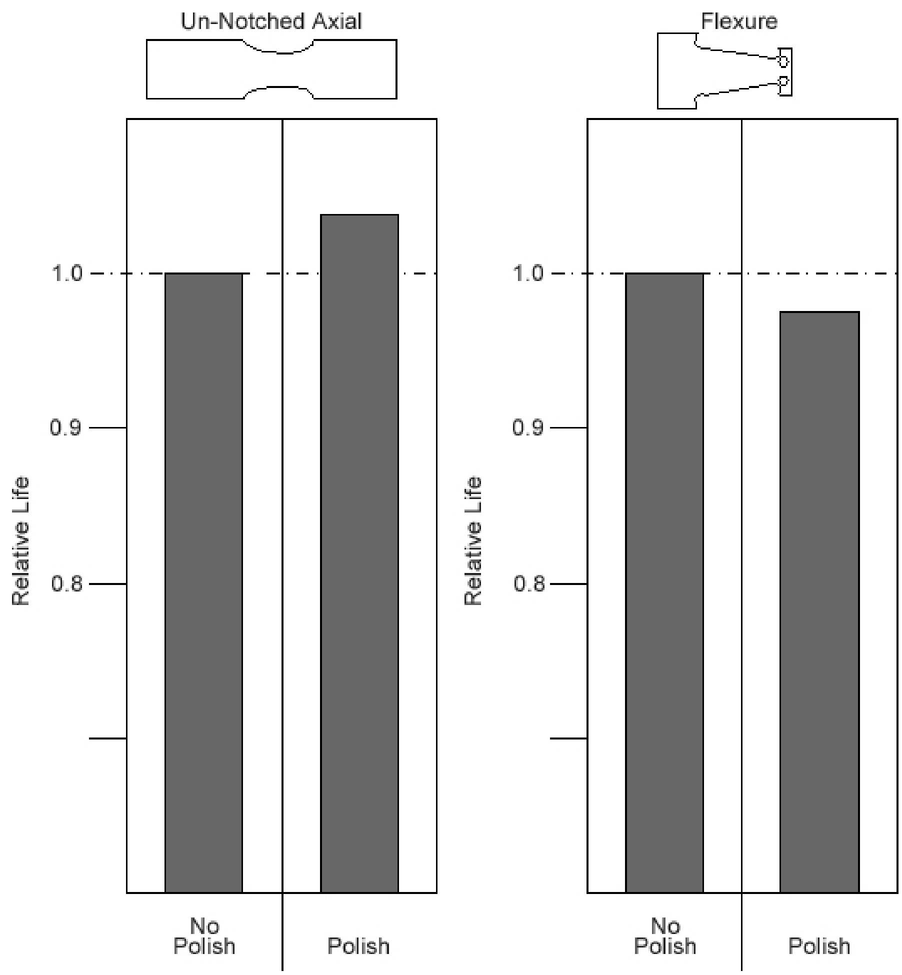

Figure 9.4-11 Fatigue Results of Un-Polished and Polished 2024-T3 Clad Sheet

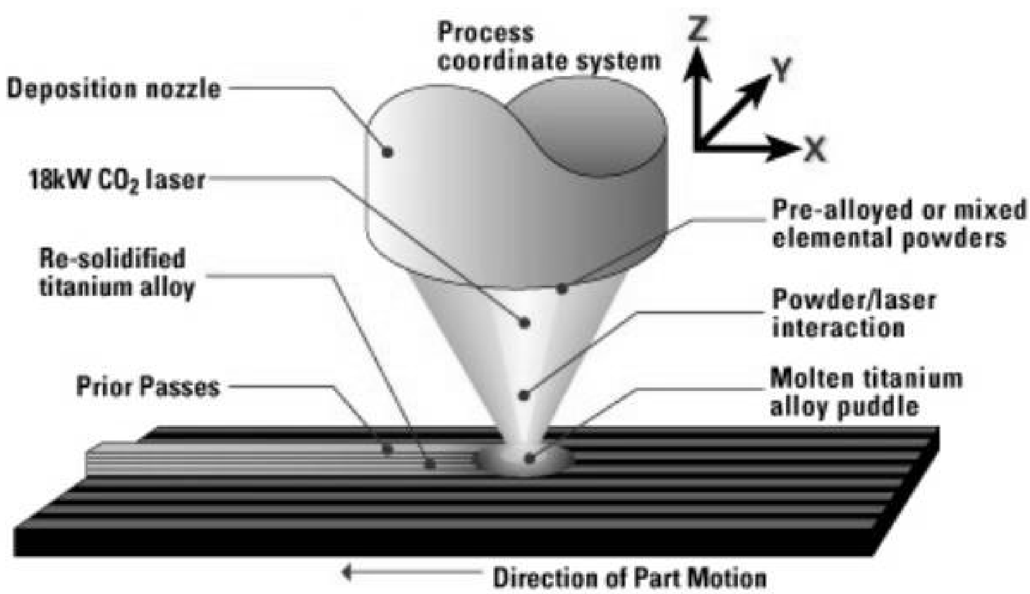

Figure 9.4-12 Laser Deposited Titanium Process Using the AeroMet™ Process

Figure 9.4-13 Sample Laser Deposited Part

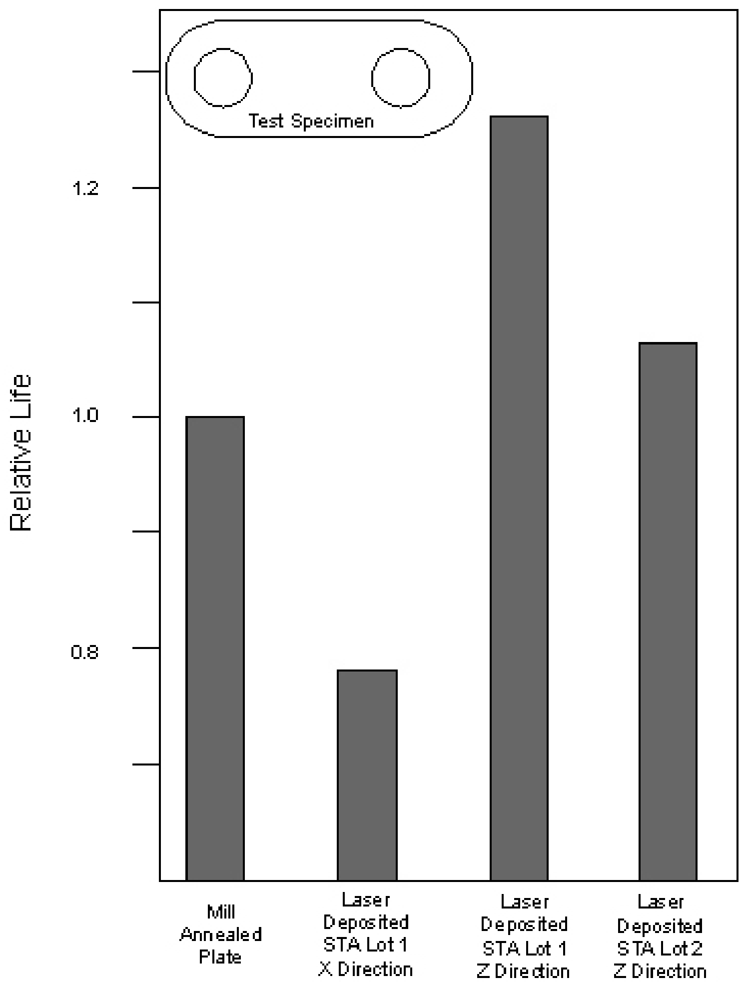

Figure 9.4-14 Fatigue Comparison of Laser Deposited Ti6Al-4V

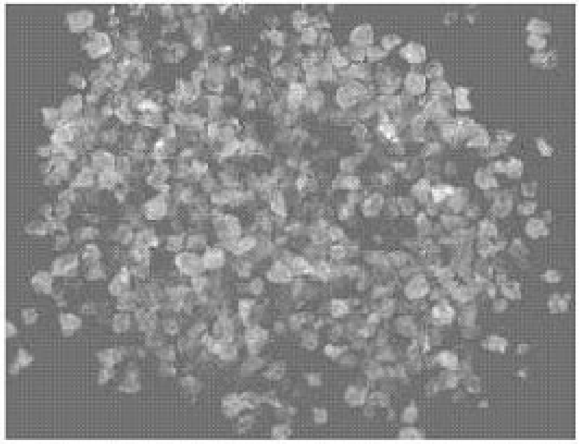

Figure 9.4-15 Nanocomposite Paint Stripping Media

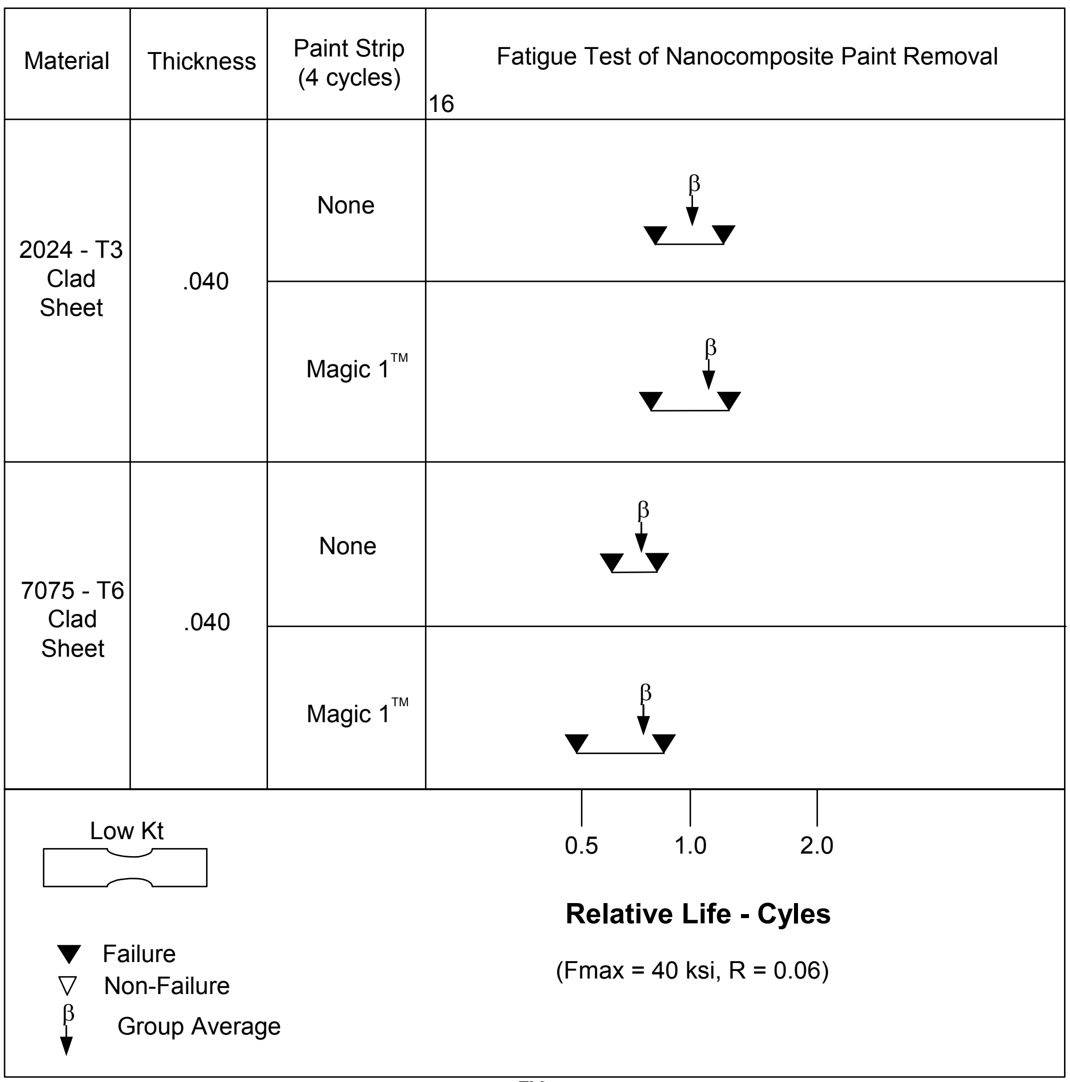

Figure 9.4-16 Magic 1™ Paint Stripping Results

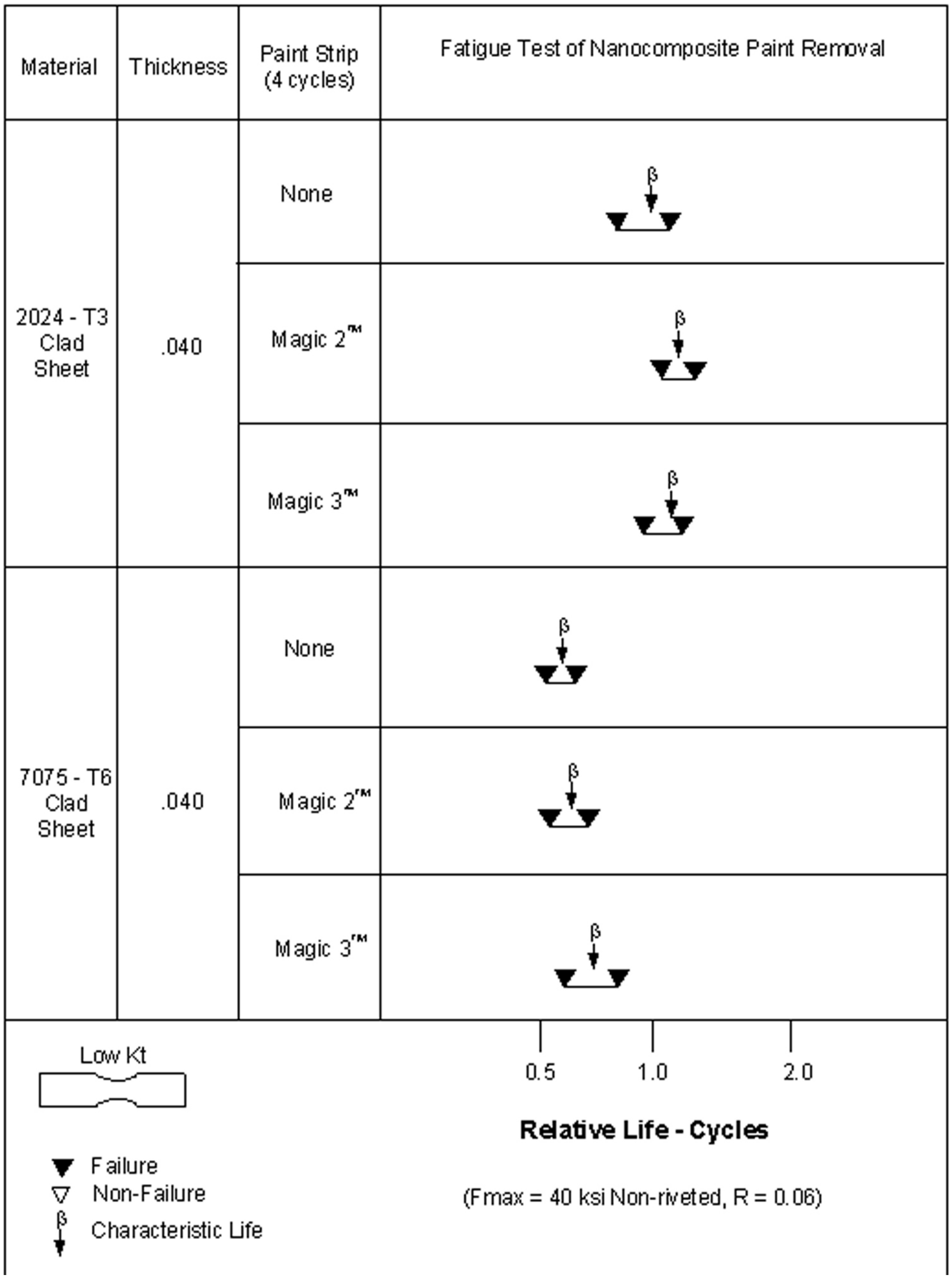

Figure 9.4-17 Magic 2™ and Magic 3™ Paint Stripping Results

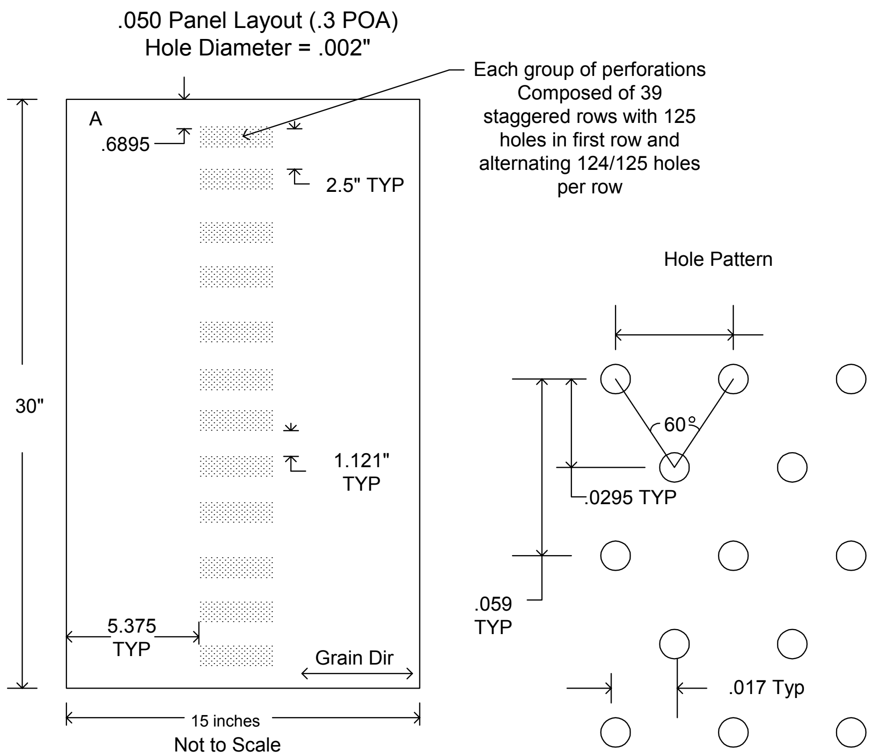

Figure 9.4-18 Laser Perforated Panels

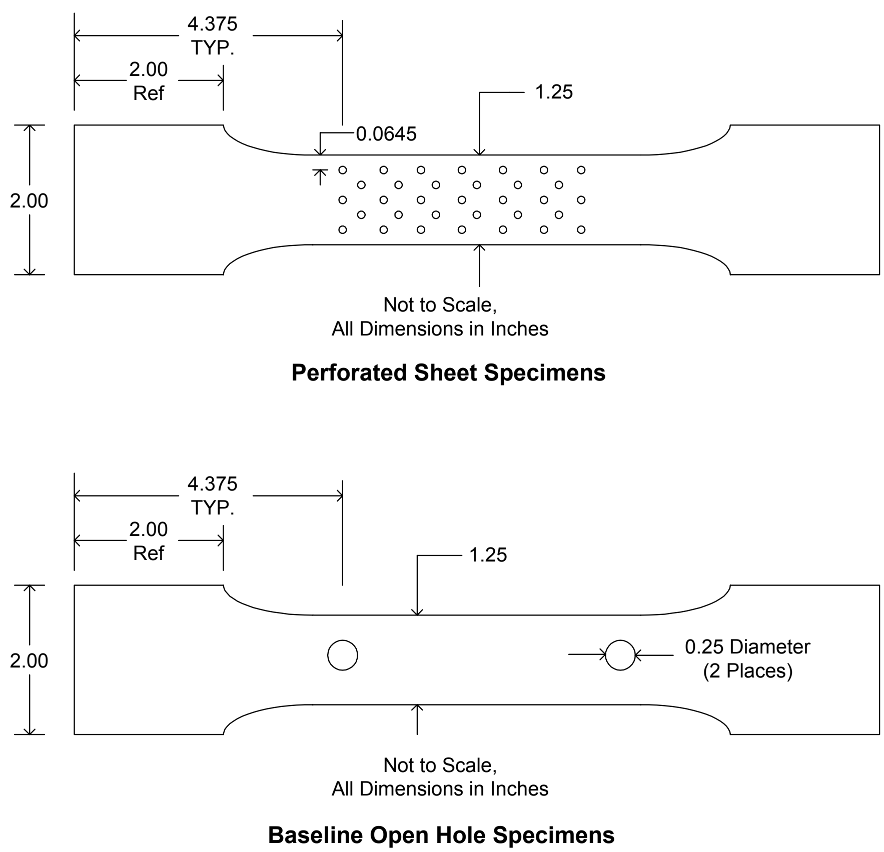

Figure 9.4-19 Fatigue Test Specimens

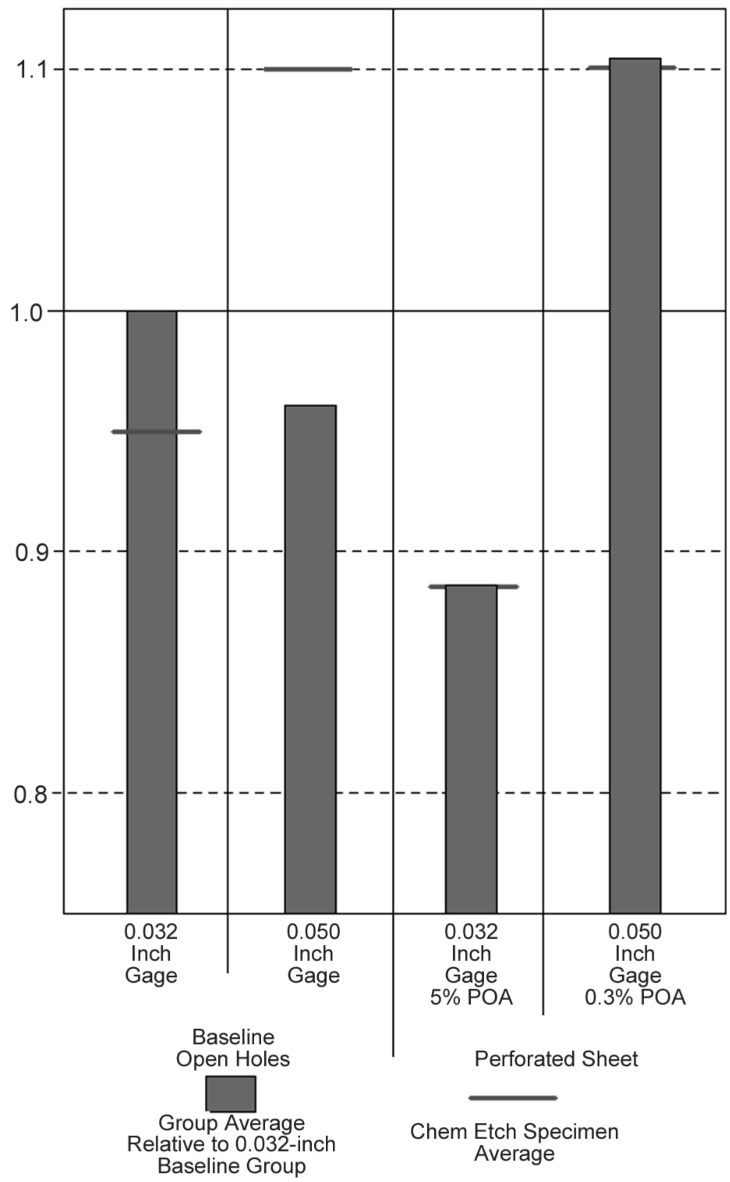

Figure 9.4-20 Perforated Sheet Test Results.

Figure 9.4-21 CNC Stylist Forming Tool and Sample Panel

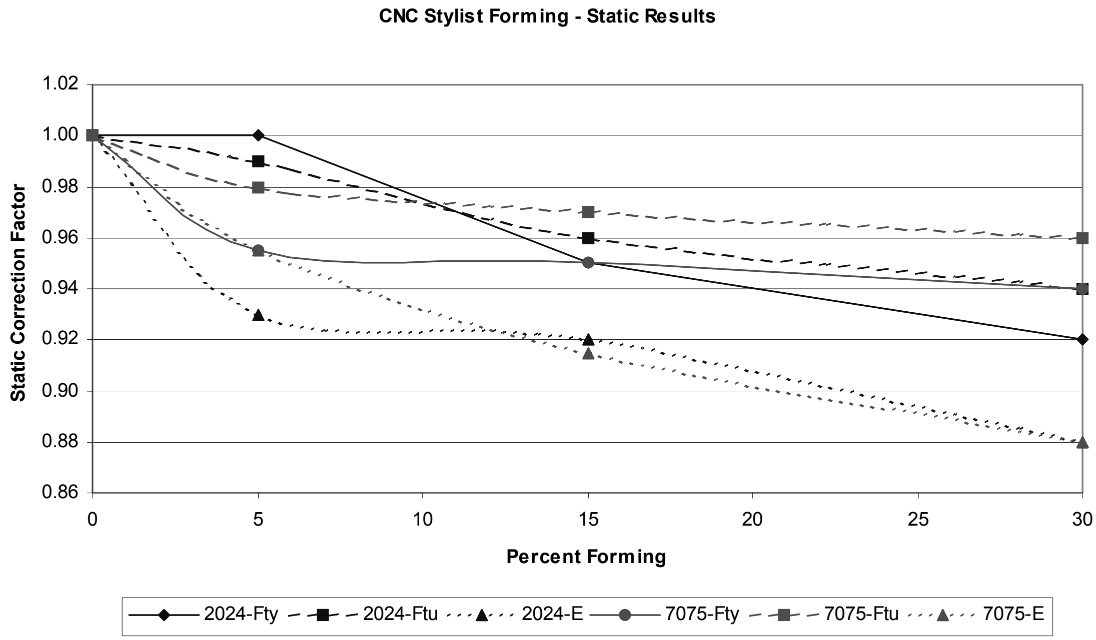

Figure 9.4-22 Fatigue Test Specimens.

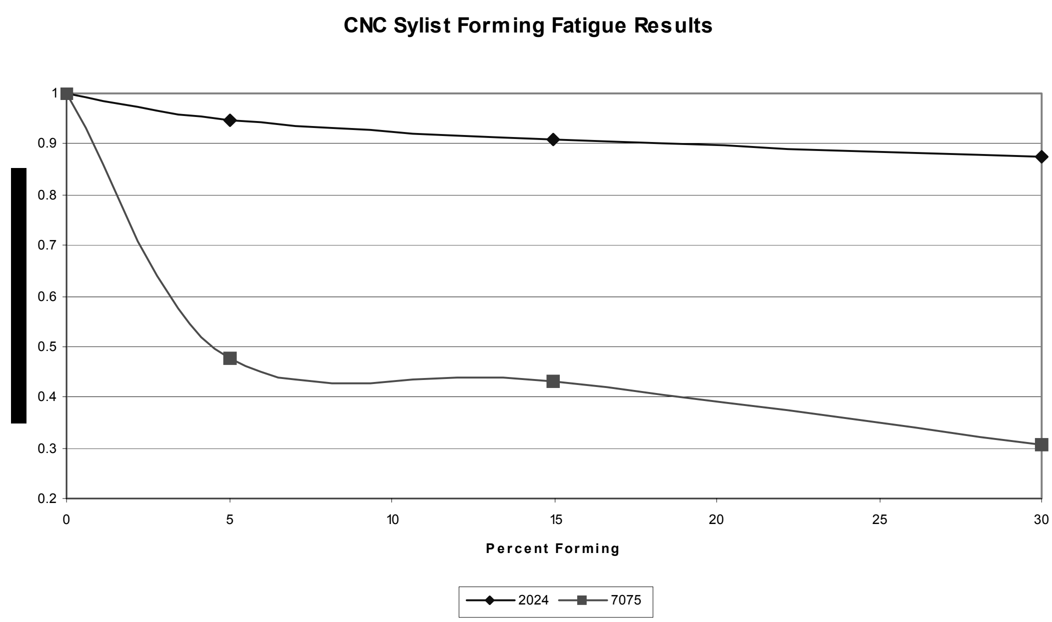

Figure 9.4-23 CNC Stylist Fatigue Results.

Unitized Structure Plug-in Models for AFGROW

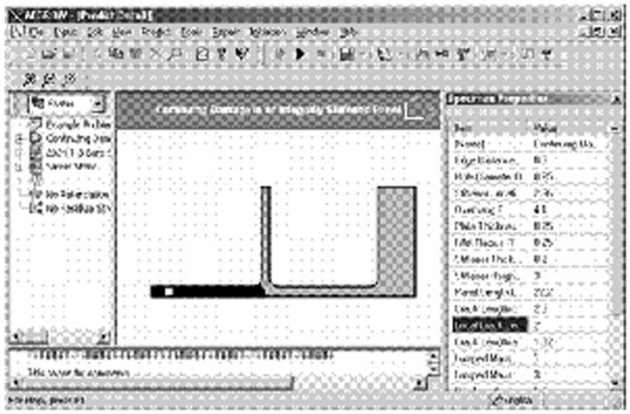

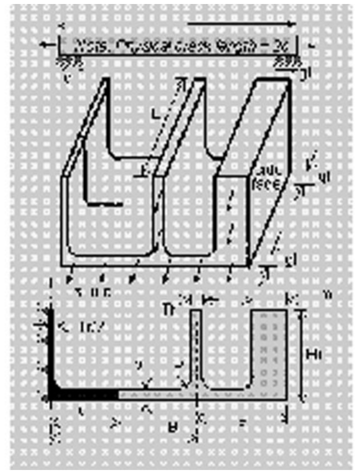

- Continuing Damage in a Integrally Stiffened Panel
- Two-Bay Central Crack in an Integrally Stiffened Panel
- AFGROW Crack Growth Analysis Can Assist in Setting Design Criteria for New Types of Structure

Figure 9.4-24

Unitized Structure Verification Testing & Correlation

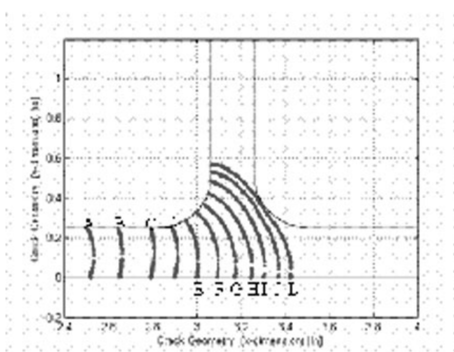

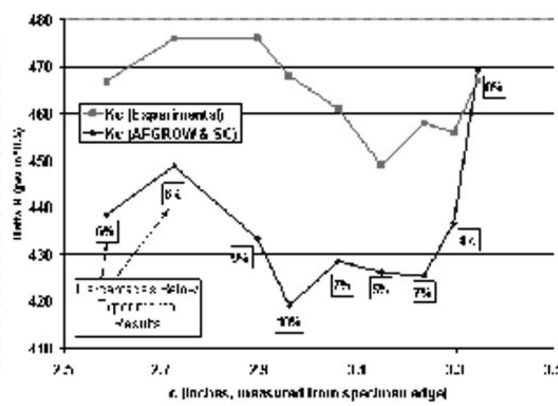

Experimental Crack Front Locations (Secant Method used to calculate K)

StressCheck Comparisons with Experimental K's

- Unitized Structure Tests in Polymethylmethacrylate (PMMA)
- Continuing Damage in a Plate Tests in PMMA
- Crack Shapes Tracked, Analyzed, Verified

Figure 9.4-25

AFGROW Plugin Capability for External-K Solutions

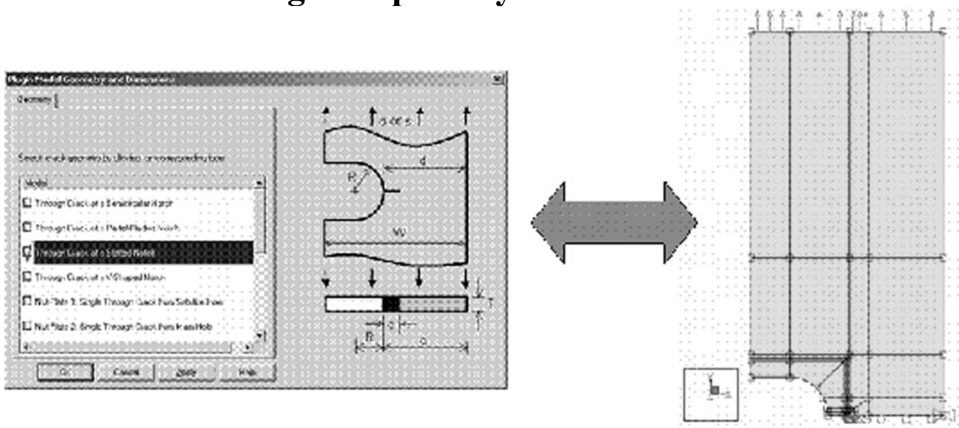

- Real-Time Stress Intensity Solutions Obtained from Parametric p-Version StressCheck® Models
- Many New Problem Classes Already Developed and Available
- New Models Built Directly into Familiar AFGROW Framework

Figure 9.4-26

AFGROW Plugin Capability for External-K Solutions

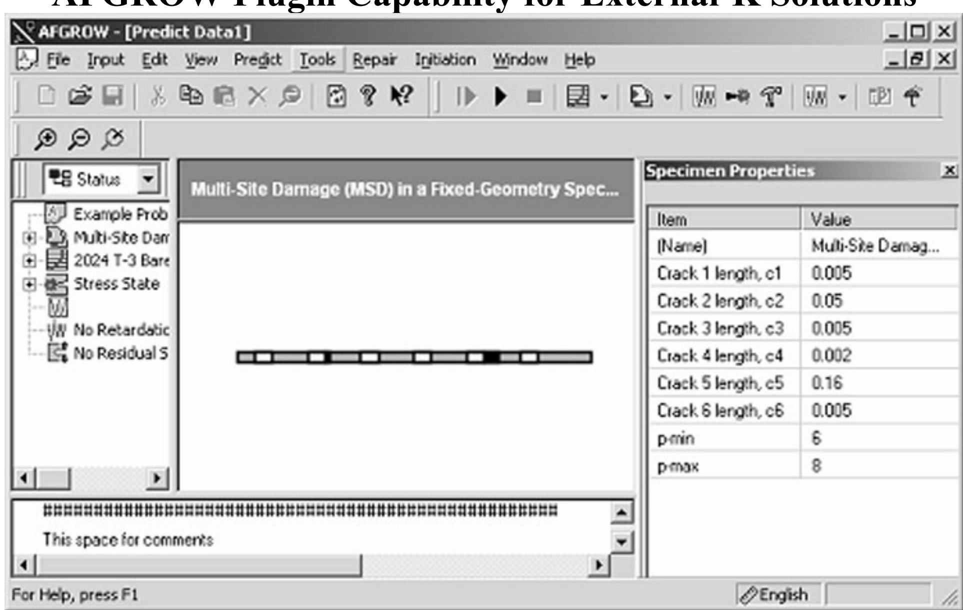

- Numerous Parameters Handled Easily
- Track Multiple Cracks, Multi-Site Damage, WFD
- No Need to Fit Solution Curves to Multiple Parametric Variations

Figure 9.4-27

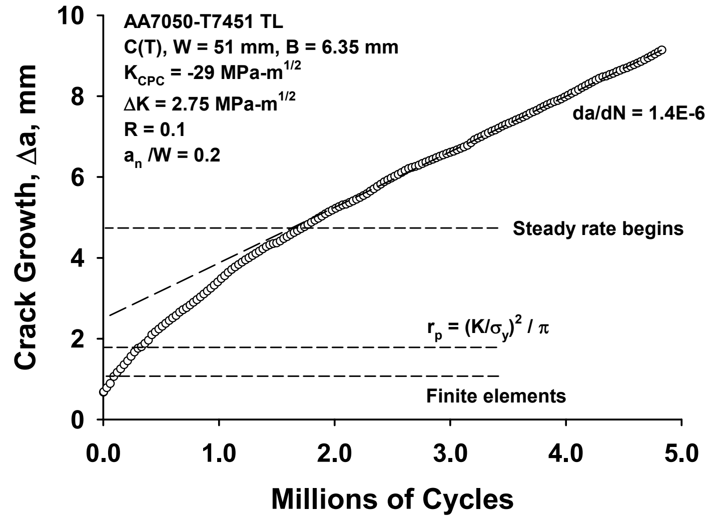

Figure 9.4-28 Crack Growth Versus Cycles Showing the Elevated Growth Rates Caused by the Residual Stress Field and Showing the Amount of Crack Growth Necessary to Establish a Steady Growth Rate.

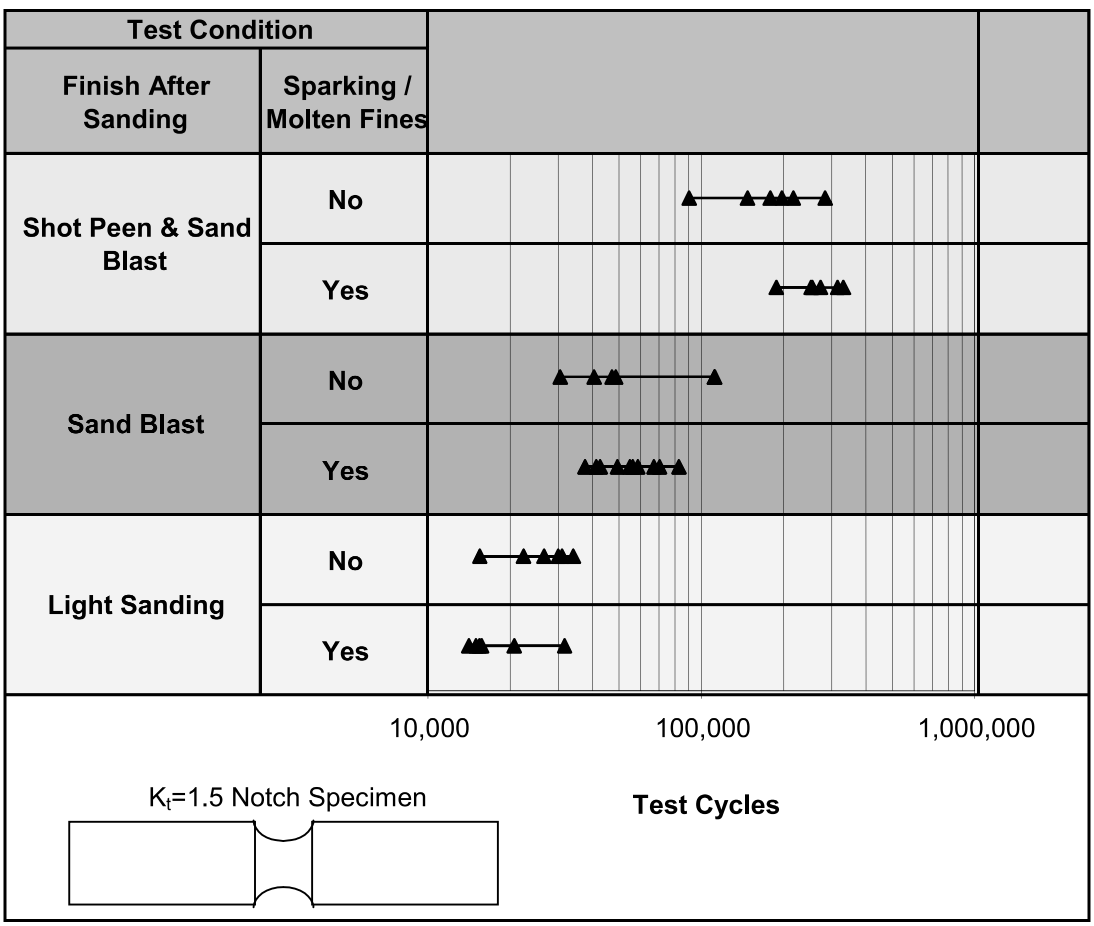

Figure 9.4-29 Flat Notch (Kt = 1.5) Fatigue Test Results, Titanium Plate Study.

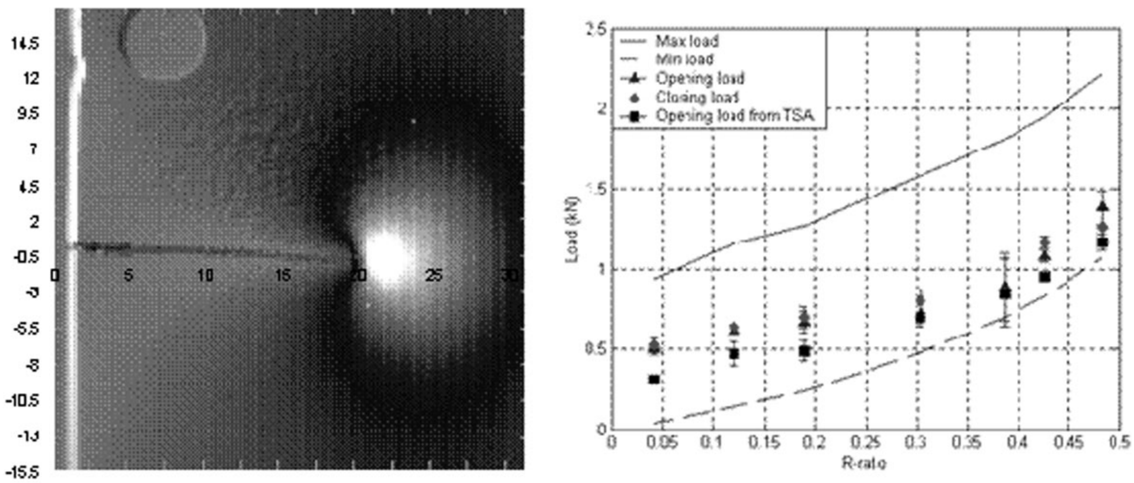

Figure 9.4-30 Thermoelastic Data From a Crack in a Compact Tension Specimen With the Locations of the Crack Tip Obtained by the New Algorithm [4] Superimposed on the Image (*left*) and Assessment of Opening Loads During Closure Compared to Compliance Data From a Back-Face Strain Gauge (*right*).

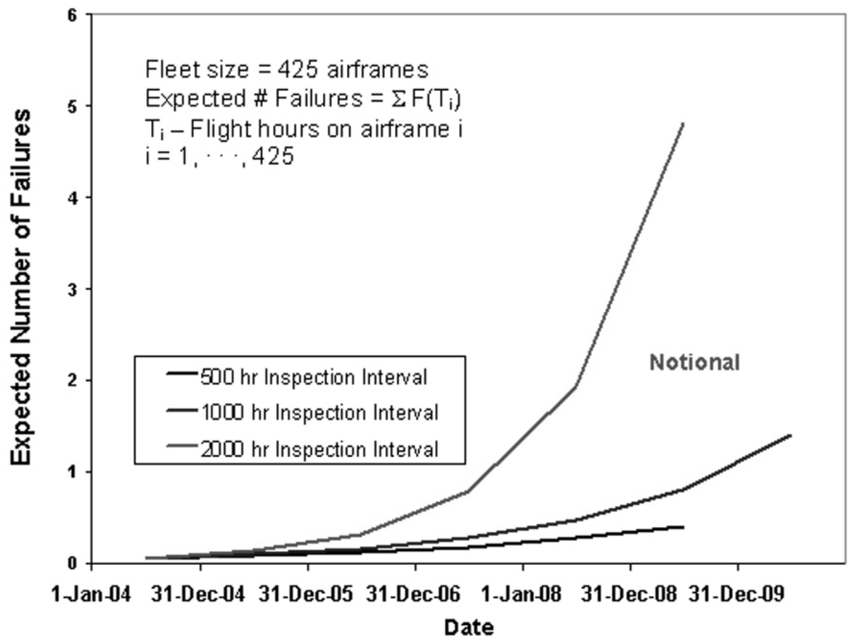

Figure 9.5-1 An Example Application of the Flight Hours to Failure Distribution is the Calculation of the Expected Number of Fleet Failures as a Function of Calendar Time. This Figure Presents Expected Numbers of Failures for Inspection Intervals of 500, 1000 and 2000 Flight Hours for a Fleet Size of 425 Airplanes.

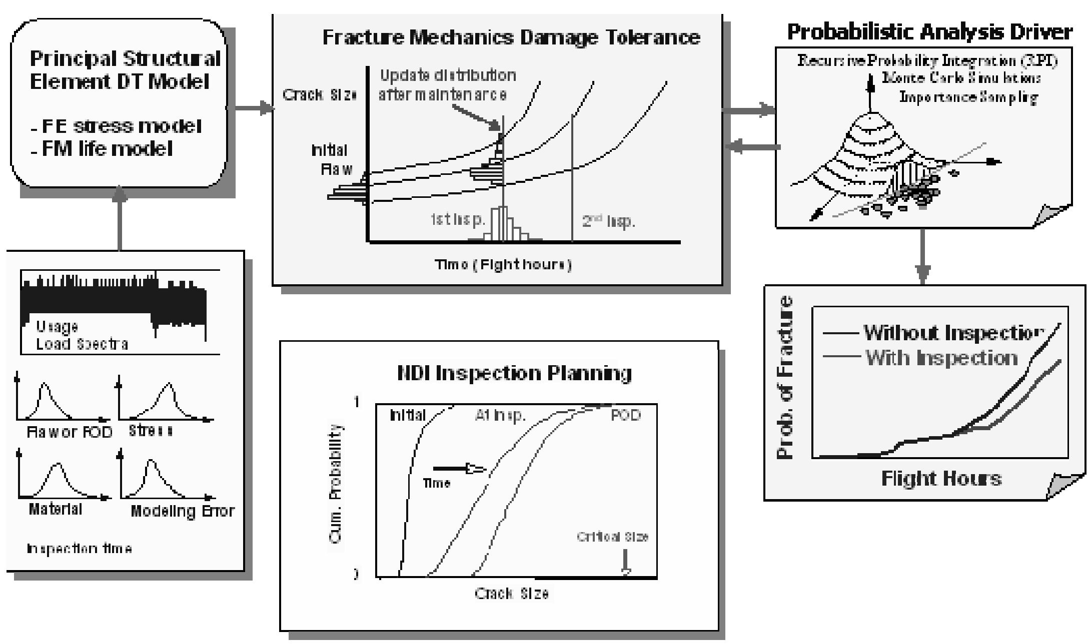

9.5-2 Probabilistic Damage Tolerance Analysis-Based Maintenance Planning

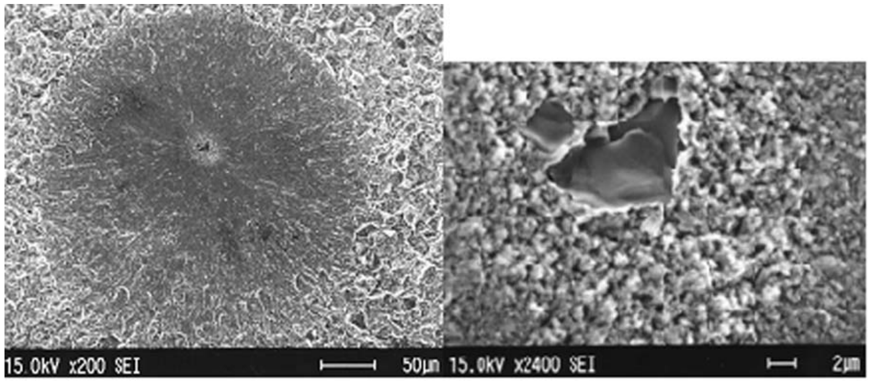

Figure 9.5-3 Scanning Electron Micrographs of a Typical Inclusion at the Origin of Fatigue Failure, High and Low Magnifications, Respectively[1].

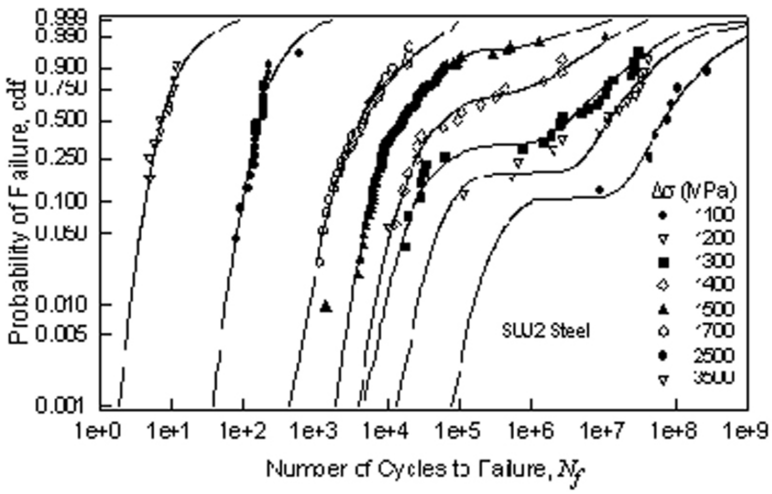

Figure 9.5-4 S-N Data for SUJ2 Steel With CDFs Computed From the Fatigue Crack Growth Model[1].

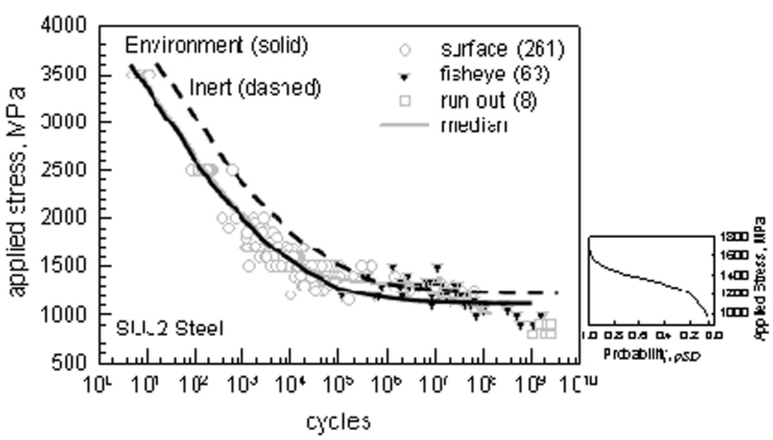

Figure 9.5-5 An Interpretation of the Median S-N Behavior for VHC Fatigue for SUJ2 Steel[1].

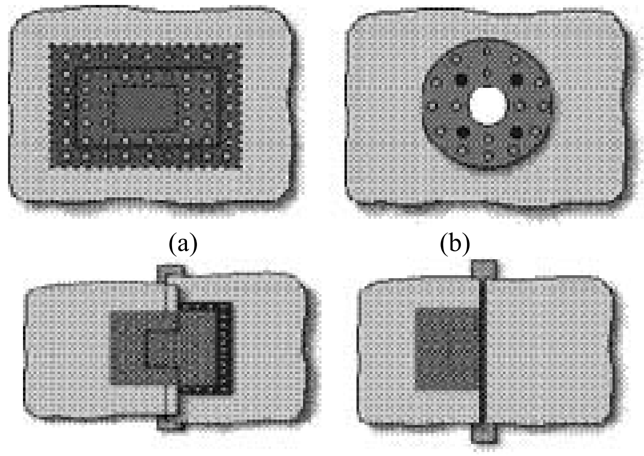

(c) (d)

Figure 9.6-1 Typical Repair Configurations for Fuselage Skin Repairs

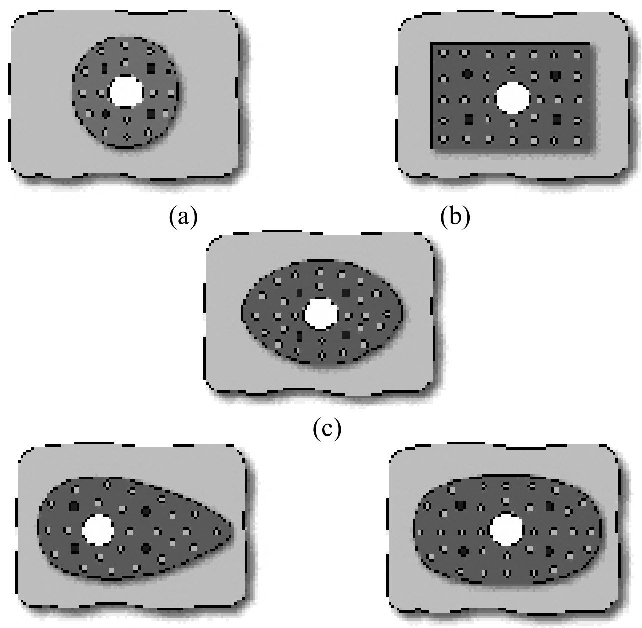

(d) (e)

Figure 9.6-2 Typical Repair Configurations for Antenna Installations

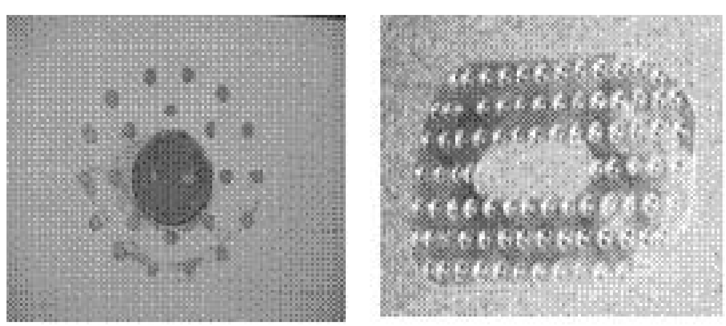

(a) (b)

Figure 9.6-3 Typical Field Repair Configurations With Irregular Fastener Patterns

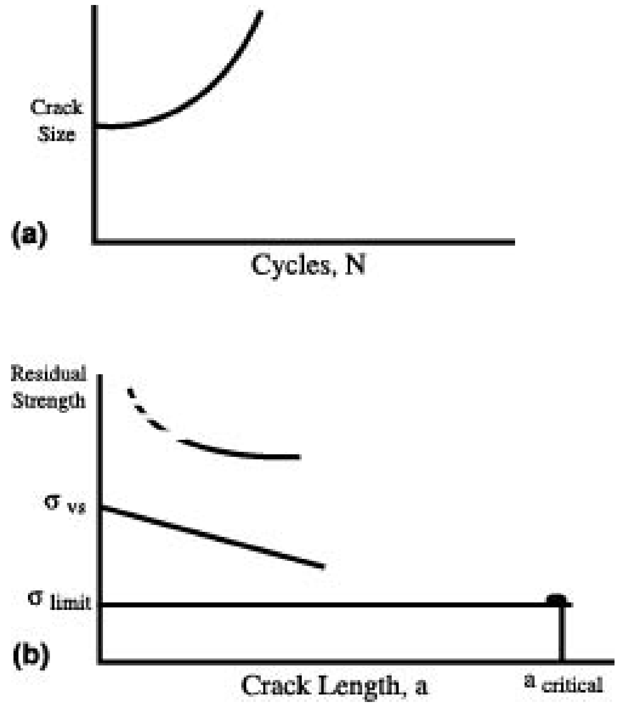

Figure 9.6-4 Typical Results From Damage Tolerance Analysis

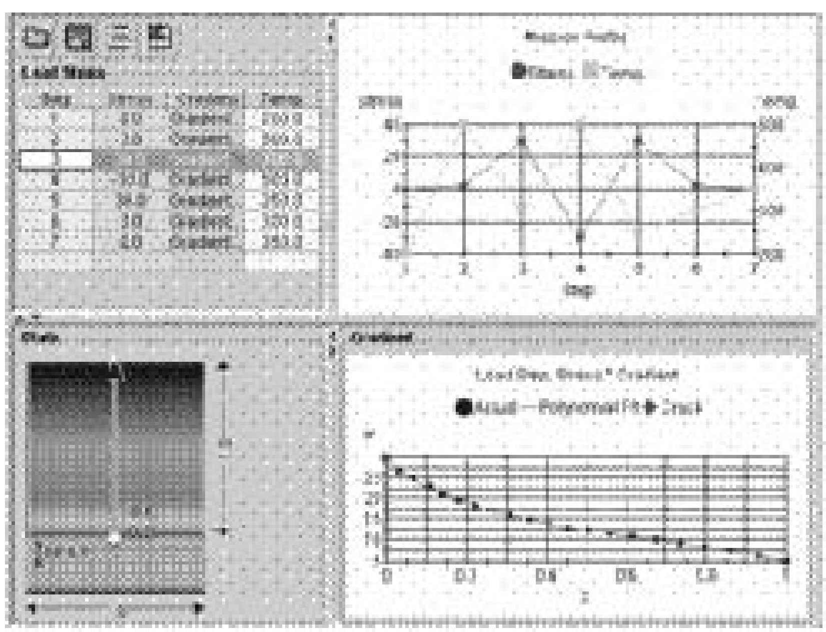

Figure 9.6-5 The Initial Framework for Surface Damage in DARWIN (Version 4.0) Includes a Mission Profile Consisting of Stresses and Temperatures at the Crack Location for Each Surface Feature

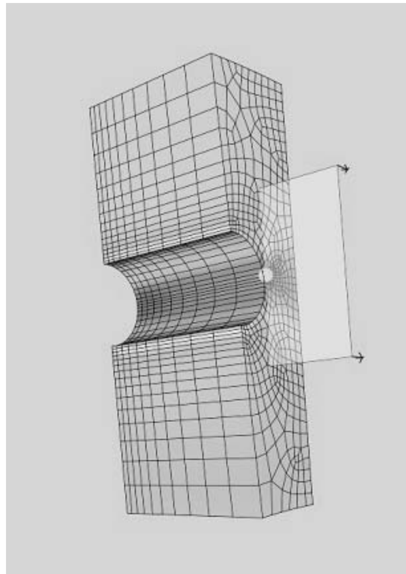

Figure 9.6-6 Capability for Modeling Surface Damage Based on Three-Dimensional Finite Element Geometry is Currently Under Development for DARWIN 5.0

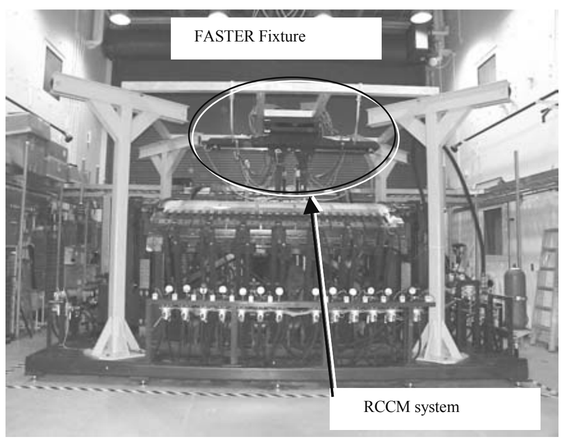

Figure 9.6-7 Full-Scale Aircraft Structural Test Evaluation and Research Facility

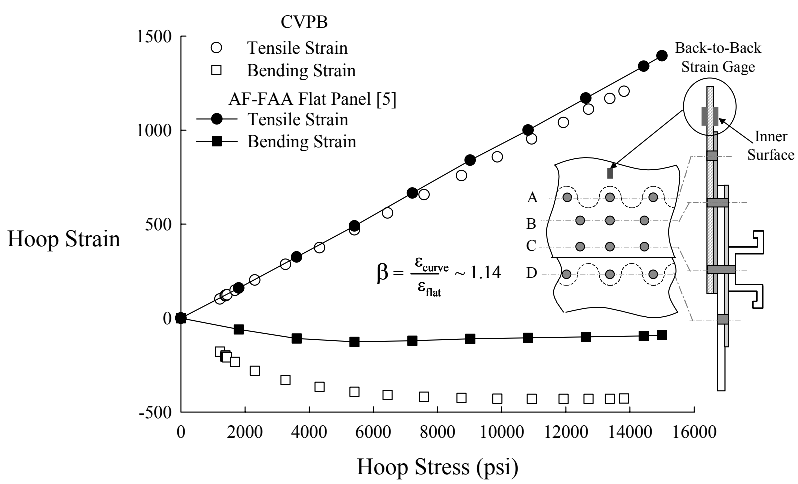

Figure 9.6-8 Strain Near the Lap Joint in a Curved Panel CVPB and a Flat Panel

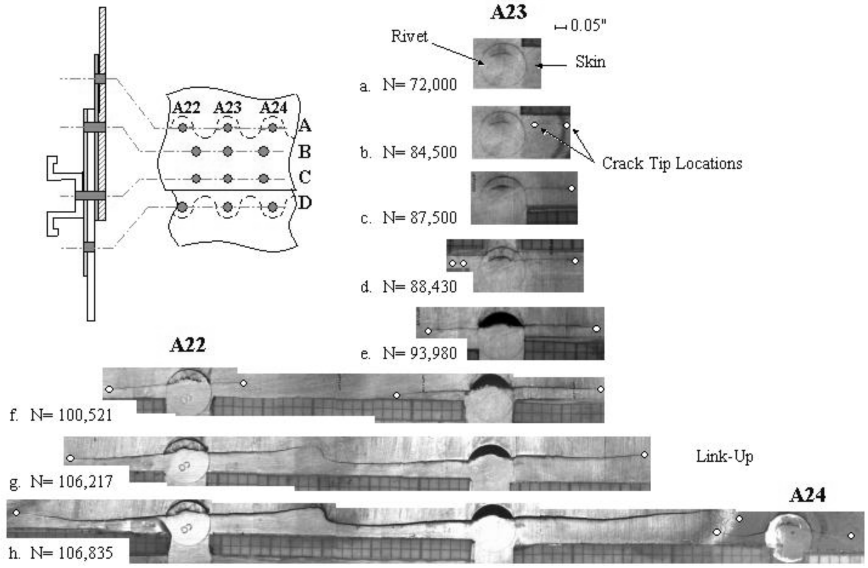

Figure 9.6-9 Crack Growth Process in the Outer Critical Rivet Row

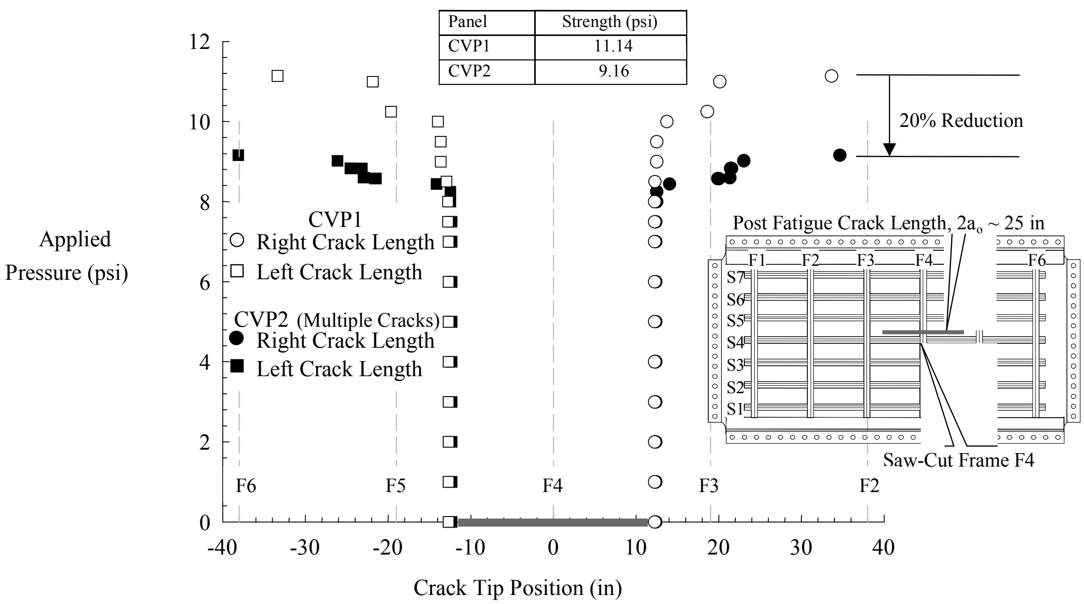

Figure 9.6-10 Residual Strength Data for Panels CVP1 and CVP2

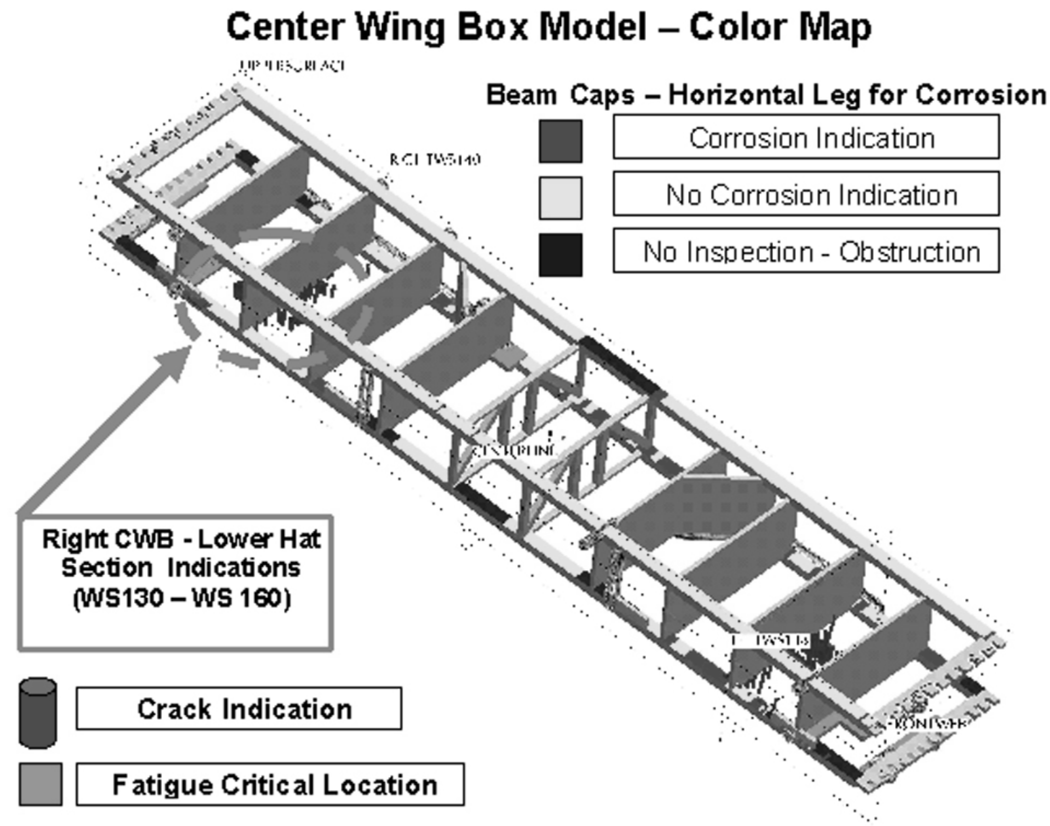

Figure 9.7-1 Phase I NDI Indications Depicted in the Notional 3-Dimensional Representation of the CWB.

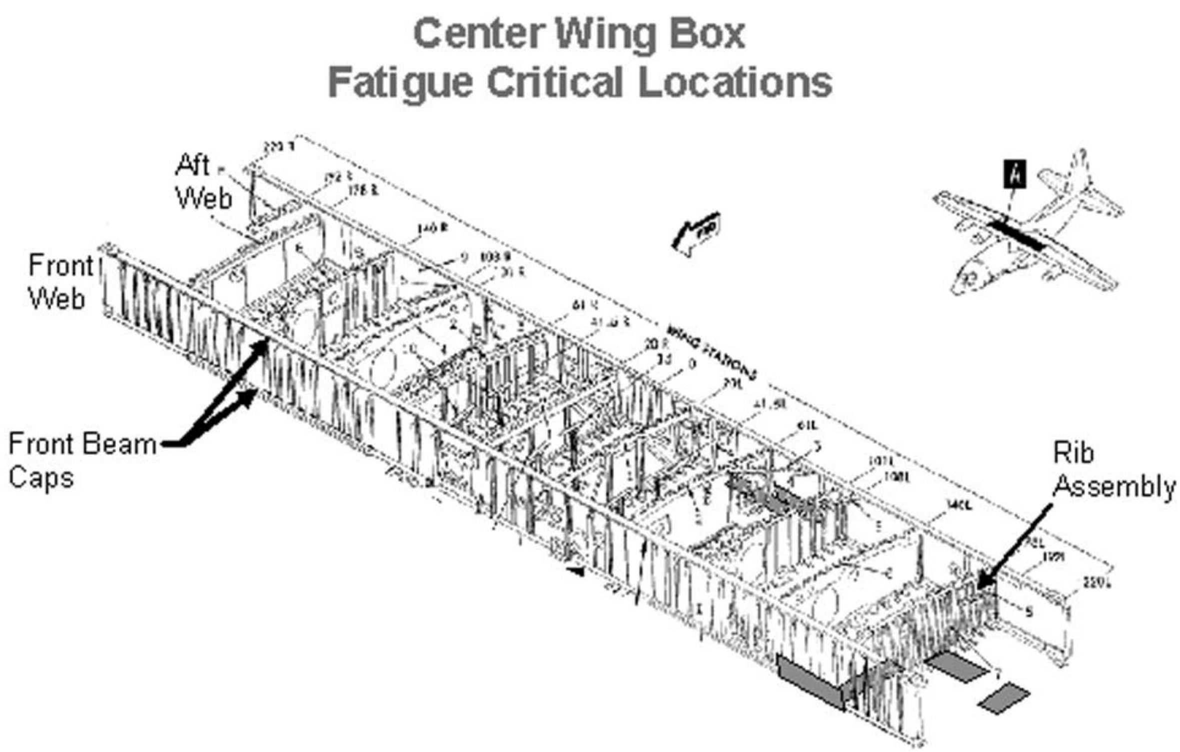

Figure 9.7-2 Spatial Locations of Select Center Wing Box FCL's. (Left Wing Positions Shown in black)

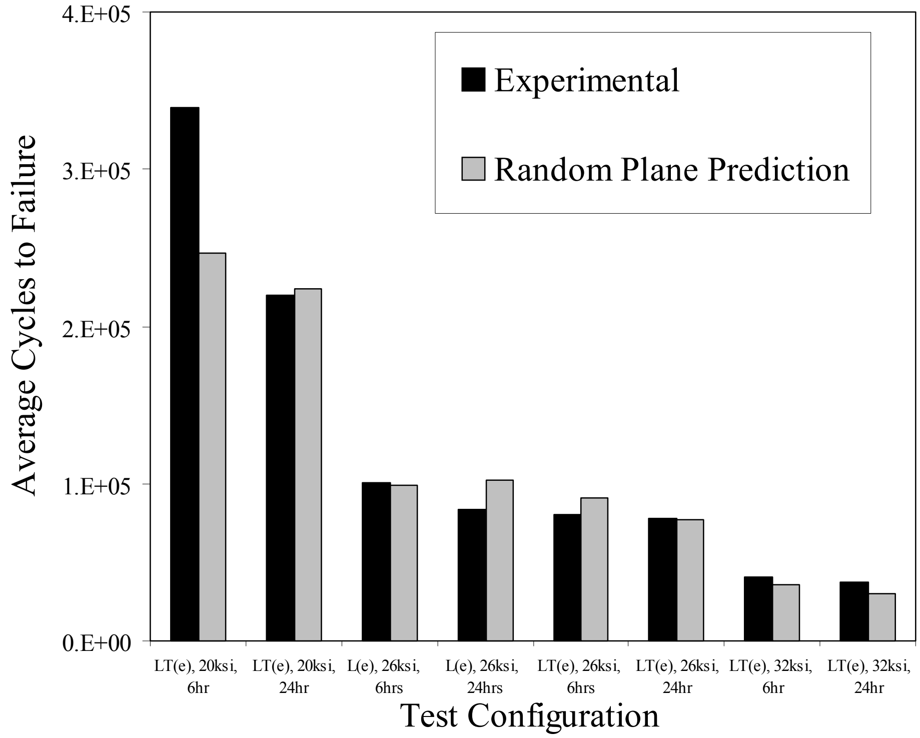

Figure 9.7-3 Comparison of Average Experimental and Predicted Lives Using the Random Plane Life Prediction Method for Eight Test Configurations as Defined by Stress Level, Specimen Orientation, and Corrosion Duration.

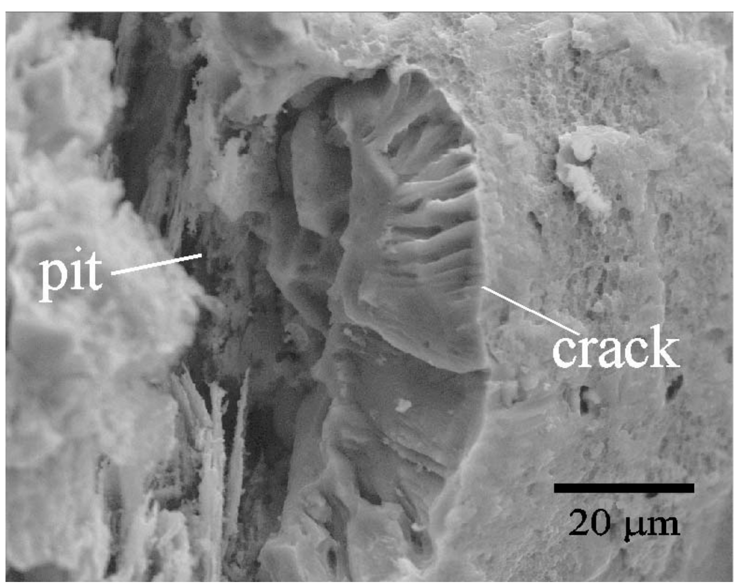

Figure 9.7-4 Longitudinal 2024-T3 Sheet Specimen Subjected to 20,159 Constant Amplitude Fatigue Cycles (Smax = 26 ksi, R = 0.02) Followed by Overloading, Exposing Early-Stage Crack as Shown.

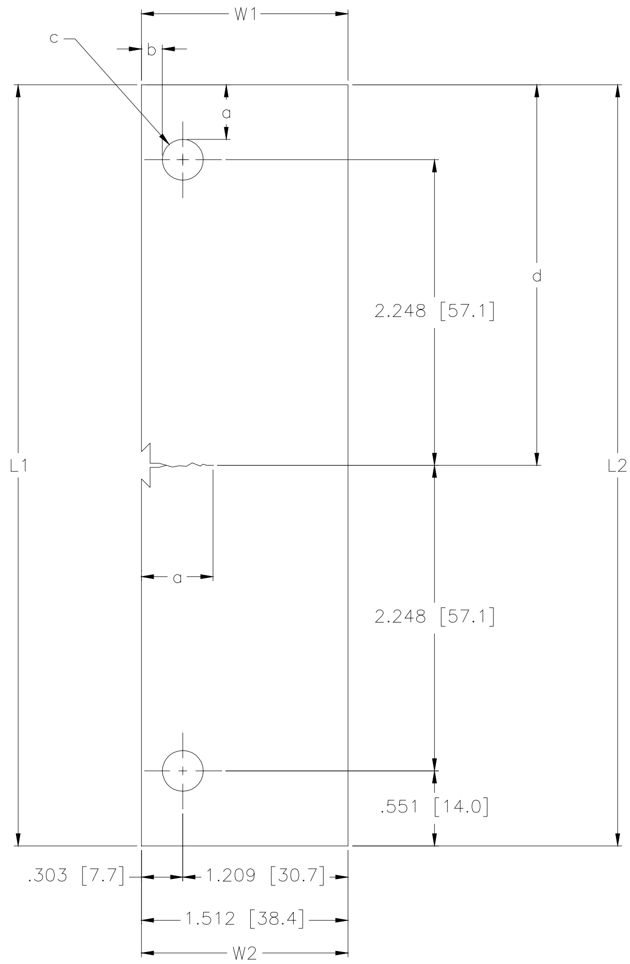

Figure 9.7-5 ESE(T) Specimen Chosen for This Test was Done so for its Thin Sheet Capabilities. The Specimen has a Thickness of 0.063 Inches. Dimensions are Given in Inches and Millimeters in Brackets.

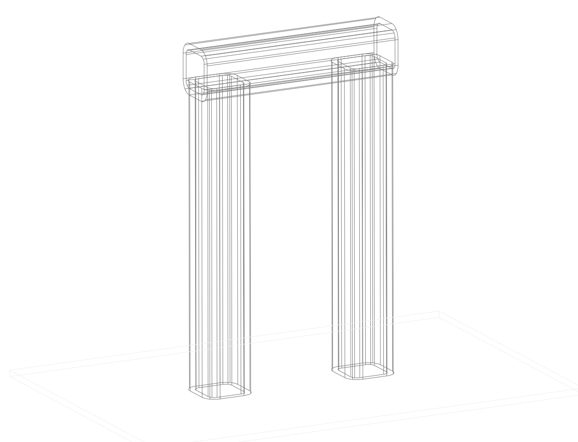

Figure 9.7-6 SCC Test Frame, Measuring 18 Inches High and 8 Inches Across, Welded to a Quarter Inch Base.

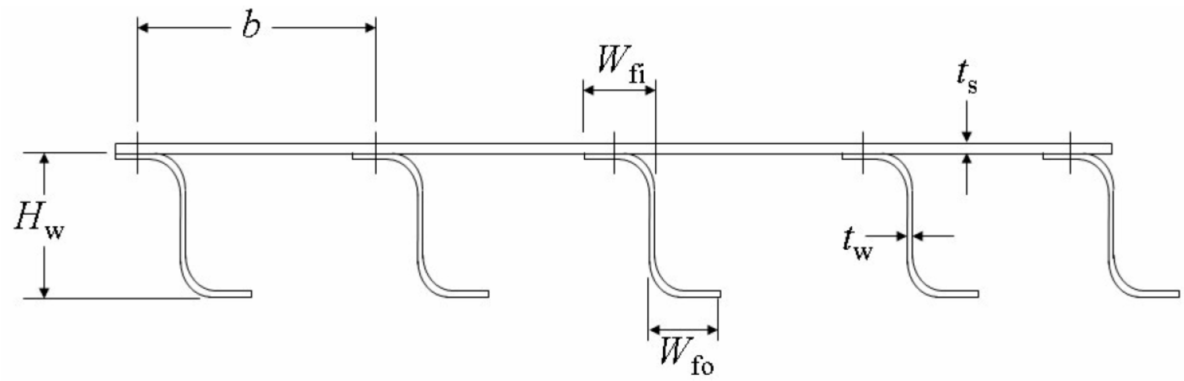

Config	t_s	t_w	W_{fi}	W_{fo}	H_w	b	L
1	2.03 (0.080)	1.78 (0.070)	16.3 (0.64)	16.3 (0.64)	37.1 (1.46)	106 (4.19)	531 (20.9)
2	2.03 (0.080)	2.03 (0.080)	16.3 (0.64)	16.3 (0.64)	37.1 (1.46)	106 (4.19)	531 (20.9)
3	2.03 (0.080)	2.03 (0.080)	15.2 (0.60)	15.2 (0.60)	28.2 (1.11)	54.4 (2.14)	279 (11.0)

Figure 9.7-7 Test Panel Cross-Section.

Table 9.7-1 Test Panel Material Properties.

Component	E GPa (Msi)	σ_U MPa (ksi)	σ_Y MPa (ksi)
Skin (7075-T6)	71.7 (10.4)	582.6–583.3 (84.5–84.6)	515.8–517.1 (74.8–75.0)
Stiffener (7075-T62)	71.7 (10.4)	568.8 (82.5)	508.9–509.5 (73.8–73.9)

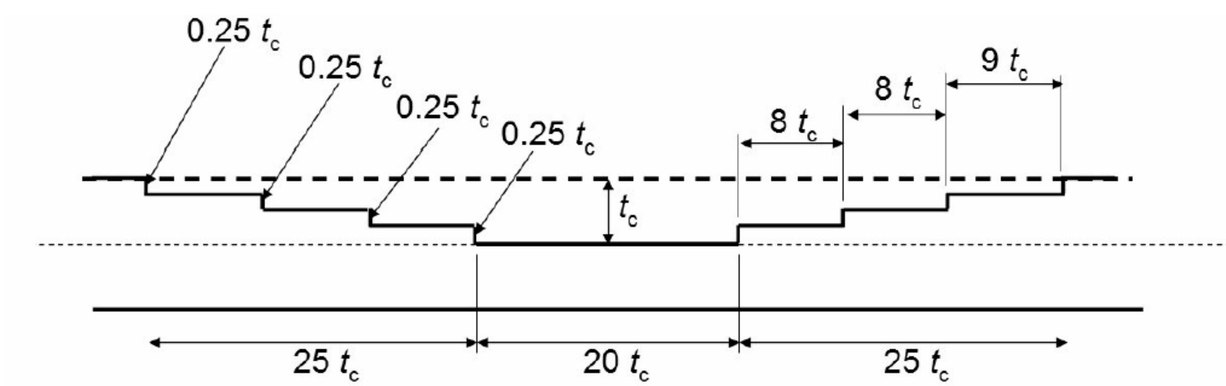

Figure 9.7-8 Panel Grindout Geometry.

Table 9.7-2 Results of Panel Testing.

Panel No.	Config No.	δ_g Pct	P_s kN (kip)	P_{max} kN (kip)	$\Delta L/L\|_{P_{max}}$ μstrain	Strength Chg[a] Pct
1	1	0%	154 (35)	405.7 (91.21)	7120	
2	1	0%	166 (37)	412.5 (92.73)	7700	
4[b]	1	37.4%	139 (31)	354.9 (79.80)	8273	
5	1	34.8%	154 (35)	395.4 (88.90)	6885	−3%
7	1	56.1%	118 (27)	376.7 (84.70)	7062	−8%
8	1	57.4%	119 (27)	382.4 (85.97)	7316	−7%
9	1	34.8%	150[c] (34)	396.6 (89.16)	7234	−3%
10	2	Fixture Failure				
11	2	0%	184 (41)	445.1 (100.07)	8180	
12	2	0%	167 (38)	444.7 (99.97)	8270	
13	2	36.1%	144 (32)	420.7 (94.58)	7750	−5%
14	2	41.9%	148 (33)	425.2 (95.59)	7870	−4%
15	2	36.4%	NR[d]	437.6 (98.38)	7860	−2%
16	2	40.6%	163 (37)	432.7 (97.28)	7710	−3%
17	2	52.9%	NR	423.4 (95.20)	7820	−5%
18	2	Fixture Failure				
19	3	0%	388 (87)	422.2 (94.93)	11,030	
20	3	0%	409 (92)	425.8 (95.73)	10,430	
22	3	41.3%	326 (73)	384.9 (86.53)	10,210	−9%
23	3	41.3%	302 (68)	383.8 (86.29)	9640	−9%
25[b,e]	3	56.1%	245 (55)	358.2 (80.52)	9782	−16%
26	3	62.6%	251 (56)	375.7 (84.47)	10,680	−11%
27	3	60.0%	234 (53)	370.1 (83.20)	10,227	−13%

[a]Compared to average of pristine results
[b]Result discarded. See text.
[c]Approximate
[d]"Not Recorded" (see text)
[e]This panel had an unusual surface finish. Hardness testing revealed a lower strength (about 10%) than other panels.

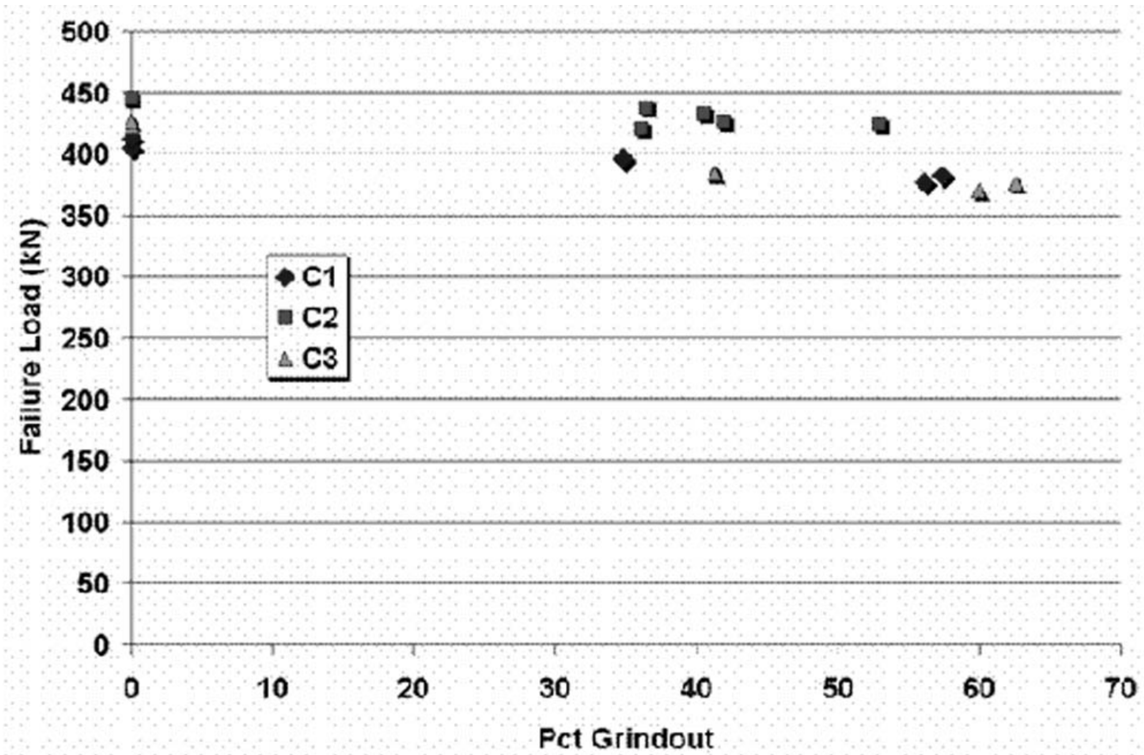

Figure 9.7-9 Buckling Panel Test Results for 3 Panel Configurations.

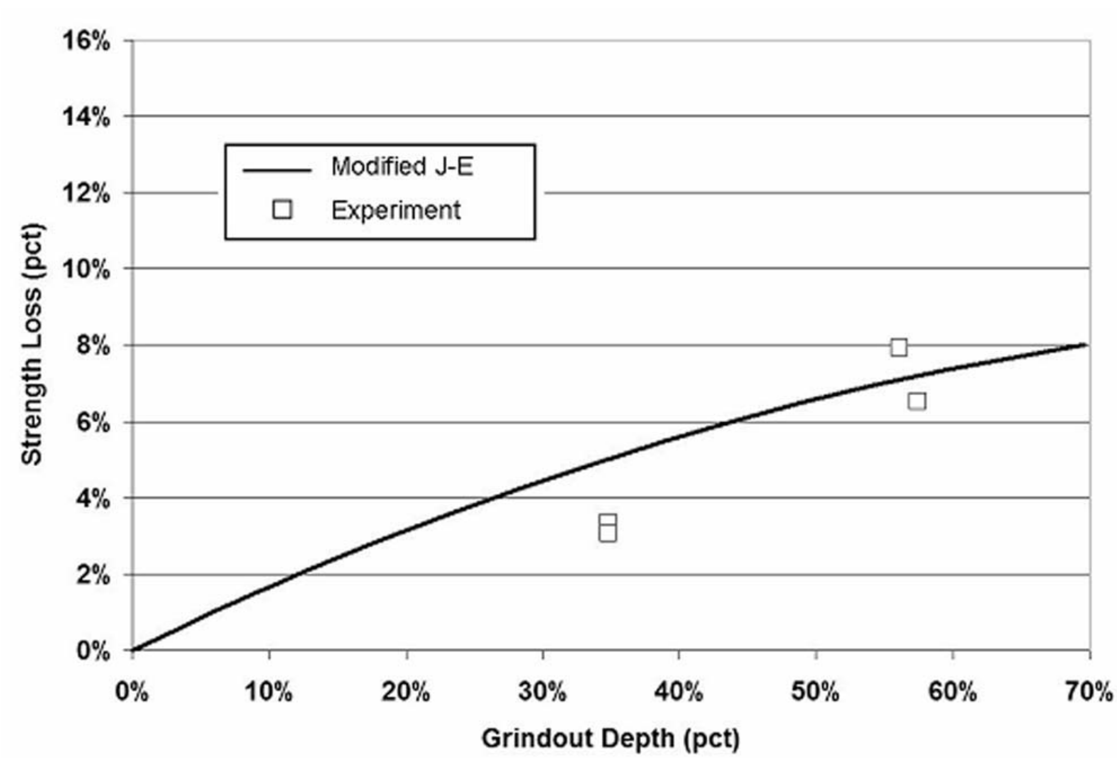

Figure 9.7-10 Configuration C1 Panel Experimental Results Versus Modified Johnson-Euler Method.

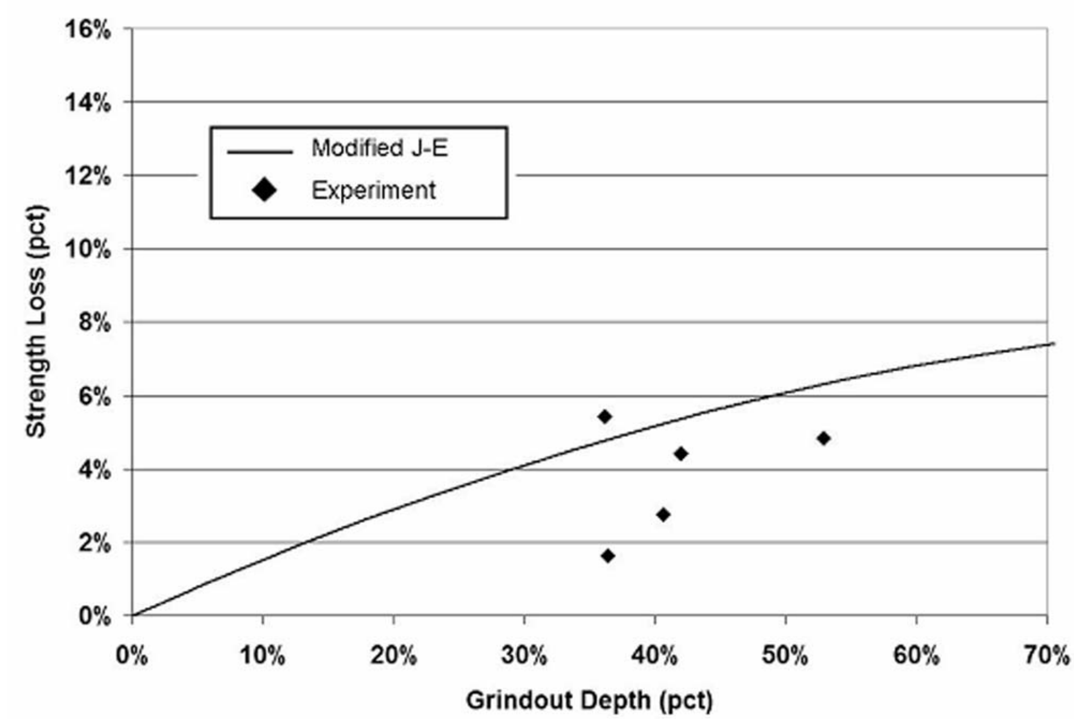

Figure 9.7-11 Configuration C2 Panel Experimental Results Versus Modified Johnson-Euler Method.

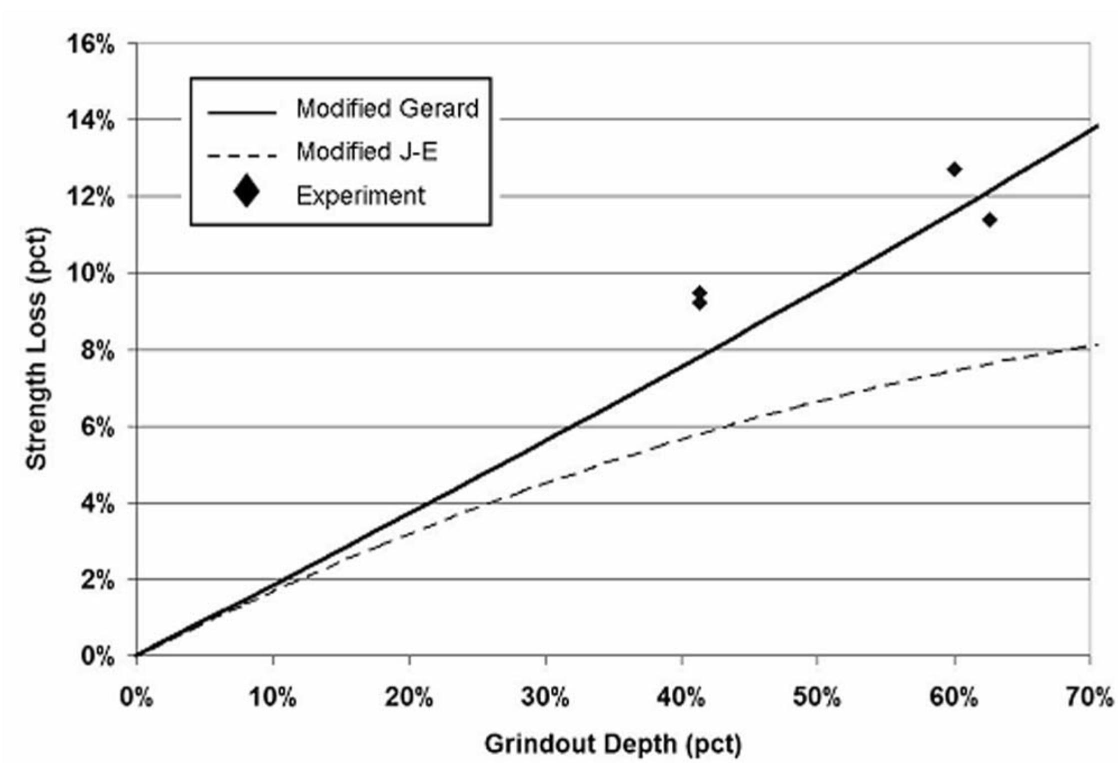

Figure 9.7-12 Configuration C3 Panel Experimental Results Versus Modified Method of Gerard. Modified Johnson-Euler Method is Shown for Referece.

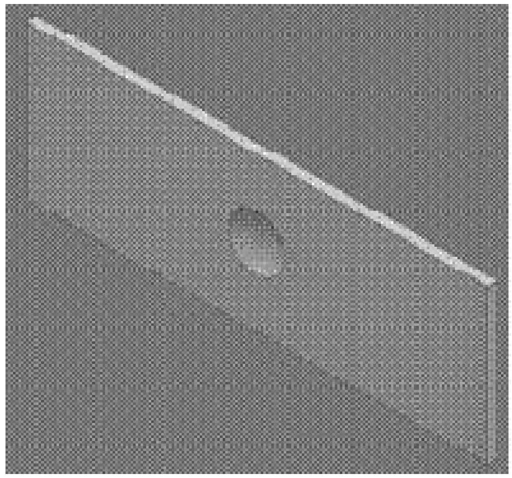

Figure 9.7-13 Specimen Designating a Thickness Loss of 70%; Width is Approximately 4 Inches and Length is 12 With an Impression Diameter of About 1.5 Inches.

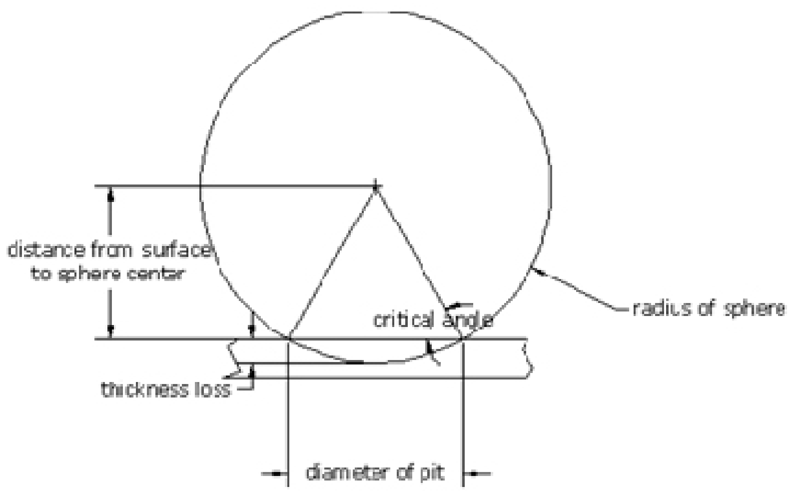

Figure 9.7-14 Cross-Section of an Arbitrary Specimen: Machined Profile Follows the Circumference of Mentioned Sphere.

Table 9.7-3 Specimens Tested With a Truncated Spectrum With Number of Cycles to Failure Given. The Actual Thickness Loss Has Been Estimated to be 5% of the Thickness Beyond the Thickness Loss Due to Machining.

	N	Thickness Loss	Log(N)	stdev(log(N))
15-1	2,533,072	20	6.4036	0.0727
15-2	1,999,413	20	6.3009	
60-1	720,987	65	5.8579	
70-2	778,681	75	5.8914	0.0076
70-3	759,659	75	5.8806	

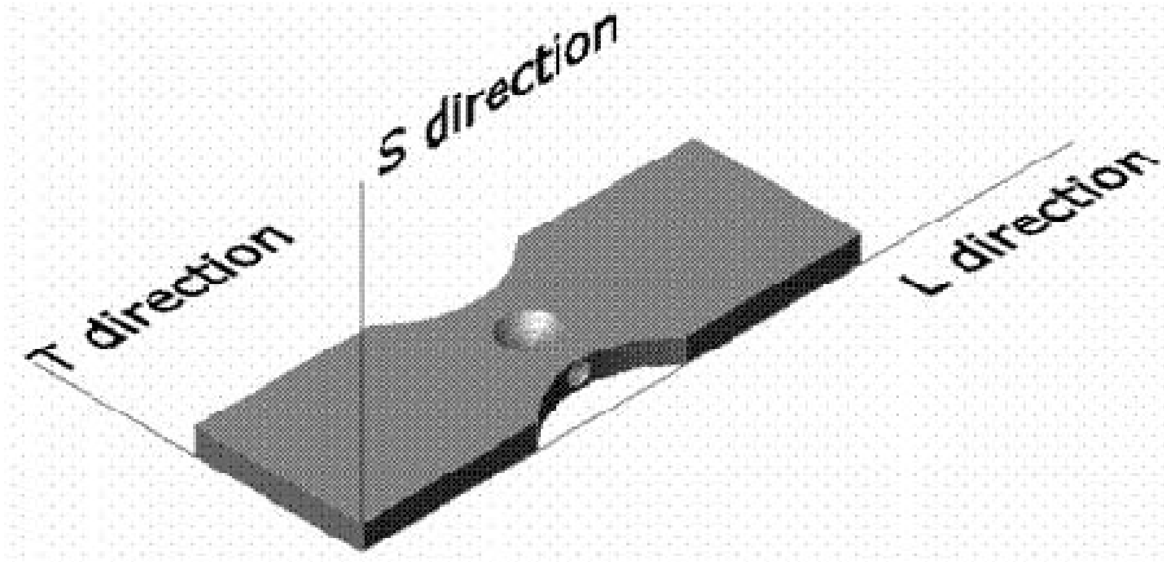

Figure 9.7-15 Material Axes Orientation for Test Specimens.

Table 9.7-4 Specimen Loading Direction and Corrosion Damage Planes.

	LT	*LS*	*LTLS*	*ST*	*LTST*
loading in L direction (spanwise)	3	3	3	0	0
loading in T direction (chordwise)	3	0	0	3	3

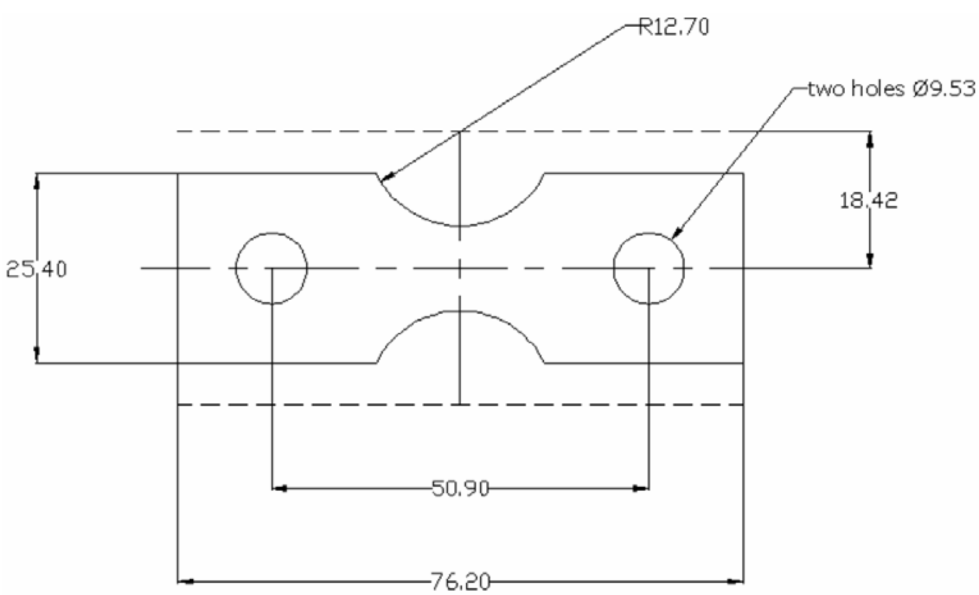

Figure 9.7-16 Specimen Dimensions (in mm).

Table 9.7-5 Results After Second (Higher Load) Spectrum Testing.

Loading Direction "L"				Loading Direction "T"			
	failed	no failure	no data		failed	no failure	no data
LTLS	2	1	0	*LTST*	3	0	0
LT	1	1	1	*LT*	0	3	0
LS	0	2	1	*ST*	1	1	1

Table 9.7-6 Number of Cycles to Failure for Second (Higher Load) Spectrum Testing. See Notes for Nucleation Site Description.

Loading Direction "L"		Loading Direction "T"	
	failed (N_f)		failed (N_f)
LTLS	2,740,914$_a$ 7,157,886$_b$	*LTST*	4,644,128$_d$ 5,120,304$_e$ 9,192,452$_f$
LT	6,015,498$_c$	*LT*	
LS		*ST*	3,251,101$_g$

a. The crack nucleated away from both corrosion sites at an "L" shape away from free surfaces. It seems as if the specimen experienced inadvertent shear loading in the test frame.

b. The crack here nucleated between corrosion on the side and on the front of the specimen. This area would be likely for failure due to the surrounding weakened ligaments.

c. This specimen had no corrosion on either side, yet it nucleated on the side of the specimen, most likely due to the K_t of the specimen design.

d. Corrosion conditions were on the front and side of the specimen and nucleated where expected -- at the side of the specimen where corrosion existed.

e. Nucleation seemed to be caused at the corner of the specimen between corrosion sites. Again, reason for this may be explained by the weakened surrounding material.

f. This nucleation occurred away from the most susceptible corner, but corrosion was not apparently a factor.

g. This specimen had corrosion only on the side and corrosion seems to be the cause for this failure as beach marks are present which have formed circumferentially to the corrosion.

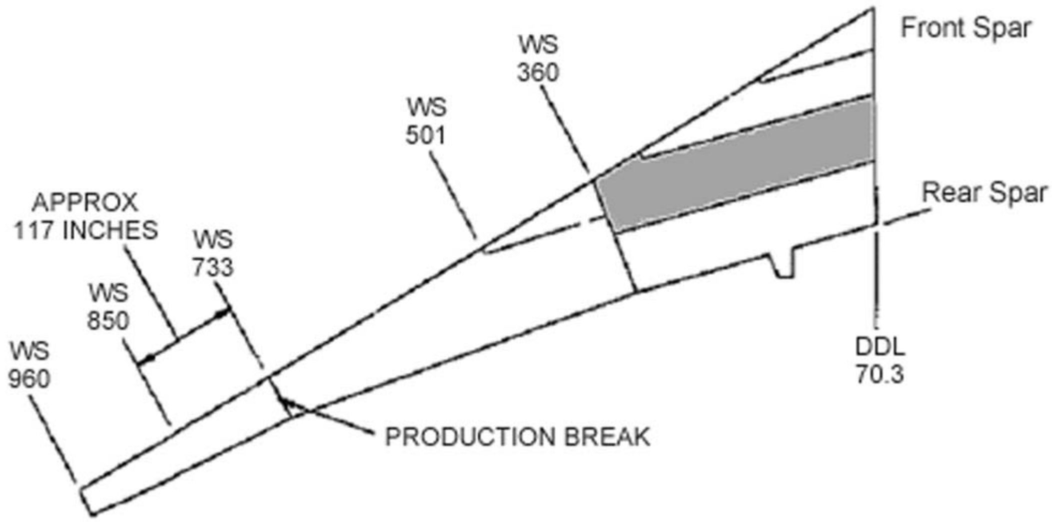

Figure 9.7-17 Wing Station Layout With Area of Interest Shaded.

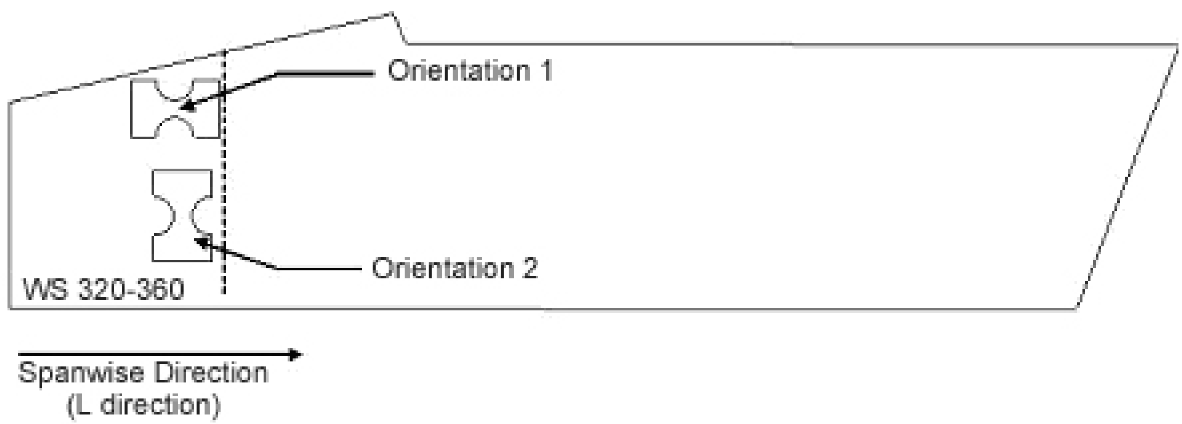

Figure 9.7-18 Wing Section 320 Through 360 on the Upper Wing Skin With Specimen Cut-Out Locations Shown.

Table 9.7-7 Results After Completion of Second, More Severe Spectrum.

Loading Direction "L"				Loading Direction "T"			
	failed	no failure	no data		failed	no failure	no data
LTLS	2	1	0	*LTST*	3	0	0
LT	1	1	1	*LT*	0	3	0
LS	0	2	1	*ST*	1	1	1

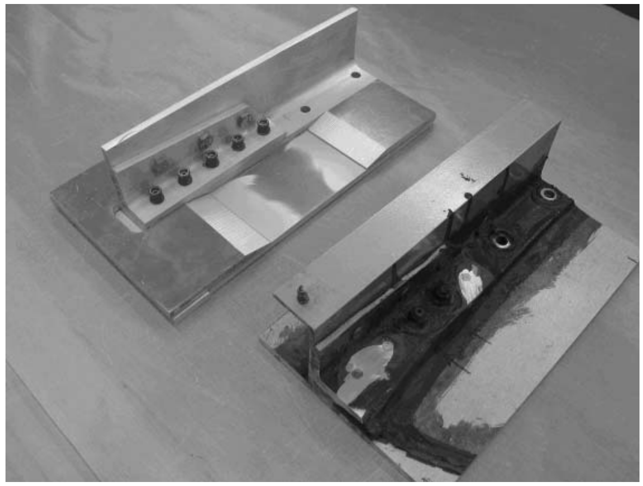

Figure 9.7-19 Prototype (L) and In-Service Specimen #1 of Transport Upper Wing Skin.

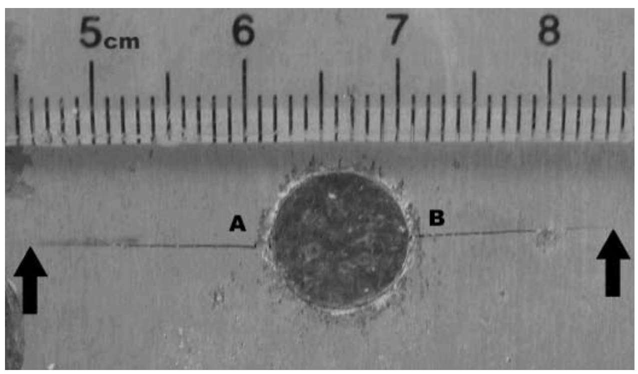

Figure 9.7-20 Two Cracks, Each About 15mm, Growing From Fastener Hole, Specimen #1.

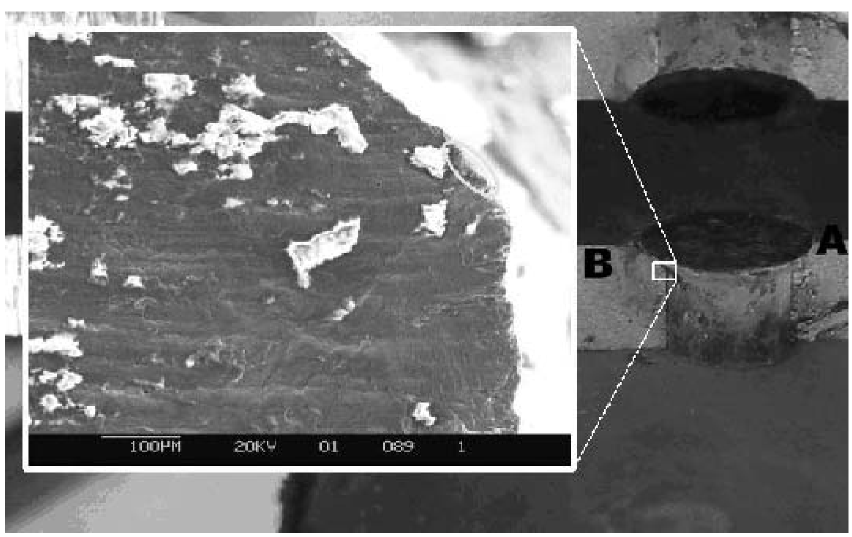

Figure 9.7-21 Crack Nucleation Site (Inclusion) on One Side of Hole, Specimen #1.

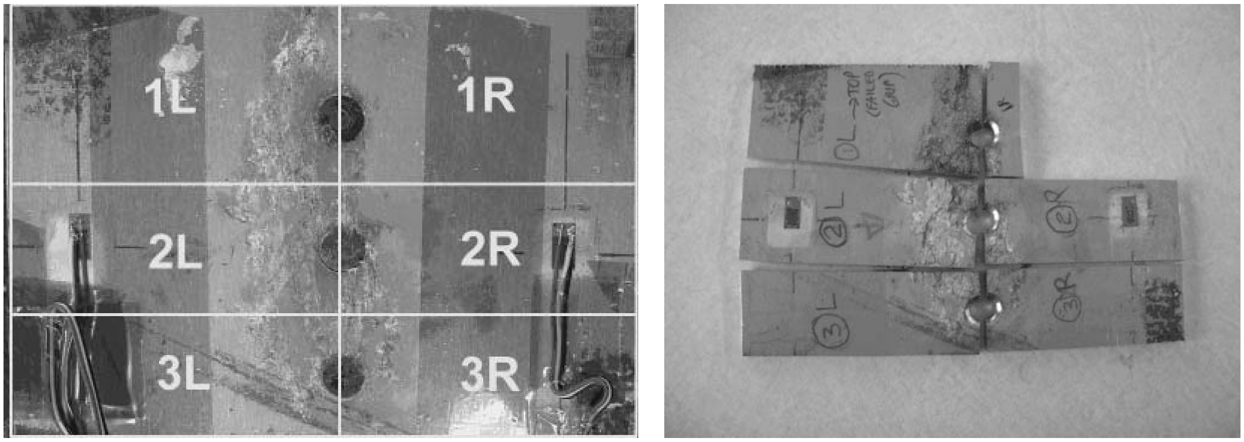

Figure 9.7-22 Sectioning of In-Service Specimen #2.

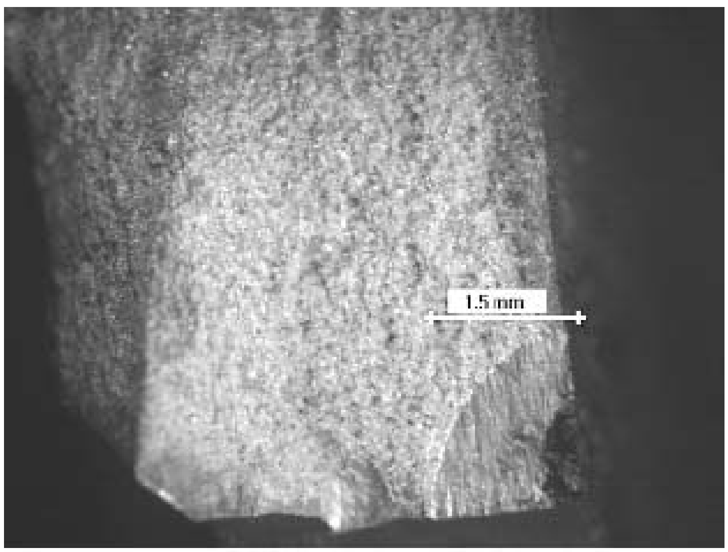

Figure 9.7-23 Corner Crack at Bottom of Fastener Hole #3, Specimen #2.

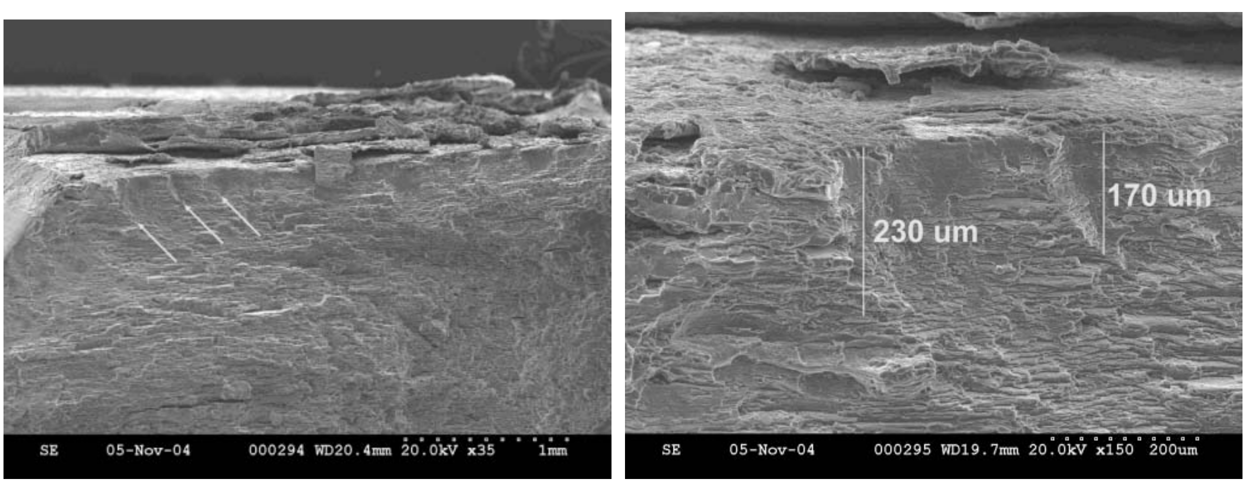

Figure 9.7-24 Early Nucleation Features Near Surface Adjacent to Countersink, Specimen #2.

Figure 9.7-25 7075-T6-0.106” Specimen With a Constituent Particle Related Crack: Corrosion Aided in Material Removal Around the Particle, and Subsequently Crack Nucleation.

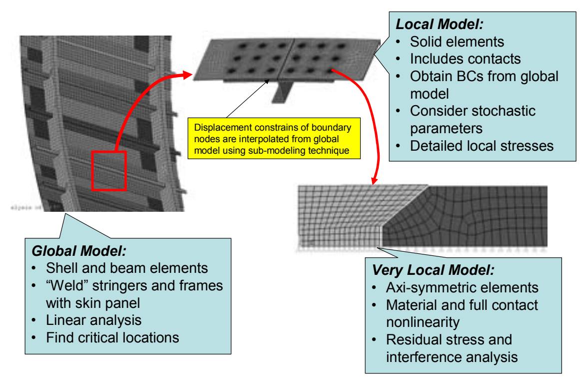

Figure 9.7-26 Multiscale Stochastic FE Approach.

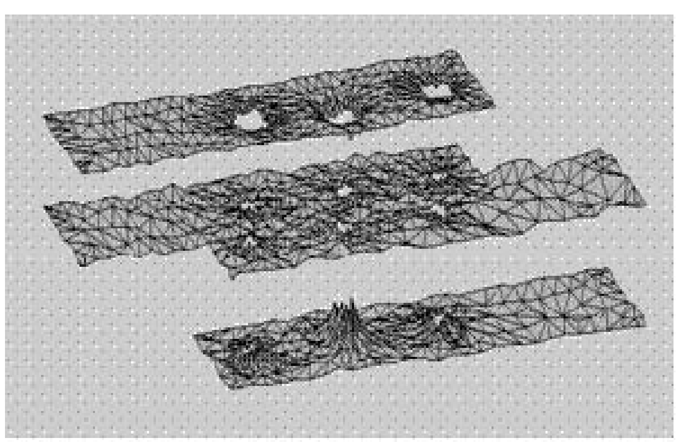

Figure 9.7-27 Simulated Stochastic Corroded Surfaces.

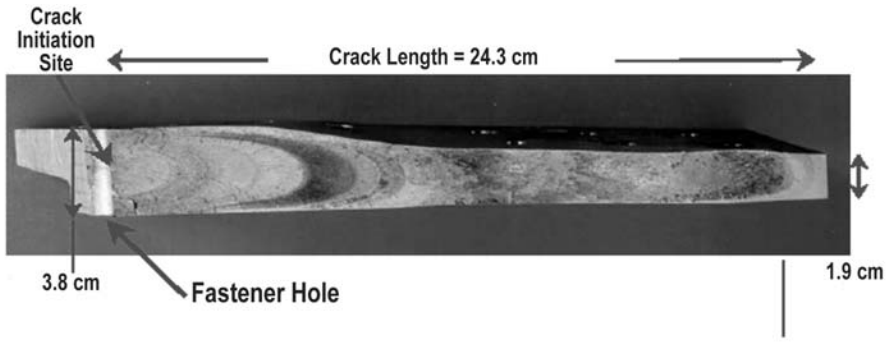

Figure 9.7-28 The Photograph Shows the Surface of a Long Crack Emanating From a Tie Box Fastener Hole.

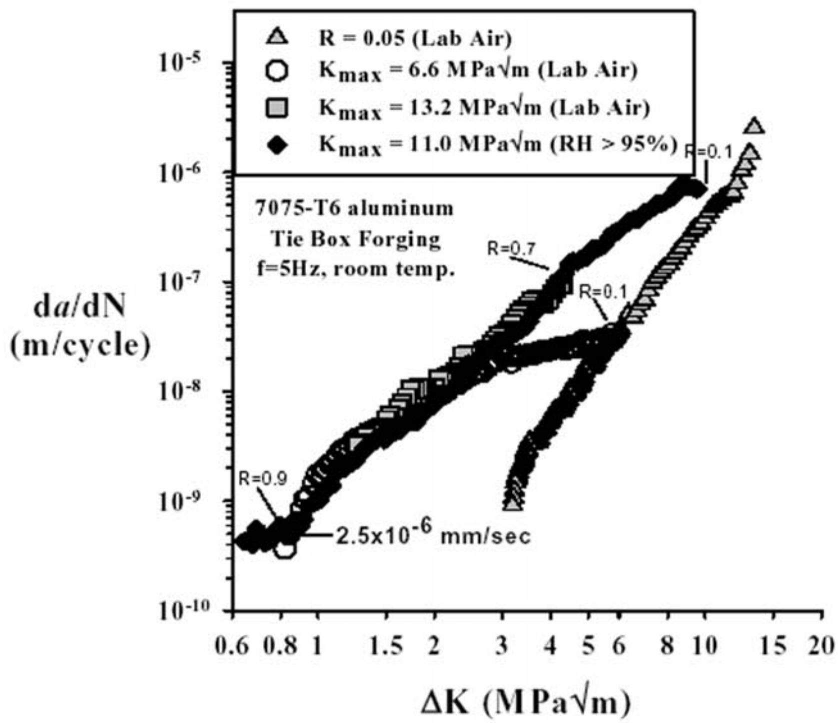

Figure 9.7-29 Plot Showing the High R (Ripple Load) and Low R Fatigue crack Growth Rate Characteristics of 7075-T6 Tie Box Forging Material Exposed to Laboratory Air and 95% Relative Humidity Air Environments.

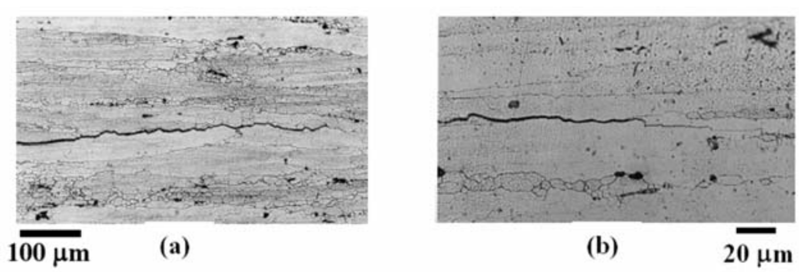

Figure 9.7-30 Optical Micrographs of an Etched Surface Showing the Near Crack-Tip Region and the IG Crack Path of (a) Crack Found in a Tie Box Forging and (b) Fatigue Crack Produced in Laboratory Air (30% to 60% RH) Using Tie Box Forging 7075-T6 Material.

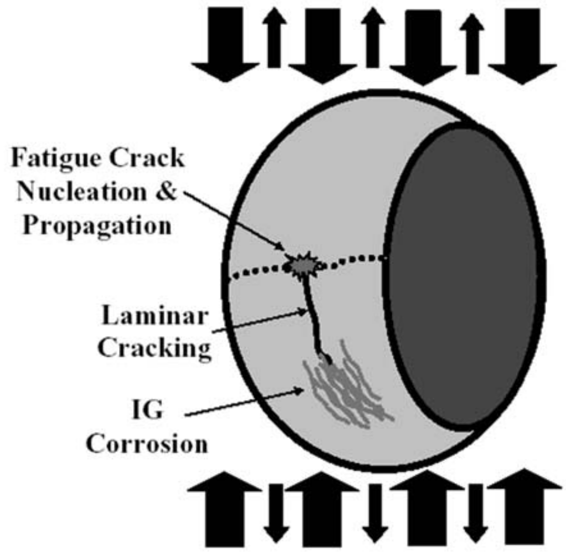

Figure 9.7-31 Schematic Showing the Test Coupon Hole and Remote Compressive (Small Tension) Loading, the IG Corrosion Region Located at the 7 O'clock Position, IG Delamination (Laminar Cracking), Region of Fatigue Crack Nucleation and Through-the-Thickness Fatigue Crack Propagation (Dashed Line).

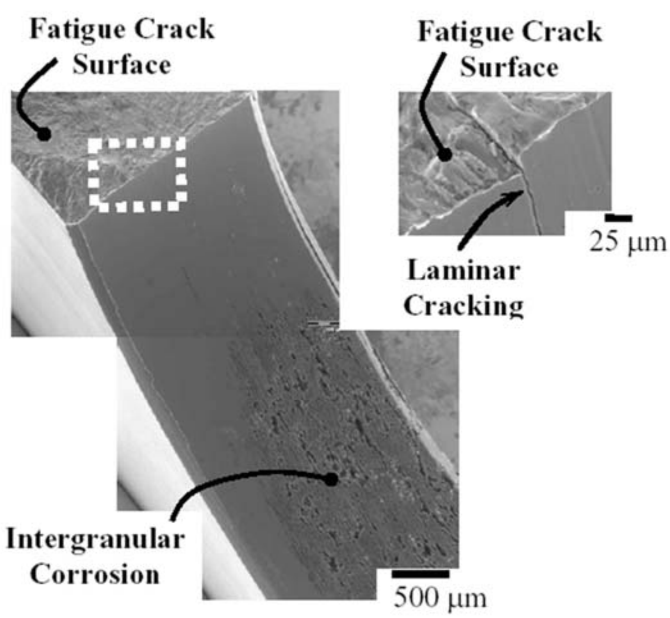

Figure 9.7-32 The Micrograph Shows the 6 to 9 O'clock Portion to the Test Coupon Hole. Noted on the Through-the-Thickness Surface is the IG Corrosion Region Located at the 7 O'clock Position and Noted at the Top of the Micrograph is the Fatigue Crack Surface. The Small Micrograph at the Upper Right Location Shows the Region of Fatigue Crack Nucleation (Dashed Square Area) at High Magnification; Here, the Laminar Crack is Clearly Seen.

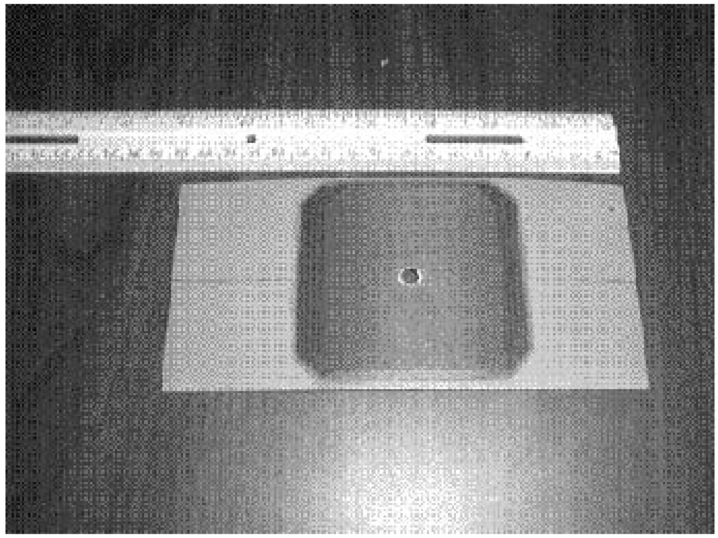

Figure 9.8-1 Test Specimen With Bonded Composite Patch.

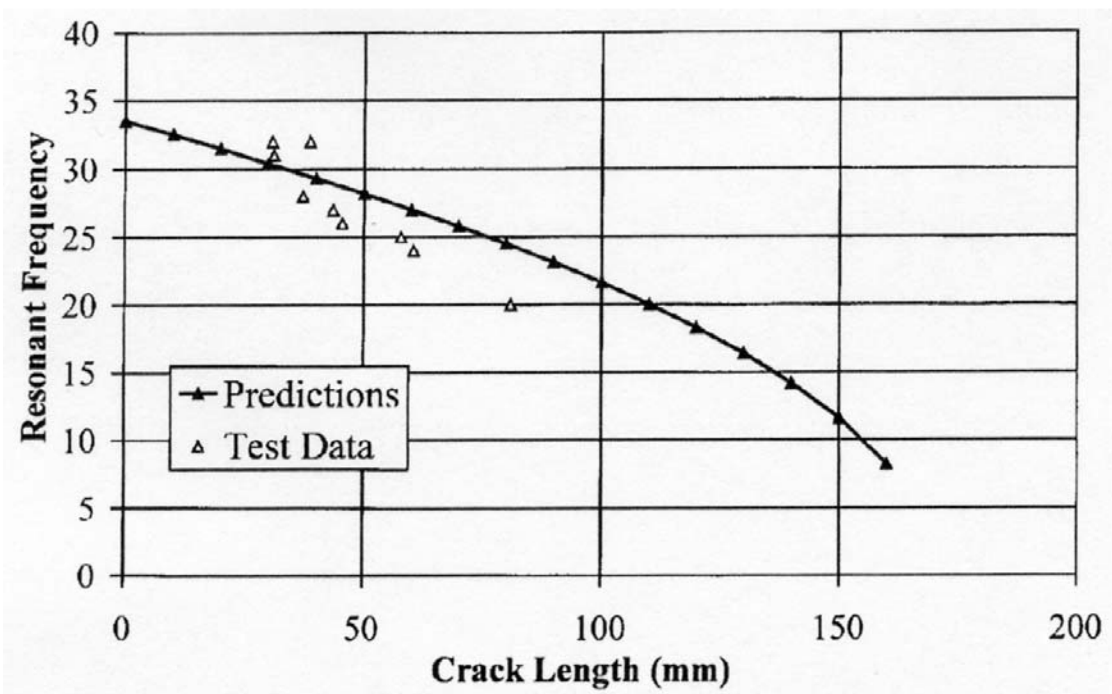

Figure 9.8-2 Predicted and Observed Resonant Frequencies at Various Crack Lengths in 170x360x1-mm Specimens With Bonded Repair Patches.

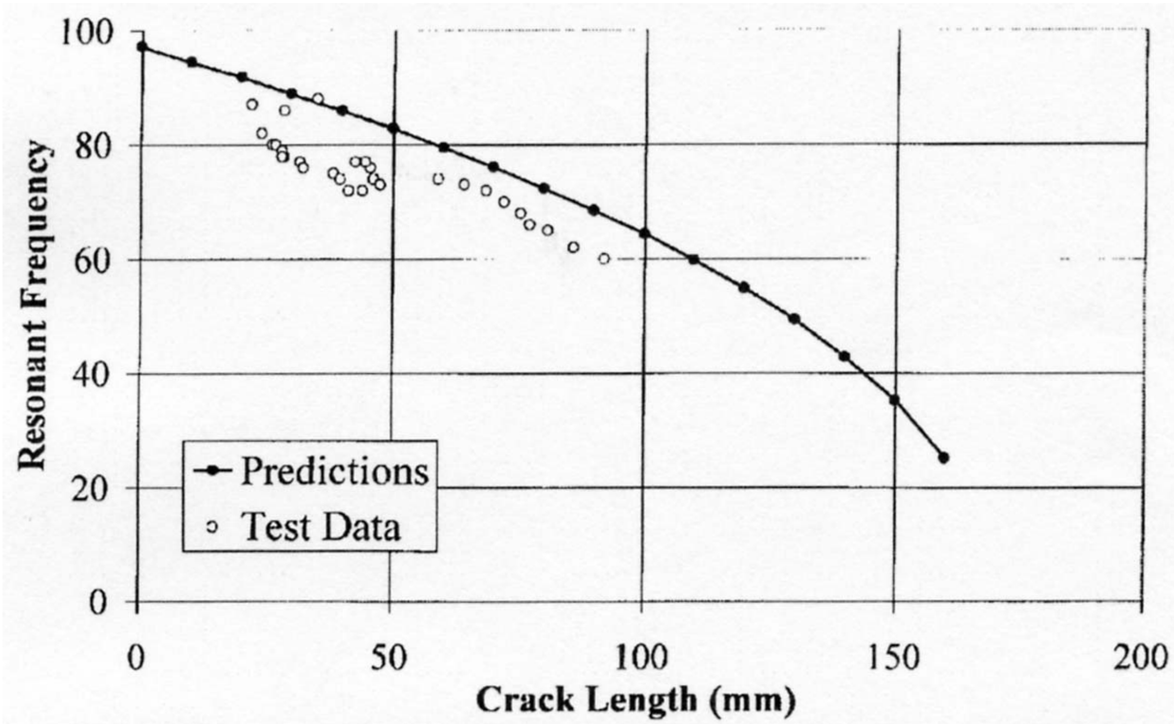

Figure 9.8-3 Predicted and Observed Resonant Frequencies at Various Crack Lengths in 170x360x3.2-mm Specimens With Bonded Repair Patches.

Figure 9.8-4 Disassembly of a Cessna 402A.

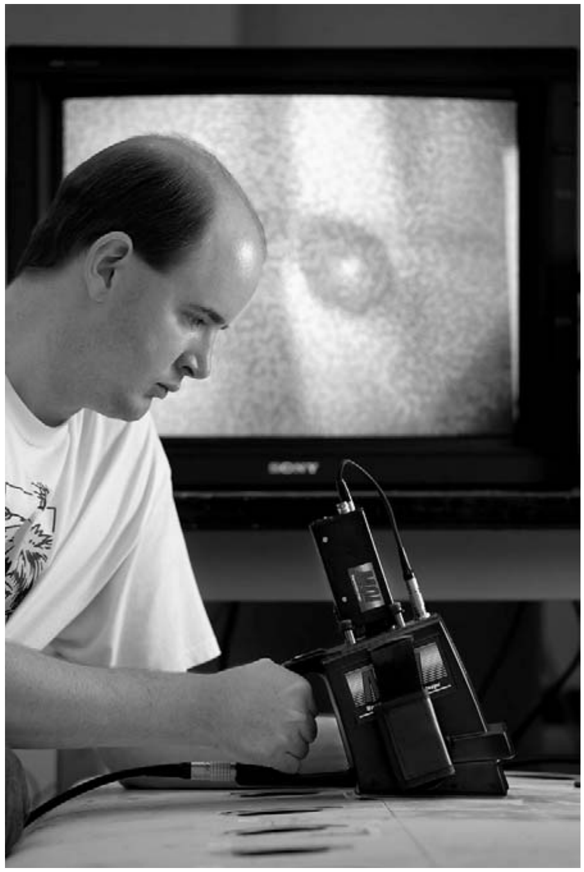

Figure 9.8-5 Magneto Optic Imaging.

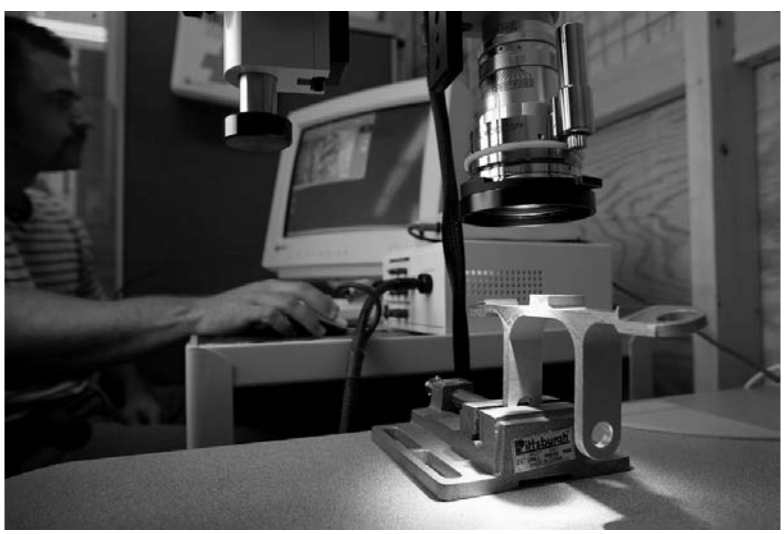

Figure 9.8-6 Microscopic Examination.

Figure 9.8-7 FAA Test Bed Aircraft.

Figure 9.8-8 ATR42-300 -- Pretest.

Figure 9.8-9 ATR42 -- Posttest.

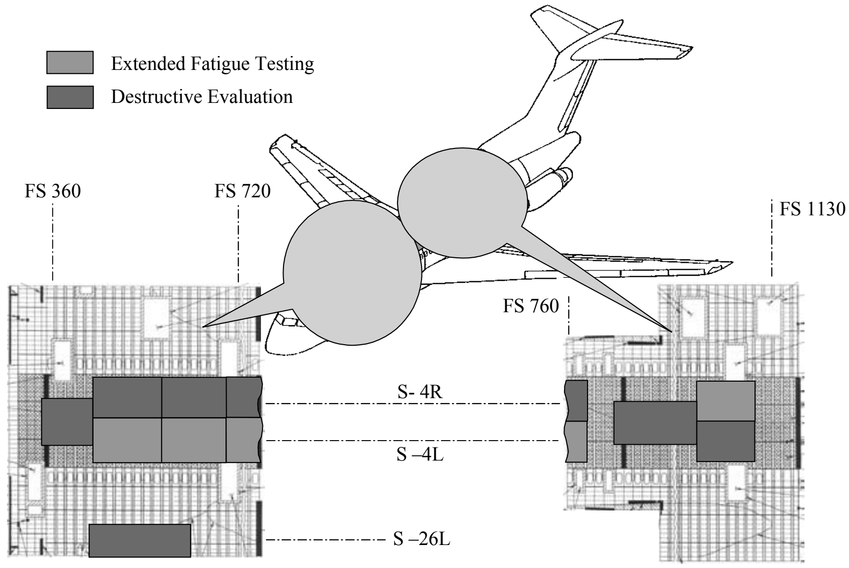

Figure 9.8-10 Sections Removed for Evaluation.

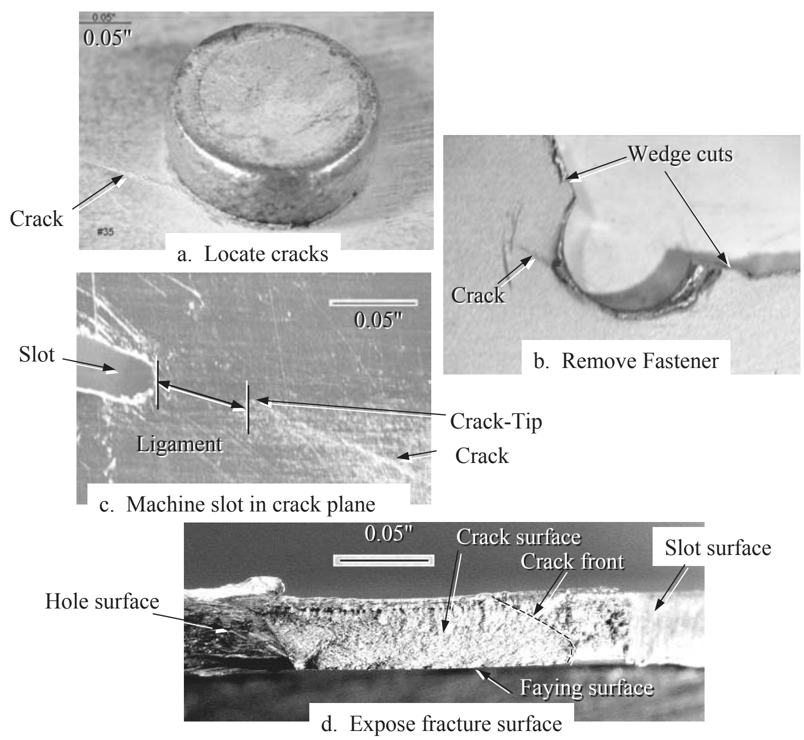

Figure 9.8-11 Disassembly Procedure for Joints.

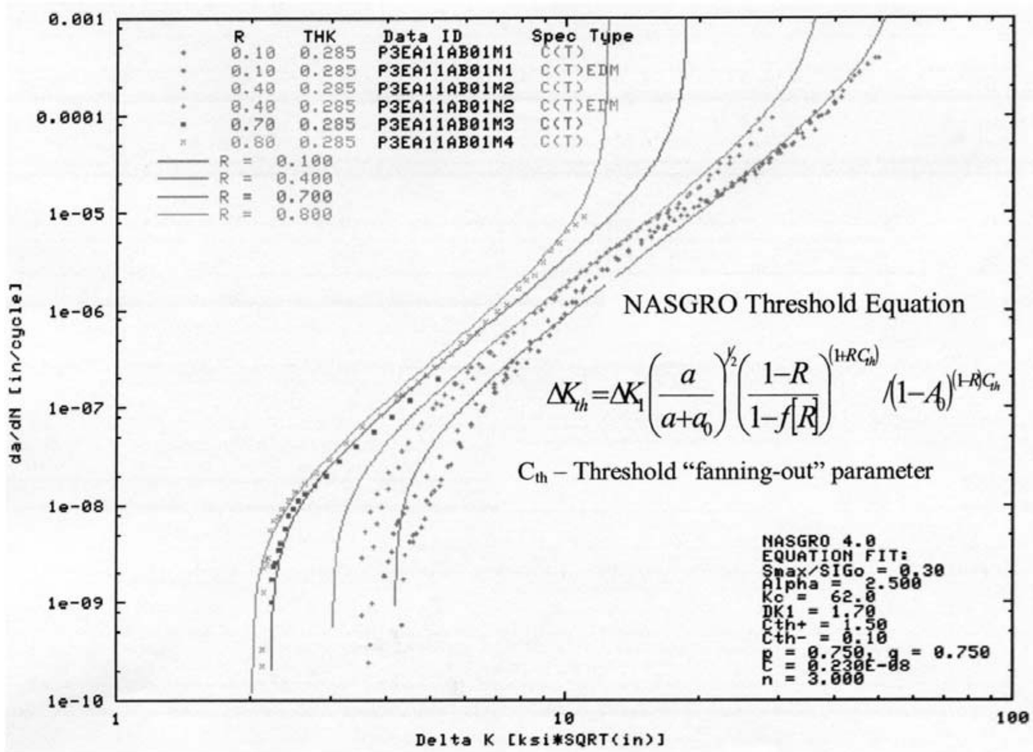

Figure 9.8-12 NASGRO Eqn. Fit for Ti-6Al-4V MA 0.25" Plt; C(T) Specimens; R = 0.1 - 0.8 data; C_{th} = 1.50.

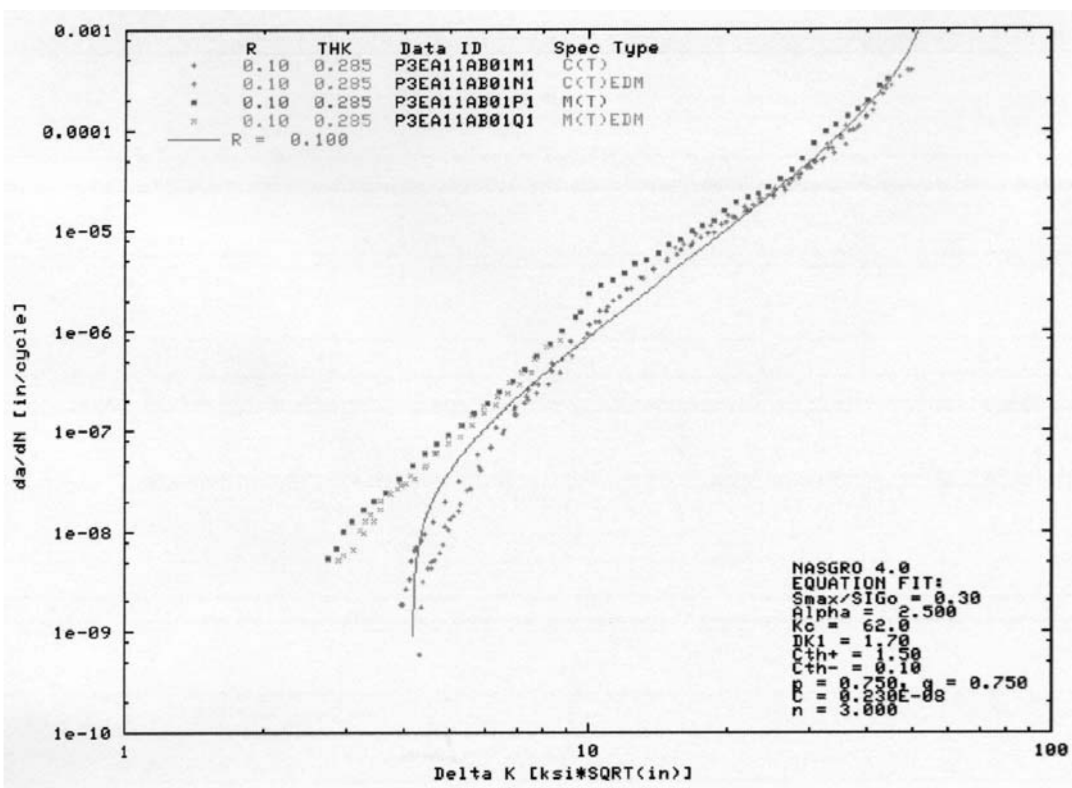

Figure 9.8-13 NASGRO Eqn. Fit for Ti-6Al-4V MA 0.25" Plt; C(T) & M(T) Specimens; R = 0.1 data; C_{th} = 1.50.

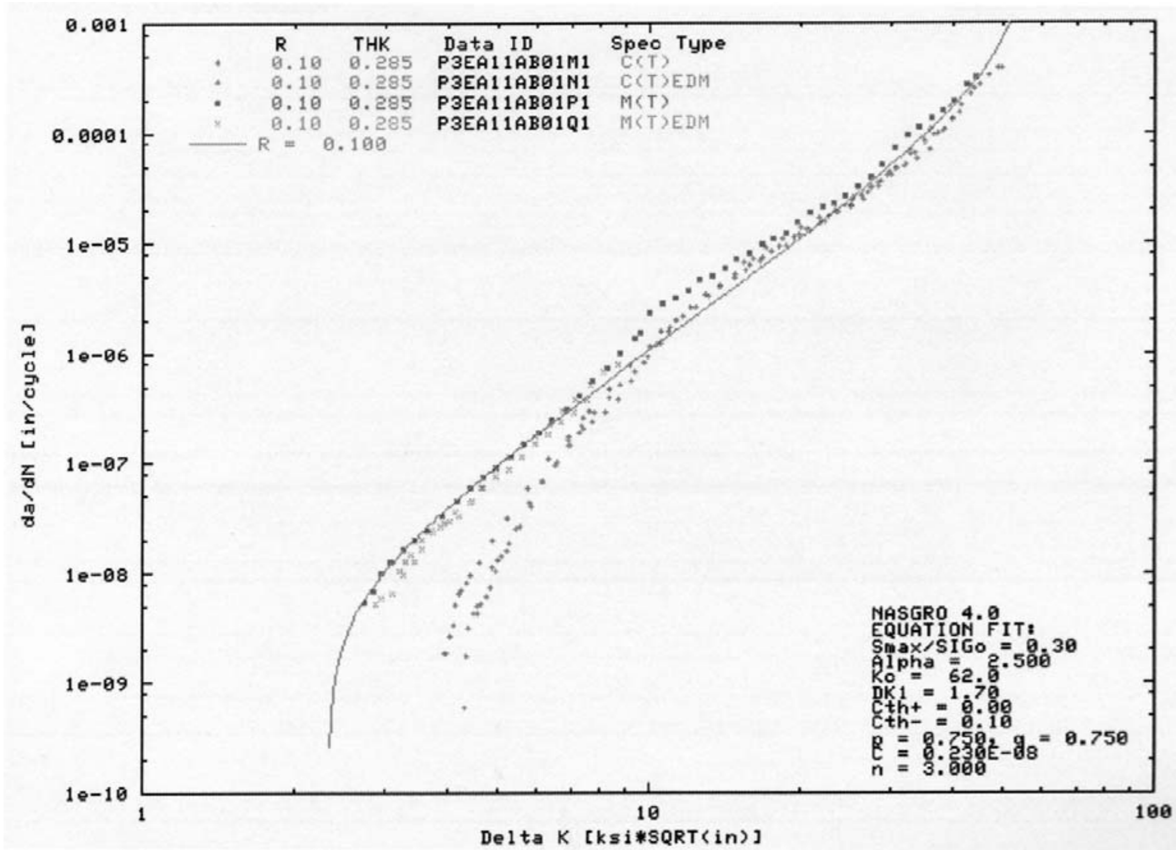

Figure 9.8-14 NASGRO Eqn. Fit for Ti-rAl-4V MA 0.25" Plt; C(T) & M(T) Specimens; R = 0.1 data; C_{th} = 0.

F/A-18 Full-Scale Testing

- Test Article (FT76/ST50)
  - FT76 Is the New Forward Fuselage Attached to the Recycled Center/Aft Fuselage (ST50) From the Previous Test Program
    - ST50 Was the Full-Scale Static Test Article
- Test Requirements
  - Complete 12,000 Hours of Fatigue Cycling
  - Complete Static Loading of All Ultimate Design Conditions

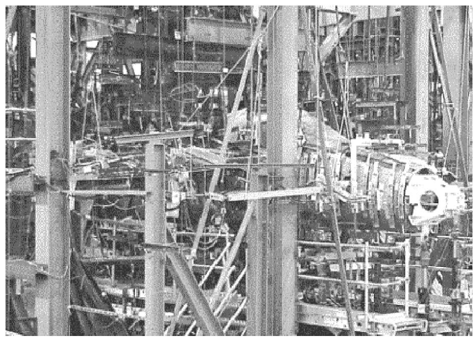

Ref.: T. Callihan
ICAF 2003

BOEING

F/A-18 Full-Scale Testing (continued)

- Test Article (FT50)
  - FT50 tested the Engineering and Manufacturing Demonstration (EMD) configuration of the aircraft.
  - Completed 18,000 Simulated Flight Hours of Fatigue Cycling

- Test Article (FT77)
  - FT77 tested the new F/A-18 Wing
  - Completed 18,000 Simulated Flight Hours of Fatigue Cycling

- Teardowns and Inspections in work

Ref.: T. Callihan
ICAF 2005

BOEING

Figure 9.8-15

F-15 FTA6 Test Articles

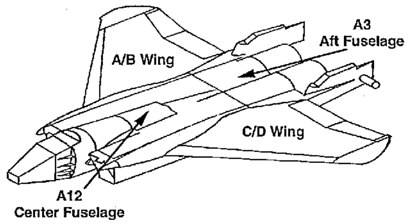

Tested at the Air Force Wright Aeronautical Lab Dec. 1988 through May 1994.

Test achieved 18133 flight hours.

Shut down after failure of the LH Intermediate spar near lower lug.

Ref.: M. Golike
ASIP 2003

Figure 9.8-16

F-15 FTA6 Teardown/ Inspection

Teardown/Inspection performed in St. Louis. Sept. 1994 through Oct. 1996.

Sample Teardown Location:

Crack C

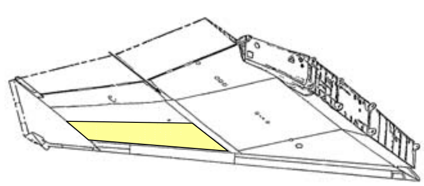

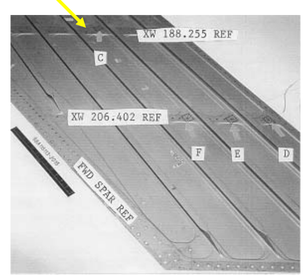

Look Up at LH Wing **Look Down at LH Wing Skin**

Failure analyses and fleet inspection definition – on going per priority order

Ref.: M. Golike
ASIP 2003

Figure 9.8-17

F-15 FTA6 Teardown Analysis Process

- Determine the spectrum appropriate for the failure location.
- Perform crack initiation and crack growth analysis. (LifeWorks used at Boeing St. Louis)
- Iterate until match is achieved.
- In general, match consists of: CI Life + CG Life = 18133, with final crack size matching final FTA6 crack size.
- Revise the F-15 A-D Durability and Damage Tolerance Assessment analysis and report. Do a DTA version of the analysis using B/P properties, theoretical loads and spectra to predict DTA lives.
- Then use these lives to revise the F-15 A-D Force Structural Maintenance Plan inspection requirements and procedures.

Ref.: M. Golike
ASIP 2003

BOEING

Figure 9.8-18

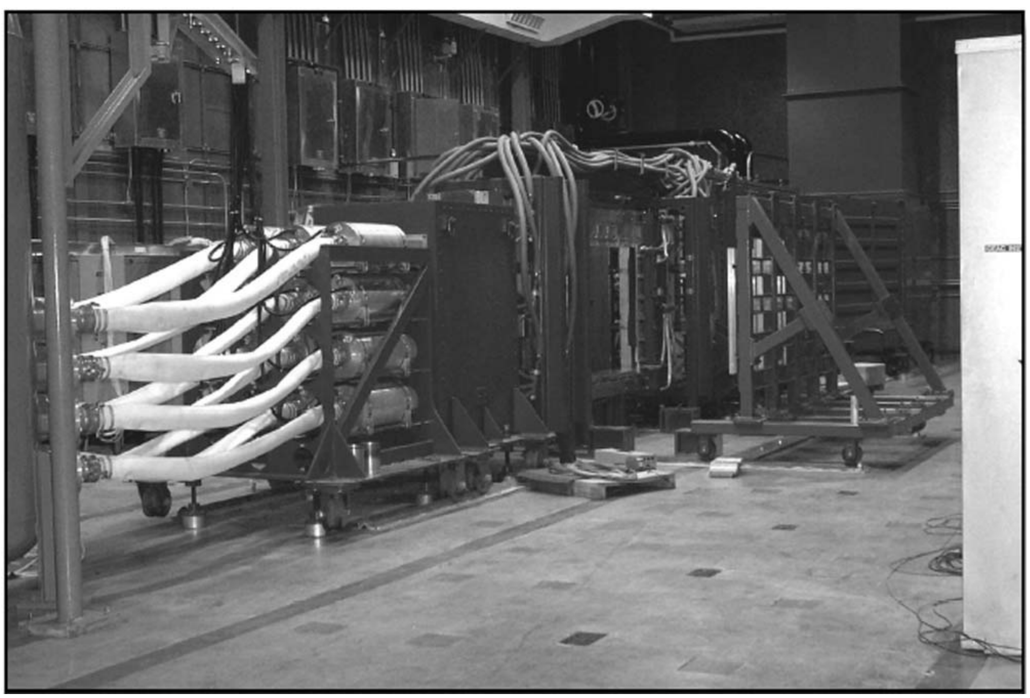

Figure 9.8-18A

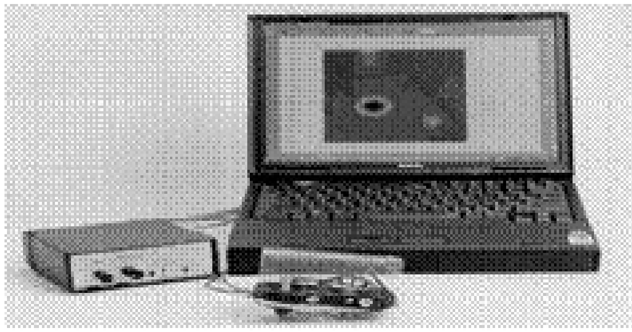

Figure 9.9-1 Computer-Aided Tap Tester.

Figure 9.9-2 Air-Coupled Ultrasonic Testing System.

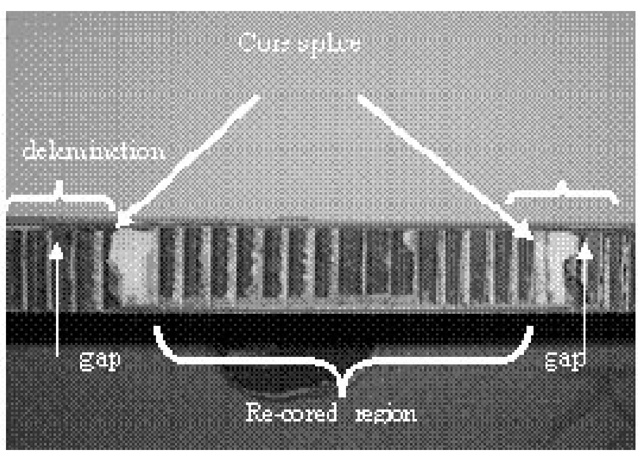

Figure 9.9-3 Cross Section of the Repaired Panel.

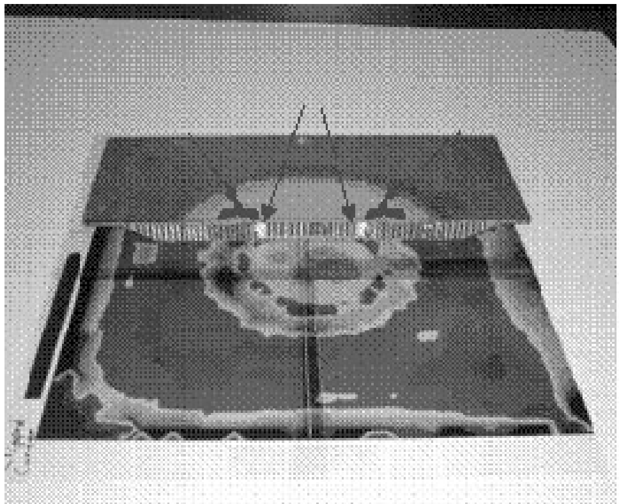

Figure 9.9-4 Correlation Between the Internal Conditions of Composite Repairs and Its Image by the CATT.

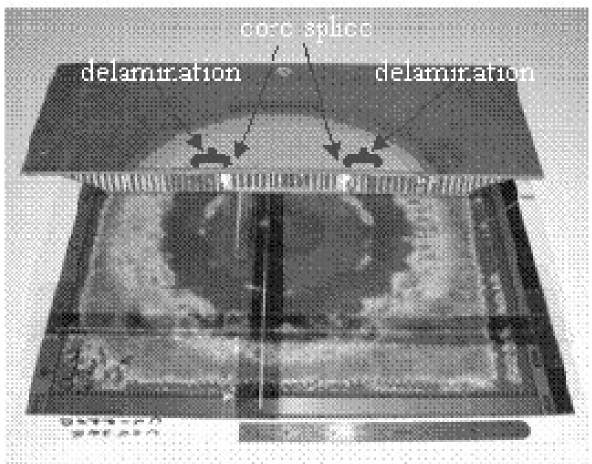

Figure 9.9-5 Correlation Between the Internal Conditions of Composite Repairs and Its Image by the AC-UT System.

Figure 9.9-6 Composite General Aviation 14 CFR Part 23 Aircraft That are Currently Being Certified.

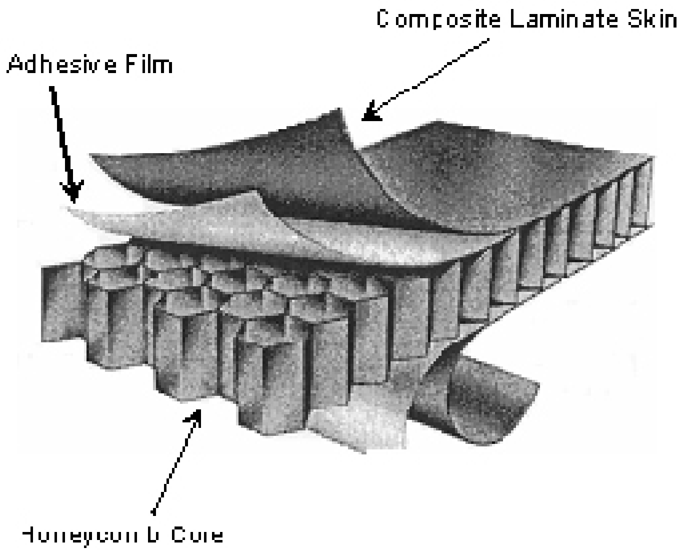

Figure 9.9-7 Basic Construction of a Honeycomb Aircraft Panel.

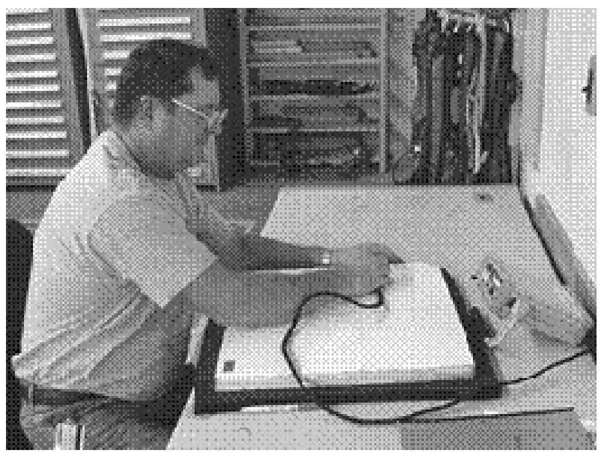

Figure 9.9-8 An Inspector Using an NDI Device on a Honeycomb Test Specimen.

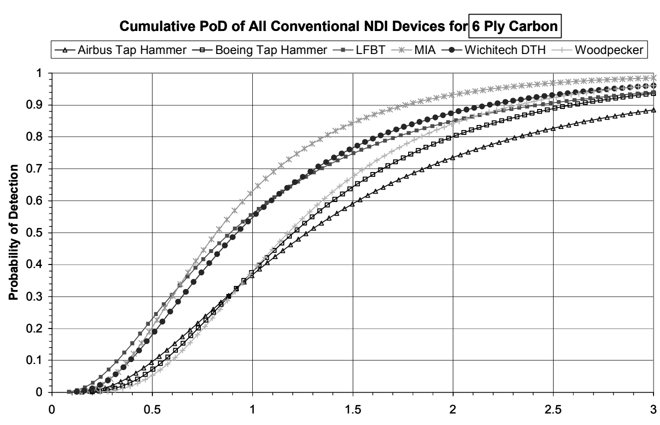

Figure 9.9-9 A Set of Typical POD Curves.

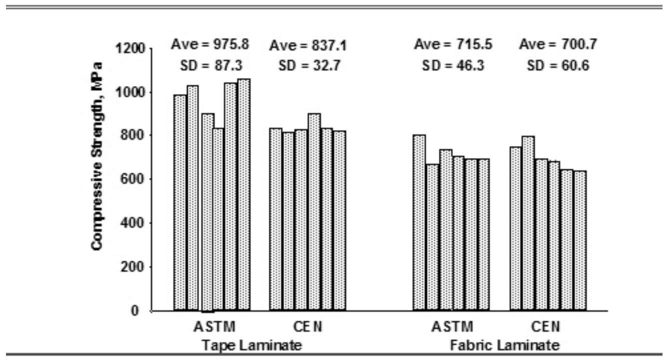

Figure 9.9-10 Comparison of ASTM and CEN Compression Test Results at Room Temperature for Tape and Fabric Unidirectional Laminates.

Figure 9.9-11 ASTM D 695 Compression Test Fixture.

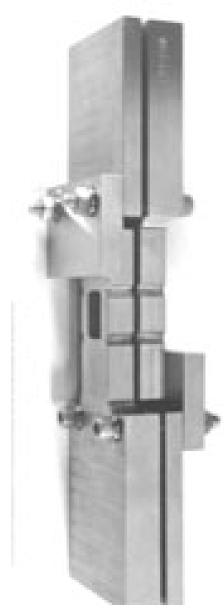

Figure 9.9-12 SACMA Compression Test Fixture.

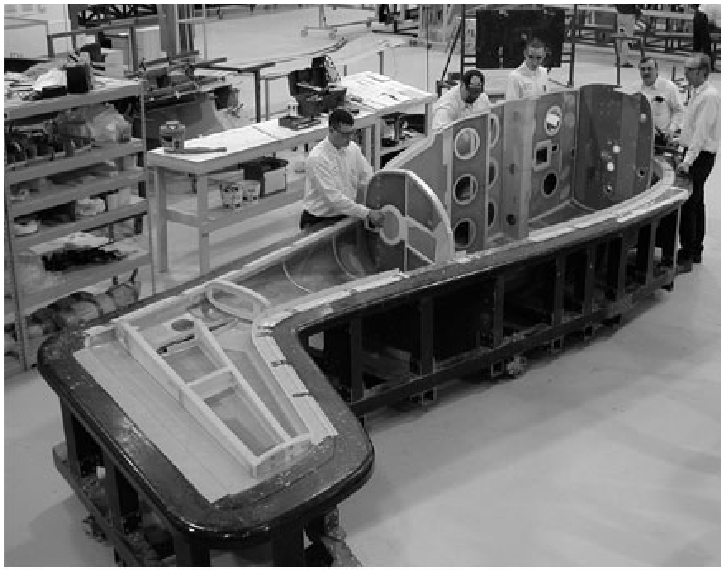

(a)

(b)

Figure 9.9-13 (a) Manufacturing a Bonded Component for a General Aviation Aircraft and (b) the Completed Aircraft in Flight.

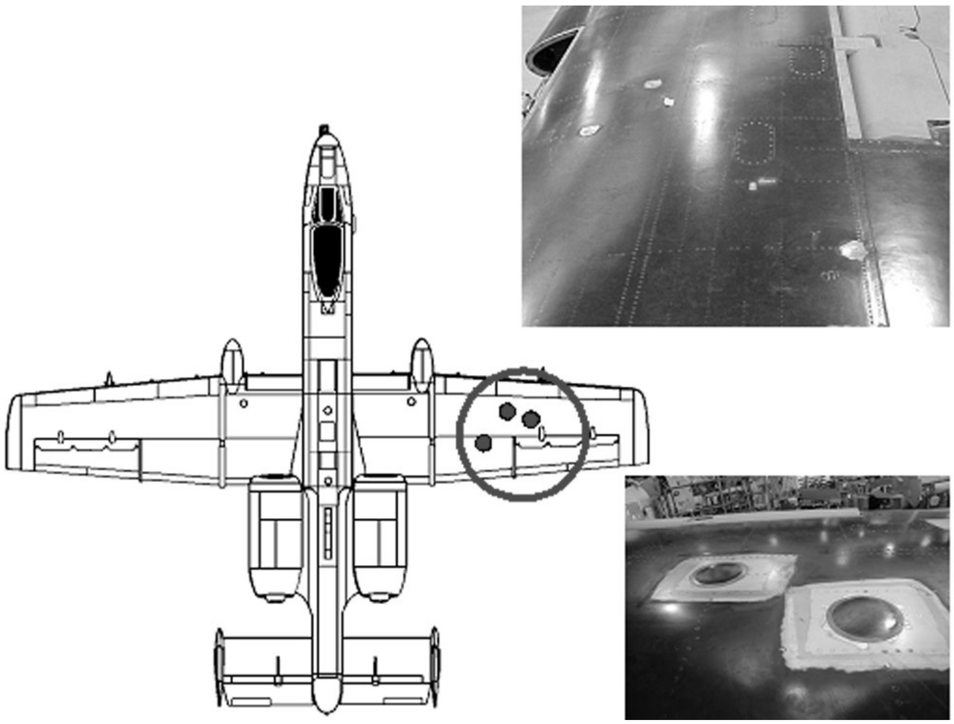

Figure 9.9-14.

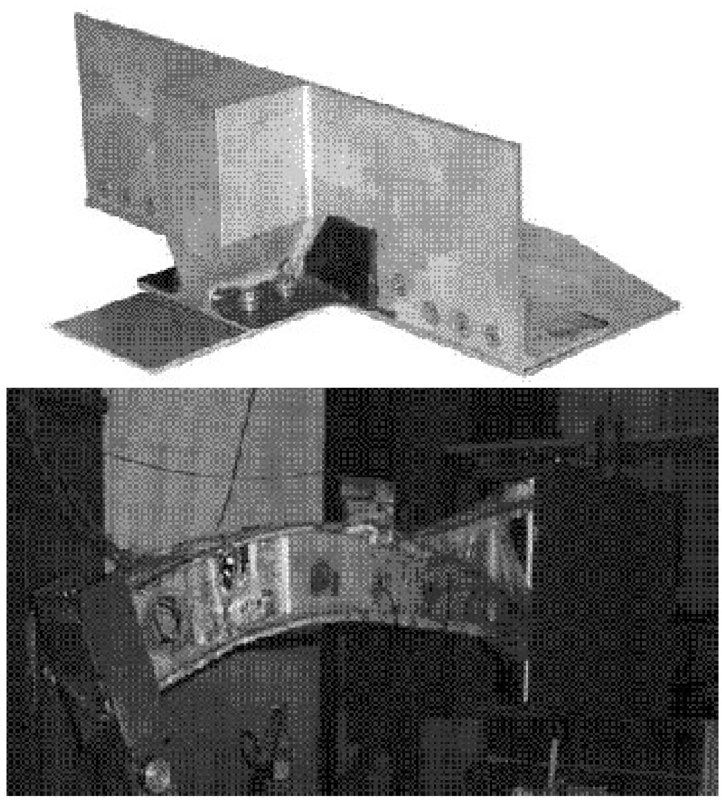

Figure 9.9-15.

Figure 9.9-16 Single Aisle and Twin Aisle Fuselage Section.

Figure 9.9-17 Horizontal Stabilizer in As-Received Condition.

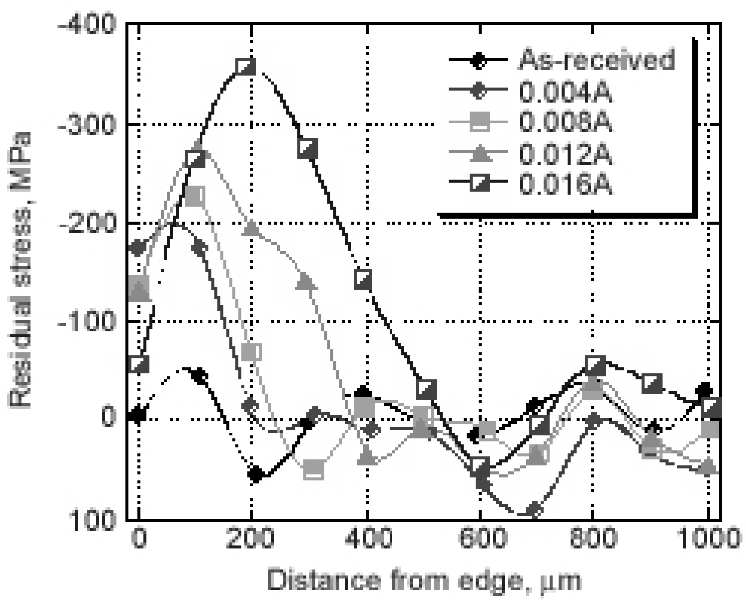

Figure 9.10-1 Residual Stresses in As-Received and Shot-Peened SENB Specimens.

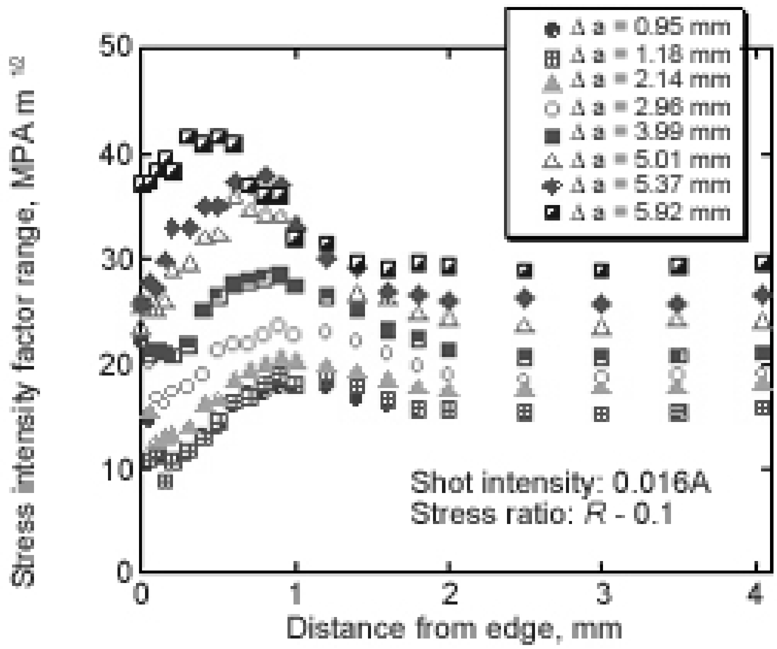

Figure 9.10-2 K in SENB Specimens With Residual Stress.

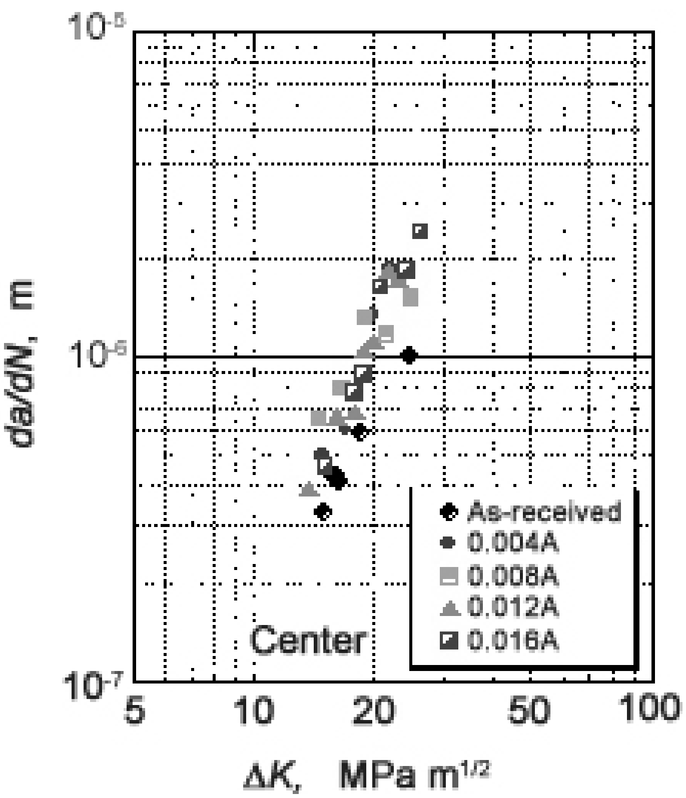

Figure 9.10-3 da'/dN Versus ΔK at Center of SENB Specimens, as Received and Shot Peened.

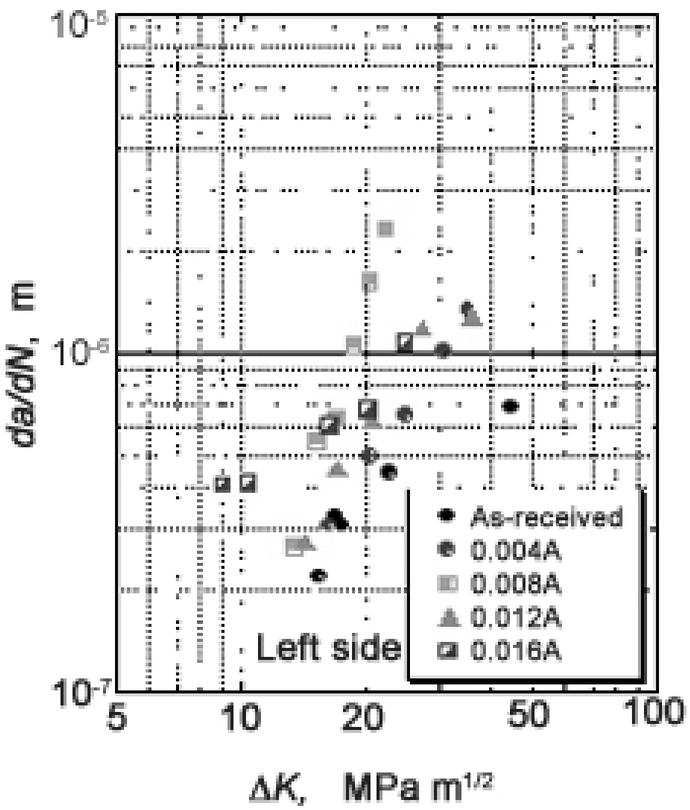

Figure 9.10-4 da'/dN Versus ΔK at Left Side of SENB Specimens, as Received and Shot Peened.

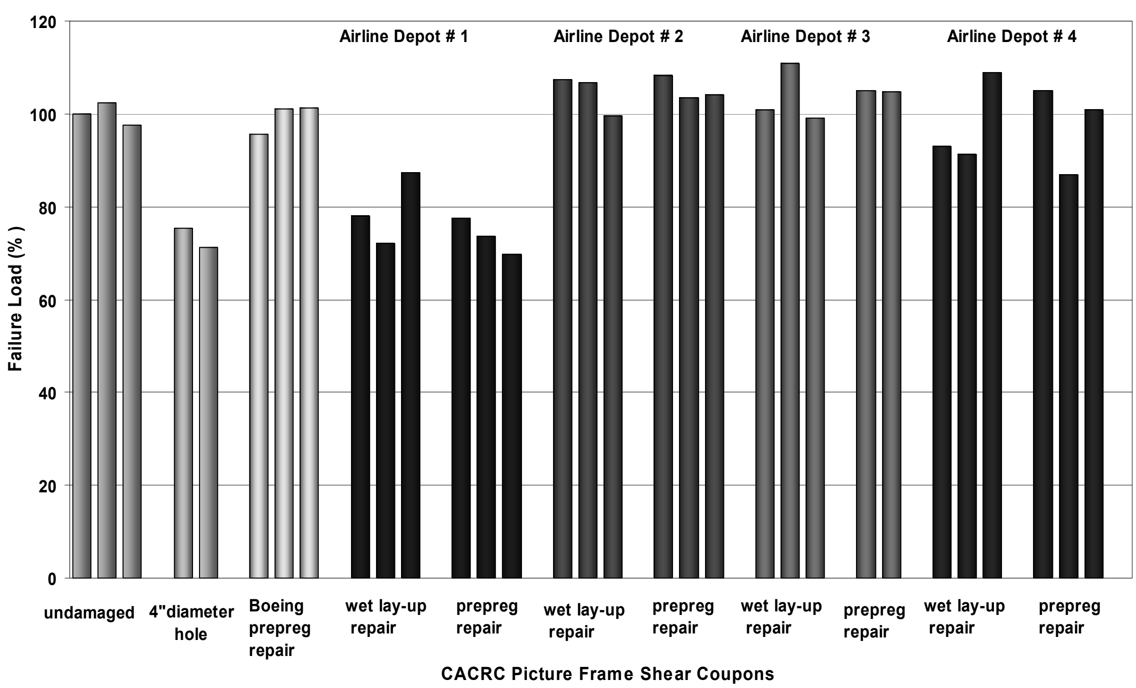

Figure 9.10-5 Performance of Field Station Repairs Versus OEM Repairs.

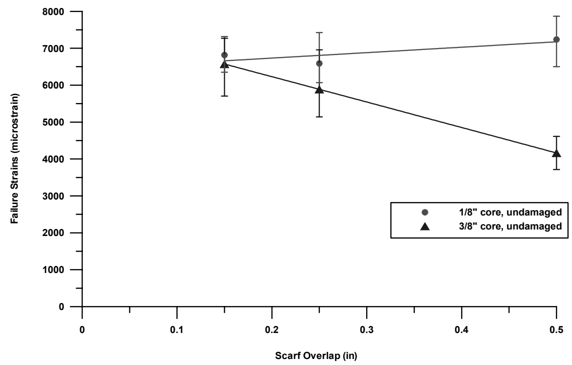

Figure 9.10-6 Effect of Core Cell Size on the Failure Strains of Undamaged Large Beams.

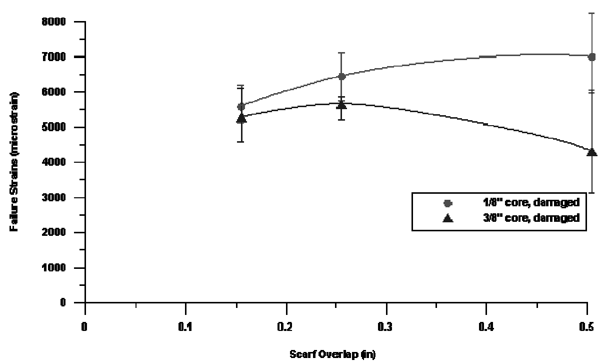

Figure 9.10-7 Effect of Core Cell Size on the Failure Strains of Damaged Large Beams.

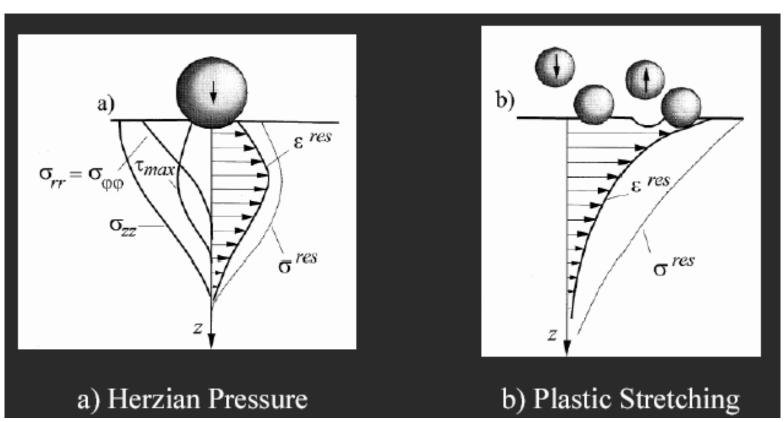

Figure 9.10-8 Mechanical Effects Due to Shot Peening.

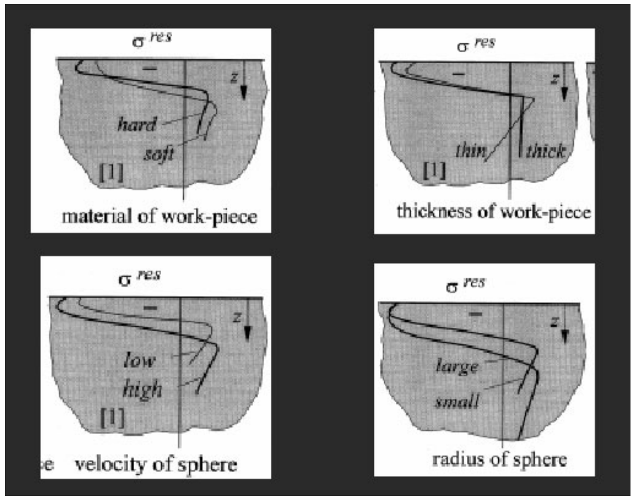

Figure 9.10-9 Influence of Shot-Peening Parameters on the Distribution of the Residual Stresses.

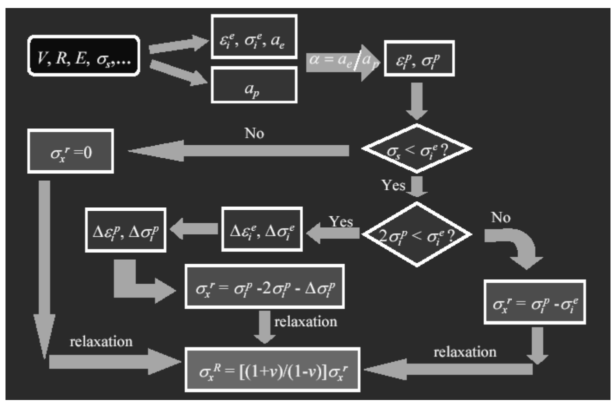

Figure 9.10-10 Flow Chart of the Enhanced Model Used to Calculate Shot-Peening-Induced Residual Stresses.

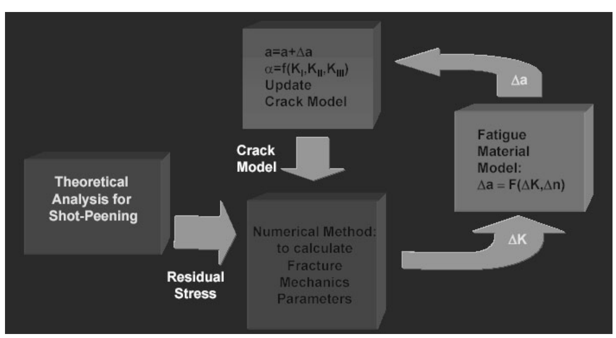

Figure 9.10-11 Modeling Fatigue Crack Growth in Shot-Peened Structural Components.

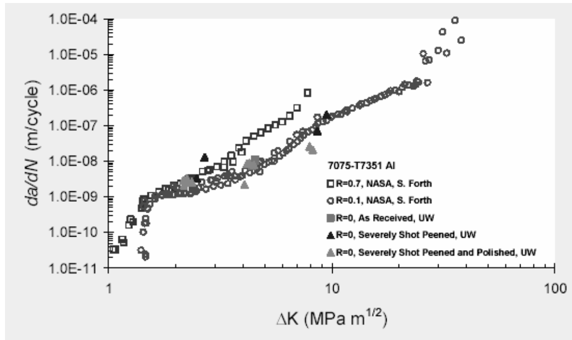

Figure 9.10-12 da/dN vs. ΔK of a Double-Edged Sharp Notch Specimen.

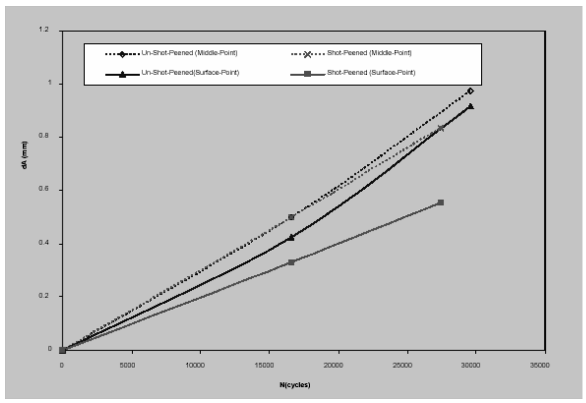

Figure 9.10-13 Effects of Shot Peening on Fatigue Crack Growth.

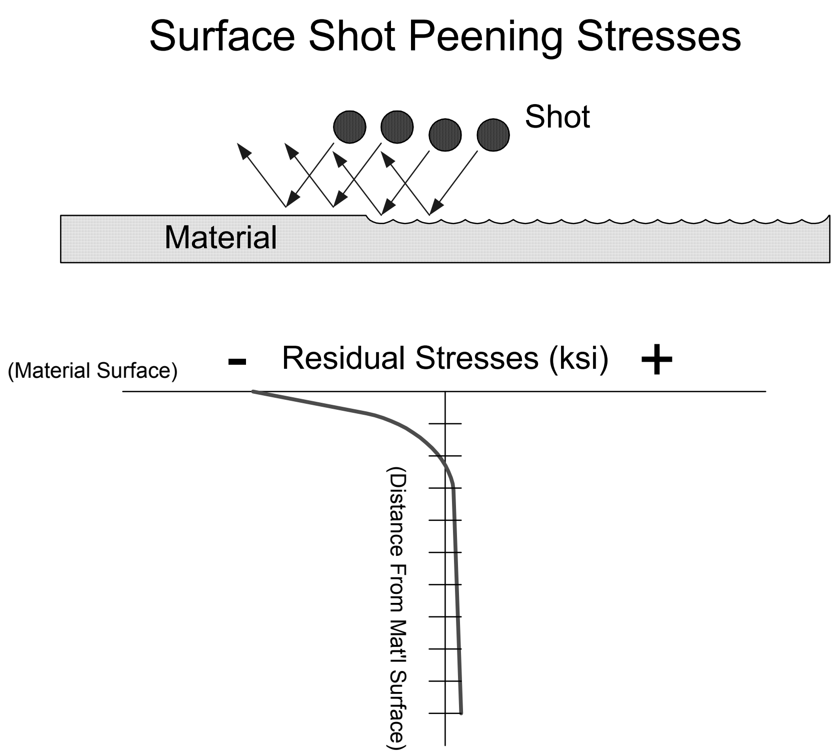

Figure 9.10-14 Shot Peen Process and Effective Residual Stress Pattern.

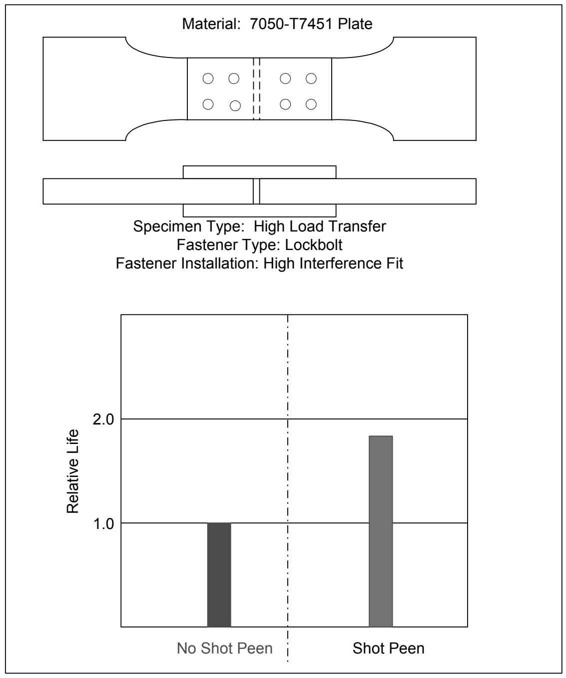

Figure 9.10-15 Typical Fatigue Life Improvement for Shot Peening.

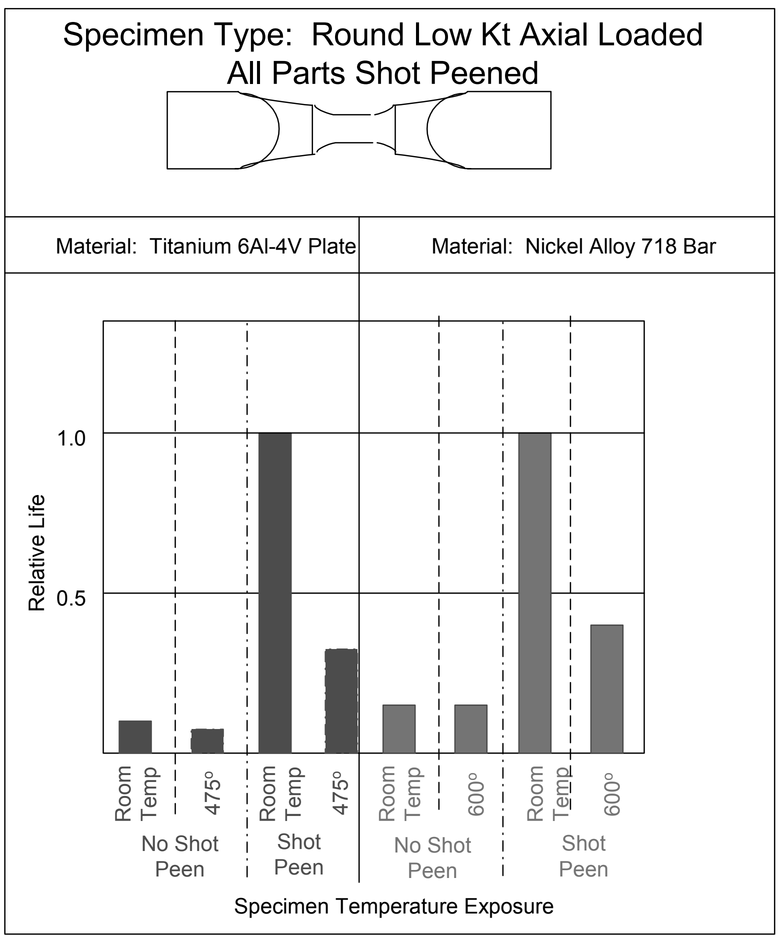

Figure 9.10-16 Effect of Temperature on Fatigue Performance of 6Al-4V Titanium and Nickel Alloy 718 (180 FTU).

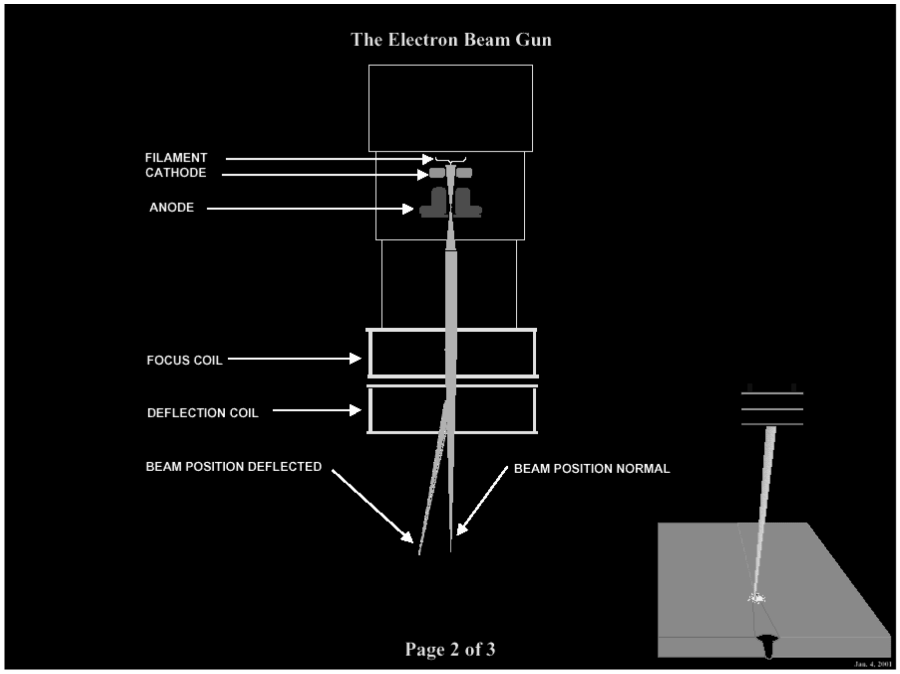

Figure 9.10-17 E-Beam Weld Process.

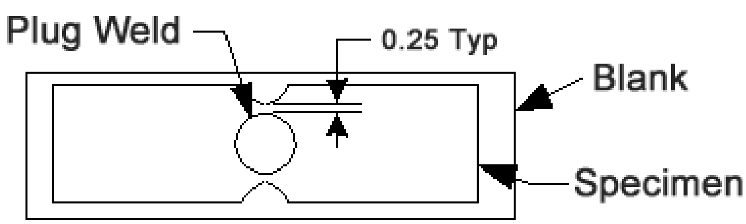

Figure 9.10-18 E-Beam Weld Specimen.

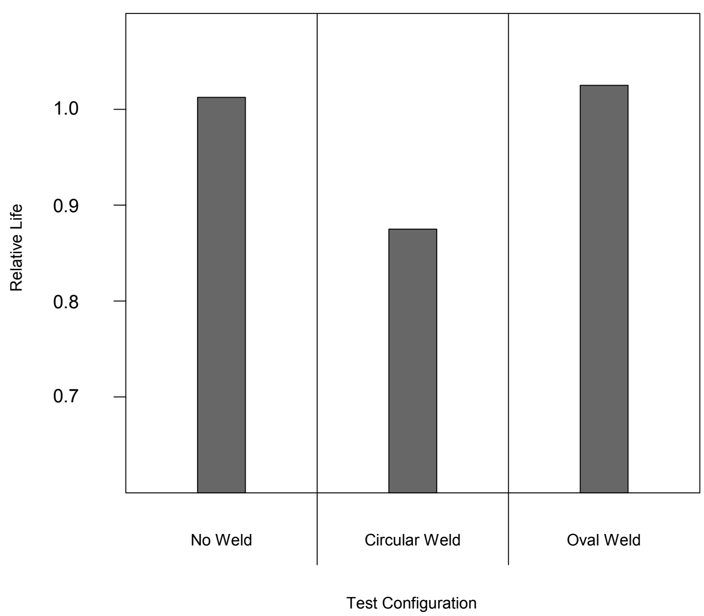

9.10-19 E-Beam Plug Weld Fatigue Results.

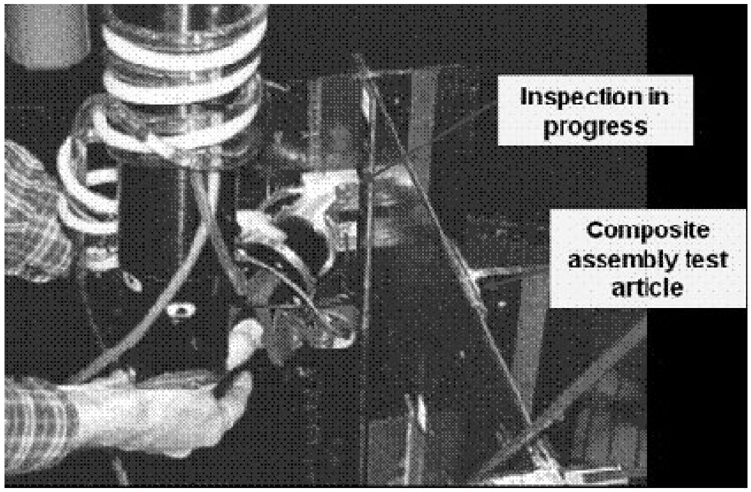

Figure 9.11-1

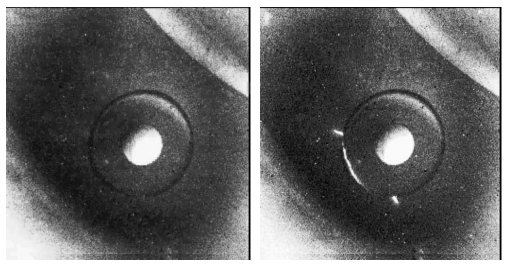

Figure 9.11-2 Crack Detection in an Aircraft Wheel Using Thermosonic Imaging
(a) Before and (b) During Sound Excitation.

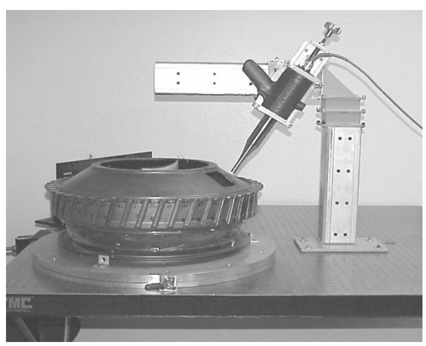

Figure 9.11-3 The FAA AANC Prototype Sonic IR System Setup to Inspect a Turbine Disk.

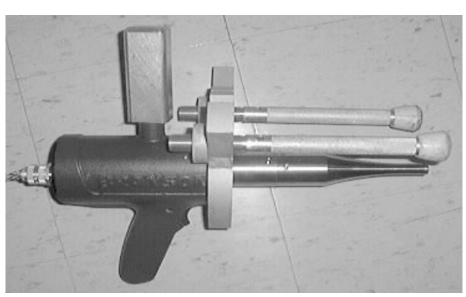

Figure 9.11-4 A Prototype Tripod Ultrasonic Source for Hand-Held Use on Aircraft.

Figure 9.11-5 An Alternative Head for the Gun With Three Active Horns.

Figure 9.11-6 Testing a Hand-Held Prototype on the AANC B737.

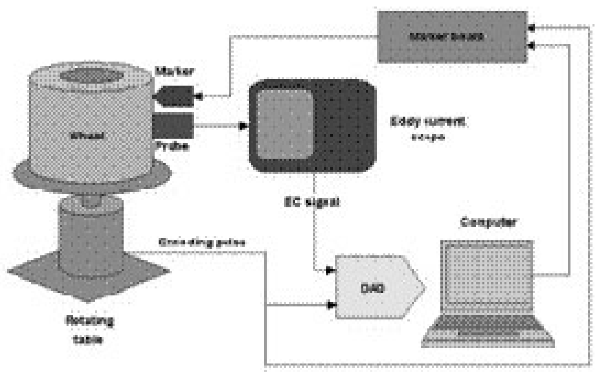

Figure 9.11-7 Schematic of the ASA System for Wheel Inspection.

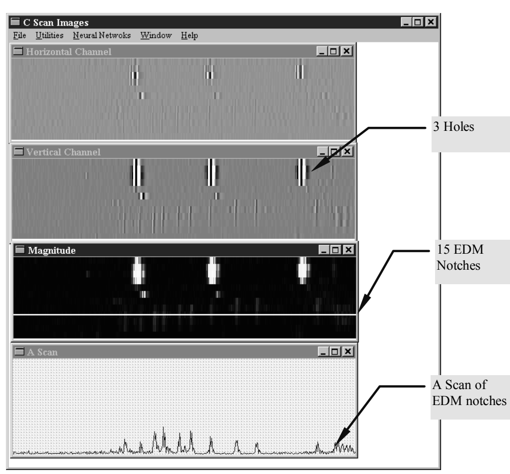

Figure 9.11-8 A Sample Image Window From a B747 Wheel Scan.

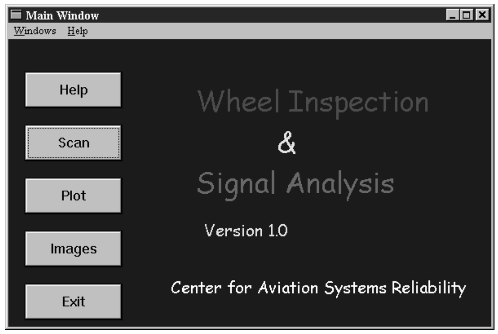

Figure 9.11-9 Main Window of the Wheel Inspection and Signal Analysis Software.

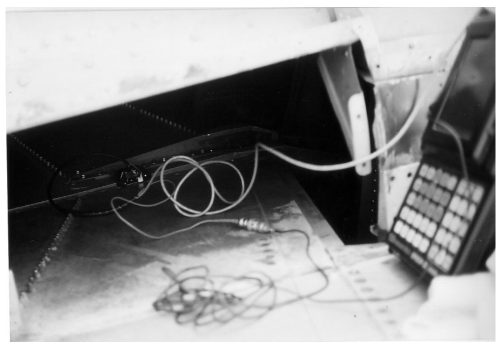

Figure 9.11-10 Ultrasonic Scanning With Dry-Coupled Probe and Portable Flaw Detector.

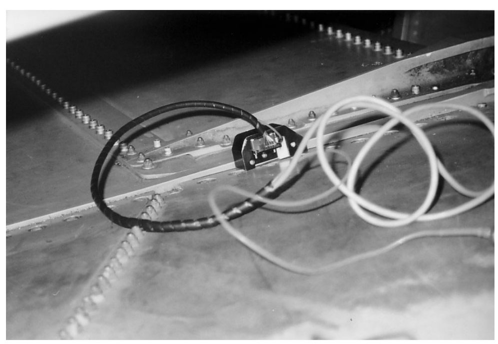

Figure 9.11-11 Dry-Coupled Ultrasonic Probe With Internal Digital Encoding Module.

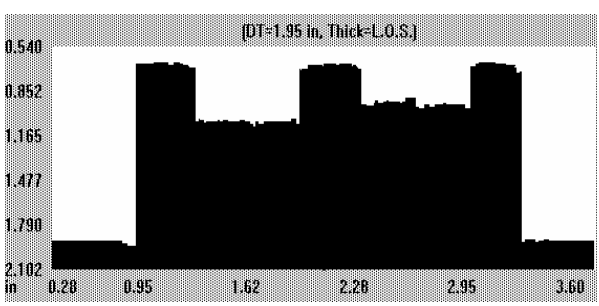

Figure 9.11-12 Measurement of Crack Lengths Using B-Scan Imaging.

Figure 9.11-13 Disassembled Cessna 402C.

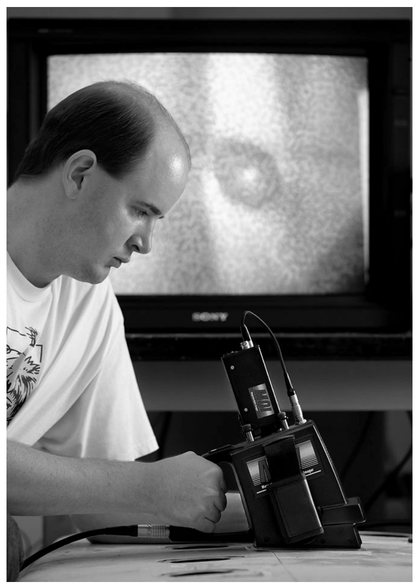

Figure 9.11-14 Magneto Optic Imaging.

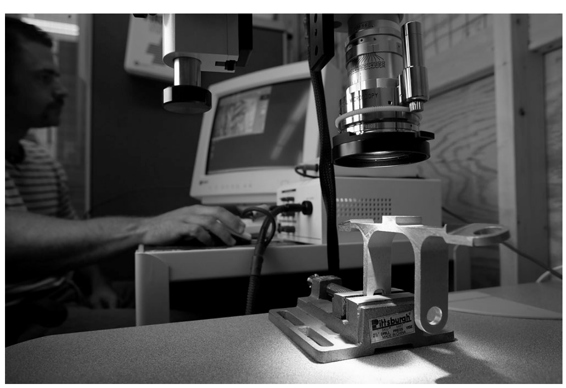

Figure 9.11-15 Microscopic Examination.

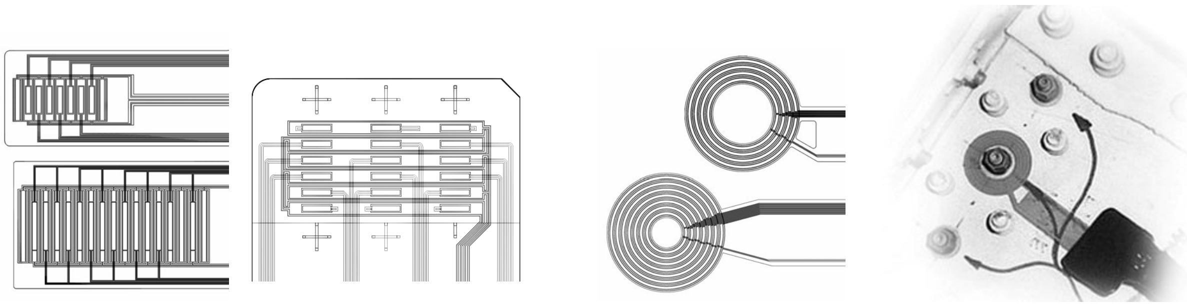

(a) (b) (c)

Figure 9.11-16 Example MWM-Array Sensor Constructs: (a) Surface Mountable Linear MWM-Arrays, FA17 (top left), FA23 (bottom left) and the FA54; (b) MWM-Rosettes for Surface Mounting and Embedding at Fastener Holes, FA06 and FA09; and (c) Application of MWM-Rosette for Full-Scale On-Aircraft Fatigue Tests.

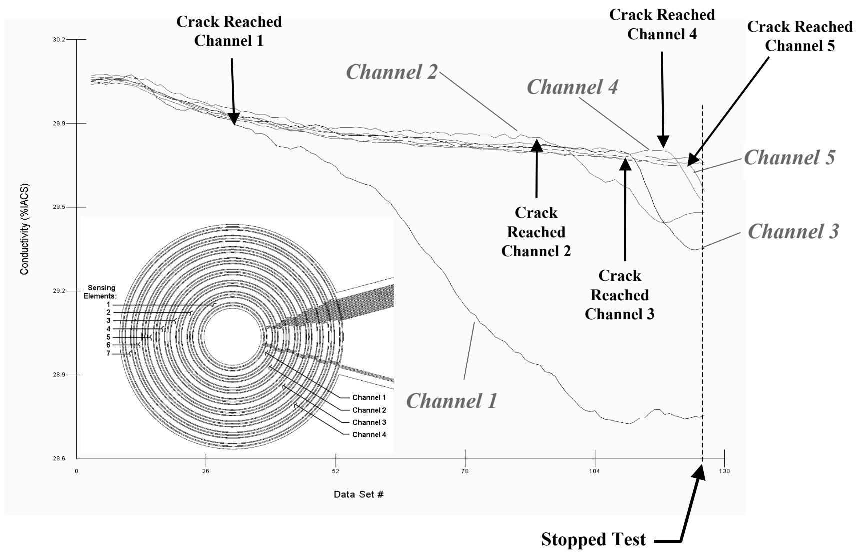

(a)

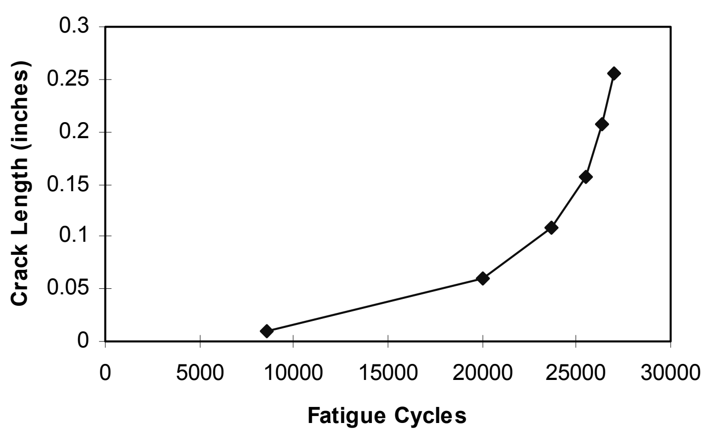

(b)

Figure 9.11-17 Fatigue Test: (a) Data With an MWM-Rosette Mounted Around a Hole in an Aluminum Dogbone Specimen; (b) Crack Length Versus Number of Cycles Data From a Fatigue Test With an Array Mounted Around a Hole in an Aluminum Alloy Specimen. Seven Channels Were Used in This Test. The Test Stopped Shortly After the Crack Reached Channel 6.

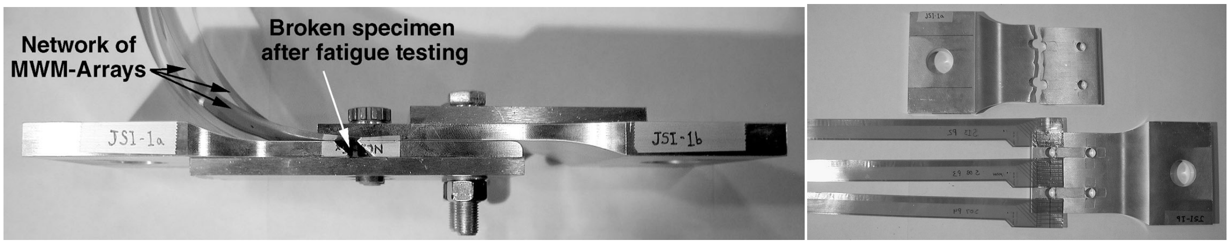

Figure 9.11-18 MWM-Arrays Were Embedded Between Skins in This 4-Hole Specimen and Successfully Monitored Crack Growth Up to Specimen Failure. The MWM-Array Sensors Remained Functional Even After the Specimen Failed.

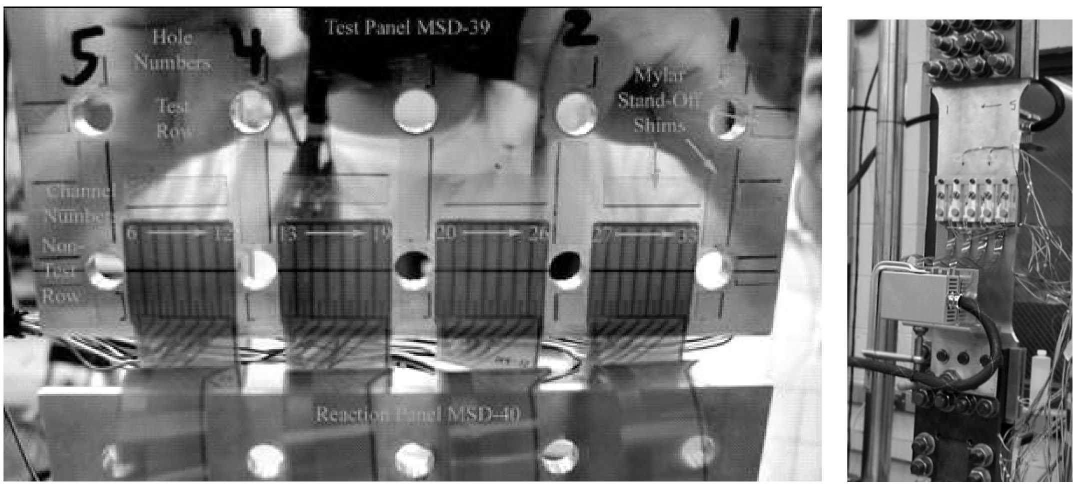

(a) (b)

Figure 9.11-19 (a) The Ten-Hole Specimen With Embedded MWM-Arrays Shown Prior to Bolting Up. (b) The Ten-Hole Specimen is Mounted in the Load Frame in the Photo on the Right. Eight 7-Channel MWM-Arryas Were Used in the Test to Monitor Fatigue in the Ligaments Between All Ten Holes.

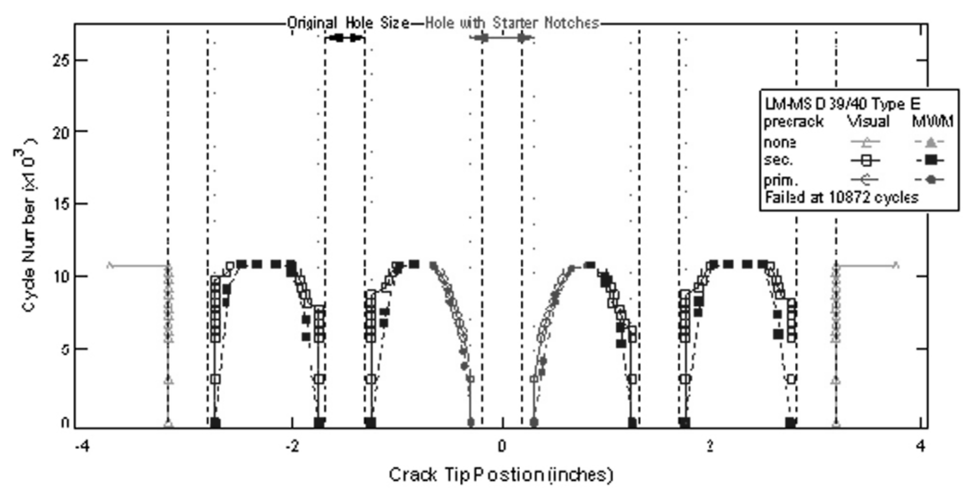

Figure 9.11-20 MWM-Array Data From the Ten-Hole Specimen. Crack Tip Position was Determined for Each Ligament Based on Affected Channels of the MWM-Array. The Colored Lines Indicate Progression of the Crack Tip Versus Cycles. The MWM-Arrays Were Able to Detect the “Buried” Cracks Before They Were Visible on the Exposed Surface.

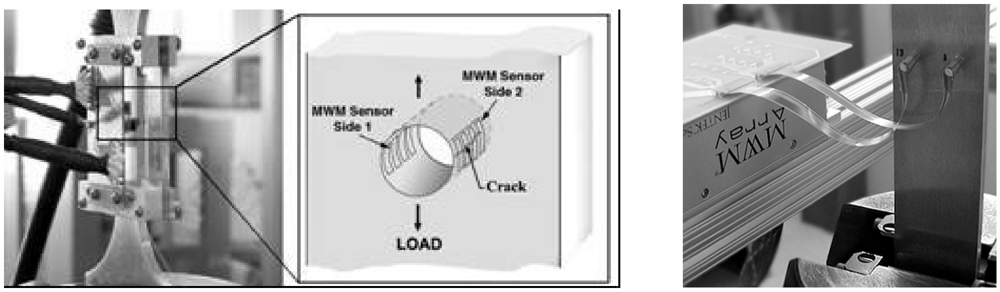

(a) Original prototype (b) (c) 2nd-generation system

Figure 9.11-21 (a) and (b) Two Seven-Channel MWM-Arrays Were Mounted Inside a Hole in an Aluminum Dog-Bone Specimen to Monitor the Area in Which Fatigue Cracks Were Likely to Form; (c) 2nd-Generation System With Two MWM-Arrays That Can Monitor Both Sides of Two Separate Holes Simultaneously.

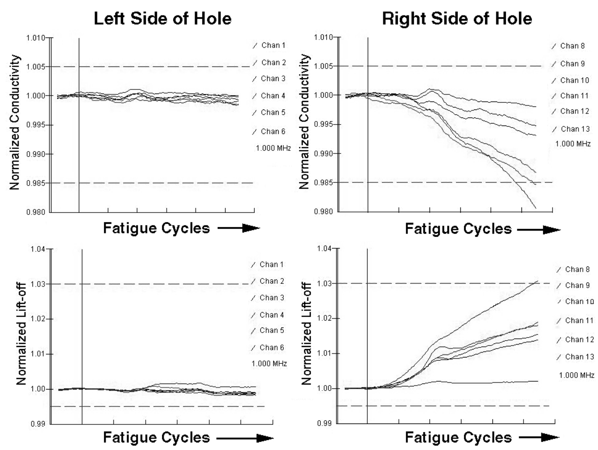

Figure 9.11-22 The MWM-Array Mounted on the Left Side of the Hole Registered Significant Changes in Conductivity and Life-Off as Load Cycling Continued.

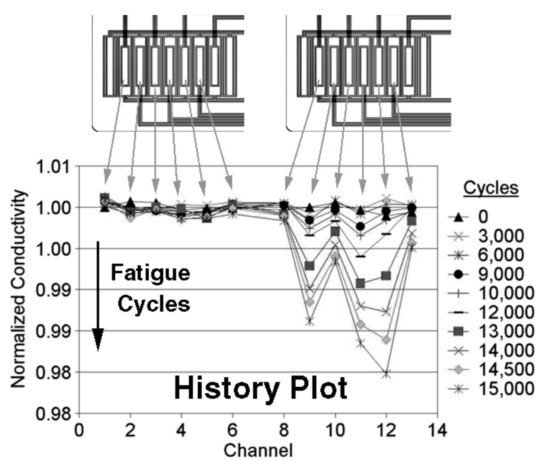

Figure 9.11-23 The History Plot Shows the Spatial Relationship of the Affected Channels. Channels 1 Through 6 Were on the Left Side of the Hole With Channels 8 Through 13 Were on the Right Side.

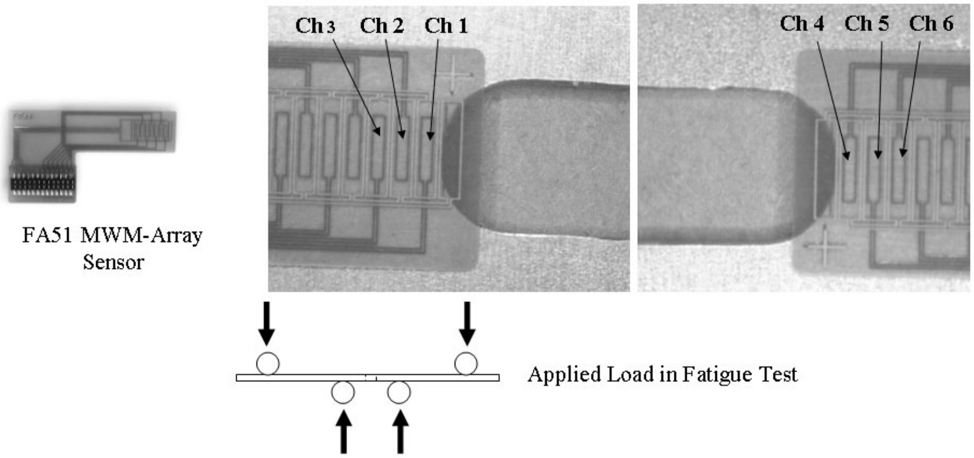

Figure 9.11-24 Setup for Real Crack Generation With MWM-Arrays Mounted at Slot Apexes in IN-718 Plate.

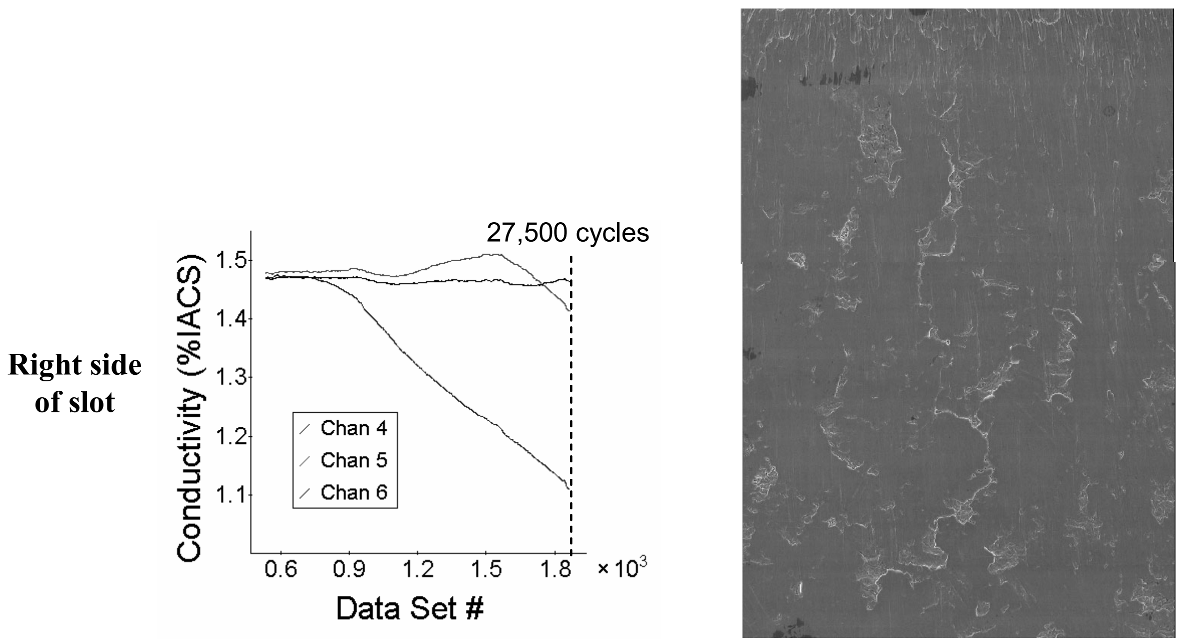

Figure 9.11-25 MWM-Array Response to a Fatigue Crack at the Right Side of the Slot Shown in Figure 9.11-24, and SEM Micrograph Showing the Detected 1 mm Crack.

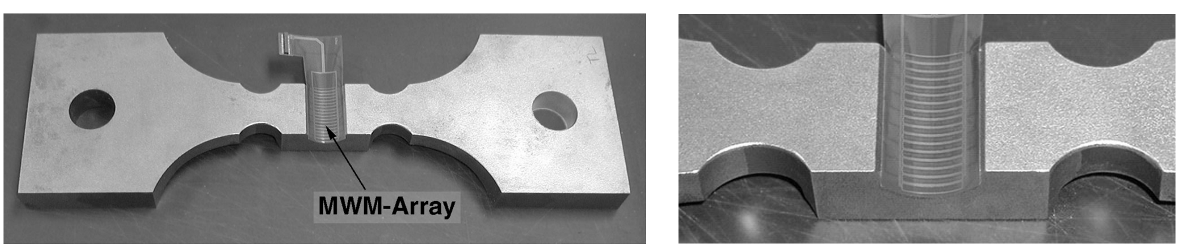

Figure 9.11-26 The Linear MWM-Array Was Mounted in the Central Cavity With Sensing Elements Across the Specimen. This 4340 Steel Specimen Had Been Shot-Peened Prior to Load-Cycling.

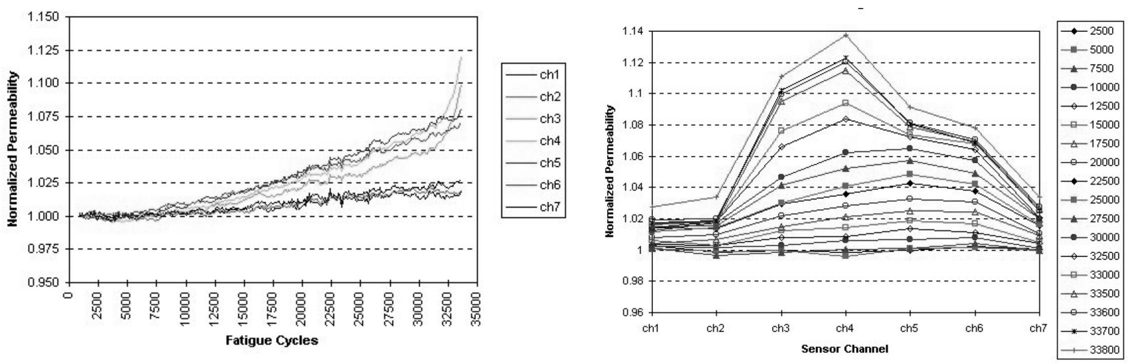

(a) (b)

Figure 9.11-27 (a) MWM Data for All Seven Channels on 4340 Shot-Peened Specimen, Plotted Versus Number of Fatigue Cycles Along the Horizontal Axis, and (b) Versus Individual Channels With Increasing Fatigue Cycles.

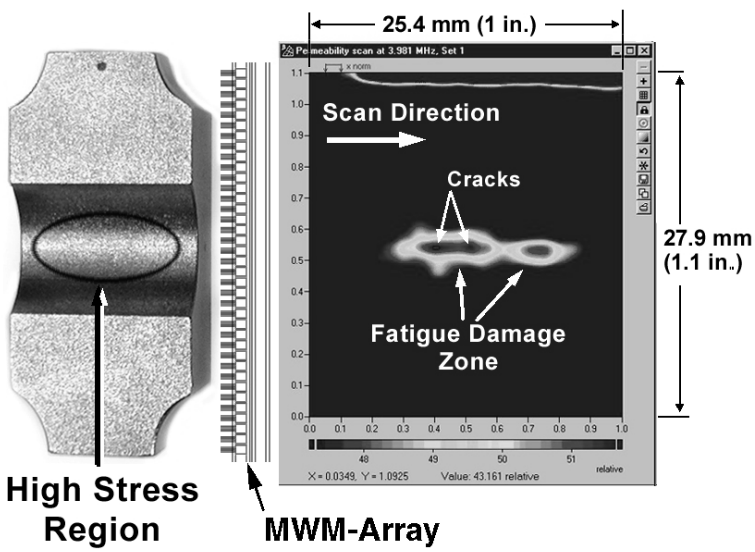

Figure 9.11-28 Central Portion of the Shot-Peened 4340 Specimen Showing High Stress Area and MWM-Array Permeability Image of High Stress Area After About 33,000 Cycles.

Figure 9.12-1 Production Laser Peening of Integrally Bladed Rotors (IBRs) for the F/A-22 Raptor Commenced at LSP Technologies, Inc. in March 2003. Red Laser Beams are Added Graphics to Illustrate the Process (left); the Actual Infrared Laser Beams are Invisible to the Human Eye. Laser Peening Increases the Damage Tolerance and Enhances the Fatigue Performance of This IBR.

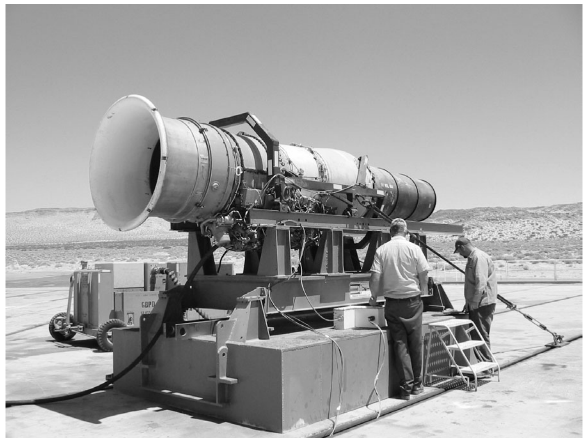

Figure 9.12-2 Engine Test Facility.

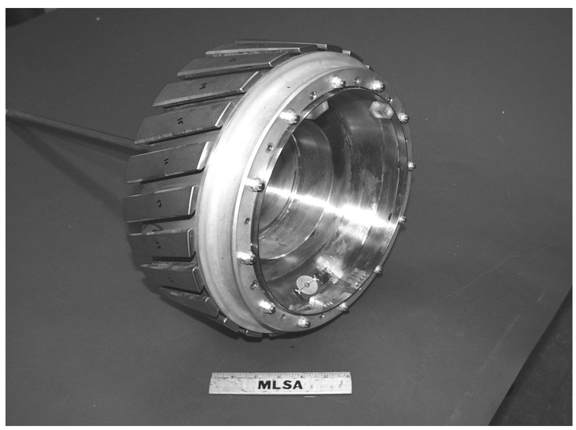

Figure 9.12-3 Instrumented Fan Disk.

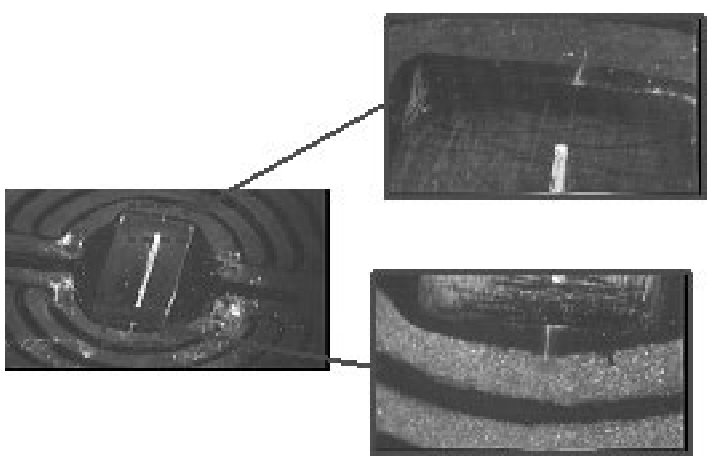

Figure 9.12-4 Finite Element Analysis of Crack.

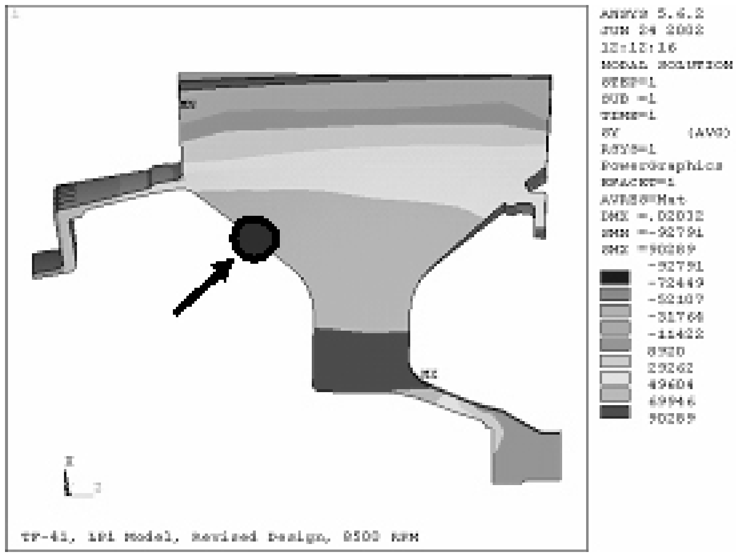

Figure 9.12-5 Crack Growth Inspection.


Figure 9.12-6 Fan Disk Failure Debris.

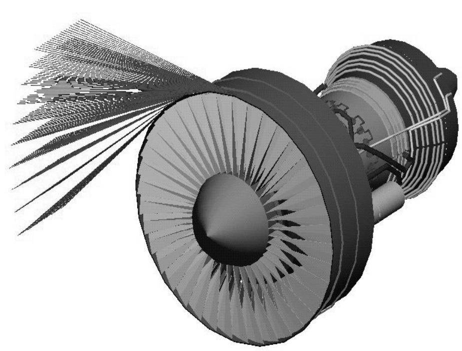
Figure 9.12-7 Engine Failure Model.

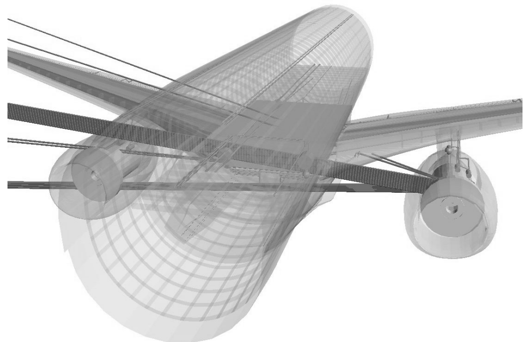

Figure 9.12-8 UEDDAM Disk Burst Analysis.

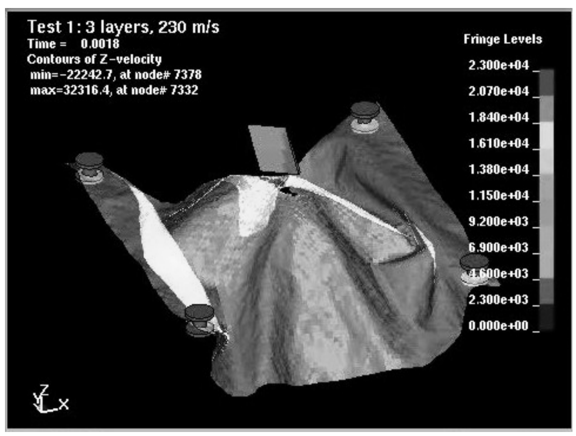

Figure 9.12-9 Simplified Model-Ballistic Simulation.

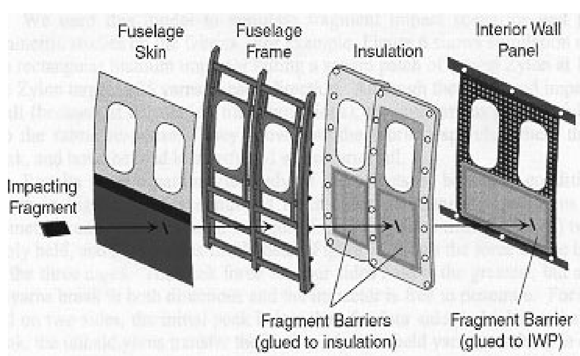

Figure 9.12-10 Armor Fabric Installation Schematic.

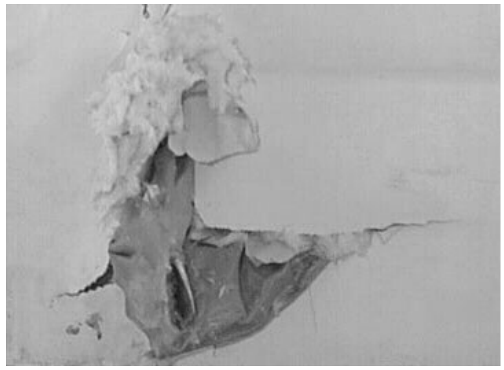

Figure 9.12-11 Fan Blade Fragment Stopped in an Interior Wall Panel.

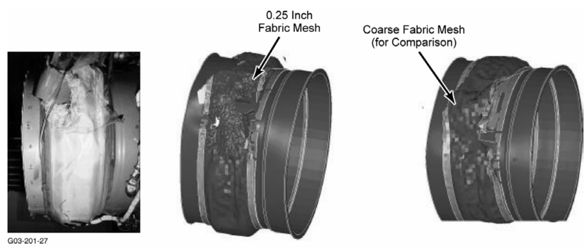

Figure 9.12-12 Engine Blade-Off Test Result and Failure Model Simulation.

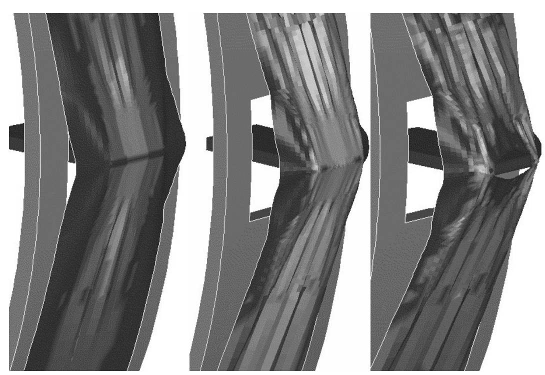

Figure 9.12-13 Model Simulation Views of an Engine Blade Penetration of a Fabric Containment Ring.

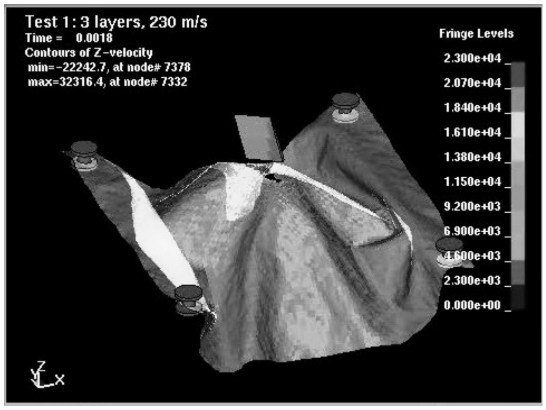

Figure 9.12-14 Model Simulation of an Uncontained Engine Blade Penetrating a Fabric Barrier.

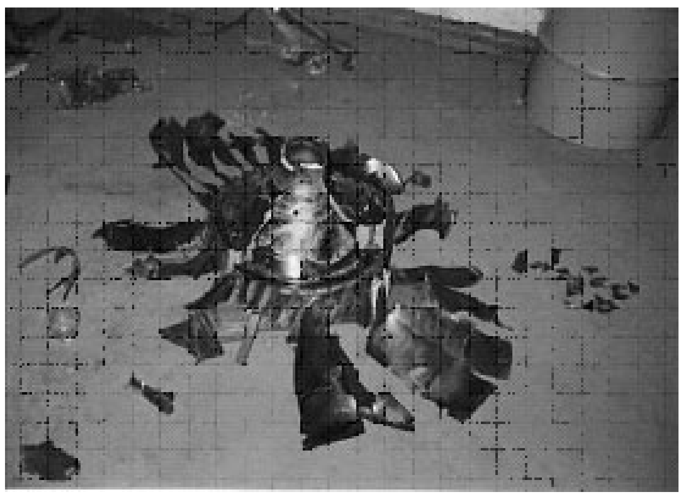

Figure 9.12-15 Fan Disk Failure Debris.

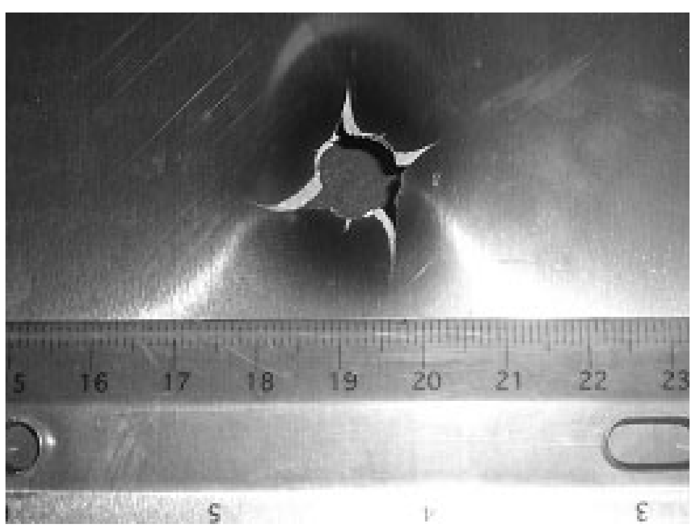

Figure 9.12-16 Ballistic Test Impact on Aluminum Plate From a 0.5” Steel Ball.

Figure 9.12-17 MWM-Array Probe Scanning Engine Disk Slot (left), Photo, Top View of MWM-Array Scanning Slot (middle), and actual MWM-Array FA35 Used for the Automated Disk Slot Inspection.

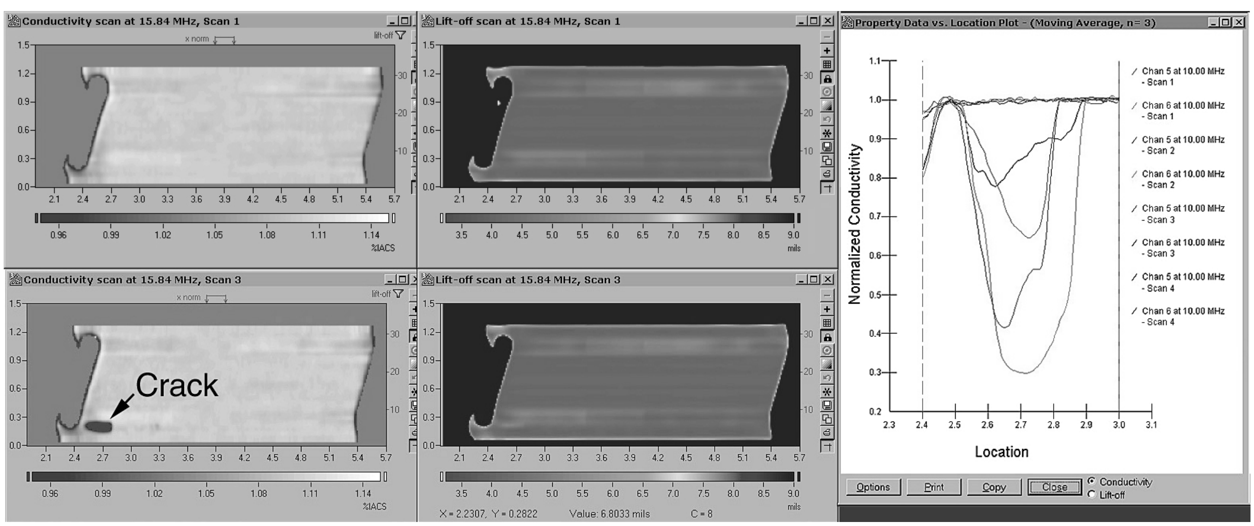

Figure 9.12-18 GridStation Results From Two Different Disk Slots Scanned Using JENTEK's Automated Engine Disk Slot Inspection System. Conductivity is Displayed Using a Blue Scale With a Crack Indication Shown in Red. Lift-Off is Displayed Using a Green-to-Red Scale Where Green Indicates Acceptable Lift-Off. A Crack Indication Can Clearly Be Seen in the Conductivity Image on the Lower Left. The B-scans at Right Show Detection of Cracks in Different Slots.

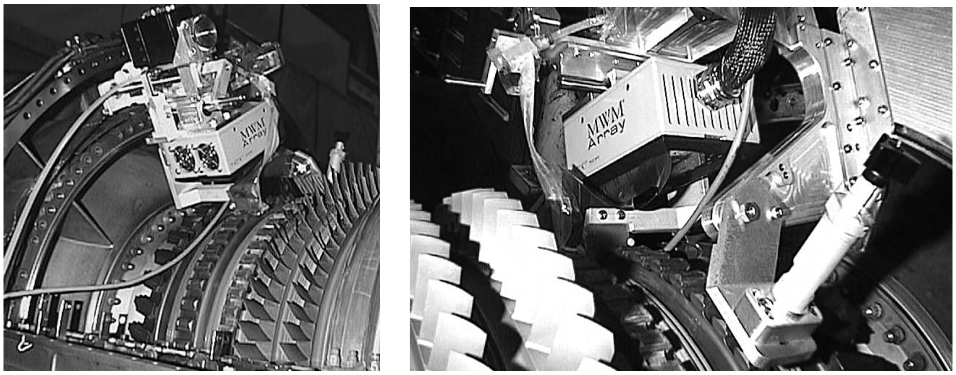

Figure 9.12-19 The “Top-Half” Fixture, Developed for Inspecting Engine Disk Slots in the Stage 1-2 Compressor Spool In-Situ, After Removal of the Upper Compressor Case, Upper Fan Duct and Blades. This Enables Automated I-Level Eddy Current Array Disk Slot Inspection.

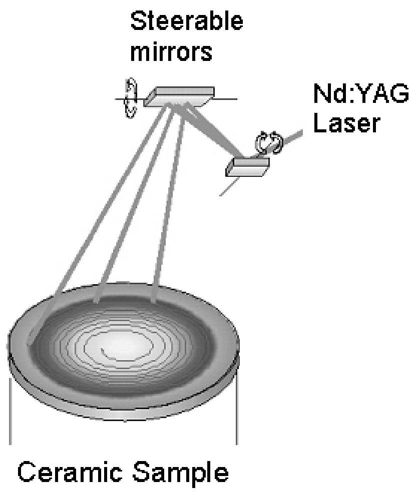

Figure 9.12-20 Schematic of the Laser Upshock Technique Applied to a Thin Silicon Nitride Disk.

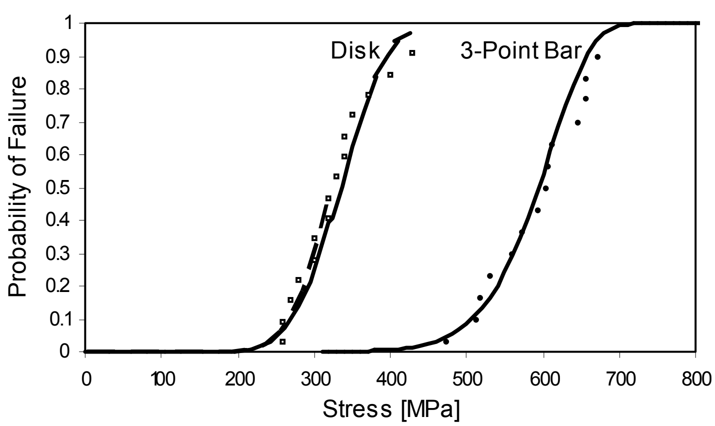

Figure 9.12-21 Silicon Nitride Disks Under Thermal Shock. Failure Probability of Disk Versus Maximum Stress Predicted Using Finite Element Analysis and Experimental Results From 3-Point Flexure Bar Data. Experimental Rupture Data is Shown as Discrete Points. The Disk Prediction is Shown Based on Analysis of Disk #3 (Solid Line) and Disk #9 (Dotted Line).

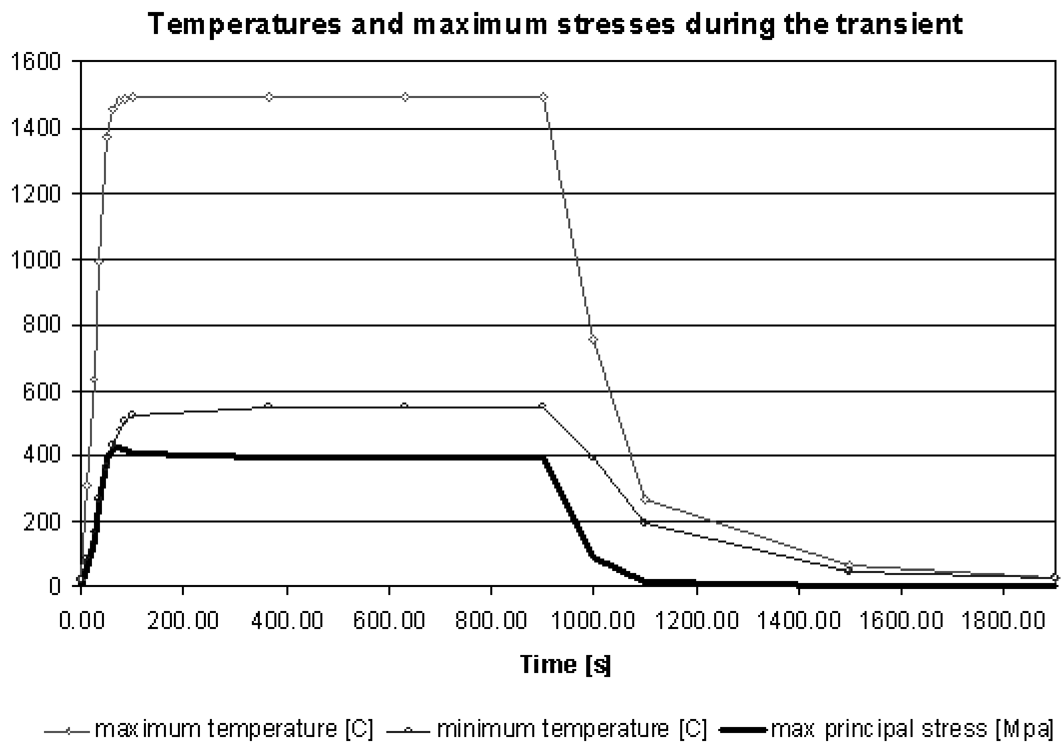

Figure 9.12-22 Maximum Temperatures and Stresses Versus Time for a Simulated Startup/Shutdown Cycle of a Ceramic Turbine Vane.

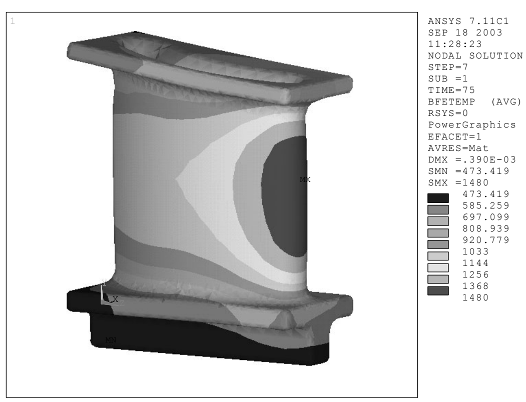

Figure 9.12-23 Finite Element Model Results Showing the Stator Vane Temperature Profile at 75 Seconds -- the Moment of Highest Loading.

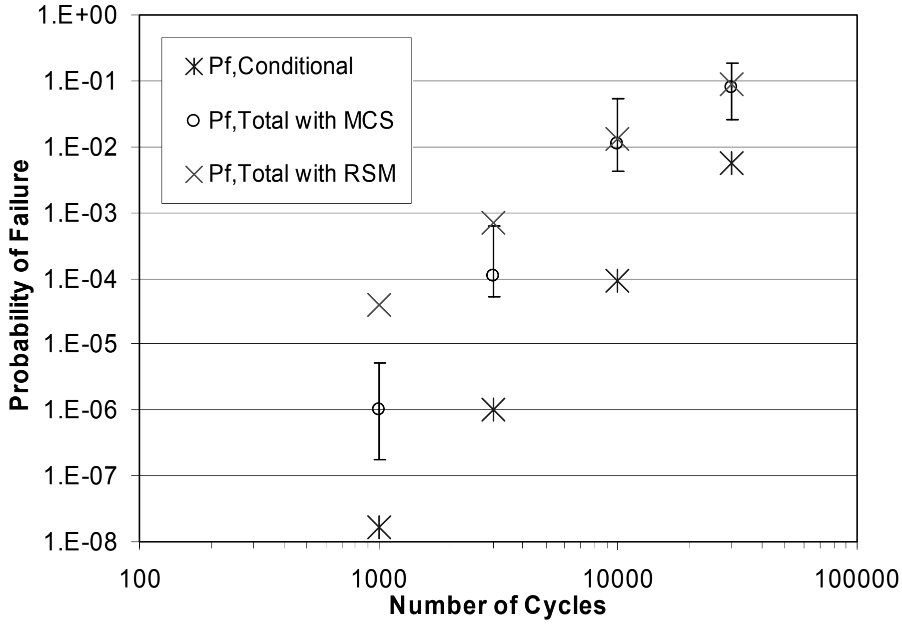

Figure 9.12-24 Results for Conditional (Deterministic) and Total Probability From the PDF Using Monte Carlo Simulation (MCS) and Response Surface Method (RSM).

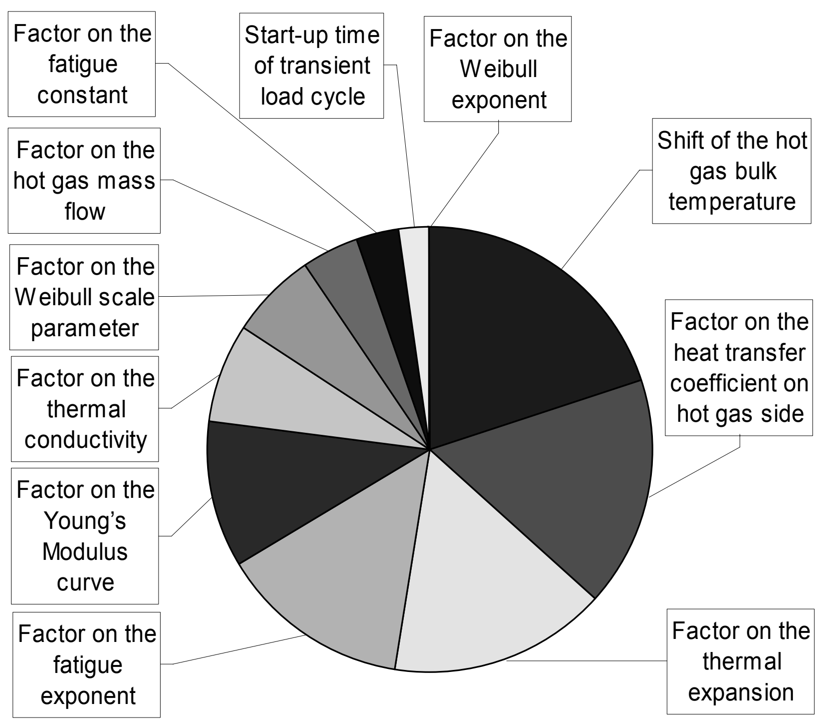

Figure 9.12-25 Sensitivity of Conditional Failure Probability at 1,000 Load Cycles With Monte Carlo Simulation.

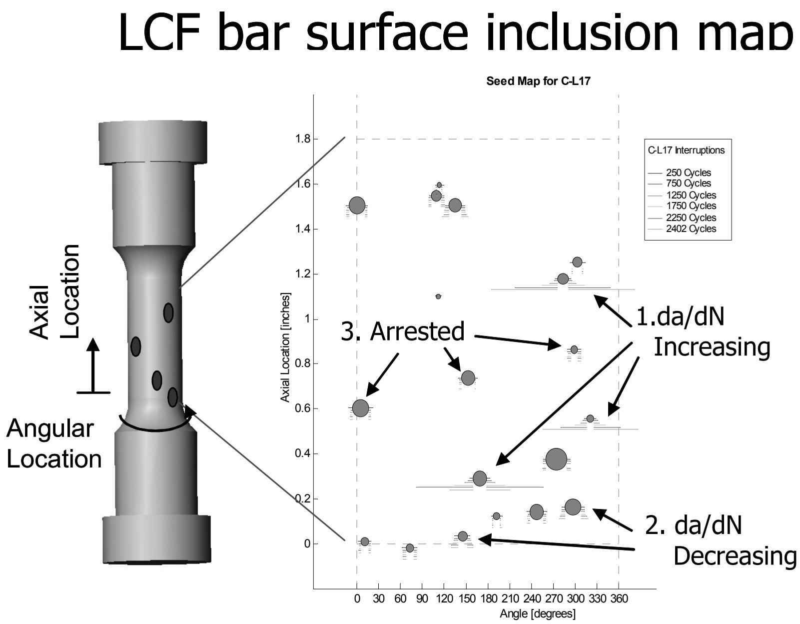

Figure 9.12-26 Map of Surface Inclusion Initiated Crack Lengths From an Interrupted Fatiuge Experiment.

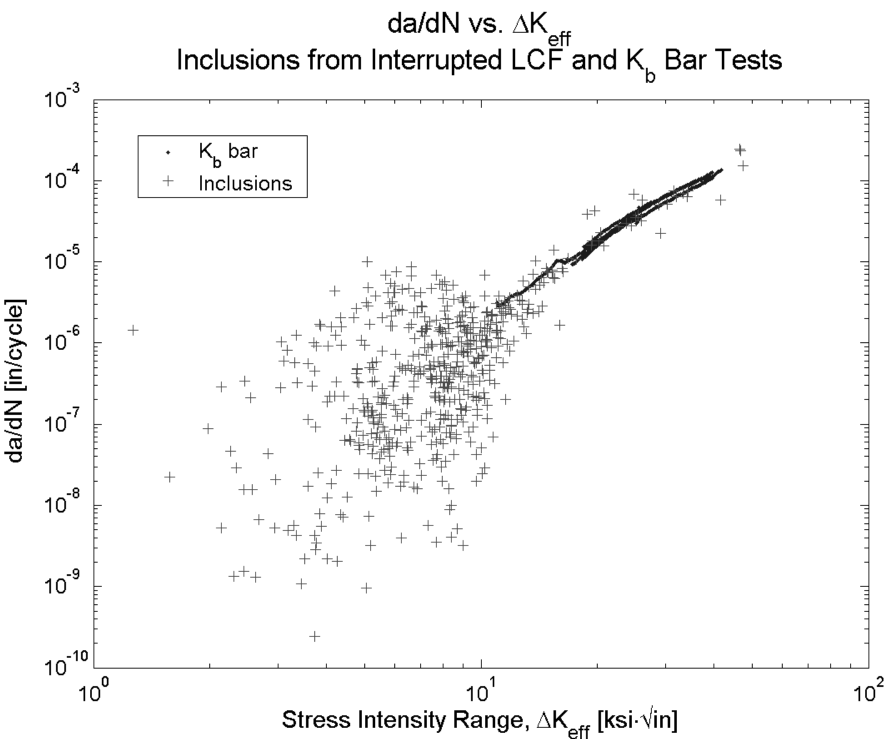

Figure 9.12-27 Crack Growth Rates for Cracks Emanating From Surface Inclusions Compared With K_b Bar Surface Crack Data.

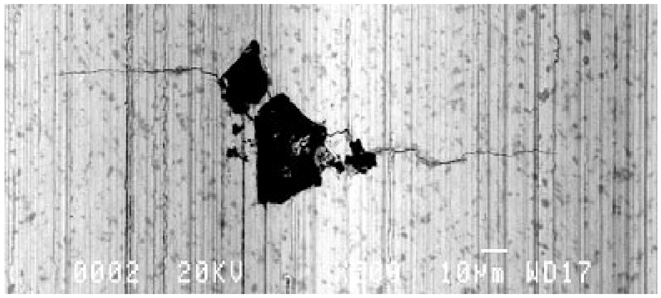

Figure 9.12-28 SEM Micrograph of Smooth LCF Test Bar Illustrating Crack Growth From an Alumina Inclusion. Note: Crack Seems to Initiate From Corners (Upper Left and Lower Right).

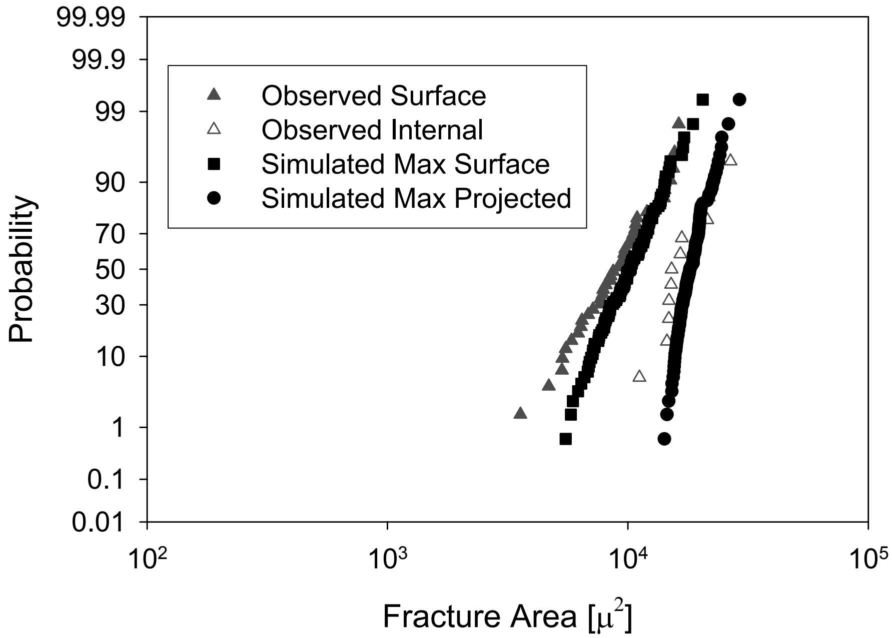

Figure 9.12-29 Fracture Area Comparison For Larger T64 Inclusions.

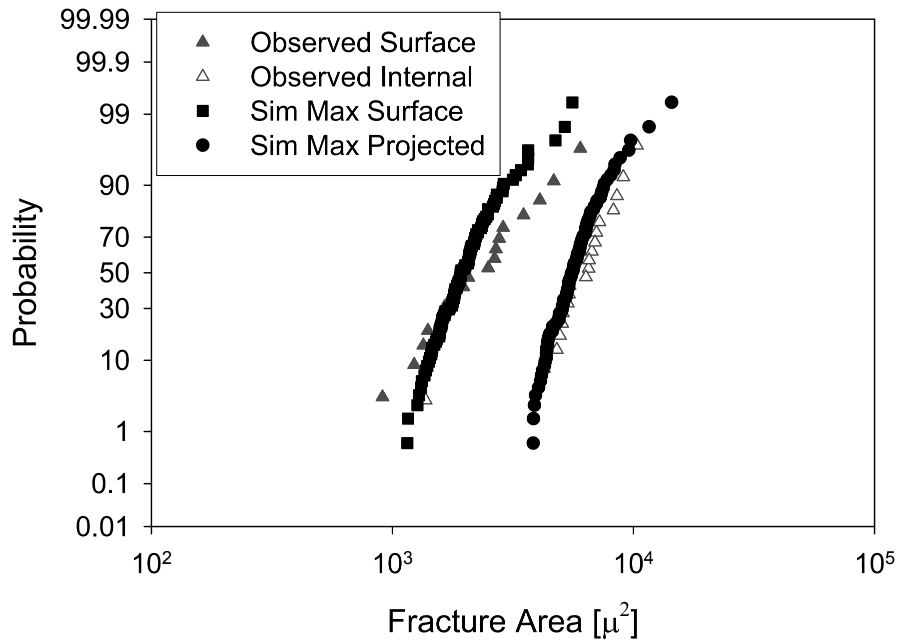

Figure 9.12-30 Fracture Area Comparison For Smaller RAM90 Inclusions.

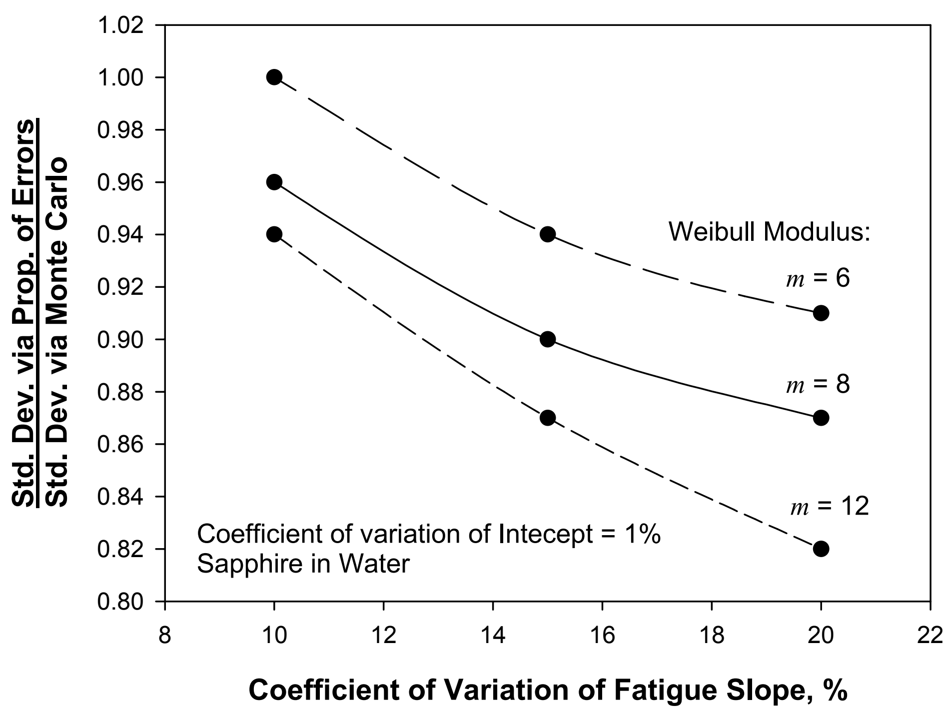

Figure 9.12-31 Comparison of Standard Deviations of Crack Growth Parameter A^* Made Via Propagation of Errors and Monte Carlo Simulation for Sapphire Tested in Water.

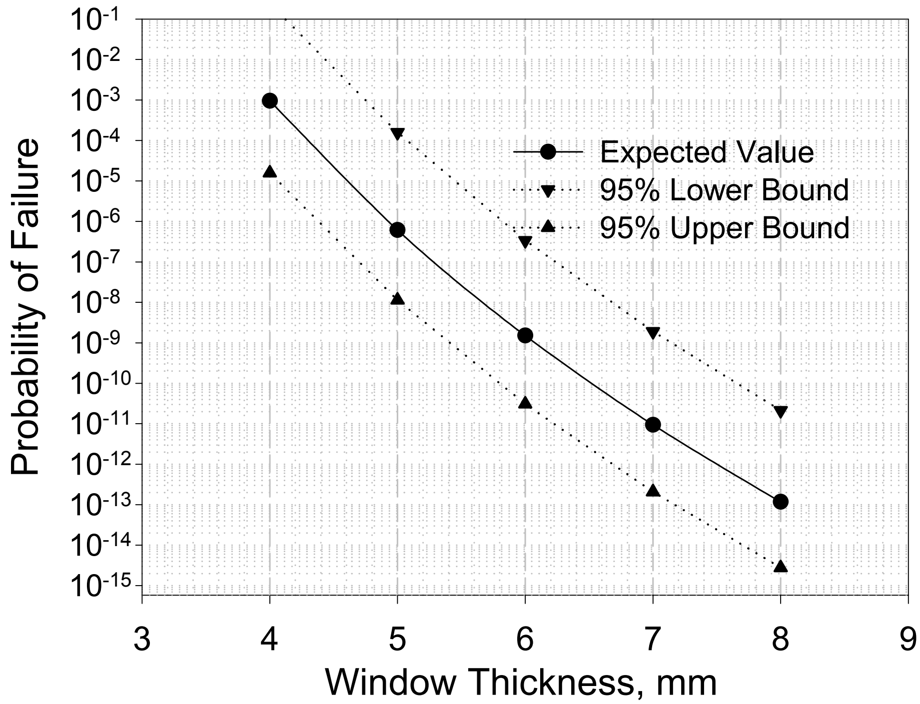

Figure 9.12-32 Lifetime Failure Probability and 95% Confidence Intervals For a Pressurized Sapphire Window.

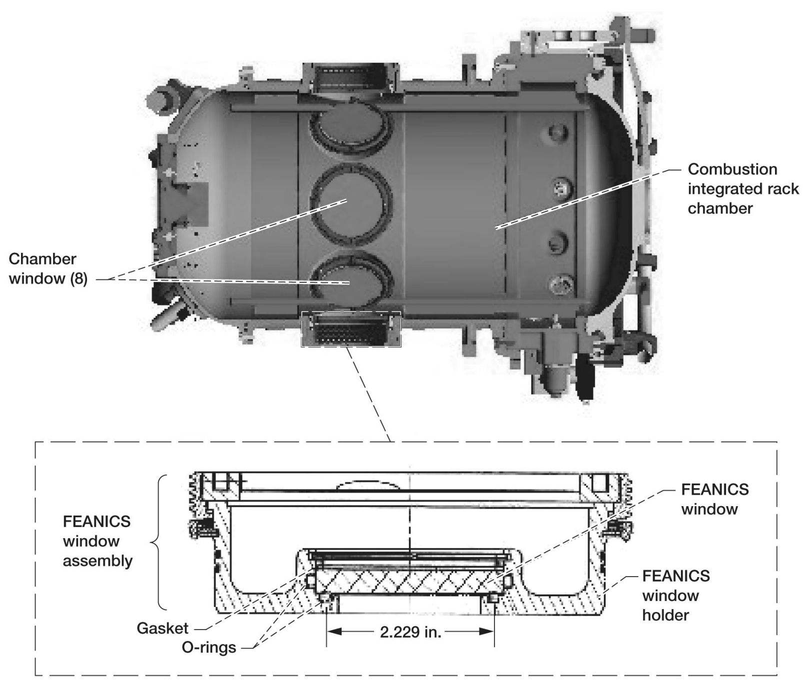

Figure 9.12-33 FEANICS (Flow Enclosure Accommodating Novel Investigations in Combustion of Solids) Module and ZnSe Window Assembly.

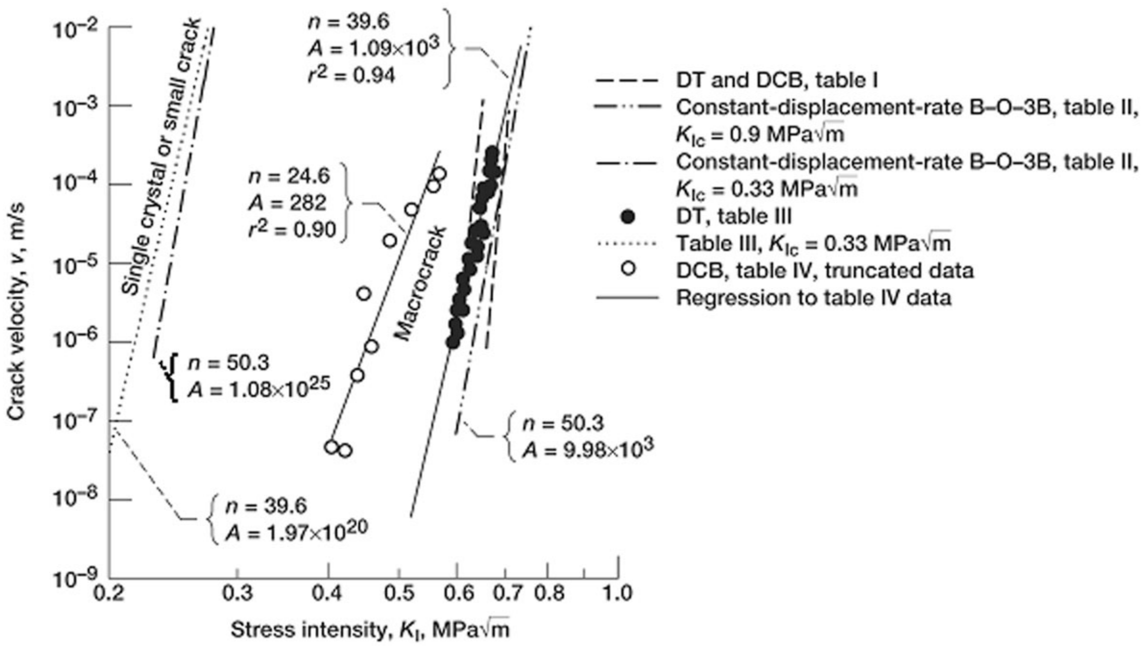

Figure 9.12-34 Crack Velocity v as a Function of Stress Intensity Factor K_I For ZnSe in Water. DCB is Double-Cantilever Beam, DT is Double Torsion, and B-O-3B is Point Loading of Circular Plates Supported by Three Balls.

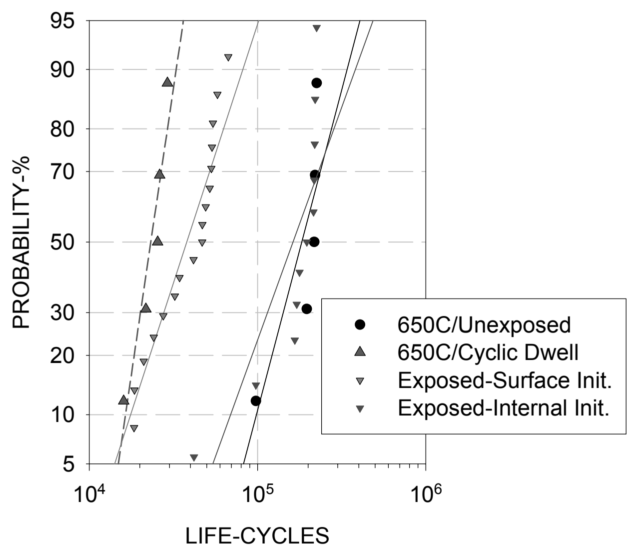

Figure 9.12-35 Udimet 720 Fatigue Lives For 0.70% Strain Range at 650°C, Including Prior Exposed, Unexposed, and Cyclic Dwell Lives Could be Generally Grouped by Failure Initiation Sites.

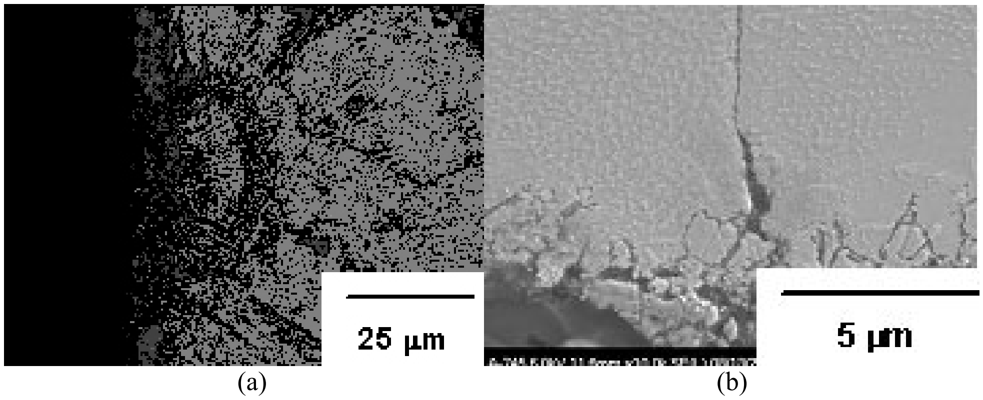

Figure 9.12-36 Fracture Surfaces (a) and Metallographic Sections (b) Showed Failures Initiated at Surface Oxidation For Many Exposed and All Cyclic Dwell Specimens of Udimet 720 and ME3.

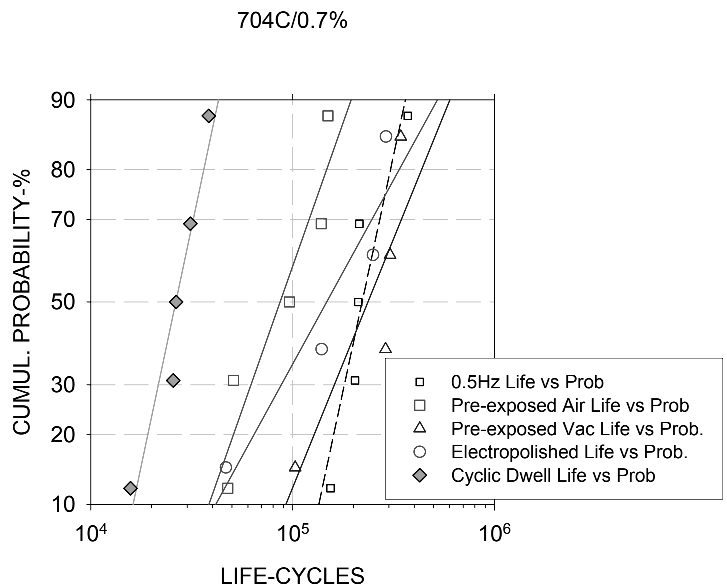

Figure 9.12-37 Controlled Experiments on ME3 For 0.70% Strain Range at 704°C Indicated Mixed Cycling and Exposure in Air is Life Limiting.

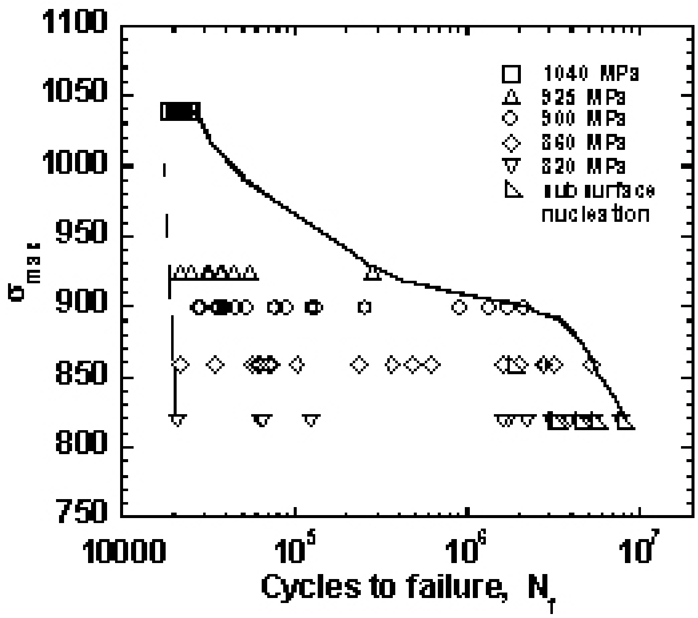

Figure 9.12-38 Fatigue Life Behavior of the Ti-6-2-4-6 Alloy.

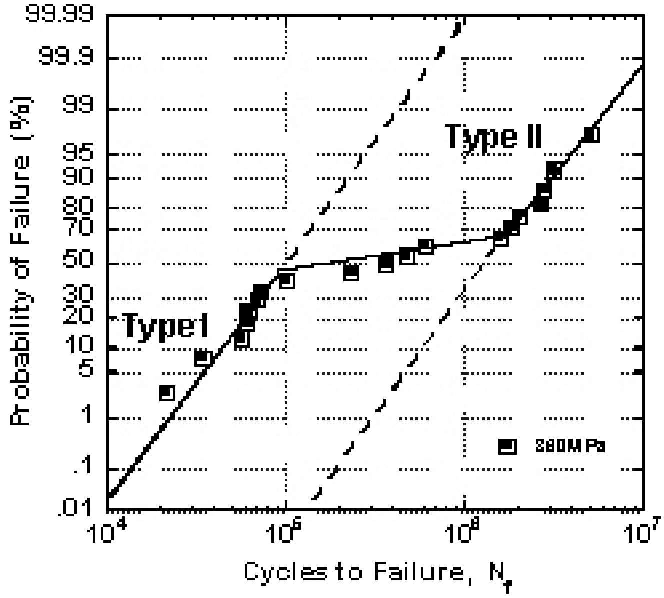

Figure 9.12-39 Step-Like Shape of Experimental Points in the CDF Space of Ti-6-2-4-6 at σ_{max} = 860 MPa.

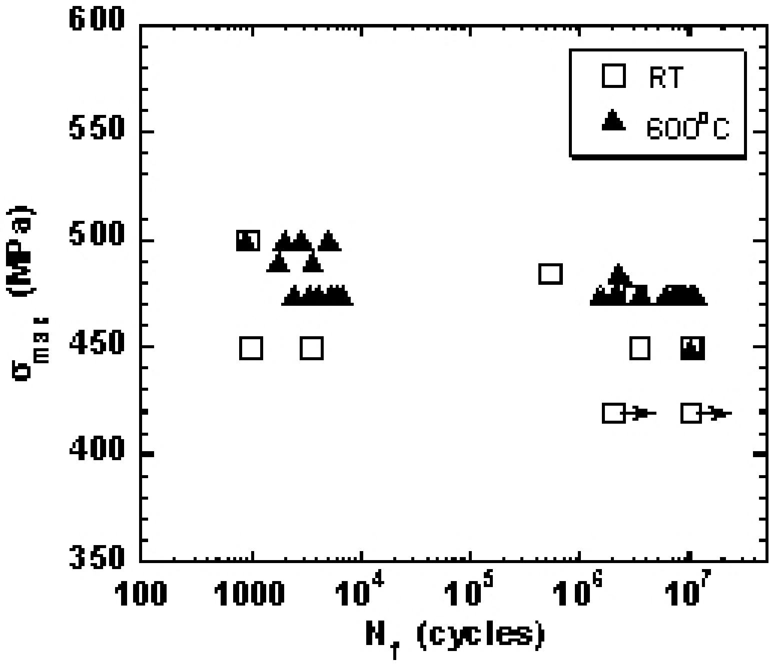

Figure 9.12-40 Fatigue Life Behavior of the γ-TiAl Based Alloy at Room Temperature and 600°C.

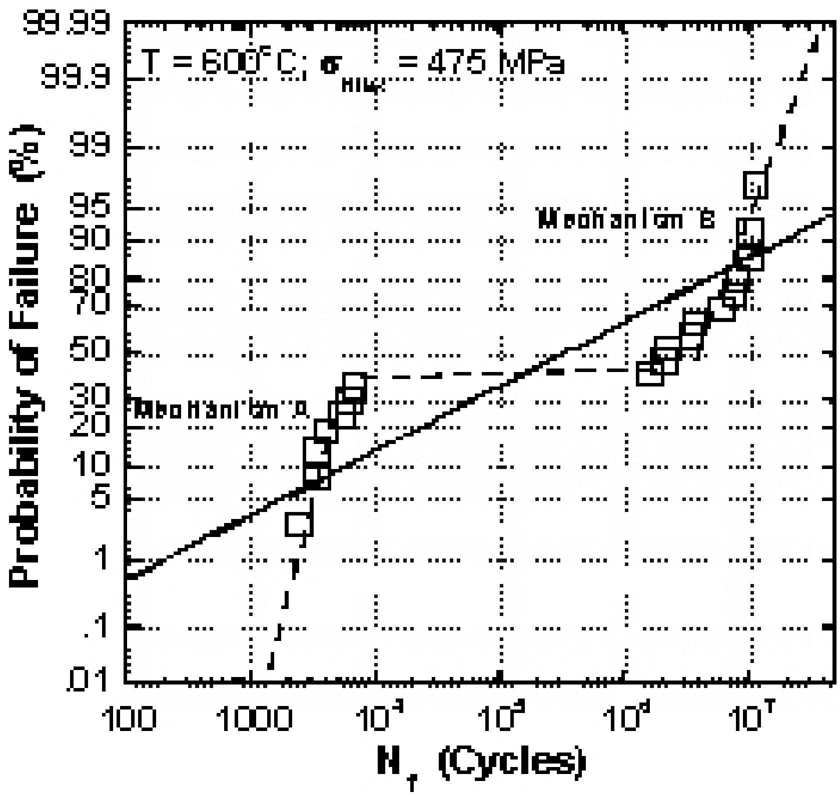

Figure 9.12-41 Step-Like Nature of the Experimental Points With Respect to the CDF in the γ-TiAl Based Alloy.

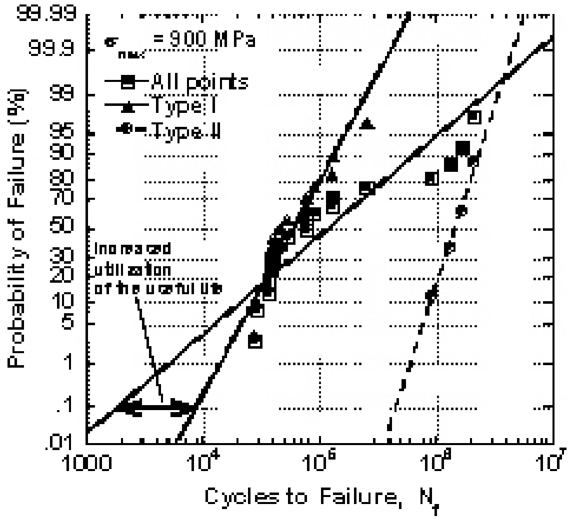

(a)

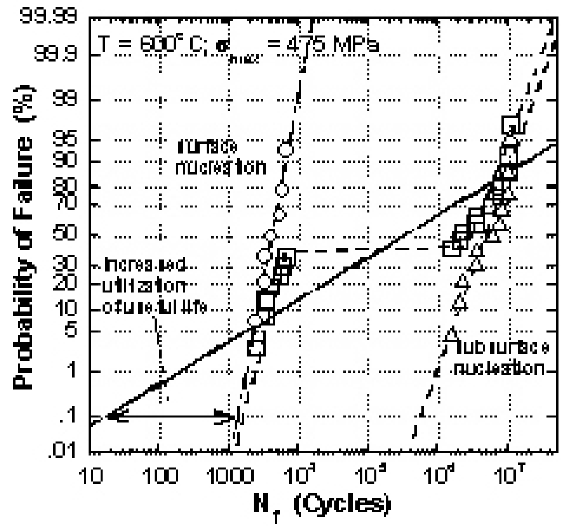

(b)

Figure 9.12-42 The Worst-Case Life Prediction Methodology in (a) TI-6-2-4-6 and (b) the γ-TiAl Based Alloy.